



IntechOpen

# Recent Advances in Analytical Chemistry

*Edited by Muharrem Ince and Olcay Kaplan Ince*





---

# Recent Advances in Analytical Chemistry

*Edited by Muharrem Ince  
and Olcay Kaplan Ince*

Published in London, United Kingdom

---



## IntechOpen





*Supporting open minds since 2005*



Recent Advances in Analytical Chemistry  
<http://dx.doi.org/10.5772/intechopen.79436>  
Edited by Muharrem Ince and Olcay Kaplan Ince

#### Contributors

Sahel Karoui, Slaheddine Kamoun, Bertrand Rochat, Mahesh Deshpande, Veena Kasture, Mahalaxmi Mohan, Machhindra Chavan, H el ene Perreault, Claudia Nelson, Raymond Bacala, Baylie Gigolyk, Evelyn Ang, Haley Neustaeter, Emy Komatsu, Oleg Krokhin, Dave Hatcher, Muslum Ilgu, Marit Nilsen-Hamilton, Meric Ozturk, Rezzan Fazlioglu, Yasemin Ozsurekci, Nikita Tavengwa, Barbara Moyo

  The Editor(s) and the Author(s) 2019

The rights of the editor(s) and the author(s) have been asserted in accordance with the Copyright, Designs and Patents Act 1988. All rights to the book as a whole are reserved by INTECHOPEN LIMITED. The book as a whole (compilation) cannot be reproduced, distributed or used for commercial or non-commercial purposes without INTECHOPEN LIMITED's written permission. Enquiries concerning the use of the book should be directed to INTECHOPEN LIMITED rights and permissions department ([permissions@intechopen.com](mailto:permissions@intechopen.com)).

Violations are liable to prosecution under the governing Copyright Law.



Individual chapters of this publication are distributed under the terms of the Creative Commons Attribution 3.0 Unported License which permits commercial use, distribution and reproduction of the individual chapters, provided the original author(s) and source publication are appropriately acknowledged. If so indicated, certain images may not be included under the Creative Commons license. In such cases users will need to obtain permission from the license holder to reproduce the material. More details and guidelines concerning content reuse and adaptation can be found at <http://www.intechopen.com/copyright-policy.html>.

#### Notice

Statements and opinions expressed in the chapters are those of the individual contributors and not necessarily those of the editors or publisher. No responsibility is accepted for the accuracy of information contained in the published chapters. The publisher assumes no responsibility for any damage or injury to persons or property arising out of the use of any materials, instructions, methods or ideas contained in the book.

First published in London, United Kingdom, 2019 by IntechOpen  
eBook (PDF) Published by IntechOpen, 2019

IntechOpen is the global imprint of INTECHOPEN LIMITED, registered in England and Wales,  
registration number: 11086078, The Shard, 25th floor, 32 London Bridge Street  
London, SE19SG – United Kingdom  
Printed in Croatia

British Library Cataloguing-in-Publication Data

A catalogue record for this book is available from the British Library

Additional hard and PDF copies can be obtained from [orders@intechopen.com](mailto:orders@intechopen.com)

Recent Advances in Analytical Chemistry  
Edited by Muharrem Ince and Olcay Kaplan Ince  
p. cm.  
Print ISBN 978-1-78985-809-9  
Online ISBN 978-1-78985-810-5  
eBook (PDF) ISBN 978-1-83962-122-2

# We are IntechOpen, the world's leading publisher of Open Access books Built by scientists, for scientists

**4,100+**

Open access books available

**116,000+**

International authors and editors

**120M+**

Downloads

**151**

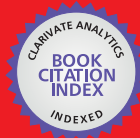
Countries delivered to

Our authors are among the  
**Top 1%**

most cited scientists

**12.2%**

Contributors from top 500 universities



**WEB OF SCIENCE™**

Selection of our books indexed in the Book Citation Index  
in Web of Science™ Core Collection (BKCI)

Interested in publishing with us?  
Contact [book.department@intechopen.com](mailto:book.department@intechopen.com)

Numbers displayed above are based on latest data collected.  
For more information visit [www.intechopen.com](http://www.intechopen.com)







# Meet the editors



Dr. Muharrem Ince received his PhD degree in Analytical Chemistry at Firat University, Turkey, in 2008. He worked at Mus Alparslan University, Turkey, from 2009 to 2012 as an assistant professor. He has been working at Munzur University since 2012. From 2013 to 2016, he served as Head of Department of Chemical Engineering at Munzur University. He is an editorial board member of several international journals. Currently, he is an associate professor at Munzur University. He is the author and coauthor of more than 25 papers published in respectable international journals. He is an expert on analytical method development, spectroscopic and chromatographic techniques, trace element analysis, food analysis, and toxicology.



Dr. Olcay Kaplan Ince received her BS degree from Hacettepe University and her PhD degree in Analytical Chemistry from Firat University in Turkey in 2008. She has been a research analytical chemist at Munzur University since 2009 in the Food Engineering Department. She was also Head of Department of Food Engineering at Munzur University, 2014–2015. She has been serving as an associate editor of the *International Journal of Pure and Applied Sciences* since 2015. She is the author of more than 28 papers published in journals with good impact factors in their area. Her research areas include atomic absorption spectroscopy, speciation, trace and toxic element analysis, analytical chemistry, instrumental analysis, problem solving in analytical chemistry, food science, and chromatography, especially high-performance liquid chromatography-mass spectrometry and gas chromatography.



# Contents

<b>Preface</b>	<b>XIII</b>
<b>Section 1</b> Sample Preparation Techniques	<b>1</b>
<b>Chapter 1</b> Quantitative and Qualitative LC-High-Resolution MS: The Technological and Biological Reasons for a Shift of Paradigm <i>by Bertrand Rochat</i>	<b>3</b>
<b>Section 2</b> Analytical Instrumentation and Methods	<b>21</b>
<b>Chapter 2</b> Modern Extraction and Cleanup Methods of Veterinary Drug Residues in Food Samples of Animal Origin <i>by Babra Moyo and Nikita Tawanda Tavengwa</i>	<b>23</b>
<b>Chapter 3</b> Contribution of Infrared Spectroscopy to the Vibrational Study of Ethylenediammonium Chloride Thiocyanate: (C <sub>2</sub> H <sub>10</sub> N <sub>2</sub> )(Cl NCS) <i>by Sahel Karoui and Slaheddine Kamoun</i>	<b>45</b>
<b>Chapter 4</b> Characterization of Whole and Fragmented Wild-Type Porcine IgG <i>by Claudia Nelson, Raymond Bacala, Baylie Gigolyk, Evelyn Ang, Haley Neustaeter, Emy Komatsu, Oleg Krokhin, Dave Hatcher and Hélène Perreault</i>	<b>65</b>
<b>Section 3</b> Separation Approaches and Validation	<b>95</b>
<b>Chapter 5</b> Bioanalytical Method Development and Validation: A Review <i>by Mahesh Mukund Deshpande, Veena Sanjay Kasture, Mahalaxmi Mohan and Macchindra J. Chavan</i>	<b>97</b>

<b>Section 4</b>	
Recent Developments and Applications in Analytical Chemistry	117
<b>Chapter 6</b>	119
Aptamers for Diagnostics with Applications for Infectious Diseases <i>by Muslum Ilgu, Rezzan Fazlioglu, Meric Ozturk, Yasemin Ozsurekci and Marit Nilsen-Hamilton</i>	

# Preface

This book presents recent and future trends in analytical methods and provides an overview of analytical chemistry, organized into four sections. As a comprehensive analytical chemistry book, it takes a broad view of the subject and integrates a wide variety of approaches. The first section of the book discusses sample preparation techniques. Topics include analytical instrumentation and methods, separation approaches and validation, and recent developments and applications in analytical chemistry. The book was written primarily for researchers in the fields of analytical chemistry, environmental chemistry, food and chemical engineering, and applied chemistry. Its aim is to explain the subject, clarify important studies, and compare and develop new and groundbreaking applications. Written by leading experts in their respective areas, it is highly recommended for professionals who are interested in analytical chemistry because it provides specific and comprehensive examples that compare new and classical methods. The book is edited by Dr. Muharrem Ince from Munzur University, Turkey. I hope the readers will find it useful.

**Muharrem Ince and Olcay Kaplan Ince**  
Munzur University,  
Tunceli, Turkey



---

Section 1

# Sample Preparation Techniques

---





# Quantitative and Qualitative LC-High-Resolution MS: The Technological and Biological Reasons for a Shift of Paradigm

*Bertrand Rochat*

## Abstract

Today, high-resolution mass spectrometry (HRMS: Q-TOF-MS, Orbitrap-MS) shows sensitive and reliable quantifications of a large variety of compounds while acquiring in high-resolution full-scan mode. Interestingly, HRMS shows equal quantitative performance than triple-quadrupole-MS (QQQ-MS), which is the MS technology traditionally used for quantification. But, in contrast to QQQ-MS that performs “narrow-minded” ion transitions (targeted prior determination), analysis using HRMS can record HR-full scan that detects virtually all ions (e.g., from  $m/z = 80$  to 1000) and gives a global picture of what is in the biological sample (diagnostic screening). This is more and more seen as a key advantage because on top of targeted and quantitative analyses, many other routine or research determinations can be performed such as qualitative (identification), simultaneous quantitative/qualitative (quan/qual), and omics (untargeted) assays. The high versatility and performance of most actual HRMS instruments placed them as new gold standards in LC-MS analysis. Indeed, only HRMS can answer new analytical requests from systems biology and personalized medicine requesting more holistic approaches with untargeted analyses (e.g., proteomics and metabolomics). In the light of the new HRMS-based paradigm, concrete examples revealing quantitative, qualitative, simultaneous quan/qual, and omics capabilities of HRMS in the context of routine and research analyses will be given.

**Keywords:** diagnostic, HRMS, high resolution, LC-MS, liquid chromatography, mass spectrometry, metabolomics, Orbitrap-MS, proteomics, quantitative, qualitative, routine, screening, Q-TOF-MS, triple-quadrupole-MS, untargeted

## 1. Introduction: analytical tools and the understanding of the biology

In life sciences, liquid chromatography coupled to mass spectrometry (LC-MS) is considered as a tool to measure molecules in biological samples. In clinical and toxicology labs, LC-MS determinations are quantitative and routinely performed and usually measured one or a few compounds [1–4]. These analyses are strongly driven by medical knowledge as well as the understanding of disease biology. Our understanding of the biology is, to a large extent, related to the available analytical tools. On the other hand, new concepts in life sciences can promote

the development of new analytical tools. The actual understanding of biological systems is presented here below. It will help to put into perspective the actual and future needs for LC-MS analysis and MS technology.

Today, we can draw three main bricks of life, genome, proteome, and metabolome (**Figure 1**), respectively, and to determine nucleic acids, proteins, and metabolites, there are various analytical tools in which, for the last two bricks, mass spectrometry (MS) plays a central role. Whereas **Figure 1** describes three equal bricks of life, the analytical tools have somehow driven DNA far ahead in terms of grants and publications. Indeed, **Figure 2** depicts the number of publications collected in PubMed database for the last 20 years in relation to these three bricks, “genome, proteome, or metabolome” and “patients” as key words. **Figure 2** reveals that the number of publications related to the genome is much higher (log scale) than for the proteome and metabolome. It underscores the efficiency of DNA chips (high-throughput sequencing) as analytical tools. **Figure 2** also reveals the higher number of publication for the proteome than for the metabolome. A steady state between these three bricks of life is expected to come in a near future because genome, proteome, and metabolome have complementary information and because recent MS technologies with improved analytical capabilities, have been launched during this last decade. These recent MS are high-resolution mass spectrometers (HRMS) and allow cheap targeted and omics/global approaches. They should promote proteome and metabolome determinations not only in research but also in routine laboratories for diagnosis purposes (e.g., clinical and toxicology labs).

The main advantages of DNA sequencing over the determination of proteins and metabolites are that (1) DNA can be multiplied (PCR), (2) the DNA sequence is (roughly) constant over the entire life, and (3) the analysis has become really affordable. On the other hand, the great advantage of the determination of the proteome and/or the metabolome over the genome is the integration of all types of interactions and memories (e.g., age) that the living system has with its environment (**Figure 3**) [5]. This last point is crucial and supports an increasing need for individual’s proteome and metabolome determination.

In addition, the concepts of “long tail disease” and “tyranny of the average” have recently emerged (**Figure 4**) [6, 7]. These concepts underscore the high number

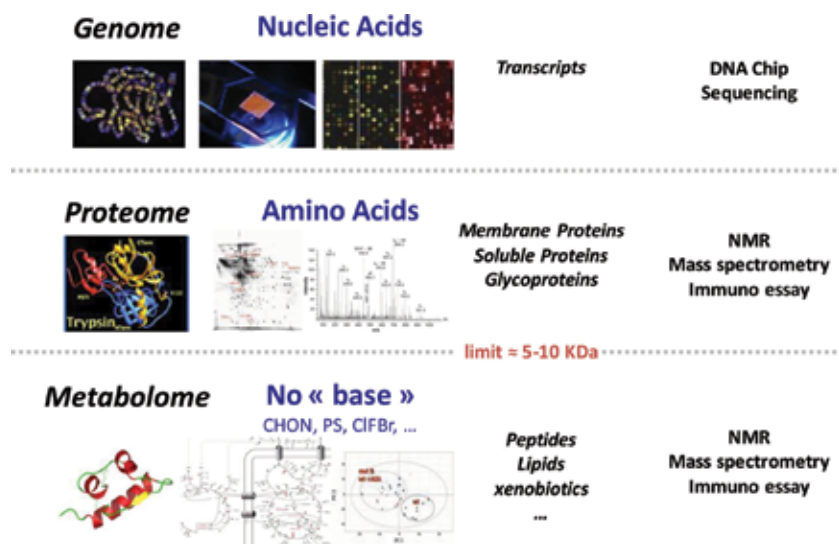


**Figure 1.**  
The three mains of life, their bases, entities, and analytical tools.

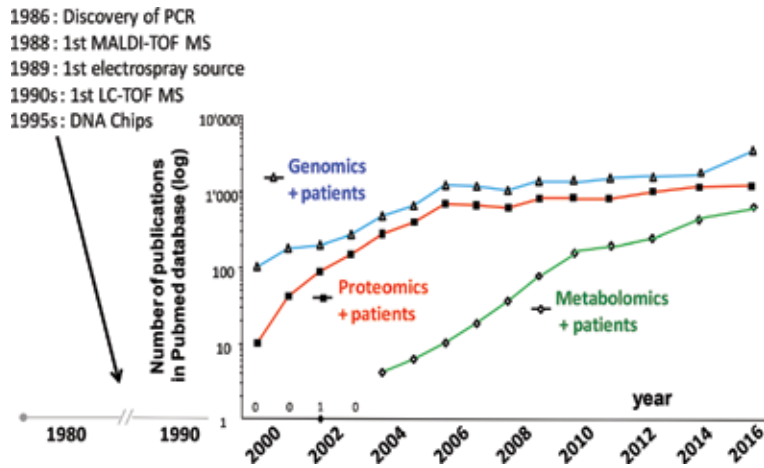


**Figure 2.** Number of publications in PubMed database in relation to three keywords, “genomics,” “proteomics,” and “metabolomics,” associated to “patients” over the last two decades.

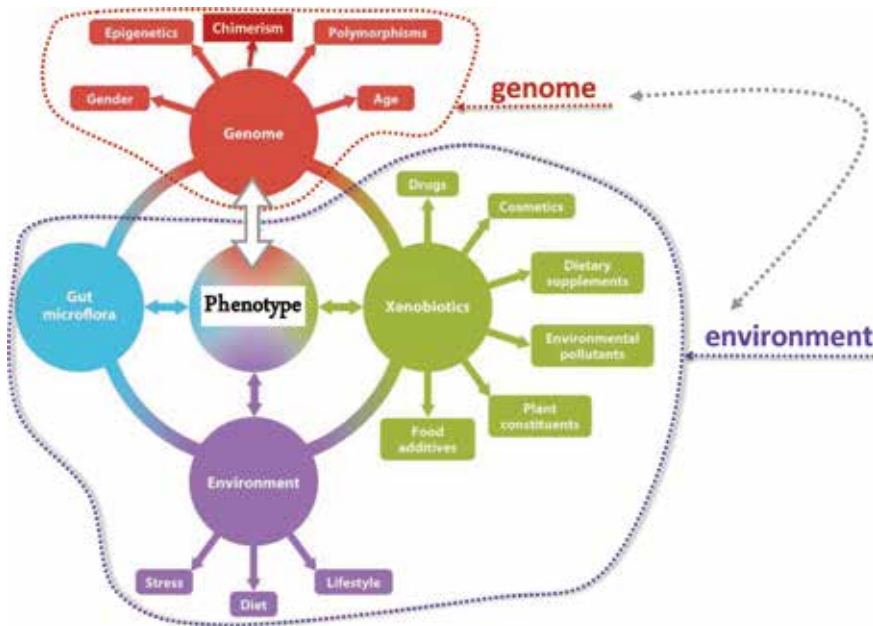


**Figure 3.** System biology and its holistic approach. The phenotype of an individual is the results of the interaction and memories of the genome and the environment. It sustains that a global approach is valuable in personalized medicine (adapted from [5]).

of low-prevalence diseases. Low-prevalence diseases represent a significant part of many diseases that are wrongly considered as homogenous (etiology or molecular mechanism of the disease) and would be diagnosed with many different biomarkers. Low-prevalence (sub-)diseases suggest that there is a need to determine more globally what is in the patient’s sample (the proteome and/or the metabolome) in order to find unexpected outsider molecules that will be at a low frequency but with a high significance as biomarkers. Eventually, these concepts promote medical doctors and bioanalysts to favor more holistic approaches for a higher consideration of individual (variations limiting the tyranny of the average) [6, 7].

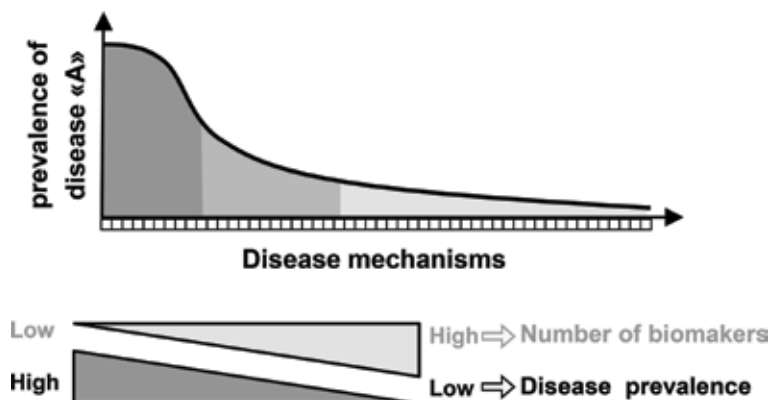


**Figure 4.** Prevalence of a disease “A” against disease mechanisms. The figure depicts a long tail curve suggesting that, beside the frequent and few molecular mechanisms or origins of the disease (left part of the curve), there are many low-prevalence subcategories of the “same” disease (right part of the curve). In this scenario, the determination of a few usual biomarkers can be useless for many patients. The potential high number of biomarkers with low prevalence but high significance suggests that untargeted acquisition and untargeted data treatment have their place in biomedical analyses.

These actual concepts in life sciences have become crucial for understanding the complexity of biological systems and for delivering better personalized diagnostics and medicine. It promotes the LC-MS instruments capable to record “global view” in one affordable analytical shot [8, 9].

## 2. LC-MS technologies

This can be useful to recall that liquid chromatography coupled to mass spectrometry (LC-MS) is composed of three parts: (1) the (U)HPLC system, (2) the atmospheric pressure ion (API) source (most frequently the API source type is an “electrospray”), and (3) the mass analyzer (**Figure 5**) [10]. The ion source is an interface between the liquid and the gas phase, where the mobile phase is vaporized, leaving the ions in the gas phase and ready to enter in the MS. Even if the second and third parts are fully integrated, the ionization chamber can rapidly be changed by another source that is designed for different flow rates or modes of ionization. The LC-MS analysis records chromatograms where  $m/z$  values (ions = mass over charge ratios) are detected (relative intensity) and depicted over time (**Figure 5**). Ions are detected as positive or negative adducts: usually  $+H^+$  but also  $+Na^+$ ,  $K^+$ ,  $NH_4^+$ , and  $-[H^+]^-$ . There are three main MS technologies (ion trap MS would be the fourth but it is not described here) that can be divided in low and high mass resolution instruments (**Figure 6**). There are triple-quadrupole (QQQ-MS), (quadrupole-)time-of-flight-MS (TOF-MS), and (quadrupole-)Orbitrap-MS (Orbi-MS; e.g., Q Exactive).

Most frequently, mass resolution ( $R$ ) is defined as  $R = m/\Delta m_{FWHM}$ , where  $[m]$  and  $\Delta m_{FWHM}$  correspond to the  $m/z$  of the ion considered and the distribution of  $m/z$  at full-width half-maximum of the peak height (FWHM), respectively ( $\Delta m_{FWHM}$  units are Da, u, or Th; **Figure 7**) [11]. Mass accuracy is defined as the delta between the theoretical and measured  $m/z$  and is given in mDa (u or mTh) or in ppm [11]. Accurate mass determination allows to extract ions with narrower mass-extraction-window (MEW) in order to construct extracted-ion chromatograms (XIC) [12].

Low- and high-resolution mass spectrometers are defined with an  $R$  value below or above 10,000, respectively. Low-resolution MS (LRMS) are QQQ-MS, whereas

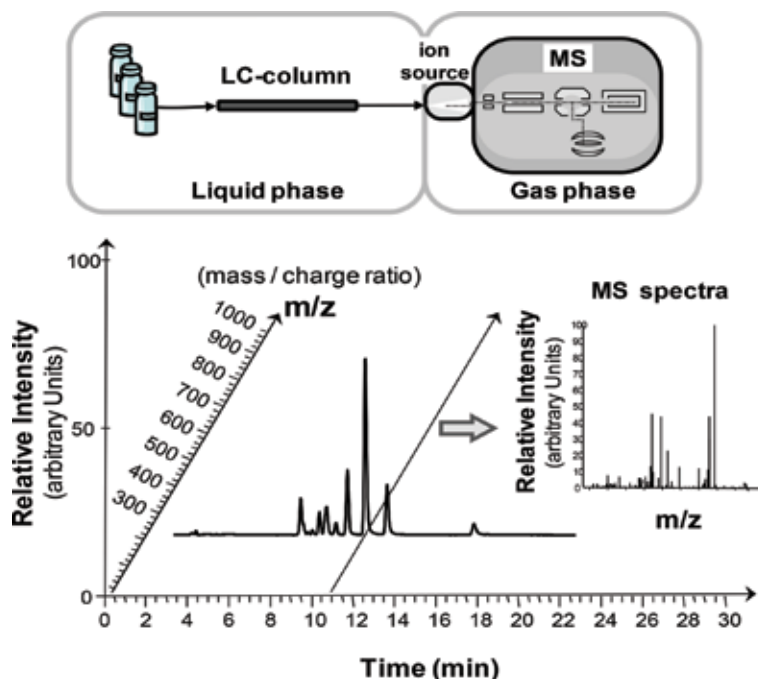


**Figure 5.** LC-MS analysis. LC-MS systems are composed of a LC part, an ion source, and a MS analyzer. LC-MS analysis is defined mainly by a retention time, a relative intensity (arbitrary units), and the ions detected ( $m/z$ , mass over charge ratio).

high-resolution MS (HRMS) are TOF-MS and Orbi-MS instruments. It is worth to note that R is not a constant value over the mass range (**Figure 8**) [12]. R values are usually given at  $m/z = 200$  and  $400$  for Orbi-MS and TOF-MS, respectively. Today, R

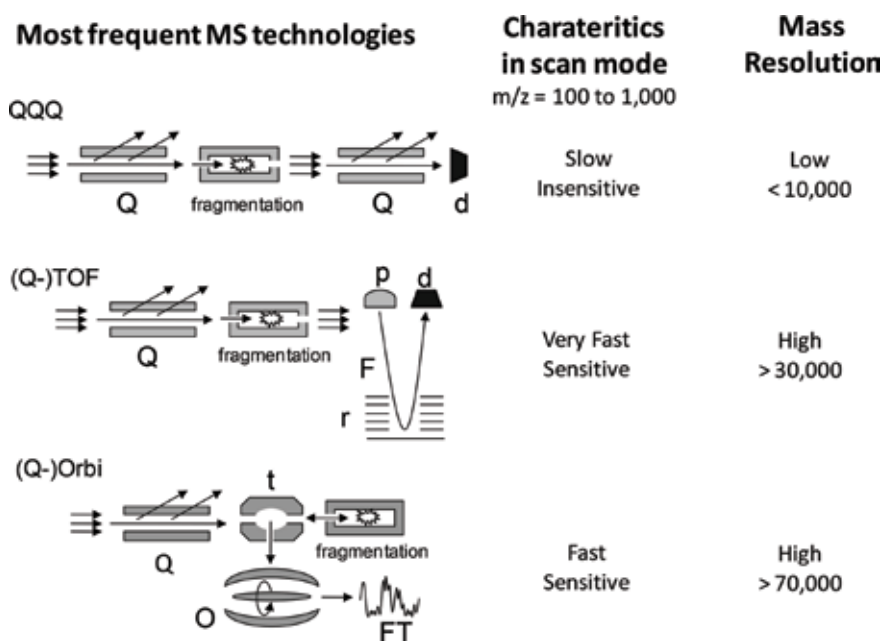


**Figure 6.** The three most frequent MS technologies and their key characteristics for scanning rate and mass resolution (adapted from [7]).

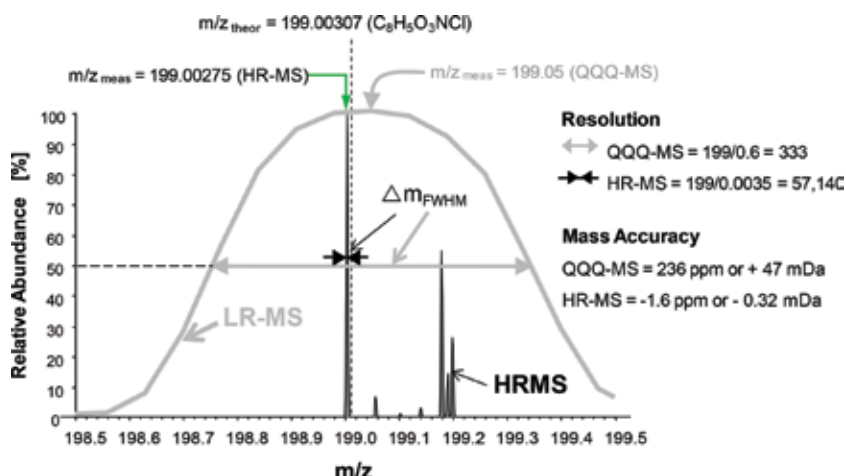


**Figure 7.** Sketch showing what are the mass resolution and the mass accuracy. Typical mass resolution and mass accuracy are exemplified.  $m/z_{meas}$  and  $m/z_{theor}$  stand for measured and theoretical  $m/z$  (adapted from [6]).

varies between 20,000 and 140,000 in (U)HPLC-MS analysis for  $m/z$  between 100 and 800. Orbi-MS has a higher R allowing a better discrimination of ions (e.g., fine isotopic distribution).

This is also of interest to know that there are slow and fast-scanning MS. In scan mode (e.g.,  $m/z$  ranging from 100 to 1000), QQQ-MS are slow and insensitive. For this reason, the acquisition mode of QQQ-MS is, in most cases, selected reaction monitoring (SRM; also called multiple reaction monitoring, MRM). In SRM acquisition, the precursor ion is selected in the first quadrupole (Q1) and fragmented in the collision cell (Q2), and an intense and specific fragment/product ion is selected

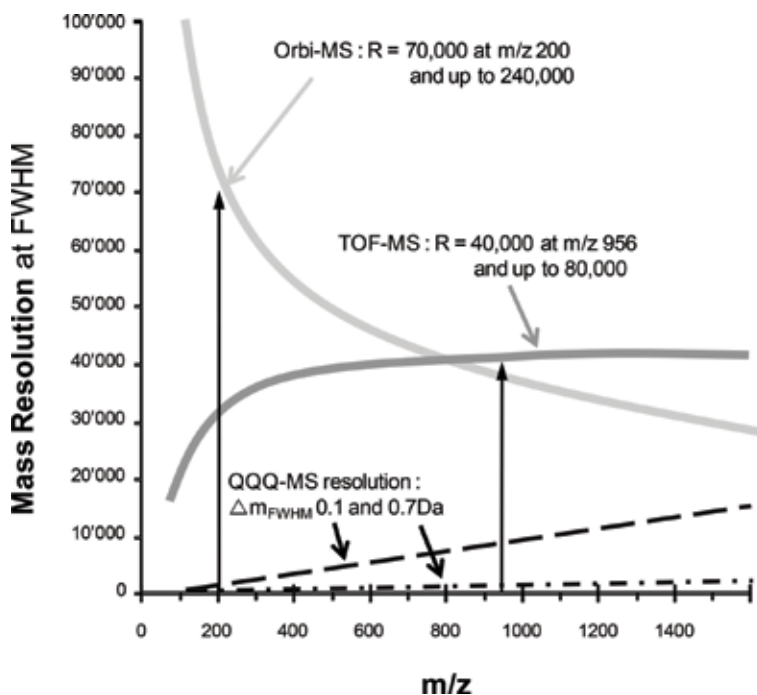


**Figure 8.** Mass resolution ( $R$ ) against the  $m/z$  range for the three most frequent MS technologies (adapted from [6]).

in the last quadrupole (Q3) prior its detection by the photomultiplier. This is an ion transition please, see **Figures 6 and 9**. In contrast, TOF- and Orbi-MS are fast-scanning instruments. Scan rates of affordable Orbi-MS depend on the resolution chosen and are typically 1.5, 3, 6, and 12 Hz (number of scans/s) at R = 140,000, 70,000, 35,000, and 17,500 (at  $m/z = 200$ ), respectively. TOF has a higher scan rate (>20 Hz) which can be an advantage if multiple acquisitions are recorded in parallel or if ion mobility is used. The main differences between the three most frequent technologies, QQQ-, Orbi-, and TOF-MS, are depicted in **Figure 6** and **Table 1**.

**Figure 10** sketches the key consequence of the differences between QQQ-MS, on one side, and TOF- and Orbi-MS, on the other side. This is related to the acquisition types that are ion transitions (SRM) and high-resolution full scan (HR-full scan). QQQ-MS *have to* acquire SRM in order to be selective and sensitive, whereas TOF- and Orbi-MS are selective *and* sensitive in the full-scan mode acquisition [13]. This means that with SRM acquisition, the bioanalyst has to know the precursor and product ions and the collision energies to apply *prior* to the analytical run. In contrast, with HRMS full-scan acquisition, the bioanalyst can use generic parameters and acquire all ions in a large mass range (e.g.,  $m/z$  from 100 to 1000) **Figure 9**. In this last scenario, a global determination is recorded allowing various kinds of retrospective, targeted, or untargeted data treatments. In this book chapter, we have defined the global ion acquisition as the HR-full scan, whereas there are various alternative possibilities defined as data-independent acquisitions (DIA; e.g.,  $MS^{ALL}$ ,  $MS^E$ ,  $MS^{SWATH}$ ) that also record virtually all ions [14, 15].

A good example of retrospective data mining is shown in the biotransformation study of tamoxifen [16]. In this study, plasma samples from patients treated with tamoxifen were extracted and analyzed with a LC-HRMS acquiring HR-full scan. Retrospective data treatment allowed to detect and determine 39 tamoxifen metabolites. A second example of post-acquisition data mining is shown in an

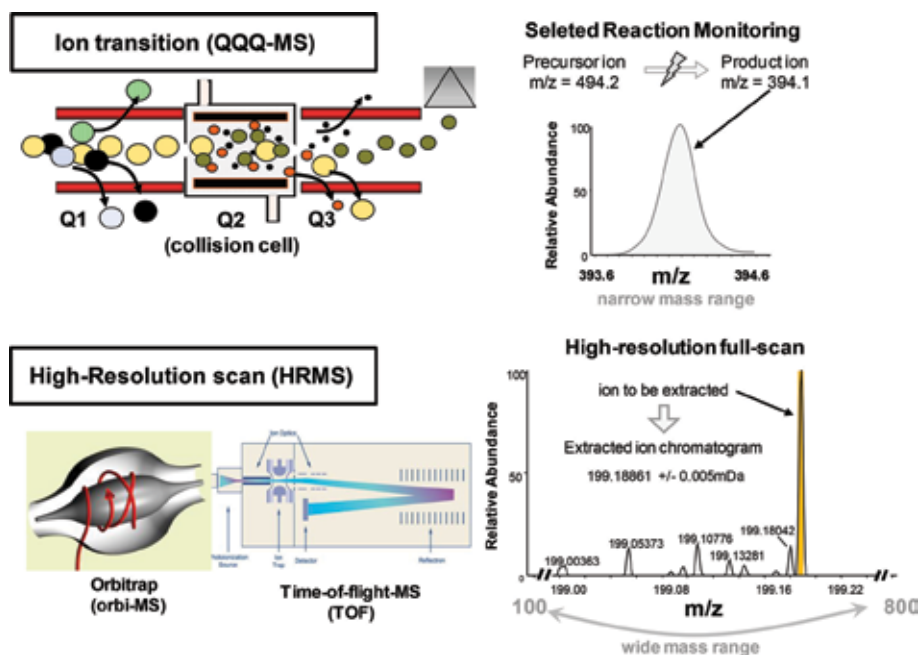


**Figure 9.** Typical acquisitions for sensitive and selective detections with low- and high-resolution MS: ion transitions (QQQ-MS) and full scan (HRMS), respectively.

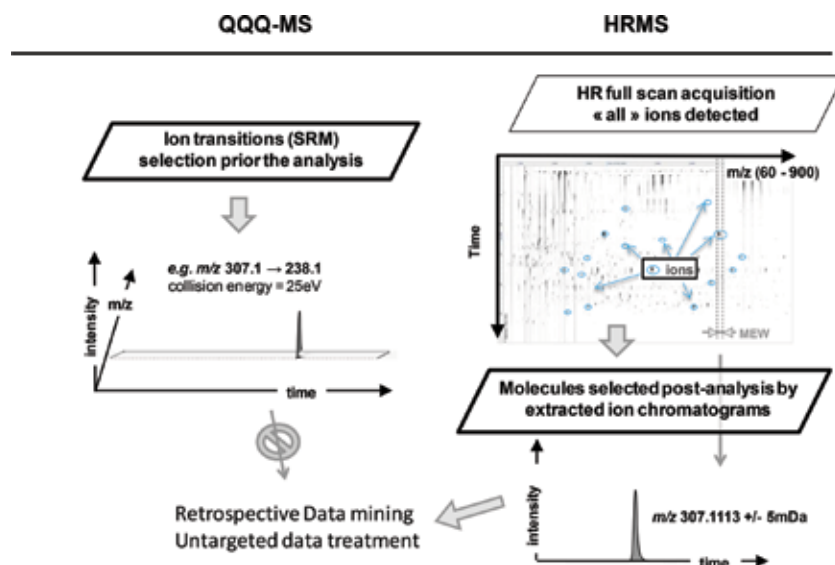


**Figure 10.**

Usual acquisitions for sensitive and selective detections on QQQ-MS and HRMS analyses. With QQQ-MS, ion transitions have to be defined before the analysis. Therefore, the selective filter is applied before the acquisition. With HRMS, the acquisition can be performed in full-scan mode where, virtually, “all” ions are recorded. The selective filter is applied after the acquisition by choosing the ions to be extracted. Typical QQQ- and HRMS acquisitions are depicted on the chromatograms.

untargeted diagnostic screening workflow where an outlier metabolite in a patient’s metabolome is revealed by the comparison with healthy people metabolomes [17]. Both examples are better described in Section 3.

Importantly, like for QQQ-MS, most actual HRMS can perform excellent quantitative determinations (see the following section) [13]. This is why today’s HRMS instruments should be considered as the new gold standard in LC-MS analyses because of their capabilities to perform quantitative, qualitative, quan/qual, and omics analyses (Figure 11) [13]. As depicted in Table 1, quantitative performance of HRMS is not better but equivalent to QQQ-MS. But the

		QQQ-MS	Q-TOF-MS	Orbi-MS
	Mass Resolution	low	high	high
Sensitivity	Global analysis *	1	3	3
	Targeted analysis **	3 (4)	(2) 3	(2) 3
Specificity	Global analysis *	1	(2) 3	3 (4)
	Targeted analysis **	3	(3) 4	4 (5)
Acquisition rate	Global analysis *	1	(3) 4	3
	Targeted analysis **	3	(2) 3	2
Sum	Global analysis *	3	8-10	9-10
	Targeted analysis **	9-10	7-10	8-10

**Table 1.**

Key analytical differences of the most frequently used mass spectrometers. This table allocates a grade according to global or targeted MS performance (one to five points for poor to excellent, respectively). Global acquisition (\*) corresponds to high-resolution full scan or data-independent acquisition (no selection of precursor ions). Targeted acquisition (\*\*) corresponds to SRM (selected reaction monitoring) or product ion scan (selection of precursor ions). The last row gives the sum of the grades (adapted from [7]).



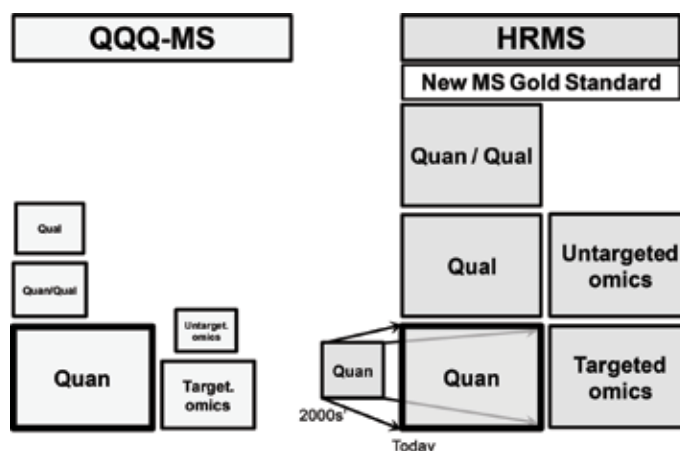


**Figure 11.**

Overview of the analytical workflows performed by QQQ-MS and HRMS. Box sizes relate to the analytical performance. Whereas quantitative (*quan*) determination is similar between LRMS (SRM; QQQ-MS) and HRMS (TOF-, Orbi-MS; HR-full scan), HRMS has much better analytical capabilities for qualitative (*qual*), simultaneous quantitative and qualitative (*quan/qual*), and omics (targeted and untargeted metabolomics and proteomics) workflows.

HRMS-unique capability to perform global and qualitative analyses is becoming more and more crucial. For one or two decades, the mind-set of bioanalysts performing LC-MS analysis was the following: QQQ-MS are the instruments of choice for routine and quantitative analyses, whereas complex and expensive HRMS instruments are dedicated to qualitative and research analyses. This is outdated. With the recent progress in HRMS technologies (both TOF and Orbi-MS), a shift of paradigm is occurring [8, 12, 18]. This shift of paradigm is based on the fact that today's HRMS instruments can perform *both* excellent quantitative and qualitative analyses. HRMS should be seen as the new gold standard mass analyzers (**Figure 11**).

In the next section, typical examples of LC-HRMS analyses are presented. HRMS represents the most versatile analytical tool allowing to perform from targeted quantification to untargeted metabolomics/proteomics [13].

### 3. Examples of quantitative and qualitative LC-HRMS analyses

#### 3.1 Quantitative performance of HRMS instruments

Today, there are many peer-review articles that compare side-by-side the quantitative performance of QQQ-MS and HRMS instruments [19–26]. These comparisons investigate the sensibility, selectivity, ease of use, calibration linearity, reliability, and robustness in real-life LC-MS analyses. This is always difficult to have an absolute comparison between two MS technologies because it is related to various parameters like the compounds studied, the two ion source designs (not the MS itself) that possibly show different sensitivities, the memory effects on column that perturb the determination of the limit of detection, the different generations of lenses/ion guides that are just behind the entrance of the MS and that usually are independent to MS technologies, etc. The frequently claimed better sensitivity of QQQ-MS over other technologies is often the result of latest hardware modifications (more efficient lenses, ion guides, etc.) introduced first in new QQQ-MS. Again, this is not related to the mass analyzer itself.

Nevertheless, a general conclusion can be drawn from these numerous articles and comparisons. Today, most HRMS instruments show similar quantitative performance than QQQ-MS [13, 19–26]. In **Figures 12–14**, adapted from recent publications (respectively Refs. [25] and [23]), the authors underscore that HRMS quantitative performance is comparable to QQQ-MS. **Figure 12** depicts LC-MS chromatograms at the limit of detection, the calibration curves, and the fold differences of the limits of detection obtained for nine drugs with a QQQ-MS (TSQ Quantum Ultra) performing ion transitions (SRM) and a HRMS (Q Exactive Focus) performing HR–full scans. No significant differences of quantitative performance were observed except the saturation of the QQQ-MS detector at the highest spiked concentrations (5000 ng/mL corresponding to 10 ng on column) [25]. **Figure 13** depicts the limits of quantification (LOQ) of 27 compounds determined in SRM and full scan with a QQQ-MS and a HRMS [23]. Here again, no significant differences in the LOQ values were observed [23]. As shown in **Figure 13**, the fold differences between QQQ-MS and Orbi-MS are below  $\approx 3x$  (or  $1/3x$ ) for 22/27 compounds. Four compounds show a more pronounced difference, between 7x and 20x, in favor of HRMS, which is probably the result of poor intensity of the fragment ions (SRM acquisition). In contrast, one compound shows a better LOQ value (8x) with the QQQ-MS. **Figure 14** shows the reliability of 25-hydroxyvitamin D3 quantification in 662 serum extracts analyzed with a QQQ-MS (SRM) and an Orbi-MS (HR–full scan) [27], exemplifying the robustness of HRMS in routine and quantitative determinations (see also [28, 29]). Similar conclusions showing the

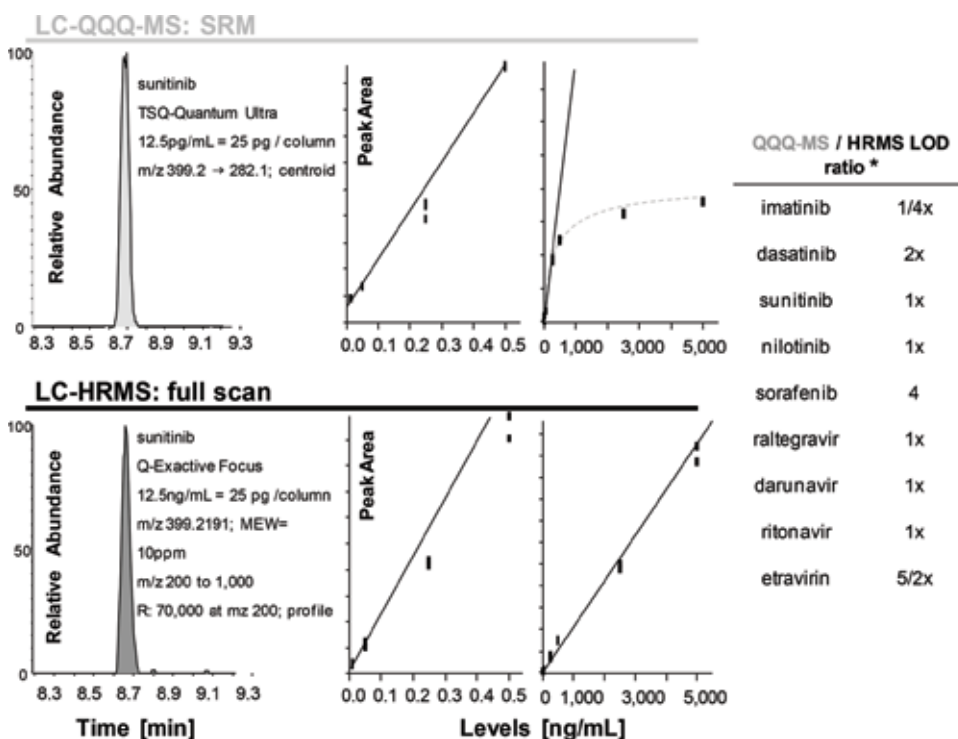


**Figure 12.** Example of side-by-side comparison of LC-MS quantification with QQQ-MS and HRMS. Chromatograms at the limit of detection (LOD) in plasma extracts, curve linearities, and LOD differences between both MS platforms are depicted, whereas QQQ-MS and HRMS acquire SRM and HR–full scan, respectively. Calibration curves at the lowest levels are similar, whereas at the highest levels, a saturation of the QQQ-MS multiplier is observed. (\*) ratio < 1 means QQQ-MS is more sensitive than HRMS and vice versa (adapted from [14]).

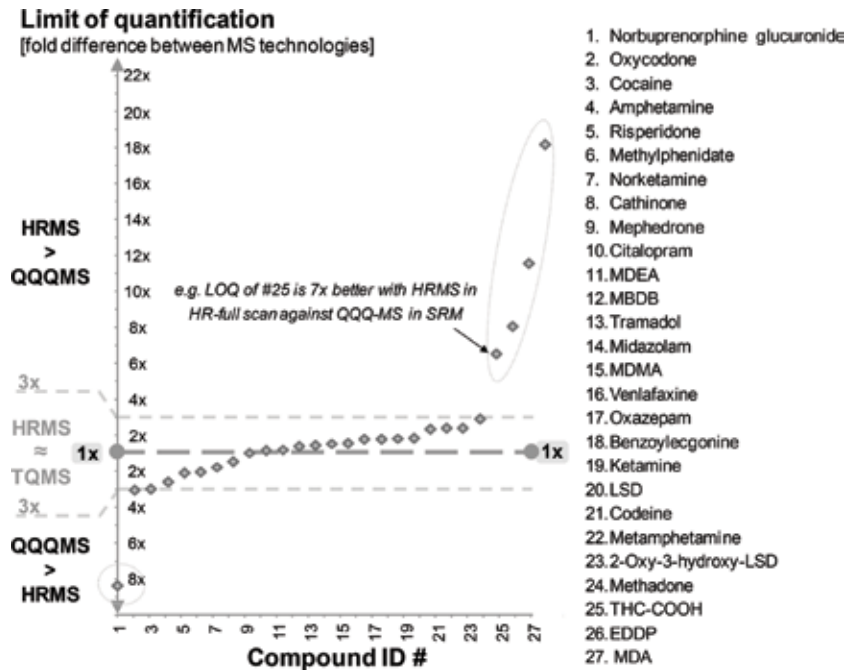


**Figure 13.** Example of side-by-side comparison of LC-MS quantification with QQQ-MS and HRMS. Limits of quantification for 27 compounds are plotted in biological extracts. Most compounds show similar LOQ values (differences <3x), whereas four compounds with probable poor intensity of the fragment ions show lower LOQ values with QQQ-MS (adapted from [20]).

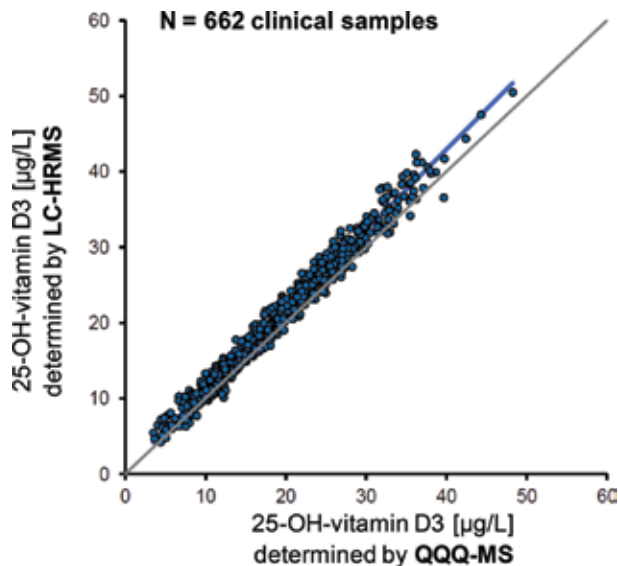


**Figure 14.** Passing and Bablok fit of 25-hydroxyvitamin D3 in 662 plasma extracts determined with QQQ-MS and HRMS acquiring SRM and full scan (adapted from [16]).

capability of routine determinations have been made for Q-TOF-MS [20, 30, 31]. If needed (e.g., poorly cleaned sample extracts or direct-flow-injection analysis), the acquisition of fragment ions can show higher selectivity or/and sensitivity in LC-HRMS analysis [25, 32].

Evidences of HRMS quantitative performance are accumulating [13], but this is not straightforward to change bioanalysts' habits that have used QQQ-MS for decades. It can be difficult to convince them to shift, whereas HRMS shows "only" similar quantitative performance as QQQ-MS. The shift in favor of HRMS still needs activation energy in order to occur. This activation energy will come from the additional and outstanding capabilities of HRMS for qualitative and untargeted determinations and the increasing needs for more global and/or untargeted approaches in the determination of biological samples [33]. Even if some laboratories will concentrate their work exclusively on targeted and quantitative analyses and will possibly keep working with predefined ion transitions on QQQ-MS, most lab heads will "feel" the additional needs for untargeted acquisitions and untargeted data treatments for routine or investigation analyses (see Introduction section and the following section). Here below, quan/qual, qualitative, and omics analysis are presented.

### 3.2 Quan/qual and qualitative analyses with HRMS instruments

The *in vivo* biotransformation study of tamoxifen represents a good example of quan/qual analysis [16]. Tamoxifen is a selective estrogen receptor modulator, used for the prevention and adjuvant treatment of estrogen-sensitive breast cancer. In this study, plasma samples from patients treated with tamoxifen (steady-state levels) were analyzed with a QQQ-MS (TSQ Quantum Ultra; SRM acquisition) or with an Orbi-MS (Exactive Plus MS; HR-full-scan acquisition). It has been shown that tamoxifen metabolites can be more active than the parent drug and that tamoxifen reactive metabolites can bind to macromolecules [33]. It was and is challenging to reveal new findings with tamoxifen because hundreds of articles have already studied *in vivo* and *in vitro* the biotransformations of tamoxifen [21].

First, in this study [16], similar plasma levels (CV < 15%) of tamoxifen and two metabolites were obtained with the QQQ-MS and the HRMS platforms. Secondly, the HR-full-scan acquisition allowed the identification of 39 circulating metabolites of tamoxifen, of which 3 were never described previously and corresponded to the sixth and seventh generations (6 and 7 biotransformation steps; **Figure 15**). Semiquantitative determinations of tamoxifen metabolites allowed to observe that some metabolites have a high plasma level variability with poor relations with the parent drug level, whereas, in contrast, other metabolites show a strong relation to tamoxifen levels (**Figure 15**). Various strategies were employed to identify tamoxifen metabolites. They consisted in the extraction of ions from possible biotransformation pathways (and chemical compositions) or from similar tamoxifen fragmentation (**Figure 15**). All these tasks were particularly simplified because of the HRMS detection selectivity (accurate mass and high-resolution spectra allowing narrow mass-extraction-windows) and because of the sensitivity of HR-full scan or MS<sup>ALL</sup> acquisitions (product scan where all precursor ions are fragmented, no selection of precursor ions in the quadrupole; see also data-independent acquisition, MS<sup>SWATH</sup>, or MS<sup>E</sup> acquisitions [13]).

This study [16] demonstrates the excellent capabilities of HRMS data for further investigations in real biological samples on top of the targeted and quantitative determinations of tamoxifen and two metabolites. Similarly, from HR-full-scan acquisition, new metabolites of hepcidin, a peptide involved in iron homeostasis in the blood, have been discovered on the side of the quantitative determination of hepcidin [28]. It underscores that HR-full-scan acquisitions allow targeted simultaneous and quantitative determinations and investigational data treatment (see also [14, 34–37]).

### 3.3 Omics analyses with HRMS instruments

In general, LC-MS omics analyses (metabolomics and proteomics) are associated to research analyses such as the discovery of biomarkers. In the new understanding

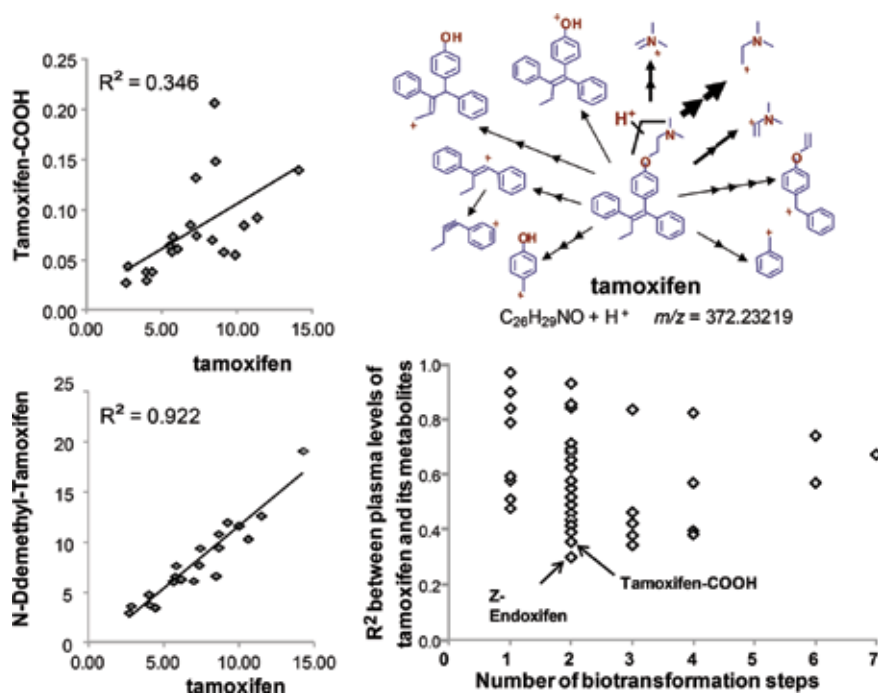


**Figure 15.** Biotransformation study of tamoxifen. Left-hand side: correlations between tamoxifen levels and two of its metabolites showing poor (top) and good (bottom)  $R^2$  coefficient. Right-hand side: top, tamoxifen fragmentation; accurate mass determination allow to assign chemical compositions and putative chemical structures to tamoxifen fragments; bottom: in-depth coverage of tamoxifen metabolite discovery resulting from HR scans and accurate mass extractions of ions (adapted from [9]).

of life sciences where a holistic approach has its place in routine analysis and where low-prevalence diseases represent a significant part (**Figure 4**), there is an increasing need for untargeted or semi-targeted LC-MS analysis as a diagnostic workflow. Here below, an untargeted diagnostic screening is presented as a metabolomics analysis [17]. This study evaluates the feasibility to perform an untargeted LC-HRMS analysis and an untargeted data treatment in a routine context.

**Figure 16** depicts this study [17] and its omics workflow. *One* serum sample (the test sample) was spiked with *one* compound. The serum sample was then extracted (protein precipitation) and analyzed with a LC-HRMS system acquiring HR-full scan from  $m/z$  60 to 900 (untargeted acquisition) this sample was compared with 95 samples from healthy persons. Unsupervised (untargeted) data treatment with a metabolomics software allowed, after the application of different filters that remove insignificant ions (>99%), to reveal the spiked compound in a short and final list of 20–50 compounds (the number of detected ions is >10,000). Whereas, in the final list, many ions were not identified (e.g., unknown adducts, isotopes, or in-source fragments) or were compounds from food intake; this untargeted diagnostic screening procedure appears feasible and reliable to reveal unexpected xenobiotics (toxicology) or higher concentrations of endogenous metabolites. Correlation(s) between clinical symptoms and metabolite outlier(s) found in a patient should be done by clinicians prior to the request for a confirmatory, targeted, and absolute quantification analysis. Such HRMS untargeted approaches could be useful as preliminary diagnostic screening when canonical and targeted processes do not establish nor reveal a clear diagnostics or disease etiology (low-prevalence disease mechanism or etiology). Similar examples that underscore or suggest the utility of untargeted acquisitions in routine analyses have been published [38, 39].

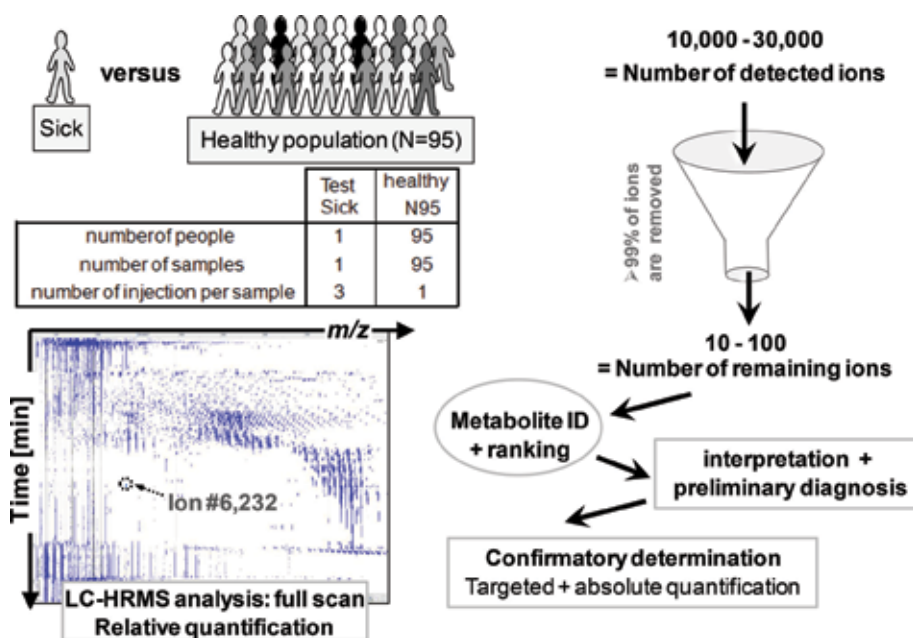


**Figure 16.** Untargeted diagnostics screening workflow. The metabolome of a human serum (containing a spiked molecule, “sick”) is determined and compared with 95 healthy serum metabolomes. HR-full scans are acquired and untargeted data treatment is performed with a metabolomics software. After removing useless ions with proper filters, the spiked molecule was identified and ranked. Revealed metabolites can be related to the patient’s symptoms, preliminary diagnosis postulated, and further confirmatory analysis performed. Such untargeted analysis can be undertaken when canonical procedures fail. This workflow is in accordance with “low-prevalence diseases” and against the “tyranny of the average” concepts (adapted from [8]).

#### 4. Conclusion and perspectives

In this book chapter, a brief review of the performance of HRMS instruments has been presented: first, on quantitative and then on qualitative, quan/qual, and omics analyses. Today, there are numerous peer-review articles showing that in quantitative analysis, most actual HRMS instruments are performing similarly to QQQ-MS. Taken into account the additional and unique HRMS capabilities for qualitative and untargeted determinations, HRMS opens new analytical possibilities that fit new requests from systems biology and its holistic/global approaches. For this reason, HRMS should be considered as the new gold standard MS systems (paradigm shift). Indeed, HRMS shows unique versatility, and bioanalysts can foresee routine or research analyses from targeted quantifications to untargeted metabolomics.

#### Acknowledgements

This chapter is also the result of various discussions with many colleagues and friends. They are anyhow part of this book chapter as I believe that, like in quantum physics, we are somehow all intricately connected. I would like to express my respectful gratitude to them. I also thank Drs. Anne Boddecs and Anne Cissencco for their humanism in regard to Matt Enset.

#### Conflict of interest

The author declares no conflict of interest.

## **Author details**

Bertrand Rochat  
Département Formation Recherche, University Hospital of Lausanne,  
PAF, Génopode, Université de Lausanne, Lausanne, Switzerland

\*Address all correspondence to: [bertrand.rochat@chuv.ch](mailto:bertrand.rochat@chuv.ch)

## **IntechOpen**

---

© 2018 The Author(s). Licensee IntechOpen. This chapter is distributed under the terms of the Creative Commons Attribution License (<http://creativecommons.org/licenses/by/3.0>), which permits unrestricted use, distribution, and reproduction in any medium, provided the original work is properly cited. 

## References

- [1] Maurer HH. Current role of liquid chromatography-mass spectrometry in clinical and forensic toxicology. *Analytical and Bioanalytical Chemistry*. 2007;**388**:1315-1325
- [2] Viette V, Hochstrasser D, Fathi M. LC-MS (/MS) in clinical toxicology screening methods. *Chimia*. 2012;**66**:339-342
- [3] Stone JA, Fitzgerald RL. Liquid chromatography-mass spectrometry education for clinical laboratory scientists. *Clinics in Laboratory Medicine*. 2018;**38**:527-537
- [4] Mbughuni MM, Jannetto PJ, Langman LJ. Mass spectrometry applications for toxicology. *Electronic Journal of the International Federation of Clinical Chemistry and Laboratory Medicine*. 2016;**27**:272-287
- [5] Johnson CH, Patterson AD, Idle JR, Gonzalez FJ. Xenobiotic metabolomics: major impact on the metabolome. *Annu Rev Pharmacol Toxicol*. 2012;**52**:37-56
- [6] Merlo J, Mulinari S, Wemrell M, Subramanian SV, Hedblad B. The tyranny of the averages and the indiscriminate use of risk factors in public health: The case of coronary heart disease. *SSM - Population Health*. 2017;**3**:684-698
- [7] Tabery J. Commentary: Hogben vs. the tyranny of averages. *International Journal of Epidemiology*. 2011;**40**:1454-1458
- [8] Rochat B. Quantitative/qualitative analysis using LC-HRMS: The fundamental step forward for clinical laboratories and clinical practice. *Bioanalysis*. 2012;**4**:1709-1711
- [9] Rochat B. Is there a future for metabotyping in clinical laboratories? *Bioanalysis*. 2015;**7**:5-8
- [10] de Hoffmann E, Stroobant V. *Mass Spectrometry. Principles and Application*. 3rd ed. Chichester: Wiley; 2007. p. 502. Available from: [www.usp.br/massa/2014/qfl2144/pdf/MassSpectrometry.pdf](http://www.usp.br/massa/2014/qfl2144/pdf/MassSpectrometry.pdf)
- [11] Brenton AG, Godfrey AR. Accurate mass measurement: Terminology and treatment of data. *Journal of the American Society for Mass Spectrometry*. 2010;**21**:1821-1835
- [12] Rochat B, Kottelat E, McMullen J. The future key role of LC-high-resolution-MS analyses in clinical laboratories: A focus on quantification. *Bioanalysis*. 2012;**4**:2939-2958
- [13] Rochat B. From targeted quantification to untargeted metabolomics. Why LC-high-resolution-MS will become a key instrument in clinical labs. *Trends in Analytical Chemistry*. 2016;**84**:151-164
- [14] Hopfgartner G, Tonoli D, Varesio E. High-resolution mass spectrometry for integrated qualitative and quantitative analysis of pharmaceuticals in biological matrices. *Analytical and Bioanalytical Chemistry*. 2012;**402**:2587-2596
- [15] Arnhard K, Gottschall A, Pitterl F, Oberacher H. Applying 'Sequential Windowed Acquisition of All Theoretical Fragment Ion Mass Spectra' (SWATH) for systematic toxicological analysis with liquid chromatography-high-resolution tandem mass spectrometry. *Analytical and Bioanalytical Chemistry*. 2015;**407**:405-414
- [16] Dahmane E, Boccard J, Csajka C, Rudaz S, Décosterd L, Genin E, et al. Quantitative monitoring of tamoxifen in human plasma extended to 40 metabolites using liquid-chromatography high-resolution mass spectrometry: New investigation



- capabilities for clinical pharmacology. *Analytical and Bioanalytical Chemistry*. 2014;**406**:2627-2640
- [17] Rochat B, Mohamed R, Sottas PE. Untargeted diagnostic screening by LC-HRMS: A feasibility study for clinical laboratories. *Metabolites*. 2018;**8**:39
- [18] Ramanathan R, Jemal M, Ramagiri S, Humpreys WG, Olah T, Korfmacher WA. It is time for a paradigm shift in drug discovery bioanalysis: From SRM to HRMS. *Journal of Mass Spectrometry*. 2011;**46**:595-601
- [19] Morin LP, Mess JN, Garofolo F. Large-molecule quantification: Sensitivity and selectivity head-to-head comparison of triple quadrupole with Q-TOF. *Bioanalysis*. 2013;**5**:1181-1193
- [20] Zacs D, Rjabova J, Pugajeva I, Nakurte I, Viksna A, Bartkevics V. Ultra high performance liquid chromatography-time-of-flight high resolution mass spectrometry in the analysis of hexabromocyclododecane diastereomers: Method development and comparative evaluation versus ultra high performance liquid chromatography coupled to Orbitrap high resolution mass spectrometry and triple quadrupole tandem mass spectrometry. *Journal of Chromatography. A*. 2014;**366**:73-83
- [21] Kaufmann A, Butcher P, Maden K, Walker S, Widmer M. Quantitative and confirmative performance of liquid chromatography coupled to high-resolution mass spectrometry compared to tandem mass spectrometry. *Rapid Communications in Mass Spectrometry*. 2011;**25**:979-992
- [22] Henry H, Sobhi HR, Scheibner O, Bromirski M, Nimkar SB, Rochat B. Comparison between a high-resolution single-stage Orbitrap and a triple quadrupole mass spectrometer for quantitative analyses of drugs. *Rapid Communications in Mass Spectrometry*. 2012;**26**:499-509
- [23] Fedorova G, Randak T, Lindberg RH, Grabic R. Comparison of the quantitative performance of a Q-Exactive high-resolution mass spectrometer with that of a triple quadrupole tandem mass spectrometer for the analysis of illicit drugs in wastewater. *Rapid Communications in Mass Spectrometry*. 2013;**27**:1751-1762
- [24] Kadar H, Veyrand B, Antignac JP, Durand S, Monteau F, Le Bizec B. Comparative study of low- versus high-resolution liquid chromatography-mass spectrometric strategies for measuring perfluorinated contaminants in fish. *Food Additives and Contaminants. Part A, Chemistry, Analysis, Control, Exposure and Risk Assess*. 2011;**28**:1261-1273
- [25] Grund B, Marvin L, Rochat B. Quantitative performance of a quadrupole-orbitrap-MS in targeted LC-MS determinations of small molecules. *Journal of Pharmaceutical and Biomedical Analysis*. 2016;**124**:48-56
- [26] Kaufmann A, Butcher P, Maden M, Walker S, Widmer M. Determination of nitrofurans and chloramphenicol residues by high resolution mass spectrometry versus tandem quadrupole mass spectrometry. *Analytica Chimica Acta*. 2015;**862**:41-52
- [27] Bruce SJ, Rochat B, Béguin A, Pesse B, Guessous I, Boulat O, et al. Analysis and quantification of vitamin D metabolites in serum by ultra-performance liquid chromatography coupled to tandem mass spectrometry and high-resolution mass spectrometry—A method comparison and validation. *Rapid Communications in Mass Spectrometry*. 2013;**27**:200-206

- [28] Rochat B, Peduzzi D, McMullen J, Favre A, Kottelat E, Favrat B, et al. Validation of hepcidin quantification in plasma using LC-HRMS and discovery of a new hepcidin isoform. *Bioanalysis*. 2013;**5**:2509-2520
- [29] Primikyri A, Papanastasiou M, Sarigiannis Y, Koutsogiannaki S, Reis ES, Tuplano JV, et al. Method development and validation for the quantitation of the complement inhibitor Cp40 in human and cynomolgus monkey plasma by UPLC-ESI-MS. *Journal of Chromatography B*. 2017;**1041-1042**:19-26
- [30] Zhou X, Meng X, Cheng L, Su C, Sun Y, Sun L, et al. Development and application of an MSALL-based approach for the quantitative analysis of linear polyethylene glycols in rat plasma by liquid chromatography triple-quadrupole/time-of-flight mass spectrometry. *Analytical Chemistry*. 2017;**89**:5193-5200
- [31] Kellmann M, Muenster H, Zomer P, Mol JGJ. Full scan MS in comprehensive qualitative and quantitative residue analysis in food and feed matrices: How much resolving power is required? *Journal of the American Society for Mass Spectrometry*. 2009;**20**:1464-1476
- [32] Rochat B. Fully-automated systems and the need for global approaches should exhort clinical labs to reinvent routine MS analysis? *Bioanalysis*. 2018;**10**:1129-1141
- [33] Rochat B. Role of cytochrome P450 activity in the fate of anticancer agents and in drug resistance: Focus on tamoxifen, paclitaxel and imatinib metabolism. *Clinical Pharmacokinetics*. 2005;**44**:349-366
- [34] Tonoli D, Varesio E, Hopfgartner G. Mass spectrometric QUAL/QUAN approaches for drug metabolism and metabolomics. *Chimia*. 2012;**66**:218-222
- [35] Partridge E, Trobbiani S, Stockham P, Scott T, Kostakis C. A validated method for the screening of 320 forensically significant compounds in blood by LC/QTOF, with simultaneous quantification of selected compounds. *Journal of Analytical Toxicology*. 2018;**42**:220-231
- [36] Li D, Cao Z, Liao X, Yang P, Liu L. The development of a quantitative and qualitative method based on UHPLC-QTOF MS/MS for evaluation paclitaxel-tetrandrine interaction and its application to a pharmacokinetic study. *Talanta*. 2016;**160**:256-267
- [37] Qu L, Fan Y, Wang W, Ma K, Yin Z. Development, validation and clinical application of an online-SPE-LC-HRMS/MS for simultaneous quantification of phenobarbital, phenytoin, carbamazepine, and its active metabolite carbamazepine 10,11-epoxide. *Talanta*. 2016;**158**:77-88
- [38] Tebani A, Afonso C, Marre S, Bekri S. Omics-based strategies in precision medicine: Toward a paradigm shift in inborn errors of metabolism investigations. *International Journal of Molecular Sciences*. 2016;**17**:E1555
- [39] Dénes J, Szabó E, Robinette SL, Szatmári I, Szőnyi L, Kreuder JG, et al. Metabonomics of newborn screening dried blood spot samples: A novel approach in the screening and diagnostics of inborn errors of metabolism. *Analytical Chemistry*. 2012;**84**:0113-10120

---

Section 2

# Analytical Instrumentation and Methods

---



# Modern Extraction and Cleanup Methods of Veterinary Drug Residues in Food Samples of Animal Origin

*Babra Moyo and Nikita Tawanda Tavengwa*

## Abstract

Extensive research on the presence of veterinary drug residues in food samples has been conducted and is still underway. The inappropriate or excessive use of veterinary drugs in food producing animals may result in trace quantities of these drugs or their metabolites in food samples. Food contamination by veterinary drug residues is one of the main challenges worldwide to public health with drug resistance being the biggest threat. One of the challenges in veterinary drug residue analysis is their occurrence in trace amounts that are normally below limits of detection of most analytical instruments. Various efficient, economical, miniaturized and environmentally friendly extraction methods have been developed in recent years to pre-concentrate these analytes before instrumental analysis to enhance their detection and also to overcome the limitations of traditional extraction methods such as liquid-liquid extraction and solid phase extraction. These methods include quick, easy, cheap, effective, rugged and safe (QuEChERS), molecularly imprinted polymers, dispersive liquid-liquid microextraction and hollow fiber liquid-phase microextraction, and they will be discussed in this chapter.

**Keywords:** veterinary drug residues, food samples, modern extraction methods, pre-concentration, miniaturization

## 1. Introduction

Food is an indispensable part of human life and supplies the energy and nutrients needed for the development and growth of the neonate [1]. However, food safety is an important issue regarding residues of veterinary drugs in foods from food producing animals. Veterinary drugs are used to prevent and treat bacterial infections as well as improve feed efficiency and to promote animal growth worldwide [2]. The use of veterinary drugs in food producing animals may result in residues of the drugs or their metabolites being present in food samples, and this might be due to the inappropriate or excessive use of these drugs [3]. Various veterinary drugs have been reported to be retained in meat and milk of food producing animals [4–6] and this might be a health problem to humans who consume these food products.

Various pre-treatment methods have been described for the extraction of veterinary drug residues in food samples, such as liquid-liquid extraction (LLE) [7–9], solid-phase extraction (SPE) [10], solid-phase micro extraction [11–14]. Pre-concentration is necessary because veterinary drug residues often occur in trace amounts. However, some of these methods are laborious and time consuming, like LLE and SPE. It is very important to develop simple, rapid and efficient methods for the determination of veterinary drug residues in foods samples. In recent years, extraction and pre-concentration techniques that are compliant to the green chemistry methods have been developed and they will be discussed in Section 6. Moreover, several countries and different international organizations such as the World Health Organization (WHO), the Food Agriculture Organization (FAO) and the European Union (EU) have set maximum residue limits (MRLs) of veterinary drug residues in food to ensure food safety.

## 2. Physicochemical properties and uses of veterinary drugs

Physicochemical properties and uses of different veterinary drug classes are described below. A few examples of the physicochemical properties of selected veterinary drugs are shown on **Table 1**. Sulfonamides (SAs) show impartially low sorption capacity to solids compared to other veterinary drugs. These are used for the treatment of bacterial infections in animal husbandry and also act as growth promotants. Sulphonamides are also used in farm animal feeds and fish cultures [15]. Examples include sulfadiazine, sulfamethazine, sulfamethoxazole and sulfaquinolaxine.

Tetracyclines (TCs), including tetracycline, oxytetracycline, chlortetracycline and doxycycline are broad-spectrum veterinary drugs with broad use in animal husbandry. They are amphoteric compounds. Generally, TCs are more stable in acidic conditions.

Quinolones (QNs) are synthetic veterinary drugs with broad-spectrum antibacterial effects. This veterinary drug class consists of plain quinolones, such as oxolinic acid and nalidixic acid and fluorinated quinolones, known as fluoroquinolones (FQs), such as ciprofloxacin, flumequine and sarafloxacin.

Amphenicols are a broad-spectrum veterinary drug group that include chloramphenicol and its metabolites, thiamphenicol and florfenicol. Florfenicol has its own metabolite, florfenicol amine. The most common member of this veterinary drug class is chloramphenicol which is effective against many bacterial strains. Its toxicity and unwanted effects have restricted its use over the past years [16, 17].

Macrolides are a class of semi-synthetic medium-spectrum veterinary drugs. The most commonly used macrolides have 12–16 membered structures. Erythromycin is the most common veterinary drug in this class. Generally, macrolides have weak characteristics and thus are unstable under acidic conditions. Examples include erythromycin, tylosin, spiramycin, tilmicosin and tulathromycin.

Beta lactam veterinary drugs consist of several groups of compounds with cephalosporins and penicillins among the most important. Penicillins are commonly used for their microbial activity against both gram-positive and gram-negative organisms. The main clean-up method of penicillins for their analysis is pre- and post-column derivatization and the commonly used detection methods are LC-MS and LC-UV. Examples of penicillins are amoxicillin, ampicillin, oxacillin and cloxacillin, and examples of cephalosporins are cephapyin, ceftiofur and cefadroxil.

Aminoglycosides are broad spectrum veterinary drugs with antibacterial and antifungal activities produced by *Streptomyces* and *Micromospora*. The use of aminoglycosides has been clinically limited to severe infections because of its toxicity. More toxic veterinary drugs in this class have been restricted to topical or oral use for the treatment of infections caused by *Enterobacteriaceae*. Less toxic aminoglycosides are

Class of veterinary antibiotic drugs	Name of antibiotic	Solubility in water (mg L <sup>-1</sup> )	pK <sub>a</sub>
Tetracyclines	Tetracycline	231	3.3
	Chlortetracycline	~8600	3.3
	Doxycycline	50,000	—
	Oxytetracycline	1 × 10 <sup>6</sup>	3.27
Sulphonamides	Sulfadiazine	77	6.5
	Sulfamethoxazole	500	8.8
	Sulfaquinoxaline	75	—
	Sulfamethazine	1500	8.43
	Macrolides	Erythromycin	2000
Quinolones	Tylosin	5000	—
	Azithromycin	<1000	—
	Ciprofloxacin	Insoluble	—
	Enrofloxacin	146	—
	Oxolinic acid	Insoluble	6.87

—, Not available.

**Table 1.**  
 Physicochemical properties of selected veterinary drugs from different classes.

used for treatment of severe sepsis caused by gram-negative aerobes. Examples of aminoglycosides are streptomycin, kanamycin, tobramycin and gentamicin.

Nitrofurans are synthetic chemotherapeutic agents used in the treatment and prevention of gastrointestinal infections caused by *Escherichia coli* and *Salmonella*. They are broadly used in cattle, cows, pigs and poultry and are administered orally or as feed additives. Examples of nitrofurans include are furazolidine, furaltadone, nitrofurantoin and nitrofurazone.

In summary of this section, generally, veterinary drugs are compounds characterized by a complex chemical structure that have very variable water solubilities, low volatilization potential, several ionizable functional groups (amphoteric molecules) and different pK<sub>a</sub> values hence they have a low bioaccumulation potential [18]. Veterinary drugs may have different functionalities within the same molecule, making them either neutral, cationic, anionic, or zwitterionic under different pH conditions. Different functionalities within a single molecule may result in its physicochemical and biological characteristics such as, sorption behavior, photo reactivity and toxicity changing with pH. Solubility and hydrophobicity are also pH dependent. The pH dependency of antibiotic solubility can affect the extraction and quantification by analytical techniques [19].

### 3. Contamination of food by veterinary drugs

The use of veterinary drugs in food producing animals can result in the presence of residues in animal derived products such meat, milk, eggs and honey. This poses a health hazard to the consumers [3]. Veterinary drugs such as macrolides, tetracyclines, sulfonamides and penicillins are also used as antibiotics in humans [20, 21]. Physicochemical properties of drugs, pharmacokinetic characteristics or biological processes of animals are factors that affect the presence of drug residues in food of animal origin. Improper drug usage and failure to observe withdrawal periods may be a reason for the occurrence of veterinary drug residues in foods derived from animals.

## 4. Health effects

The threat of food contamination by veterinary drug residues is one of the major challenges to public health worldwide [3]. The presence of low levels of veterinary drug residues may not have a negative impact on public health. However, the substantial use of drugs may increase the risk of adverse effects of these residues to humans [3, 22, 23]. Continuous ingestion of veterinary drug residues can promote the development of drug resistance bacterial strains in an individual, resulting in resistance to treatment with the same antibiotics when need arises [24–26]. Veterinary drug traces also have harmful effects on humans, such as allergic reactions, liver damage, yellowing of teeth and gastrointestinal disturbance [27]. Sulphonamides can cause drug intoxication and hypersensitivity. Signs of hypersensitivity and intoxication are fever and anemia respectively.

Manuring, treatment of animals and disposal of carcasses, offals, urine, feces and unused products can contaminate the environment with veterinary drugs [28]. An excessive use of antibiotics in commercially reared animals does not only affect humans, it can also affect the food chain leading to ecological imbalances. For example, a deficient management of the livestock carcasses can lead to antibiotic resistance in the scavengers that ingest them, like vultures [24–26]. The disposal of medicated animals should be regulated to minimize the risk in scavenger birds.

## 5. Maximum residual limits

The MRL values for food products result from calculations based upon the acceptable daily intake. MRL values depend on chronic toxicity of the antibiotic in question. More toxic drugs have lower MRL values compared to moderately toxic drugs. Prohibited substances are pharmacologically active substances for which an MRL cannot be established because of their toxicity and these include substances such as chloramphenicol, nitrofurans and nitroimidazoles. The kidney is the most important organ of drug excretion and that might be the reason why for most drugs it is allocated a higher MRL. For example, in the European Union (EU), countries have established a MRL of 200, 100, and 300  $\mu\text{g kg}^{-1}$  for liver, muscle and kidney tissues, respectively for enrofloxacin and ciprofloxacin. The MRL set by the EU Committee for veterinary medicinal products is 200  $\mu\text{g kg}^{-1}$  in muscles, liver and kidneys of animal origin, 40  $\mu\text{g kg}^{-1}$  in milk, and 150  $\mu\text{g kg}^{-1}$  in eggs for the macrolide drugs. **Table 2** shows some MRL values for different foods of animal origin.

Class of veterinary drugs	Target veterinary drug	Matrix	MRL ( $\mu\text{g kg}^{-1}$ )
Sulphonamides	Sulphonamides	Milk, fish and other seafood	100
	Sulphonamides	Eggs	Not allowed
Quinolones	Danofloxacin, enrofloxacin-ciprofloxacin and oxolinic acid	Muscle	100
	Enrofloxacin and ciprofloxacin	Eggs	Not allowed
	Enrofloxacin and ciprofloxacin	Liver	200
	Enrofloxacin and ciprofloxacin	Kidney	300
Macrolides	Macrolides	Muscle, liver and kidneys	200



Class of veterinary drugs	Target veterinary drug	Matrix	MRL ( $\mu\text{g kg}^{-1}$ )
	Macrolides	Milk	40
	Macrolides	Eggs	150
Tetracyclines (single/total)	Tetracycline, oxytetracycline, chlortetracycline and doxycycline	Muscle, milk	100
Tetracyclines (single/total)	Tetracycline, oxytetracycline, chlortetracycline and doxycycline	Eggs	200

**Table 2.**  
 Maximum residue limit for veterinary drug residues in food samples according to European Community, Commission Regulation (EU) No. 37/2010.

## 6. Pre-concentration techniques

Veterinary drug residues in food of animal origin are of great concern to regulatory agencies and consumers, hence reliable extraction methods for rapid, selective and sensitive detection of these residues are necessary to ensure food safety [29]. There are various extraction methods that have been used in veterinary drug residues analysis in food samples, such as liquid-liquid extraction (LLE) [30–32] and solid phase extraction (SPE) [33, 34]. These methods suffer a number of drawbacks even though they perform their tasks adequately. Both LLE and SPE are environmentally unfriendly due to the large amounts of organic solvents they use, they are time consuming and labor intensive. Another disadvantage of SPE is that cartridges are costly.

Promising extraction and pre-concentration techniques for veterinary drug residues that have been explored recently by many researchers include dispersive liquid-liquid microextraction (DLLME) [5, 6, 35, 36], hollow fiber based liquid-phase microextraction (HFLPME) [37–40] and quick, easy, cheap, effective, rugged and safe (QuEChERS) [4, 41–43] where the general trend is compliance with green chemistry principles. Veterinary drug residues occur at trace levels as low nanogram per gram [4, 37] hence the need to pre-concentrate. The application of QuEChERS, DLLME, HFLPME and molecularly imprinted polymers (MIPs) for the extraction and pre-concentration of veterinary drug residues in food samples will be discussed below and summarized in **Table 3**.

The food industry also needs the development of new methods that are fast, easy and cheap for routine analysis of residues in food samples. The latest trend in drug residue analysis is the development of generic methods that are capable of monitoring a wide variety of compounds, belonging to different veterinary drug classes. This has proven to be challenge due to the varying chemistries and physicochemical properties of veterinary drugs from different classes, as a result, multi-class methods for veterinary drugs are still not so widespread although they are strongly required.

### 6.1 QuEChERS

The quick easy cheap effective rugged safe (QuEChERS) method is an extraction technique that employs an organic solvent and phase separation using high salt content, in some cases followed by dispersive solid phase extraction (d-SPE) for sample clean up. The QuEChERS method, which was originally developed for pesticide analysis in fruits and vegetables [44, 45], has recently been proposed for the analysis of veterinary drugs in different food matrices [4, 41, 43, 46]. Recent applications of this method are discussed below.

Target antibiotic	Food matrix	Analytical technique	Extraction technique	Concentration of antibiotic detected	LOD	LOQ	Recovery (%)	References
Seven macrolides	Milk	LC-MS/MS	QuEChERS based on acetonitrile extraction + a mixture of salts (sodium sulfate, sodium chloride and potassium carbonate)	—	0.84 $\mu\text{g kg}^{-1}$	2.79 $\mu\text{g kg}^{-1}$	89–97	[41]
Six multi-residues	Bovine milk	LC-MS/MS	QuEChERS based on acetonitrile followed by a cleanup with d-SPE based C <sub>18</sub> , PSA and sodium acetate	—	—	—	84.18–115.99	[42]
Sixteen multi-residues	Preserved eggs	UHPLC-MS/MS	QuEChERS based on water, acetonitrile with 1% acetic acid followed by a cleanup using d-SPE with C <sub>18</sub> and PSA as sorbents	—	0.1–0.9 $\mu\text{g kg}^{-1}$	0.3–3.0 $\mu\text{g kg}^{-1}$	73.8–127.4	[43]
Three SAs	Chicken breast	HPLC-DAD	QuEChERS based on acetonitrile and water with 1% CH <sub>3</sub> CO <sub>2</sub> H followed by a cleanup using d-SPE Oasis HLB as a sorbent.	—	10 and 13 $\mu\text{g kg}^{-1}$	25–30 $\mu\text{g kg}^{-1}$	75.4–98.7	[46]
Seven TCs	Beef	LC-MS/MS	DLLME, methanol was a disperser solvent and dichloromethane was an extracting solvent	38.4 and 82.3 $\mu\text{g kg}^{-1}$	2.2–3.6 $\mu\text{g kg}^{-1}$	74–11.5 $\mu\text{g kg}^{-1}$	80–105	[5]
Several SAs	Milk	HPLC-FD	Traditional DLLME (extraction solvent (1 mL chloroform) and dispersive solvent (1.9 mL acetonitrile)	—	0.73–1.21 $\mu\text{g L}^{-1}$	—	92.9–104.7	[36]
Six FQs	Milk	HPLC-UV	DLLME was coupled to QuEChERS	—	—	2.5–15 $\mu\text{g kg}^{-1}$	74.1–101.4	[35]
Four TCs	Milk and eggs	HPLC-UV	IL-DLLME ([C <sub>6</sub> MIM][PF <sub>6</sub> ]) as an extraction solvent, FIL-NOSM a disperser solvent)	—	0.08–1.12 $\mu\text{g kg}^{-1}$	—	94.1–102.1	[6]

Target antibiotic	Food matrix	Analytical technique	Extraction technique	Concentration of antibiotic detected	LOD	LOQ	Recovery (%)	References
Florfenicol and Chloramphenicol	Pasteurized Milk	HPLC-UV	Traditional DLLME (chloroform as an extracting solvent and water as a dispenser solvent)	62.4 $\mu\text{g kg}^{-1}$ florfenicol	12.2 and 12.5 $\mu\text{g kg}^{-1}$	36.6 and 37.5 $\mu\text{g kg}^{-1}$	—	[53]
Five QNs and four TCs	Milk, honey, fish, liver and muscles of lamb	HPLC-DAD	HFLPME (0.1 mol L <sup>-1</sup> nitric acid and sodium chloride was the acceptor phase, 10% w/v Aliquat-336 in 1-octanol)	24.8 ng g <sup>-1</sup> danofloxacin 37.5 ng g <sup>-1</sup> tetracycline	0.5–20 ng g <sup>-1</sup>	1.25–40 ng g <sup>-1</sup>	—	[37]
Four TCs	Milk	HPLC-UV	HF-DLLME (chloroform as an extracting solvent and water as a dispenser solvent)	—	0.95–3.6 $\mu\text{g L}^{-1}$	5–15 $\mu\text{g L}^{-1}$	92.38–107.3	[38]
Three TCs	Bovine milk	HPLC-UV	Carrier mediated three phase HFLPME (0.1 M phosphoric acid, 1.0 M sodium chloride with pH = 1.6 as an acceptor phase, 0.05 M disodium hydrogen phosphate (pH between 9.1 and 9.5) as donor phase and 10% (w/v) of Aliquat-336 in octanol as an SLM.	6.0–27.4 $\mu\text{g L}^{-1}$	0.5–1.0 $\mu\text{g L}^{-1}$	0.5–1.0 $\mu\text{g L}^{-1}$	-	[39]
Tylosin	Milk	UV/Vis	HFLPME-TiO <sub>2</sub> (TiO <sub>2</sub> was dispersed in 1-octanol)	—	0.21 $\mu\text{g L}^{-1}$	—	89–99	[40]
Eight FQs, eight SAs and four TCs	Pork	UPLC-PDA	Mixed template MIP-MSPD (0.15 g MIMP, methanol/water (2:8, v/v) as a washing solvent, methanol/acetic acid (9:1, v/v) as an eluting solvent)	—	0.5–3.0 ng g <sup>-1</sup>	1.5–6.0 ng g <sup>-1</sup>	92–99	[57]

Target antibiotic	Food matrix	Analytical technique	Extraction technique	Concentration of antibiotic detected	LOD	LOQ	Recovery (%)	References
Four TCs	Pork, milk and eggs	HPLC-PDA	MIP-SPE (30 mg MIP particles, 0.01 mol L <sup>-1</sup> trifluoroacetic acid, pH 3.0 as the loading solvent, methanol/acetic acid (9:1, v/v) as the elution solvent)	52 ng mL <sup>-1</sup> ; TC 87 ng mL <sup>-1</sup> ; oxytetracycline in milk only	20–40 ng mL <sup>-1</sup>	50–80 ng mL <sup>-1</sup>	74–93	[58]
Ten macrolides	Swine, cattle and chicken muscles	LC-MS/MS	MIP-SPE (20 mg MIP particles, 10% methanol in water as the washing solvent, 5% ammonia in methanol as the elution solvent)	—	0.1–0.4 µg kg <sup>-1</sup>	0.3–1.0 µg kg <sup>-1</sup>	60.7– 100.3	[56]
Ten FQs	Fish	HPLC-FLD	DMIP-MSPD (50 mg MIP particles, 20% methanol in water as the washing solvent, 1% trifluoroacetic acid in acetonitrile as the elution solvent)	—	0.06– 0.22 ng g <sup>-1</sup>	—	64.4–102.7	[59]
Three FQs	Milk	HPLC-UV	Mini-MISPE (40 mg MIP particles, water as the washing solvent, methanol-acetic acid (19:1, v/v) as the elution solvent)	Ciprofloxacin: 0.21 and 0.25 g mL <sup>-1</sup>	1.5–2.3 ng mL <sup>-1</sup>	5.0–7.5 ng mL <sup>-1</sup>	87.2–106.1	[60]
TCs	Milk	Fluorescent sensing	CDs@MIPs (40 mg MIP particles, 1% (v/v) trichloroacetic acid solution was a solvent)	ND	5.48 nM	—	97.3–105.3	[61]

—, Not mentioned; ND, not detected.

**Table 3.** Modern analytical techniques in the analysis of antibiotic residues in food samples.

da Costa et al. [41] developed a modified QuEChERS extraction technique using acetonitrile, followed by the addition of a mixture of salts (sodium sulfate, sodium chloride and potassium carbonate) for the extraction of seven macrolide drugs in milk followed by analysis on liquid chromatography and tandem mass spectrometry (LC-MS/MS). Sodium sulfate and sodium chloride removed water from samples promoting the salting out effect while acetonitrile was used for deproteination. Potassium carbonate salt was included to elevate the extraction pH to around 9.5 promoting an increase in the recovery, since macrolides have a pKa between 6.6 and 9.2. The limit of detection (LOD) and limit of quantification (LOQ) were 0.84 and 2.79  $\mu\text{g kg}^{-1}$  respectively and recoveries were ranging between 89 and 97%. No further clean-up step such as an additional d-SPE step was required, hence reducing time, cost and labor.

In another study by Wang et al. [42], a modified QuEChERS extraction technique based on octadecylsilane ( $\text{C}_{18}$ ), primary secondary amine (PSA) and sodium acetate for six multi-residue veterinary drugs in bovine milk followed by analysis using LC-MS/MS. The QuEChERS method was optimized for use in the determination of multi-class veterinary drug residues in fatty foods (milk) using response surface methodology. The amounts of  $\text{C}_{18}$ , PSA, and sodium acetate used in this study were determined by the response surface methodology variables. PSA,  $\text{C}_{18}$  and sodium acetate have a dissolving effect on milk-fat globules and hence, resulting in higher recoveries (84.18–115.99%) compared to da Costa et al. [41]. Organic solvents, such as acetonitrile, methanol and ethanol, are commonly employed in the precipitation of proteins in biological matrices. For all residues, the LOQs were low enough to quantify the analytes below their MRLs.

Li et al. [43] employed the QuEChERS method followed by d-SPE coupled to ultrahigh-performance liquid chromatography tandem mass spectrometry for the multi-residue analysis of 16 veterinary drugs belonging to three classes (macrolides, quinolones, and sulfonamides) in preserved eggs. Graphitized carbon black was used as a comparative d-SPE sorbent. The recoveries of all veterinary drugs decreased with the addition of graphitized carbon black, while purification with a conjugation of PSA and  $\text{C}_{18}$  in the presence of magnesium sulfate resulted in better results. The results demonstrated good linearity, accuracy, precision, LOD (0.1–0.9  $\mu\text{g kg}^{-1}$ ) and LOQ (0.3–3.0  $\mu\text{g kg}^{-1}$ ) which indicated that the proposed method was highly sensitive and could efficiently determine trace amounts.

Machado et al. [46] developed a QuEChERS method followed by analysis on the high performance liquid chromatography (HPLC) with a diode array detector (DAD) for the simultaneous determination of sulfadiazine, sulfamethoxazole and sulfamethoxypyridazine in chicken breast samples. The LODs ranged between 10 and 13  $\mu\text{g kg}^{-1}$  and the LOQs ranged between 25 and 30  $\mu\text{g kg}^{-1}$  while recoveries ranged between 75.4 and 98.7%. SPE was done for comparison and recoveries lower than 70% were obtained. However, SPE, proved to reduce the matrix effect compared to the QuEChERS method.

## **6.2 Liquid phase microextraction**

Traditional sample preparation techniques such as liquid-liquid extraction (LLE) have drawbacks in spite of the substantial use of this method over the years. The LLE method is tedious, time consuming and uses large amounts of toxic organic solvents which are non-compliant to the green analytical chemistry (GAC) principles. In order to overcome these drawbacks, new extraction techniques that are simple, rapid and inexpensive, miniaturized and have the ability of automation have been developed in recent years [47]. The efforts of various researchers in this area have resulted in the development of a new extraction technique known as

liquid-phase microextraction (LPME). LPME offers an alternative to SPME [48]. LPME can be divided into three main modes which are single-drop microextraction (SD-LPME), hollow fiber liquid phase microextraction (HFLPME) and dispersive liquid-liquid microextraction (DLLME). Among these modes of LPME, HFLPME and DLLME have been the most used because of the advantages that they offer [47]. SD-LPME is the least used mode because excessive stirring tends to break up the droplet, extraction is time consuming and reaching equilibrium can be a challenge. This disadvantage overrides the advantage that this method has, which is the enormous reduction of volumes of organic solvent it uses [49].

These methods are cheap and do not have sample carryover problems that are associated with SPME [48]. LPME offers advantages such as high recovery and high enrichment factors, simplicity of operation, rapidity and they are also environment friendly [50]. Below is a summary of some studies that have used DLLME and HFLPME for the extraction of veterinary drug residues from food samples.

### 6.2.1 Dispersive liquid-liquid microextraction

Rezaee and co-workers [51] introduced DLLME as a new LLE technique for the determination of polyaromatic hydrocarbons and pesticides. The application of DLLME in the extraction of veterinary drugs in literature has increased over the years [5, 6, 35, 36]. This technique is based on a ternary component solvent system including an extraction solvent, disperser solvent and an aqueous sample and is known as traditional DLLME. The advantages of traditional DLLME are the microliter-level volumes required for extraction and dispersive solvents and short extraction times. However, the disadvantage of traditional DLLME is the use of organic solvents as the extraction and dispersive solvents.

Modified modes of DLLME have been invented recently and they include, low-density solvent based DLLME (LDS-DLLME), solidified floating organic drop DLLME (SFO-DLLME), effervescence assisted DLLME, air assisted dispersive liquid-liquid microextraction (AA-DLLME), surfactant assisted DLLME (SA-DLLME) and cloud point DLLME (CP-DLLME), ionic liquid DLLME (IL-DLLME) [6] to address the disadvantages associated with traditional DLLME. Despite these disadvantages, DLLME is more advantageous in terms of short total time, low cost and feasibility compared with other liquid-phase microextraction techniques [52]. Below is research that has been done recently on veterinary drugs in food samples using DLLME.

Mookantsa et al. [5] employed traditional DLLME for the extraction of seven tetracyclines from beef where methanol was a disperser solvent and dichloromethane was an extracting solvent followed by LC-MS/MS. Recoveries of spiked blank muscle samples at three levels (50, 100 and 150  $\mu\text{g kg}^{-1}$ ) ranged from 80–105%. LODs and LOQs ranged from 2.2 to 3.6  $\mu\text{g kg}^{-1}$  and from 7.4 to 11.5  $\mu\text{g kg}^{-1}$  respectively. Concentrations of chlortetracycline and oxytetracycline were detected in bovine muscle samples to be between 38.4 and 82.3  $\mu\text{g kg}^{-1}$  which is lower than the stipulated European Union MRL of 100  $\mu\text{g kg}^{-1}$ . DLLME was compared to a South African National Accreditation System accredited d-SPE method and the t-test showed that the results obtained by the methods had no significant difference. However, DLLME was simple, fast, inexpensive and uses very low volumes of organic solvents hence more greener compared to d-SPE.

In a study done by Karami-Osboo et al. [35], DLLME was coupled to QuEChERS for the determination of six fluoroquinolones using HPLC with ultra-violet (UV) detection. The dried supernatant from the QuEChERS method was resuspended in 1.0 mL of a 10% acetic acid-acetonitrile mixture, combined with 200  $\mu\text{L}$  of chloroform and rapidly injected into 4 mL of deionized water. The cloudy solution

was centrifuged for 5 minutes at 4500 rpm. By coupling QuEChERS to DLLME, the authors removed matrix interference, which is a common problem with the detection of fluoroquinolones. The method showed good recoveries (74.1–101.4% for all analytes) and low LOQs (below 2.5  $\mu\text{g kg}^{-1}$  for danofloxacin and below 15  $\mu\text{g kg}^{-1}$  for all other FQs).

Arroyo-Manzanares et al. [36] used traditional DLLME for the determination of several sulfonamides in milk. The analytes were detected by HPLC with fluorescence detection. The authors also compared their optimized DLLME procedure to QuEChERS. Proteins were precipitated using trichloroacetic acid and then filtered. The DLLME extraction procedure was optimized using a central composite design. The optimum volumes for chloroform as an extraction solvent and acetonitrile as a dispersive solvent were 1 and 1.9 mL, respectively. DLLME resulted in lower LODs (0.73–1.21  $\mu\text{g L}^{-1}$ ) than QuEChERS (1.15–2.73  $\mu\text{g L}^{-1}$ ) and higher recoveries (92.9–104.7% compared to 83.6–97.1%, when samples were spiked with sulfonamides at 150  $\mu\text{g L}^{-1}$ ). However, QuEChERS proved to be more reproducible than DLLME with lower relative standard deviation values of 2.9–7.1 and 3.0–9.7%, respectively.

In another study by Karami-Osboo et al. [53], traditional DLLME coupled to HPLC-UV was used for the determination of chloramphenicol and florfenicol residues in milk samples where chloroform was used as extraction solvent and the deproteinized milk as a disperser solvent. The blank milk samples were spiked at three levels, 150, 300 and 600  $\mu\text{g}$  of each chloramphenicol and florfenicol per kg of milk and recoveries were between 69.1 and 79.4%. The LODs for chloramphenicol and florfenicol were 12.5 and 12.2  $\mu\text{g kg}^{-1}$  respectively whereas the LOQs were 37.5 and 36.6  $\mu\text{g kg}^{-1}$  respectively. Despite the use of florfenicol not being permitted for milk producing animals from which milk is produced for human consumption, it was detected in one of the samples at a concentration of 62.4  $\mu\text{g kg}^{-1}$ .

Ionic liquids (ILs), consisting of organic cations and inorganic or organic anions with melting points at or below 100°C, have been widely applied as green solvents to improve extraction and enrichment performance as compared to the traditional use of organic solvents. A significant advantage of this method is that the metathesis reaction and extraction are accomplished in one step making it rapid and suitable for high-throughput analysis. Gao et al. [6] used functionalized ionic liquid-based non-organic solvent microextraction (FIL-NOSM) based on 1-butyl-3-methylimidazolium naphthoic acid salt ( $[\text{C}_4\text{MIM}][\text{NPA}]$ ) with strong acidity for the determination of TCs in milk and eggs. The use of  $[\text{C}_4\text{MIM}][\text{NPA}]$  in the FIL-NOSM method eliminated the pH adjustment step because of its strong acidity which saves as a pH regulator. This proposed method provided high extraction efficiency, less pretreatment time and requires non-organic solvents for determination of trace TC concentrations in complex animal-based food matrices. Moreover, no organic solvent was utilized in this IL-based DLLME procedure making this method more environmentally friendly. The LODs were between 0.08 and 1.12  $\mu\text{g kg}^{-1}$  in milk and egg samples. The recoveries ranged from 94.1 to 102.1%.

### *6.2.2 Hollow fiber liquid phase microextraction*

Hollow fiber liquid phase microextraction is a mode of LPME that uses a porous polypropylene hollow fiber for immobilization of organic solvent in its pores. The development of HFLPME provides a way to stabilize the extraction droplet in SD-LPME by placing it in a hollow fiber [54]. The main consumable material is the hollow fiber membrane, which is lower than other methods in cost and sample consumption [38]. The different modes of HFLPME are static, dynamic, two and three phase. The advantages of HFLPME are high enrichment, high degree of sample clean-up and low solvent consumption. The disadvantage

of HFLPME procedure is that it is slow with extraction times ranging from 15 to 45 minutes and target analytes may partly be trapped in the supporting liquid membrane (SLM) [39]. Another disadvantage is that there is no complete setup commercially available for this method although hollow fibers are commercially available [55]. Below are some recent studies on veterinary drug residues that have been carried out using HFLPME.

Tajabadi et al. [37] used a carrier mediated three phase HFLPME prior to analysis on the HPLC-DAD for the simultaneous determination of the veterinary drug residues of four TCs and five QNs in a wide range of animal source food samples such as fish, milk and honey as well as the liver and muscles of lamb and chicken. Multivariate curve resolution-alternative least squares was used for resolving some overlapped peaks in multivariate data of HPLC-DAD and made possible the simultaneous analysis of nine TCs and QNs in minimum time. LODs and LOQs for the different veterinary drugs ranged between 0.5–20 and 1.25–40 ng g<sup>-1</sup>. Danofloxacin was detected at a concentration of 24.8 ng g<sup>-1</sup> in chicken liver, tetracycline was detected at 37.5 ng g<sup>-1</sup> in lamb liver which are less than the stipulated MRLs according to EU 37/2010 and the rest of the veterinary drugs were not detected.

Xu et al. [38] employed a carrier mediated three phase hollow fiber membrane based dynamic liquid-liquid microextraction coupled with HPLC-UV detection for the residue analysis of TCs in milk samples without deproteinization and defatting, but the milk samples were diluted five folds. A peristaltic pump was used to promote mass transfer between the carrier and the operated solution. The standard addition method was used to eliminate the matrix effect. Octanol containing 20% (w/w) Aliquat-336 was used as a SLM, 0.05 M disodium hydrogen phosphate, pH 9.0 containing the sample was a donor phase and solutions of 1.0 mol L<sup>-1</sup> sodium chloride and phosphoric acid (pH = 1.0) were used as the acceptor solvent. The LOD and LOQ were in the range of 0.95–3.6 and 5–15 µg L<sup>-1</sup> respectively. The recoveries in spiked samples ranged from 92.38 to 107.3%.

A similar study was carried out by Shariati et al. [39] where tetracycline, oxytetracycline and doxycycline were extracted from bovine milk, human plasma and water samples using a carrier mediated three phase HFLPME prior analysis on the HPLC-UV. The acceptor solvent was 0.1 M phosphoric acid, 1.0 M sodium chloride with pH = 1.6, 0.05 M disodium hydrogen phosphate (pH between 9.1 and 9.5) containing the sample as the donor phase and 10% (w/v) of Aliquat-336 in octanol as a SLM. The LOD and LOQ were 0.5–1.0 and 0.5–1.0 µg L<sup>-1</sup> respectively which are lower compared to the ones obtained by Xu et al. [38] proving that fiber membrane-based dynamic liquid-liquid microextraction is a more efficient extraction method. All the milk samples contained TCs in the range of 6.0–27.4 µg L<sup>-1</sup> that was below the MRL as set by the EU.

From the two studies that are above it can be concluded that passive transport of TCs in the absence of the carrier is difficult because of existence of TCs as zwitterionic forms (at the studied conditions) in solution and hence they have a very small tendency to pass through the impregnated organic solvent. A unique advantage of the carrier mediator Aliquat-336 is that it stays in a cationic form in all pH ranges.

Sehati et al. [40] coupled HFLPME to nanomaterials, where TiO<sub>2</sub> nanomaterials were dispersed in 1-octanol and used it to fill the lumen of a HF. Then, they sealed the two ends of the HF with orthodontic stainless steel wires. The LPME took place by putting the HF into the milk samples for the extraction of tylosin. This method allowed obtaining recovery percentages in the range 89–99% and despite using an ultraviolet-visible spectrophotometer for the determination of tylosin, an LOD of 0.21 mg L<sup>-1</sup> was achieved which proves the efficiency of the extraction method that was used.



### 6.3 Molecularly imprinted polymers

Molecularly imprinted polymers (MIPs) are synthesized using a template, functional monomer, cross-linker and an initiator. MIPs are selective towards the target molecules, allowing them to be eluted from the SPE cartridge almost free of co-extracted compounds compared to classical sorbents used for clean-up procedures [56]. SPE sorbents such as C<sub>18</sub>, hydrophilic lipophilic balanced (HLB) material, diatomite, N-propylethylenediamine, alumina and Florisil are susceptible to interferences by impurities in biological samples and the cartridges can only be used once [57]. Therefore, it is important to develop simple, rapid and environmentally friendly methods. MIPs overcome the above-mentioned drawbacks of traditional SPE sorbents. MIPs are stable under different harsh conditions (extreme pH, high pressures and high temperatures) and can be reused several times [58]. Below are a few studies where MIPs were applied in the solid phase extraction of veterinary drug residues in food samples.

In a study conducted by Song et al. [56], a MIP-SPE method combining LC-MS/MS was developed to determine the residues of macrolide drugs in animal derived foods. Tylosin was used as a virtual template and the synthesized MIPs were used as the selective sorbent for packing SPE cartridge. A system of sodium borate buffer solution (pH = 10.0) and ethyl acetate was selected for the extraction of the residues of macrolides from muscle samples. Mean recoveries of 10 target analytes were in the range of 60.7–100.3%. Compared with the conventional SPE cartridges (approximately 60–90%), the MISPE cartridge was highly selective and obtained higher recoveries for the 10 macrolides drugs. The LOD and LOQ values ranged between 0.1–0.4 and 0.3–1.0 µg kg<sup>-1</sup> respectively. The results indicated that the sensitivity of the proposed method for the determination of 10 macrolide drugs residues in animal muscle samples was acceptable.

Wang et al. [57] used a mixed-template molecularly imprinted polymer (MMIP) coupled with matrix solid phase dispersion (MSPD) to recognize eight FQs, eight SAs and four TCs from pork samples following analysis with ultraperformance liquid chromatography with a photo diode array detector. The LOD and LOQ were 0.5–3.0 and 1.5–6.0 ng g<sup>-1</sup> respectively. The recoveries ranged between 92 and 99%. MMIPs were compared to C<sub>18</sub> and diatomaceous earth dispersing sorbents. The obtained chromatograms showed that the two sorbents were able to achieve the satisfactory purification effects, but the recoveries of the 20 drugs from the two sorbents (70–95%) were lower than that from MMIP.

In another study by Feng et al. [58], a MIP-SPE method combining HPLC was developed to determine the residues of TC drugs in animal derived foods. A template for MIP synthesis was selected among doxycycline, oxytetracycline and chlortetracycline for enhanced enrichment factors. Results showed that one milk sample contained TC residue (52 ng mL<sup>-1</sup>) and another milk sample contained oxytetracycline residue (87 ng mL<sup>-1</sup>), but the residue levels were lower than their MRLs in milk (100 ng mL<sup>-1</sup>). Results of other samples were negative. In order to compare the purification effect of MIP-SPE with conventional SPE, the extracts of TCs fortified blank milk (100 ng mL<sup>-1</sup>) were purified with three commercial SPE cartridges containing different sorbents (strong cation exchange phase, HLB and C<sub>18</sub>) and there were different interfering peaks around TCs peaks in the chromatograms, revealing inferior purification performances of these sorbents. MIP-SPE proved to be specific, sensitive and accurate for the extraction of TCs residues.

Dummy molecularly imprinted polymers (DMIPs) based on the matrix solid phase dispersion method for the extraction of FQs from fish prior to analysis on the HPLC with fluorescence detection were used by Sun et al. [59]. The use of

DMIPs was to prevent any possible template leakage which could still happen even after thorough washing steps. Template leakage could have a serious impact on the accuracy of the analytical method or made it not suitable for simultaneous analysis of the whole class of FQs. This problem has become one of the major areas of concern in sample pre-treatment methods of MIPs. Good recoveries, low LODs and excellent accuracy demonstrated the suitability of the DMIP sorbent for pre-treatment of FQs in fish samples. The use of DMIP resulted in less matrix interferences compared to directly extracted samples and no co-eluted peaks were observed in the chromatogram. The LOD was 0.06–0.22 ng g<sup>-1</sup> and recoveries ranged between 64.4 and 102.7%.

Wang et al. [60] used an inorganic-organic co-functional monomer, methacrylic acid-vinyltriethoxysilane (MAA-VTES) for the synthesis of molecularly imprinted microspheres (MIMs). The obtained MAA-VTES based MIMs exhibited good recognition and selectivity to FQs and were successfully applied as selective sorbents of a miniaturized home-made solid phase extraction device for the determination of ofloxacin, lomefloxacin and ciprofloxacin in milk samples. The LODs and the LOQs of FQs were 1.5–2.3 and 5.0–7.5 ng mL<sup>-1</sup>, respectively. The average recoveries for the analyte were in the range of 87.2–106.1%. Ciprofloxacin was detected in two samples as 0.21 and 0.25 ng mL<sup>-1</sup> which were below the MRL established by EU (100 g kg<sup>-1</sup>). Due to the efficiency of the developed co-functional monomer based mini-MISPE-HPLC method, it was possible to analyze the target compounds in milk samples at ng mL<sup>-1</sup> level.

A selective and eco-friendly sensor for the detection of tetracycline by grafting imprinted polymers onto the surface of carbon quantum dots was used by Hou et al. [61]. A simple microwave-assisted approach was utilized to fabricate the fluorescent imprinted composites rapidly for the first time, which could shorten the polymerization time which normally takes 8–24 hours and simplify the experimental procedure. In this study polymerization took about 1 hour. The development of fluorescent molecularly imprinted composites might be a promising method for rapid analysis in complex samples in future. TCs were not detected in milk samples. Recoveries ranged from 97.3 to 105.3%.

## **7. Challenges and future trends**

In high-fat foods like milk and meat, veterinary drug residues may bind to lipoproteins and extraction solvents forming emulsions and foam, especially polar veterinary drugs which may decrease recoveries and hence, affecting separation and analysis [56, 62]. Extracting analytes from biological samples using modern extraction techniques like DLLME has some challenges. In traditional DLLME, prior to a DLLME procedure on a complex matrix such as milk, lipids and proteins must be eliminated since they can act like surfactants and disrupt the interfacial tension at the droplet surface, constraining phase separation [63]. During the sample pre-treatment step, salts are added for analyte partitioning, phase separation, buffering and for reducing the amounts of co-extracted matrix that could hinder the transfer of analytes from the aqueous phase to the organic phase [5].

TCs are challenging drugs for analytical analysis because they are hydrophilic compounds with high solubility in aqueous media. They have both acidic and basic functionalities, and therefore exist in various forms at different pH conditions [39]. Moreover, they can form complexes with divalent metal ions and silanolic groups on the HPLC column which may result in severe peak tailing [64]. Reverse phase-HPLC with mobile phases containing acids such as phosphoric, acetic and tartaric acids can be used to reduce peak tailing or an RP-amide

column can be used. The ability of the RP-amide column to separate TCs might be explained by the hydrogen bonding between the amide functionality of the column and the hydroxyl functionality of TCs. Another challenge is that TCs are prone to photo-degradation.

Overlapping peaks during multi-residual analysis when using HPLC-DAD is a challenge. Multivariate curve-resolution coupled to alternating least squares to calculate the exact peak area of overlapping compounds was used by Tajabadi et al. [37], hence more sensitive analytical instruments such as the LC-MS/MS are required for multi-residual analysis. Moreover, the solubilization procedure of veterinary drug residues is a rate-limiting step in multi-residual analysis.

The matrix effect still remains an issue when extracting veterinary drug residues using the QuEChERS method from complex samples such as meat, and hence reducing the sensitivity of chromatographic instruments [46].

## **8. Future trends**

The world is moving towards the use of greener solvents and hence promoting the principles of GAC, therefore, it can be envisioned that most extraction methods still making use of organic solvents may be completely eliminated in future. Currently greener solvents such ionic liquids are widely used in microextraction procedures as dispersive or extraction solvents according to their different solubilities in DLLME.

Electrochemical sensors and their relative detection strategies, with the advantages of high sensitivity, simplicity and rapid response, have attracted considerable attention in recent years. Among them, aptasensors are considered as one of the most promising research directions owing to the employment of an aptamer. Aptamers, with the advantage of high affinity and specificity to targets, low price and easy to be synthetic in vitro, have provided a broad prospect for developing electrochemical sensing system.

## **9. Conclusion**

Expanding agriculture, aquaculture and apiculture practices have resulted in increased levels of infections among species. Various classes of veterinary drugs including QNs, TCs,  $\beta$ -lactams, SAs and others exhibit activity against both gram-positive and gram-negative bacteria, hence they are widely used to treat or prevent diseases. However, extended use of these veterinary drugs has led to food safety issues worldwide and hence a need for developing sensitive methods for their determination. The focus of this chapter has been to present the trends in modern extraction and clean-up techniques of veterinary drug residues from food samples of animal origin, with milk being the most studied matrix because of its importance on the diet of humans and one of the most consumed foods in the world. Even though some of these veterinary drugs such as chloramphenicols have been banned in some countries due to their dangerous side effects on humans they are still detected in food samples because farmers are not adhering to EU regulations. Generally, in most studies these veterinary drug residues are below stipulated MRLs. Although most extraction methods that are emerging are promising, multi-residual analysis is still a challenge.

## **Author details**

Babra Moyo and Nikita Tawanda Tavengwa\*  
Department of Chemistry, School of Mathematical and Natural Sciences,  
University of Venda, Thohoyandou, South Africa

\*Address all correspondence to: [nikita.tavengwa@univen.ac.za](mailto:nikita.tavengwa@univen.ac.za)

## **IntechOpen**

---

© 2019 The Author(s). Licensee IntechOpen. This chapter is distributed under the terms of the Creative Commons Attribution License (<http://creativecommons.org/licenses/by/3.0>), which permits unrestricted use, distribution, and reproduction in any medium, provided the original work is properly cited. 

## References

- [1] Nagpal R, Behare PV, Kumar M, Mohania D, Yadav M, Jain S, et al. Milk, milk products, and disease free health: An updated overview. *Critical Reviews in Food Science and Nutrition*. 2012;52:321-333
- [2] Liu Y, Yang H, Yang S, Hu Q, Cheng H, Liu H, et al. High-Performance Liquid Chromatography using pressurized liquid extraction for the determination of seven tetracyclines in egg, fish and shrimp. *Journal of Chromatography, B: Analytical Technologies in the Biomedical and Life Sciences*. 2013;917-918
- [3] Beyene T. Veterinary drug residues in food-animal products its risk factors and potential effects on public health. *Journal of Veterinary Science Technology*. 2016;7(1):1-7
- [4] Gómez-Ramírez P, Jiménez-Montalbán PJ, Delgado D, Martínez-López E, María-Mojica P, Godino A, et al. Development of a QuEChERS method for simultaneous analysis of antibiotics in carcasses for supplementary feeding of endangered vultures. *Science of the Total Environment*. 2018;626:319-327
- [5] Mookantsa SOS, Dube S, Nindi MM. Development and application of a dispersive liquid-liquid micro-extraction method for the determination of tetracyclines in beef by liquid chromatography mass spectrometry. *Talanta*. 2016;148:321-328
- [6] Gao J, Wang H, Qu J, Wang H, Wang X. Development and optimization of a naphthoic acid-based ionic liquid as a “non-organic solvent micro-extraction” for the determination of tetracycline antibiotics in milk and chicken eggs. *Food Chemistry*. 2017;215:138-148
- [7] Pyrzynska K. Novel selective sorbents for solid-phase extraction. *Chemist-Analyst*. 2003;48:781-795
- [8] Poole CF. New trends in solid-phase extraction. *Trends in Analytical Chemistry*. 2003;22:362-373
- [9] Fontanales N, Marcé RM, Borrull F. New materials in sorptive extraction techniques for polar compounds. *Journal of Chromatography, A*. 2007;1152:14-31
- [10] Fang GZ, He JX, Wang S. Multiwalled carbon nanotubes as sorbent for on-line coupling of solid-phase extraction to high-performance liquid chromatography for simultaneous determination of 10 sulfonamides in eggs and pork. *Journal of Chromatography A*. 2006;1127:12-17
- [11] Zheng M, Zhang M, Peng G, Feng Y. Monitoring of sulfonamide antibacterial residues in milk and egg by polymer monolith microextraction coupled to hydrophilic interaction chromatography/mass spectrometry. *Analytica Chimica Acta*. 2008;625:160
- [12] Herrera-Herrera AV, González-Curbelo MA, Hernández-Borges J, Rodríguez-Delgado MA. Carbon nanotubes applications in separation science: A review. *Analytica Chimica Acta*. 2012;734:1-30
- [13] Ravelo-Pérez LM, Herrera-Herrera AV, Hernández-Borges J, Rodríguez-Delgado MA. Carbon nanotubes: Solid-phase extraction. *Journal of Chromatography A*. 2010;1217:2618-2641
- [14] Scida K, Stege PW, Haby G, Messina GA, García CD. Recent applications of carbon-based nanomaterials in analytical chemistry: critical review. *Analytica Chimica Acta*. 2011;691:6-17

- [15] Nollet LML. Food Analysis by HPLC. 2nd revised and expanded ed. Marcel Dekker, Inc.; pp. 621-670
- [16] Hauser AR. Antibiotics Basics for Clinicians: The ABCs of Choosing the Right Antibacterial Agent. 2nd ed. Philadelphia, PA, USA: Lippincott Williams & Wilkins; 2007
- [17] Manivasagan P, Venkatesan J, Sivakumar K, Kim SK. Marine actinobacterial metabolites: Current status and future perspectives. *Microbiological Research*. 2013;**168**:311-332
- [18] Thiele-Bruhn S, Seibicke T, Schulden HR, Leinweber P. Sorption of pharmaceutical antibiotics on whole soils and particle size fractions. *Journal of Environmental Quality*. 2004;**33**:1331-1342
- [19] Fatta-Kassinos D, Meric S, Nikolaou A. Pharmaceutical residues in environmental waters and wastewater: Current state of knowledge and future research. *Analytical and Bioanalytical Chemistry*. 2011;**399**:251-275
- [20] Shao B, Chen D, Zhang J, Wu Y, Sun C. Determination of 76 pharmaceutical drugs by liquid chromatography-tandem mass spectrometry in slaughterhouse wastewater. *Journal of Chromatography A*. 2009;**1216**:47
- [21] Zhang G, Fang B, Liu Y, Wang X, Xu L, Zhang Y. Development of a multi-residue method for fast screening and confirmation of 20 prohibited veterinary drugs in feedstuffs by liquid chromatography tandem mass spectrometry. *Journal of Chromatography B*. 2013;**936**:10
- [22] Beyene T, Tesega B. Rational veterinary drug use: Its significance in public health. *Journal of Veterinary Medicine and Animal Health*. 2014;**6**:302-308
- [23] Samanidou V, Nisyriou S. Multi-residue methods for confirmatory determination of antibiotics in milk. *Journal of Separation Science*. 2008;**31**:2068-2090
- [24] Blanco G, Junza A, Barrón D. Food safety in scavenger conservation: Diet-associated exposure to livestock pharmaceuticals and opportunist mycoses in threatened Cinereous and Egyptian vultures. *Ecotoxicology and Environmental Safety*. 2017;**135**:292-301
- [25] Blanco G, Junza A, Barrón D. Occurrence of veterinary pharmaceuticals in golden eagle nestlings: Unnoticed scavenging on livestock carcasses and other potential exposure routes. *Science of the Total Environment*. 2017;**586**:355-361
- [26] Pitarch A, Gil C, Blanco G. Oral mycoses in avian scavengers exposed to antibiotics from livestock farming. *Science of the Total Environment*. 2017;**605-606**:139-146
- [27] Jing T, Gaol XD, Wang P, Wang Y, Lin YF, Hu XZ, et al. Determination of trace tetracycline antibiotics in foodstuffs by liquid chromatography-tandem mass spectrometry coupled with selective molecular-imprinted solid-phase extraction. *Analytical and Bioanalytical Chemistry*. 2009;**393**:2009-2018
- [28] Margalida A, Bogliani G, Bowden CGR, Donazar JA, Genero F, Gilbert M, et al. Science and regulation, One health approach to use of veterinary pharmaceuticals. *Science*. 2014;**346**:1296-1298
- [29] Lu YK, Zhang JQ, Guo YZ, Zhang W, Sun HW. Determination of tetracyclines residues in egg, milk, and milk powder by online coupling of a precolumn packed with molecular imprinted hybrid composite materials to RPHPLC-UV. *Journal of Liquid Chromatography & Related Technologies*. 2015;**38**:1-7

- [30] Hernández-Mesa M, Carbonell-Rozas L, Cruces-Blanco C, García-Campaña AM. A high-throughput UHPLC method for the analysis of 5-nitroimidazole residues in milk based on salting-out assisted liquid-liquid extraction. *Journal of Chromatography B*. 2017;**1068-1069**:125-130
- [31] Jank L, Martins MT, Arsand JB, Motta TMC, Hoff RB, Barreto F, et al. High-throughput method for macrolides and lincosamides antibiotics residues analysis in milk and muscle using a simple liquid-liquid extraction technique and liquid chromatography-electrospray-tandem mass spectrometry analysis (LC-MS/MS). *Talanta*. 2015;**144**:686-695
- [32] Moreno-González D, Rodríguez-Ramírez R, del Olmo-Iruela M, García-Campaña AM. Validation of a new method based on salting-out assisted liquid-liquid extraction and UHPLC-MS/MS for the determination of betalactam antibiotics in infant dairy products. *Talanta*. 2017;**167**:493-498
- [33] Yu Y, Tao Y, Chen D, Wang Y, Huang L, Peng D, et al. Development of a high performance liquid chromatography method and a liquid chromatography-tandem mass spectrometry method with the pressurized liquid extraction for the quantification and confirmation of sulfonamides in the foods of animal origin. *Journal of Chromatography B*. 2011;**879**:2653-2662
- [34] Sichilongo KF, Muckoya VA, Nindi MM. A rapid and sensitive LC-MS/MS method for the determination of multi-class residues of antibiotics in chicken liver. *South African Journal of Chemistry*. 2015;**68**:1-6
- [35] Karami-Osboo R, Hossein Shojaee M, Miri R, Kobarfard F, Javidnia K. Simultaneous determination of six fluoroquinolones in milk by validated QuEChERS-DLLME HPLC/FLD. *Analytical Methods*. 2014;**6**(15):5632-5638
- [36] Arroyo-Manzanares N, Gamiz-Gracia L, Garcia Campana AM. Alternative sample treatments for the determination of sulfonamides in milk by HPLC with fluorescence detection. *Food Chemistry*. 2014;**143**:459-464
- [37] Tajabadi F, Ghambarian M, Yamini Y, Yazdanfar N. Combination of hollow fiber liquid phase microextraction followed by HPLC-DAD and multivariate curve resolution to determine antibacterial residues in foods of animal origin. *Talanta*. 2016;**160**:400-409
- [38] Xu H, Mi HY, Guan MM, Shan HY, Fei Q, Huan YF, et al. Residue analysis of tetracyclines in milk by HPLC coupled with hollow fiber membranes-based dynamic liquid-liquid micro-extraction. *Food Chemistry*. 2017;**232**:198-202
- [39] Shariati S, Yamini Y, Esrafil A. Carrier mediated hollow fiber liquid phase micro-extraction combined with HPLC-UV for preconcentration and determination of some tetracycline antibiotics. *Journal of Chromatography B*. 2009;**877**:393-400
- [40] Sehati N, Dalali N, Soltanpour S, Dorraji MSS. Extraction and pre-concentration of tylosin from milk samples through functionalized TiO<sub>2</sub> nanoparticles reinforced with a hollow fiber membrane as a novel solid/liquid phase micro-extraction technique. *Journal of Separation Science*. 2014;**37**:2025-2031
- [41] da Costa RP, Spisso BF, Pereira MU, Monteiro MA, Ferreira RG, da Nobrega AW. Innovative mixture of salts in the quick, easy, cheap, effective, rugged, and safe method for the extraction of residual macrolides in milk followed by analysis with liquid chromatography and tandem mass spectrometry.

Journal of Separation Science. 2015;**38**:3743-3749

[42] Wang YL, Liu Z, Ren J, Guo BH. Development of a method for the analysis of multiclass antibiotic residues in milk using QuEChERS and liquid chromatography-tandem mass spectrometry. *Foodborne Pathogens and Disease*. 2015;**12**(8):693-703

[43] Li Y, Chen Z, Wen S, Hou X, Zhang R, Ma M. Multiresidue Determination of Antibiotics in Preserved Eggs Using a QuEChERS-Based Procedure by Ultrahigh-Performance Liquid Chromatography Tandem Mass Spectrometry. *Acta Chromatographica*; 2018;**30**(1):9-16

[44] Anastassiades M, Lehotay S. Fast and easy multiresidue method employing acetonitrile extraction/partitioning and “dispersive solid-phase extraction” for the determination of pesticide residues in produce. *Journal of AOAC International*. 2003;**86**:412-431

[45] Berendsen BJA, Stolker LAAM, Nielen MWF. Selectivity in the sample preparation for the analysis of drug residues in products of animal origin using LC-MS. *TrAC Trends in Analytical Chemistry*. 2013;**43**:229-239

[46] Machado SC, Landin-Silva M, Mai PP, Rath S, Martins I. QuEChERS-HPLC-DAD method for sulphonamides in chicken breast. *Brazilian Journal of Pharmaceutical Sciences*. 2013;**49**(1):155-166

[47] Sharifi V, Abbasi A, Nosrati A. Application of hollow fiber liquid phase micro-extraction and dispersive liquid-liquid micro-extraction techniques in analytical toxicology. *Journal of Food and Drug Analysis*. 2016;**24**:264-276

[48] Quigley A, Cummins W, Connolly D. Dispersive liquid-liquid micro-extraction in the analysis of milk and

dairy products: A review. *Journal of Chemistry*. 2016;**2016**:12

[49] Lopez-Darias J, German-Hernandez M, Pino V, Afonso AM. Dispersive liquid-liquid micro-extraction versus single-drop micro-extraction for the determination of several endocrine-disrupting phenols from seawaters. *Talanta*. 2010;**80**(5):1611-1618

[50] Hadjmohammadi M, Karimiyan H, Sharifi V. Hollow fibre-based liquid phase micro-extraction combined with high performance liquid chromatography for the analysis of flavonoids in *Echinophora platyloba* DC and *Mentha piperita*. *Food Chemistry*. 2013;**141**:731-735

[51] Rezaee M, Assadi Y, Milani Hosseini MR, Aghaee E, Ahmadi F, Berijani S. Determination of organic compounds in water using dispersive liquid-liquid microextraction. *Journal of Chromatography A*. 2006;**1116**:1-9

[52] Al-Saidi HM, Emara AA. The recent developments in dispersive liquid-liquid micro-extraction for pre-concentration and determination of inorganic analytes. *Journal of Chemistry*. 2013;**11**:1343-1351

[53] Karami-Osboo R, Miria R, Javidnia K, Kobarfard F. Simultaneous chloramphenicol and florfenicol determination by a validated DLLME-HPLC-UV method in pasteurized Milk. *Iranian Journal of Pharmaceutical Research*. 2016;**15**:361-368

[54] Ghambarian M, Yamini Y, Esrafil A. Developments in hollow fiber based liquid-phase micro-extraction: Principles and applications. *Microchimica Acta*. 2012;**177**:271-294

[55] Gjelstad A, Pedersen BS. Perspective: Hollow fibre liquid-phase micro-extraction—Principles, performance, applicability, and future directions. *Scientia Chromatographica*. 2013;**5**:181-189



- [56] Song X, Zhou T, Liu Q, Zhang M, Meng C, Li J, et al. Molecularly imprinted solid-phase extraction for the determination of ten macrolide drugs residues in animal muscles by liquid chromatography-tandem mass spectrometry. *Food Chemistry*. 2016;**208**:169-176
- [57] Wang GN, Zhang L, Song YP, Liu JX, Wang JP. Application of molecularly imprinted polymer based matrix solid phase dispersion for determination of fluoroquinolones, tetracyclines and sulfonamides in meat. *Journal of Chromatography B*. 2017;**1065-1066**:104-111
- [58] Feng MX, Wang GN, Yang K, Liu HZ, Wang JP. Molecularly imprinted polymer-high performance liquid chromatography for the determination of tetracycline drugs in animal derived foods. *Food Control*. 2016;**69**:171-176
- [59] Sun X, Wang J, Li Y, Yang J, Jina J, Shaha SM, et al. Novel dummy molecularly imprinted polymers for matrix solid-phase dispersion extraction of eight fluoroquinolones from fish samples. *Journal of Chromatography A*. 2014;**1359**:1-7
- [60] Wang H, Wang R, Han Y. Preparation of molecular imprinted microspheres based on inorganic-organic co-functional monomer for miniaturized solid-phase extraction of fluoroquinolones in milk. *Journal of Chromatography B*. 2014;**949-950**:24-29
- [61] Hou J, Li H, Wang L, Zhang P, Zhou T, Ding H, et al. Rapid microwave-assisted synthesis of molecularly imprinted polymers on carbon quantum dots for fluorescent sensing of tetracycline in milk. *Talanta*. 2016;**146**:34-40
- [62] Huang JF, Lin B, Yu QW, Feng YQ. Determination of fluoroquinolones in eggs using in-tube solid-phase microextraction coupled to high-performance liquid chromatography. *Analytical and Bioanalytical Chemistry*. 2006;**384**:1228-1235
- [63] Vinas P, Campillo N, López-García I, Hernández-Córdoba M. Dispersive liquid-liquid microextraction in food analysis. A critical review microextraction techniques. *Analytical and Bioanalytical Chemistry*. 2014;**406**:2067-2099
- [64] Zhu J, Snow DD, Cassada DA, Monson SJ, Spalding RF. Analysis of oxytetracycline, tetracycline, and chlortetracycline in water using solid-phase extraction and liquid chromatography-tandem mass spectrometry. *Journal of Chromatography. A*. 2001;**928**:177



# Contribution of Infrared Spectroscopy to the Vibrational Study of Ethylenediammonium Chloride Thiocyanate: (C<sub>2</sub>H<sub>10</sub>N<sub>2</sub>) (Cl NCS)

*Sahel Karoui and Slaheddine Kamoun*

## Abstract

The C<sub>2</sub>H<sub>10</sub>N<sub>2</sub> Cl NCS (EDCT) compound is characterized by using infrared spectroscopy. The infrared spectrum of the title compound was recorded (400–4000 cm<sup>-1</sup>) at room temperature and discussed, essentially in terms of vibrational modes of [C<sub>2</sub>H<sub>10</sub>N<sub>2</sub>]<sup>2+</sup> cations and [SCN]<sup>-</sup> and [Cl]<sup>-</sup> anions. Ethylenediammonium thiocyanate chloride crystallizes, at room temperature, in the triclinic system, space group P1 (C<sub>1</sub>). The entities [C<sub>2</sub>H<sub>10</sub>N<sub>2</sub>]<sup>2+</sup>, [SCN]<sup>-</sup> and [Cl]<sup>-</sup> occupy sites of symmetry (C<sub>1</sub>). Several ground state thermodynamic parameters were calculated using the ab initio Hartree-Fock (HF) and DFT (B3LYP) methods with 6-31++G (d, p) and 6-311++G (d, p) basic sets such as vibration frequencies, rotation constants, and optimized molecular geometry. The comparison between the theoretical and experimental infrared spectrum showed good agreement.

**Keywords:** ethylenediammonium chloride thiocyanate, IR, vibrational spectra, DFT calculations

## 1. Introduction

This chapter is devoted to the characterization of C<sub>2</sub>H<sub>10</sub>N<sub>2</sub> Cl NCS by infrared vibrational spectroscopy. These studies make it possible to highlight the structural analogies and to possibly provide some additional information to those obtained by X-ray diffraction. In this chapter, we used group theory; indeed, this valuable tool allows both to count the normal vibration modes of vibration of a crystal and to describe these vibrations in symmetrical coordinate terms. In addition, an attempt is made to assign the various modes of vibration to all the bands that have appeared. It is based on predictions theories and previous work carried out on similar compounds. Infrared is a research tool can also provide exquisite structural insights into the molecule and characterizes the vibrational modes of the molecules and has enfolded within it much information on chemical structure [1]. The combined use of FT-IR spectroscopy extracts most of the obtainable information and these are the popular tools in the chemist and physicist. Amine, amino acid and Schiff bases [2–6] have recently been the focus of coordination chemists due to their

preparative accessibilities, structural varieties, and varied denticities. With those purposes, first, the EDCT was synthesized [7] and then characterized it by Infrared Spectroscopy. Simultaneously, to obtain the ground state optimized geometries and the vibrational wavenumbers of the different normal modes, we carried out the ab initio HF and DFT calculations. Here, the hybrid B3LYP method was used together with the 6-31++G (d, p) and 6-311++G (d, p) basis sets [8].

## 2. Experimental details

### 2.1 Synthesis

The title compound has been obtained by mixing, in stoichiometric proportions, a solution of ethylenediamine, a freshly prepared solution of thiocyanic acid HSCN and a solution of potassium halide. KX (X = Cl) [7].

### 2.2 IR spectroscopy

Infrared absorption spectrum was recorded at room temperature in the 400–4000  $\text{cm}^{-1}$  frequency range on a Perkin-Elmer spectrometer equipped with a Universal ATR Accessory (UATR).

### 2.3 Computational details

Numerous studies [9–12] have shown that the method DFT-B3LYP in combination with the bases 6-31++G (d, p) and 6-311++G (d, p) allowed to determine with precision energies, molecular structures and infrared vibratory frequencies. In the ground state the molecular structure of the  $\text{C}_2\text{H}_{10}\text{N}_2\text{Cl}$  NCS (EDCT) phase calculated was optimized by the use of the DFT/B3LYP methods with the methods 6-31++G (d, p) and 6-311++G (d, p) base set, and the calculated optimized structure was used in vibrational frequency calculations. The calculated harmonic vibratory frequencies and the minimal energy of the geometric structure were scaled by (B3LYP) with the base set 6-31++G (d, p) and 6-311++G (d, p). HF/DFT calculations for EDCT are performed using GAUSSIAN 03W program [13, 14]. On the other hand, the energies of the frontier orbital's were used to calculate the gap energy values and some interesting descriptors in order to predict their reactivities and behaviors at the same level of theory [14–17].

## 3. Results and discussion

### 3.1 Molecular geometry

The structure of the EDCT belongs to  $C_i$  point group symmetry and its molecular structure is obtained from GAUSSIAN 03W and GAUSSVIEW programs are shown in **Figure 1**. The molecule contains one diprotonated ethylenediammonium cation, one  $\text{Cl}^-$  and one  $\text{SCN}^-$  anions. The comparative optimized structural parameters such as bond lengths and bond angles are presented in **Table 1**. The comparative graphs of bond lengths and bond angles of ethylenediammonium chloride thiocyanate for two sets are presented in **Figures 2** and **3** respectively. Most of the optimized bond lengths are slightly higher than the experimental values, depending on the theoretical values, because the theoretical calculations belong to isolated molecules in the gas phase and the experimental results to solid state molecules. The

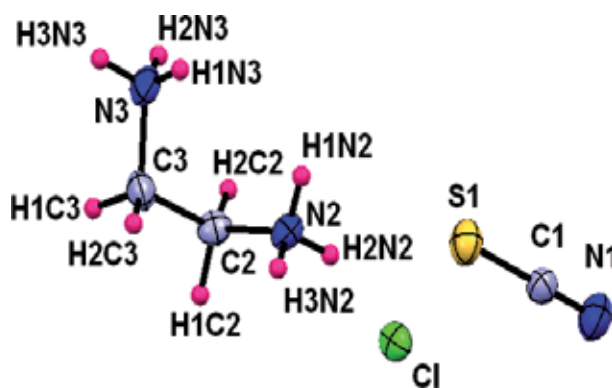


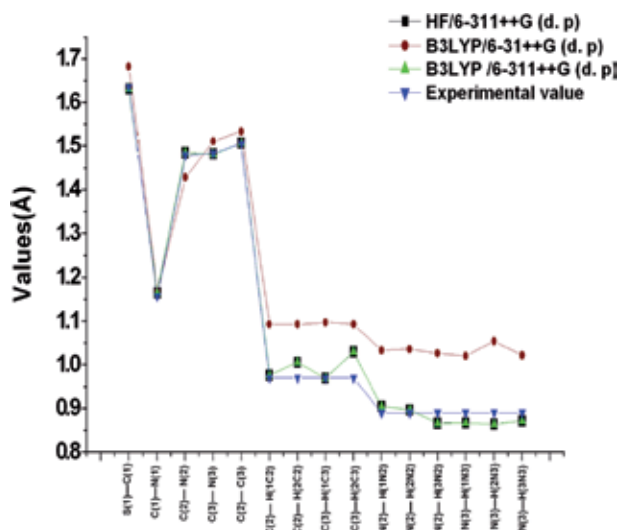
**Figure 1.**  
 Molecular structure of ethylenediammonium chloride thiocyanate.

Geometrical parameters	Methods			Experimental value [12]
	HF/6-311++G (d. p)	B3LYP/6-31++G (d. p)	B3LYP/6-311++G (d. p)	
<b>Bond length (Å)</b>				
S(1)–C(1)	1.6314	1.6324	1.6324	1.6358(12)
C(1)–N(1)	1.1651	1.1687	1.1651	1.1573(16)
C(2)–N(2)	1.4847	1.4284	1.4847	1.4798(14)
C(3)–N(3)	1.4817	1.5107	1.4817	1.4834(15)
C(2)–C(3)	1.5066	1.5334	1.5066	1.5054(15)
C(2)–H(1C2)	0.9763	1.0926	0.9763	0.9700
C(2)–H(2C2)	1.0059	1.0927	1.0059	0.9700
C(3)–H(1C3)	0.9694	1.0971	0.9694	0.9700
C(3)–H(2C3)	1.0299	1.0930	1.0299	0.9700
N(2)–H(1 N2)	0.9048	1.0333	0.9048	0.8900
N(2)–H(2N2)	0.8967	1.0357	0.8967	0.8900
N(2)–H(3N2)	0.8660	1.0264	0.8660	0.8900
N(3)–H(1N3)	0.8665	1.0202	0.8665	0.8900
N(3)–H(2N3)	0.8639	1.0540	0.8639	0.8900
N(3)–H(3N3)	0.8715	1.0219	0.8715	0.8900
<b>Bond angle (°)</b>				
N(1)–C(1)–S(1)	173.60	170.71	171.76	178.48(11)
N(2)–C(2)–C(3)	114.00	115.16	114.16	113.06(9)
N(3)–C(3)–C(2)	113.46	113.75	113.72	112.98(9)
C(2)–N(2)–H(1N2)	109.86	111.45	111.44	109.5
C(2)–N(2)–H(2N2)	107.14	111.99	112.00	109.5
C(2)–N(2)–H(3N2)	110.63	112.81	112.83	109.5

Geometrical parameters	Methods			
	HF/6-311++G (d, p)	B3LYP/6-31++G (d, p)	B3LYP/6-311++G (d, p)	Experimental value [12]
C(3)-N(3)-H(1N3)	112.06	113.78	113.77	109.5
C(3)-N(3)-H(2N3)	111.40	112.73	112.77	109.5
C(3)-N(3)-H(3N3)	107.78	107.37	107.38	109.5
N(2)-C(2)-H(1C2)	107.63	106.91	106.89	109.0
N(2)-C(2)-H(2C2)	105.68	105.49	105.65	109.0
N(3)-C(3)-H(2C3)	106.94	107.64	107.64	109.0
N(3)-C(3)-H(1C3)	107.95	105.96	105.94	109.0
C(2)-C(3)-H(1C3)	107.81	108.17	108.14	109.0
C(2)-C(3)-H(2C3)	111.33	111.69	111.62	109.0
C(3)-C(2)-H(1C2)	111.34	111.77	111.73	109.0
C(3)-C(2)-H(2C2)	107.22	108.54	108.49	109.0
H(1C2)-C(2)-H(2C2)	109.25	107.86	107.81	107.8
H(2C3)-C(3)-H(1C3)	110.86	108.27	108.30	107.8
H(1N2)-N(2)-H(2N2)	106.29	103.41	103.45	109.5
H(1N2)-N(2)-H(3N2)	108.76	108.24	108.27	109.5
H(2N2)-N(2)-H(3N2)	108.54	108.53	108.59	109.5
H(1N3)-N(3)-H(2N3)	112.15	112.78	112.80	109.5
H(1N3)-N(3)-H(3N3)	106.29	103.84	103.89	109.5
H(2N3)-N(3)-H(3N3)	107.41	107.83	107.88	109.5
N(2)-C(2)-C(3)-N(3)	74.53	74.32	74.36	72.09 (12)

**Table 1.**

Optimized geometrical parameters for ethylenediammonium chloride thiocyanate computed at HF/6-311++G (d, p), B3LYP/6-31++G (d, p) and B3LYP/6-311++G(d, p) basis sets.

**Figure 2.**

Bond length differences between theoretical (HF and DFT) approaches.

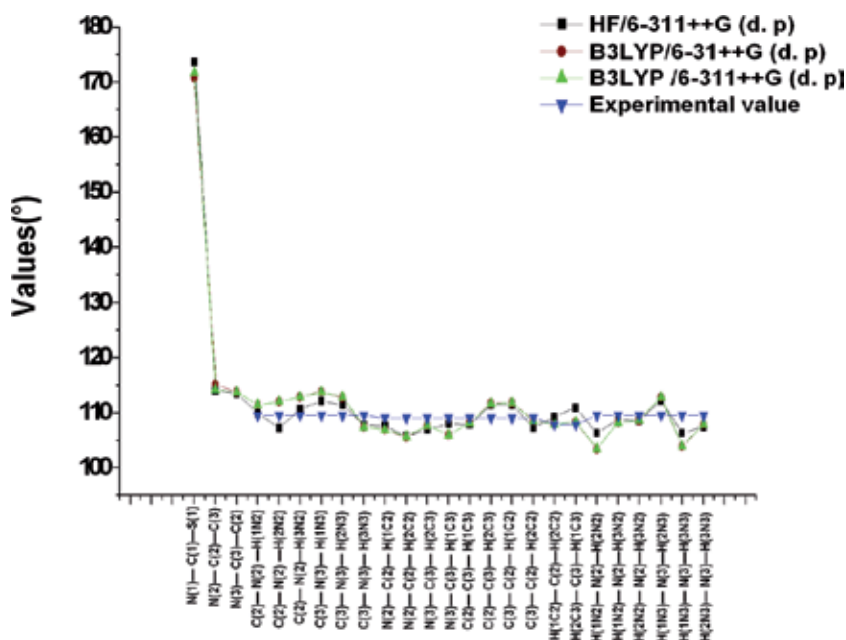


**Figure 3.**  
 Bond angle differences between theoretical (HF and DFT) approaches.

angles and binding lengths of B3LYP are compared with those of HF, the formers are generally larger than later and the values calculated by B3LYP are well correlated with the experimental data. The parameters (the vibration frequencies and the thermodynamic properties) represent a good approximation. The data presented in **Table 1** show that the theoretical HF and DFT levels (B3LYP/6-311++G (d, p)) generally estimate the same values for some link lengths and angles. The calculated C—N bond lengths are found same at two positions (C2—N2 and C3—N3) is 1.4847 and 1.5066 Å (HF and DFT), 0.0049 and 0.0012 Å, respectively, differed from the experimental value 1.4798(14) and 1.5054(15) Å [15–17]. The  $[\text{C}_2\text{H}_{10}\text{N}_2]^{2+}$  dication shows an eclipsed conformation. The calculated N—C—C—N torsion angle is 74.53° (HF and DFT), 2.44° differed from the experimental value 72.09(12)° [7]. The thiocyanate ion, present as a monodentate ligand, is almost linear. The calculated angle is 173.60° but the experimental value 178.48 (11)° and an average calculated and experimental C—S and C—N bond lengths are 1.6314 and 1.1651, 1.6358 (12) and 1.1573 (16) Å [7], respectively.

### 3.2 Vibrational analysis

#### 3.2.1 Contribution of IR spectrometry to the vibrational study of $\text{C}_2\text{H}_{10}\text{N}_2 \text{Cl NCS}$

##### 3.2.1.1 Theoretical analysis of $\text{C}_2\text{H}_{10}\text{N}_2 \text{Cl NCS}$ vibrations

The factor group method of classifying fundamental vibrational modes of crystals, as developed by Bhagavantam and Venkatarayudu [18], is certainly the most powerful method of treating  $\text{C}_2\text{H}_{10}\text{N}_2 \text{Cl NCS}$  crystal structure. The unit cell of  $\text{C}_2\text{H}_{10}\text{N}_2 \text{Cl NCS}$  contains 18 atoms which correspond to 54 degrees of vibrational freedom. To simplify the discussion of the IR data, the vibrational modes will be considered in two groups: the internal modes of  $\text{SCN}^-$  anions and  $(\text{C}_2\text{H}_{10}\text{N}_2)^{2+}$  cations. Ethylenediammonium thiocyanate chloride crystallizes, at room temperature,

in the triclinic system, space group P1 ( $C_1$ ). The entities  $[C_2H_{10}N_2]^{2+}$ ,  $[SCN]^-$  and  $[Cl]^-$  occupy sites of symmetry ( $C_1$ ).

### 3.2.1.2 Counting by the factor group method

The number of normal modes of vibration of the group  $SCN^-$  isolated of ideal symmetry  $C_{\infty v}$  is given by the representation:

$$\Gamma_{SCN} = 2A_1 + E_1 \quad (1)$$

While that of an isolated group  $[C_2H_{10}N_2]^{2+}$  of symmetry  $C_{2v}$  is given by the irreducible representation:

$$\Gamma_{[C_2H_{10}N_2]^{2+}} = 11A_1 + 8A_2 + 9B_1 + 8B_2 \quad (2)$$

The correlation diagram is given in **Table 2**. The counting of the main vibrations of this compound by the factor group method leads to the following results:

- Overall vibration representation:  $\Gamma_{(ni)} = 54Ag + 54Au$
- Translation modes:  $\Gamma_{(T')} = 9Ag + 9Au$
- Rotation mode:  $\Gamma_{(R')} = 5Ag + 5Au$
- The representation of the internal vibrations is:  $\Gamma_{(ni)} = 40Ag + 40Au$

The analysis in terms of internal vibrations, rotation  $R'$  and translation  $T'$ , is given in **Table 3** with their activities in IR.

### 3.2.1.3 Enumeration by the site group method

This method was used in order to have a detailed description of the symmetry and the nature of the internal vibrations (deformation in the plane or out of the plane, symmetrical or asymmetrical elongation, torsion, etc.).

#### 3.2.1.3.1 Vibrations of $[C_2H_{10}N_2]^{2+}$ in group ( $C_1$ )

To describe the vibrations of the organic cation, we considered separately the vibrations of the groups ( $-NH_3$ ) and ( $-CH_2-$ ) and the skeleton  $(C_2N_2)^{2+}$ .

##### a. Description of the normal modes of vibration of the grouping ( $\text{—NH}_3$ )

The group ( $\text{—NH}_3$ ) supposed free, has the symmetry  $3m$  ( $C_{3v}$ ), it presents nine internal vibrations schematized in **Figure 4**.

$$2A_1 + A_2 + 3E \quad (3)$$

Each group ( $\text{—NH}_3$ ) occupies a site ( $C_1$ ) in the cation. The use of correlation tables allows us to describe the symmetry of these vibrations in the molecular group of the cation (**Table 4**). The result is:

$$\Gamma_{NH_3} = 18Ag + 18Au \quad (4)$$



	Molecular group (G.M)	Group of site (G.S)	Factor group (G.F)
	$C_{\infty v}$	$C_1$	$C_1$
Anion (SCN) <sup>-</sup> ( $C_{\infty v}$ )	$2A_1 = \Sigma^+ (v_1, v_2)$ $E_1 = \Pi (\delta)$	$4A$	$4A_g (v_1, 2\delta, v_2)$ $4A_u (v_1, 2\delta, v_2)$

	Molecular group (G.M)	Group of site (G.S)	Factor group (G.F)
	$C_{2v}$	$C_1$	$C_1$
Cation ( $C_2H_{10}N_2$ ) <sup>2+</sup> ( $C_1$ )	$11A_1$ $8A_2$ $9B_1$ $8B_2$	$36A$	$36A_g$ $36A_u$

**Table 2.**  
 Internal mode correlation diagrams of  $C_2H_{10}N_2$  Cl NCS in  $C_i$ .

b. Description of the normal modes of vibration of the grouping ( $\text{—CH}_2\text{—}$ )

The group ( $\text{—CH}_2\text{—}$ ) supposed free, has the symmetry  $mm_2$  ( $C_{2v}$ ), it has six internal vibrations schematized in **Figure 5**.

$$2A_1 + A_2 + B_1 + 2B_2 \quad (5)$$

The ( $\text{—CH}_2\text{—}$ ) groups occupy  $E(C_1)$  sites in the cation, the correlation method allows us to determine their vibrational symmetry in the  $C_1$  molecular group of the cation (**Table 5**). The result is:

$$\Gamma_{CH_2} = 12A_g + 12A_u \quad (6)$$

$C_i$	$n_i$	$n_i$	$R'$			$T'$			Activity				
			EDA ( $C_{2v}$ )	SCN <sup>-</sup> ( $C_{\infty v}$ )	Cl <sup>-</sup> ( $C_1$ )	EDA ( $C_{2v}$ )	SCN <sup>-</sup> ( $C_{\infty v}$ )	Cl <sup>-</sup> ( $C_1$ )	EDA ( $C_{2v}$ )	SCN <sup>-</sup> ( $C_{\infty v}$ )	Cl <sup>-</sup> ( $C_1$ )	IR	R
<b>Ag</b>	54	36	4	0	3	2	0	3	3	3	3	-	+
<b>Au</b>	54	36	4	0	3	2	0	3	3	3	3	+	-

**Table 3.**  
 Enumeration of internal and external modes of  $C_2H_{10}N_2$  Cl NCS in  $C_i$ .

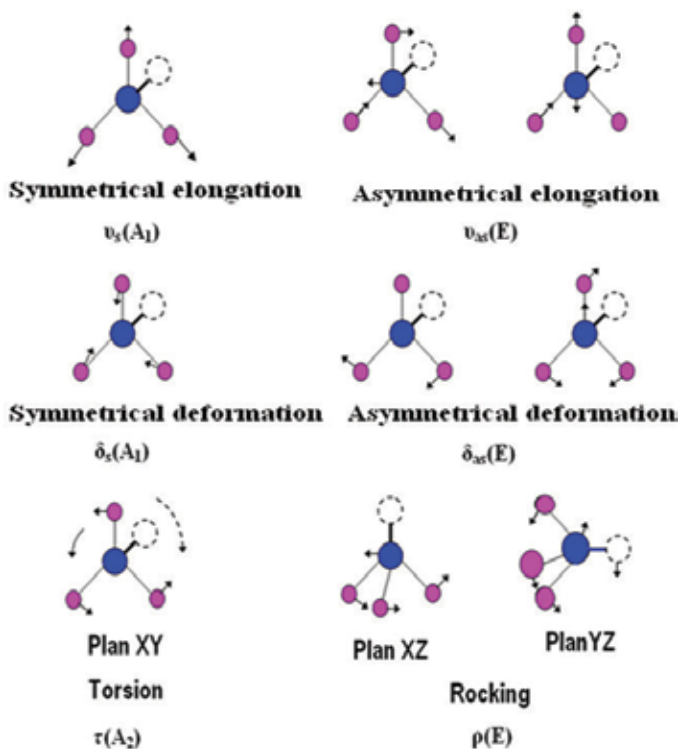


**Figure 4.**  
Normal modes of vibration of groups ( $-NH_3$ ) of symmetry  $3m$  ( $C_{3v}$ ).

c. Description of the vibration modes of the skeleton ( $NC_2N$ )

To describe the vibrations of the skeleton ( $NC_2N$ ), the corresponding symmetrical coordinates as a function of the internal coordinates have been calculated as follows:

- Increased C—N bonds:  $\Delta r_i$  ( $i = 1, 2$ )
- Increased C—C bonds:  $\Delta r_3$
- Increase of the CCN bond angles:  $\Delta \varphi_i$  ( $i = 1, 2$ )
- Torsion of DC links:  $\tau_{CC}$

GM ( $-NH_3$ )	( $-NH_3$ )	GM ( $-NH_3$ )	GS ( $-NH_3$ )	GF (Crystal)
$3m C_{3v}$	$m C_s$	$2mm C_{2v}$	$C_1$	$C_i$
$(\nu_s, \delta_s) 2A_1$ $(\delta_t) A_2$ $(\nu_s, \delta_s, \delta_t) 3E$	$5A'$ $4A''$	$5A_1$ $4A_2$ $5B_1$ $4B_2$	$18A$	$18Ag (2\nu_s, 2\delta_s, 4\nu_s, 4\delta_s, 2\delta_t, 4\delta_t)$ $18Au (2\nu_s, 2\delta_s, 4\nu_s, 4\delta_s, 2\delta_t, 4\delta_t)$

**Table 4.**  
Internal modes of ( $-NH_3$ ) in ( $C_i$ ).

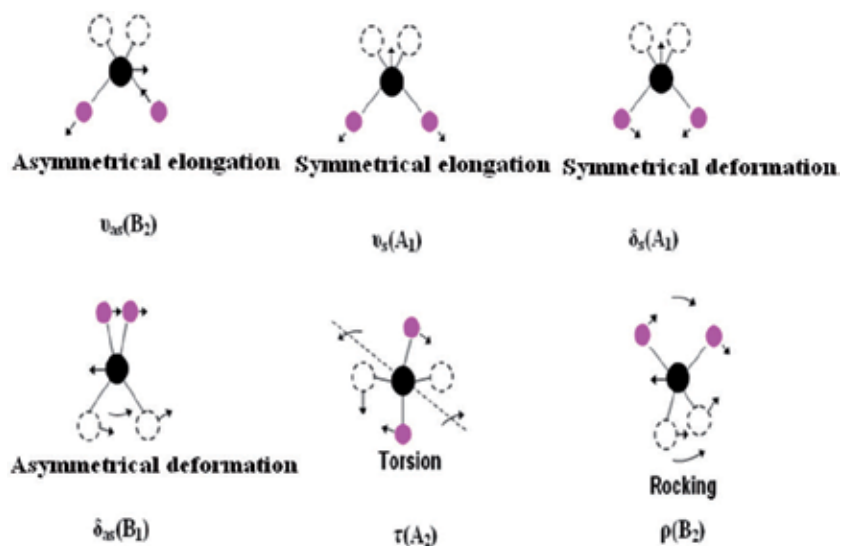


**Figure 5.**  
 Normal modes of vibration of  $(-CH_2-)$  of symmetry  $mm_2$ ,  $(C_{2v})$ .

The number of coordinates is  $6 = 3N - 6$  ( $N$ : number of atoms in the backbone, here  $N = 4$ ). Using the transforms of each coordinate under the symmetry operations of the point group  $C_s$  corresponding to the cation, six symmetrized coordinates were calculated (Table 6). At each coordinate a vibration mode has been assigned. These vibrations are shown schematically in Figure 6. The description of the normal modes of the  $NC_2N$  backbone and their activities in IR are shown in Table 7. The irreducible representation of the internal vibration modes of the skeleton in  $C_i$  is:

$$\text{Skeletal} = 6A_g + 6A_u \quad (7)$$

d. Description of the vibration modes of  $SCN^-$

The internal vibrations of the  $SCN^-$  anion have already been studied [2], they are described in terms of symmetrized coordinates as a function of the internal coordinates. These modes are divided in the group  $C_{\infty v}$  as follows:

$$\Gamma_{(SCN^-)} = 2A_1(\Sigma^+) + E_1(\Pi) \quad (8)$$

GM $(-CH_2)$	$(-CH_2)$	GM $(-CH_2)$	GS $(-CH_2)$	GF (Crystal)
$mm_2 C_{2v}$	$m C_s$	$mm_2 C_{2v}$	$E C_1$	$C_i$
$(\nu_s, \delta_s) 2A_1$ $(\delta_t) A_2$ $(\delta_a) B_1$ $(\nu_a, \delta_a) B_2$	$3A'$ $3A''$	$3A_1$ $3A_2$ $3B_1$ $3B_2$	$12A$	$12A_g (2\nu_s, 2\delta_s, 2\nu_a, 2\delta_a, 2\delta_t, 2\delta_a)$ $12A_u (2\nu_s, 2\delta_s, 2\nu_a, 2\delta_a, 2\delta_t, 2\delta_a)$

**Table 5.**  
 Internal modes of  $(-CH_2-)$  in  $(C_i)$ .

Class	Symmetric coordinate	Vibration modes
A <sub>1</sub>	$S_{1\ 1}^A = \frac{1}{\sqrt{2}}(\Delta r_1 + \Delta r_2)$ $S_{2\ 1}^A = \Delta r_3$ $S_{3\ 1}^A = \frac{1}{\sqrt{2}}(\Delta \varphi_1 + \Delta \varphi_2)$	Symmetrical elongation C-N: $\nu_s$ (C-N) Symmetrical elongation C-C: $\nu_s$ (C-C) Symmetrical deformation in the plane CCN: $\delta_s$ (CCN)
B <sub>1</sub>	$S_{6\ 2}^B = \tau_{cc}$	Twist out of the plane CCN: $\tau_{cc}$
B <sub>2</sub>	$S_{4\ 1}^B = \frac{1}{\sqrt{2}}(\Delta r_1 - \Delta r_2)$ $S_{5\ 1}^B = \frac{1}{\sqrt{2}}(\Delta \varphi_1 - \Delta \varphi_2)$	Asymmetrical elongation C-N: $\nu_{as}$ (C-N) Asymmetrical deformation in the plane CCN: $\delta_{as}$ (CCN)

**Table 6.**  
Symmetric vibrational coordinates of NC<sub>2</sub>N in (C<sub>2v</sub>).

These vibrations are shown schematically in **Figure 7**. The vibrational analysis in terms of internal vibrations is given in **Table 8**. The distribution of normal SCN group modes and their IR activity are shown in **Table 9**. The irreducible representation of the internal vibration modes of SCN<sup>-</sup> in C<sub>i</sub> is:

$$\Gamma_{\text{SCN}^-} = 4A_g + 4A_u \quad (9)$$

### 3.3 Group theory analysis

The comparisons of the experimental infrared spectra for EDCT, by using HF/6-311++G (d, p), (B3LYP) 311++G (d, p) and (B3LYP)/6-31++G (d, p) theory level, with the corresponding average predicted demonstrate good correlations as observed in **Figure 8**. Using the split triple valence base as well as the diffuse and polarization functions for computed harmonic vibratory frequencies of EDCT, 6-31++G (d, p) and 6-311++G (d, p), the frequencies FT-IR observed for various vibration modes were presented in **Table 10**. The comparative values of IR intensities activities are presented in **Table 11** and their corresponding graph given in **Figure 9**. The comparative graph of vibratory frequencies calculated by the HF and

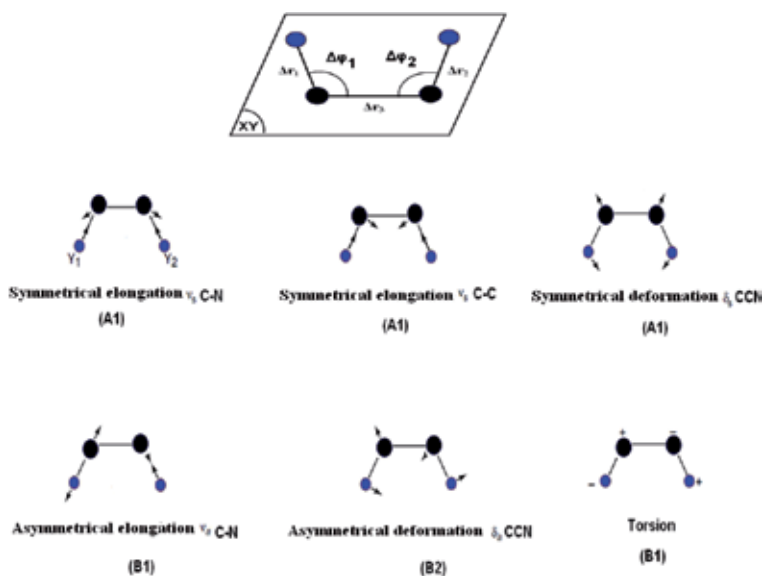


**Figure 6.**  
Normal modes of NC<sub>2</sub>N skeleton vibration in (C<sub>2v</sub>).

Description of mnv	C <sub>2v</sub>	C <sub>1</sub> (site group)	C <sub>i</sub> (factor group)
<b>Valence</b>			
$\nu_s(\text{CN})$	A <sub>1</sub> (IR, R)	A(IR, R)	Ag(R) + Au(IR)
$\nu_{as}(\text{CN})$	B <sub>1</sub> (IR, R)	A(IR, R)	Ag(R) + Au(IR)
$\nu_s(\text{CC})$	A <sub>1</sub> (IR, R)	A(IR, R)	Ag(R) + Au(IR)
<b>Deformation</b>			
$\delta_s(\text{CCN})$	A <sub>1</sub> (IR, R)	A(IR, R)	Ag(R) + Au(IR)
$\delta_{as}(\text{CCN})$	B <sub>1</sub> (IR, R)	A(IR, R)	Ag(R) + Au(IR)
<b>Torsion</b>			
$\tau_{\text{CC}}$	B <sub>2</sub> (IR, R)	A(IR, R)	Ag(R) + Au(IR)

**Table 7.**  
 Distribution of normal skeleton vibration modes in C<sub>2</sub>H<sub>10</sub>N<sub>2</sub> Cl NCS.

DFT methods to HF/6-311++G (d, p), B3LYP/6-31++G (d, p) and B3LYP/6-311++G (d, p). The basic sets for the EDCT are shown in **Figure 10**. It appears from the figure that the frequencies calculated by B3LYP with 6-31++G (d, p) of basis sets are closer to the experimental frequencies as HF method with 6-311++G (d, p) base set.

### 3.4 Bands assignments

#### 3.4.1 NH<sub>3</sub> modes

The asymmetric stretching  $\nu_{as}(\text{NH}_3)$  of symmetries (Ag + Au) are observed in IR at 3325 and 3326 cm<sup>-1</sup>. The symmetric stretching  $\nu_s(\text{NH}_3)$  of symmetries (Ag + Au) are observed in IR at 3210 cm<sup>-1</sup>. The asymmetric deformation  $\delta_{as}(\text{NH}_3)$  of symmetry (Ag + Au) observed IR at 1500 and 1570 cm<sup>-1</sup>. The symmetric deformation  $\delta_s(\text{NH}_3)$  of symmetries (Ag + Au) are observed in IR at 1467 cm<sup>-1</sup>. The Rocking  $\delta_\rho(\text{NH}_3)$  of symmetries (Au) are observed only in IR at 493 and 498 cm<sup>-1</sup>. The torsion  $\delta_\tau(\text{NH}_3)$  of symmetries (Au) observed in IR at 483 cm<sup>-1</sup>. The rocking and twisting modes are assigned as predicted by the calculations and in accordance with the expected regions for similar compounds [7, 8, 19, 20], as observed in **Table 10**.

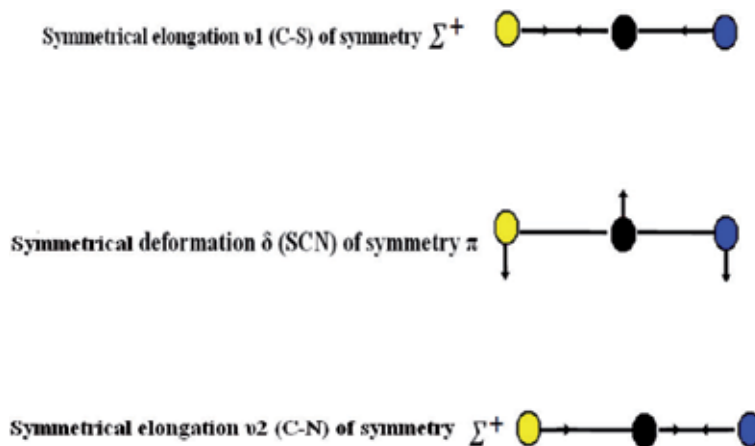


**Figure 7.**  
 Normal modes of vibration of the anion SCN<sup>-</sup> in (C<sub>2v</sub>).

	Mode	Molecular group	Group of site	Factor group	Activity	
		(G.M)	(G.S)	(G.F)	IR	R
		$C_{\infty v}$	$C_1$	$C_1$		
Anion (SCN) <sup>-</sup> (C <sub>∞v</sub> )	(ν <sub>1</sub> , ν <sub>2</sub> )	2Σ <sup>+</sup>	4A	4Ag(ν <sub>1</sub> , 2δ, ν <sub>2</sub> )	-	+
	(δ)	Π		4Au(ν <sub>1</sub> , 2δ, ν <sub>2</sub> )	+	-

**Table 8.**  
Internal modes of (SCN)<sup>-</sup> in (C<sub>∞v</sub>).

### 3.4.2 CH<sub>2</sub> modes

By comparison with previous works reported on similar compounds containing [C<sub>2</sub>H<sub>10</sub>N<sub>2</sub>]<sup>2+</sup> [21], we have attributed the bands observed in IR at 3222 and 2427 cm<sup>-1</sup> to asymmetric stretching ν<sub>as</sub>(CH<sub>2</sub>) and symmetric ν<sub>s</sub>(CH<sub>2</sub>) of symmetries (Ag + Au), respectively. The asymmetric deformation δ<sub>as</sub>(CH<sub>2</sub>) and symmetric δ<sub>s</sub>(CH<sub>2</sub>) is observed at 1452 and 1200 cm<sup>-1</sup> in IR spectrum at 1341 and 1454 cm<sup>-1</sup>. The calculated frequencies of B3LYP/6-31++G (d, p) and B3LYP/6-311++G (d, p) methods for CH<sub>2</sub> asymmetric and as asymmetric vibrations showed excellent agreement with recorded spectrum as well as literature data. The Rocking δ<sub>p</sub> (CH<sub>2</sub>) of symmetries (Ag + Au) are observed in IR at 1000 cm<sup>-1</sup>. The torsion δ<sub>τ</sub>(CH<sub>2</sub>) of symmetry (Ag + Au) observed in IR at 1124 cm<sup>-1</sup>. The rocking and twisting modes are assigned as predicted by calculations, as indicated in **Table 10**.

### 3.4.3 Skeletal modes

The NCCN skeleton gives six normal modes of vibration that may be described as three skeleton stretching (2ν<sub>CN</sub> + 1ν<sub>CC</sub>), two NCCN deformation modes and one torsional mode around the C—C bond. The symmetrical elongations of the symmetry skeleton ν<sub>s</sub> (CC) of symmetries (Ag + Au) appear in IR at 750 cm<sup>-1</sup>. The asymmetric stretching ν<sub>as</sub>(CN) of symmetries (Ag + Au) observed in IR at 544 cm<sup>-1</sup>. The symmetric stretching ν<sub>s</sub>(CN) of symmetries (Au) observed in IR at 532 cm<sup>-1</sup>. The asymmetric deformation δ<sub>as</sub>(CCN) of symmetry (Ag + Au), is observed in IR at 435 cm<sup>-1</sup>. The symmetric deformation δ<sub>s</sub>(CCN) of symmetry (Au) observed only in IR at 430 cm<sup>-1</sup>.

### 3.4.4 Internal modes of the thiocyanate group (SCN<sup>-</sup>)

The thiocyanate group (SCN<sup>-</sup>) has four vibrations in the C<sub>∞v</sub> group: two of valence denoted [ν<sub>1</sub>(CS), ν<sub>2</sub>(CN)] of symmetry (Σ<sup>+</sup>) and a doubly degenerate deformation

Description of mnv	C <sub>∞v</sub>	G.S (C <sub>1</sub> )	C.G (G.F)
<b>Valence</b>			
ν <sub>1</sub> (CS)	A <sub>1</sub> (IR, R)	A(IR, R)	2A <sub>g</sub> (R) + 2A <sub>u</sub> (IR)
ν <sub>2</sub> (CN)	A <sub>1</sub> (IR, R)	A(IR, R)	2A <sub>g</sub> (R) + 2A <sub>u</sub> (IR)
<b>Deformation</b>			
δ(SCN)	E <sub>1</sub>	A(IR, R)	2A <sub>g</sub> (R) + 2A <sub>u</sub> (IR)

**Table 9.**  
Description of the normal modes of SCN<sup>-</sup> in C<sub>2</sub>H<sub>10</sub>N<sub>2</sub> Cl NCS.

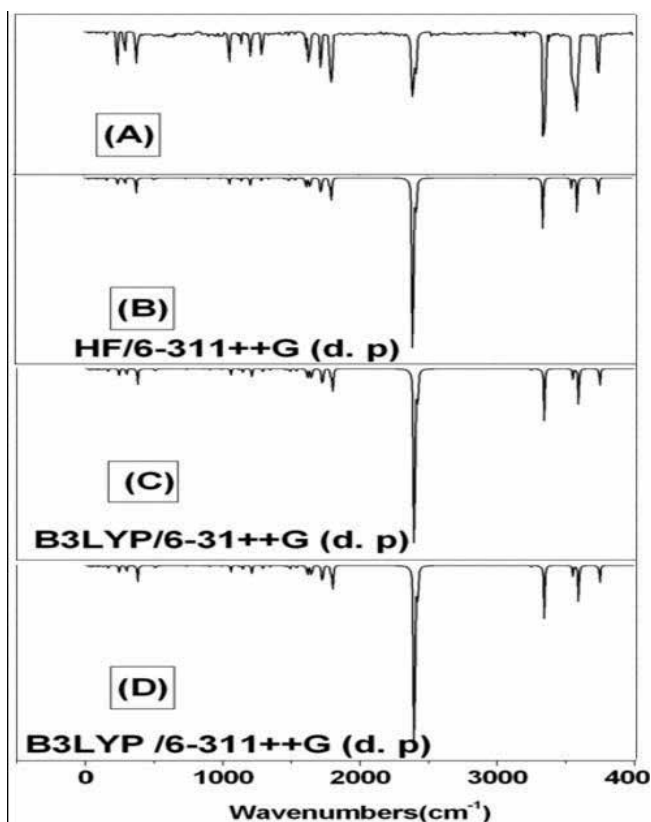


**Figure 8.** (A) Experimental infrared spectrum of  $C_2H_{10}N_2 Cl NCS$  in the solid phase compared with the calculated with: (B) (HF)/6-311++G (d, p), (C) B3LYP/6-31++G (d, p) and (D) B3LYP/6-311++G (d, p).

Mode nos.	Theoretical wavenumbers (cm <sup>-1</sup> )				Vibrational assignments
	FT-IR	HF/ 6-311++G (d,p)	B3LYP/ 6-31++G (d,p)	B3LYP/ 6-311++G(d,p)	
1	-	3746	3746	3749	Combination bands + 2 x $\delta_s(NH_2)$
2	-	3740	3740	3742	
3	-	3590	3590	3593	
4	-	3537	3536	3551	
5	3365(ep)	3341	3343	3349	
6	3326(m)	3318	3320	3332	$\nu_s(NH_2)$
7	3325(m)	3311	3307	3302	$\nu_s(NH_2)$
8	3210(m)	3250	3259	3262	$\nu_s(NH_2)$
9	-	3262	3241	3247	$\nu_s(CH_2)$
10	2427(m)	2404	2409	2413	$\nu_s(CH_2)$
11	2400(F)	2400	2399	2390	2x $\delta_s(CH_2)$
12	-	1805	1800	1809	
13	1787(ep, f)	1791	1797	1801	Combination bands + 2x $\delta_s(CH_2)$ 2x $\nu_s(CC)$
14	-	1785	1784	1782	
15	1718(ep, f)	1726	1727	1734	
16	1710(f)	1719	1723	1718	
17	1638(f)	1629	1643	1636	
18	1616(m)	1629	1623	1623	$\nu_s(C-N)$

19	1617(f)	1619	1613	1611	Combination bands
20	1580	1587	1582	1580	$\delta_{\nu}(\text{NH}_2)$
21	1530(m)	1532	1533	1539	$\delta_{\nu}(\text{NH}_2)$
22	1467(f)	1471	1466	1491	$\delta_{\nu}(\text{NH}_2)$
23	1439(m)	1438	1437	1433	$\delta_{\nu}(\text{CH}_2)$
24		1341	1345	1340	$\delta_{\nu}(\text{CH}_2)$
25		1287	1289	1297	$\delta_{\nu}(\text{CH}_2)$
26	1200(H)	1204	1208	1211	$\delta_{\nu}(\text{CH}_2)$
27	-	1135	1146	1126	$\delta_{\nu}(\text{CH}_2)$
28	1124(H)	1122	1122	1121	$\delta_{\nu}(\text{CH}_2)$
29	-	1050	1057	1061	$\delta_{\nu}(\text{CH}_2)$
30	1000 (F)	990	990	996	$\delta_{\nu}(\text{CH}_2)$
31	906(f)	909	901	921	Combination bands
32	878 (m)	831	864	874	Combination bands
33	758(f)	741	738	738	$\nu(\text{CC})$
34	541(f)	531	536	530	$\nu(\text{CN})$
35	532(f)	531	518	512	$\nu(\text{CN})$
36	498(f)	499	488	481	$\delta_{\nu}(\text{NH}_2)$
37	493(m)	496	487	482	$\delta_{\nu}(\text{NH}_2)$
38	483(m)	473	475	471	$2^{\circ} \delta_{\nu}(\text{NH}_2)$
39	450 (f)	458	450	451	$\nu(\text{C}-\text{S})$
40	448(f)	441	449	446	$\nu(\text{C}-\text{S})$
41	435(sp, f)	436	431	429	$\delta_{\nu}(\text{CCN})$
42	430(f)	429	421	428	$\delta_{\nu}(\text{CCN})$
43	421(f)	426	421	421	$\delta(\text{SCN})$
44	408(f)	402	406	402	$\delta(\text{SCN})$
45	-	83	83	81	$\delta_{\nu}(\text{NH}_2)$
46		76	72	72	Modes externes de $(\text{C}_2\text{H}_6\text{N}_2)^+(\text{Cl}^-)\text{SCN}^-$
47	-	42	44	45	
48	-	30	28	36	

**Table 10.**

Observed, HF/6-31++G (d, p), B3LYP/6-31++G (d, p) and B3LYP/6-311++G (d, p) level calculated vibrational frequency of ethylenediammonium chloride thiocyanate.

vibration denoted  $\delta_1$  (SCN) of symmetry ( $\pi$ ). From the bibliographic results [22–28] and the analysis by group theory, an attempt to attribute these vibrations observed in IR is illustrated in **Table 10**. The deformation  $\delta_1$  (SCN) of symmetry (1Au) is observed in IR at 409 and 424  $\text{cm}^{-1}$ . The calculated frequencies of B3LYP/6-31++G (d, p) and



Mode nos.	Calculated with HF/6-311++G (d. p)		Calculated with B3LYP/6-31++G (d. p)		Calculated with B3LYP/6-311++G (d. p)		
	IR intensity	Mode nos.	IR intensity	IR intensity	IR intensity	IR intensity	
1	14.48	25	12.72	13.50	19.57	15.30	14.59
2	15.73	26	24.56	9.27	18.75	10.22	22.15
3	7.17	27	32.62	6.33	36.54	4.37	34.14
4	20.26	28	30.24	12.70	33.84	10.60	31.04
5	13.87	29	0.11	13.85	1.40	17.22	0.40
6	9.54	30	23.90	9.61	131.09	791	129.89
7	28.49	31	12.19	27.24	9.80	27.24	9.09
8	45.53	32	176.12	73.75	149.02	70.95	141.72
9	111.58	33	199.40	87.48	190.70	87.08	188.76
10	29.05	34	82.23	6.61	48.96	8.11	42.56
11	2.12	35	13.39	166.12	62.76	186.03	62.76
12	6.16	36	65.01	12.53	99.11	13.63	99.11
13	31.58	37	64.34	3.41	161.00	5.11	159.11
14	12.29	38	194.80	37.30	83.40	35.20	83.40
15	18.08	39	955.17	5.35	398.06	3.15	518.06
16	2.11	40	595.05	7.87	173604	8.07	102.36
17	0.73	41	5.95	3.34	2.72	1.04	1.79
18	25.97	42	190.52	17.59	189.07	12.09	199.17
19	41.46	43	2.82	9.63	4.62	10.03	4.32
20	2.43	44	0.69	67.12	523.90	61.02	503.60
21	55.16	45	1.88	12.97	118.46	10.17	111.16
22	66.06	46	9.01	42.44	380.52	41.01	370.12
23	93.86	47	121.09	79.33	117.71	89.83	115.51
24	28.19	48	111.24	32.91	90.63	27.11	77.83

**Table 11.**  
 Comparative values of IR intensities activities between HF/6-31++G (d. p), B3LYP/6-31++G (d. p) and B3LYP/6-311++G (d. p) of ethylenediammonium chloride thiocyanate.

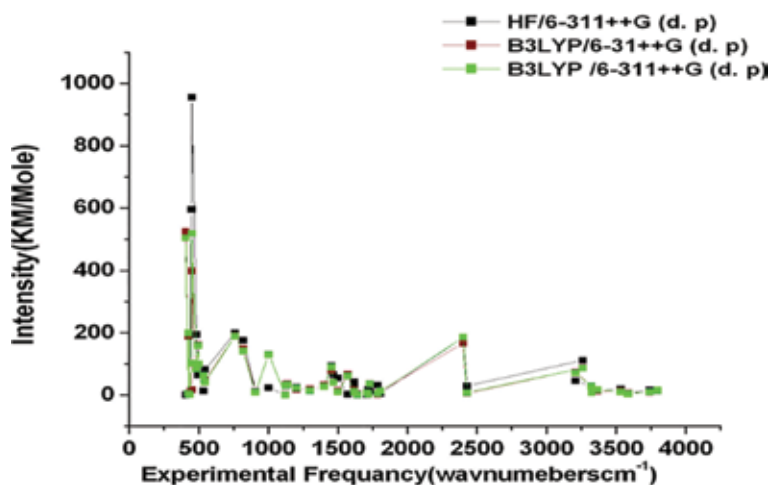


**Figure 9.**  
 Comparative graph of IR intensities by HF and DFT (B3LYP).

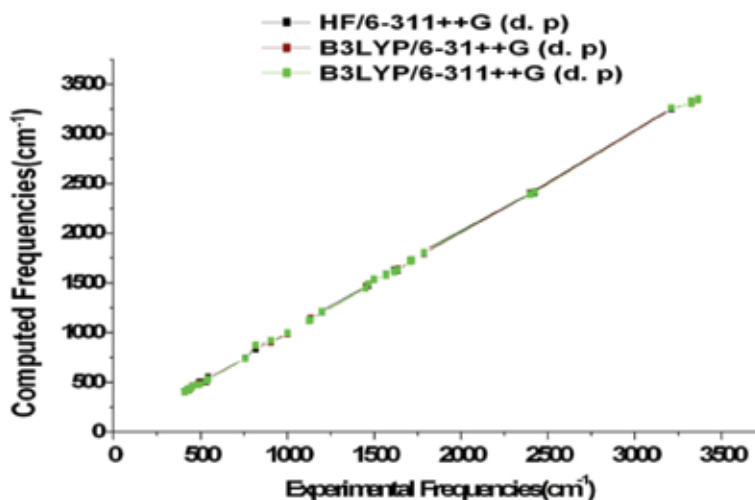


**Figure 10.**

Comparative graphs of computed frequencies (HF and DFT) with experimental frequencies.

B3LYP/6-311++G (d, p) methods for SCN deformation symmetric vibrations showed excellent agreement with recorded spectrum as well as literature data. We note a rise of degeneracy of the symmetry  $\pi$  of  $\delta_1$  (SCN) with a burst of  $33 \text{ cm}^{-1}$ . The symmetric stretching  $\nu_1$  (C=S) of symmetries (1Ag + 1Au) are observed in IR at  $450$  and  $484 \text{ cm}^{-1}$ . The calculated frequencies of B3LYP/6-31++G (d, p) and B3LYP/6-311++G (d, p) methods for C=S symmetric vibrations showed excellent agreement with recorded spectrum as well as literature data. The symmetric stretching  $\nu_2$  (C=N) of symmetries (1Ag + 1Au), predicted by the group theory, are observed in IR at  $1616 \text{ cm}^{-1}$ .

### 3.5 Other molecular properties

Several calculated thermodynamic parameters are presented in **Table 12**. Scale factors have been recommended [29] for an accurate prediction in determining the

Parameters	HF/6-311++ (d, p)	B3LYP/6-31++ (d, p)	B3LYP/6-311++G (d, p)
Zero point vibration energy	105.84889	100.34649	98.57158
Rotational constants	1.55409	1.63393	1.55409
	0.47626	0.52535	0.47626
	0.37522	0.46146	0.37522
Rotational temperature	0.07458	0.07842	0.07458
	0.02286	0.02521	0.02286
	0.01801	0.02215	0.01801
<b>Energy</b>			
Translational	0.889	0.889	0.889
Rotational	0.889	0.889	0.889
Vibrational	108.982	105.524	105.017
Total	110.759	107.302	107.394
<b>Molar capacity at constant volume</b>			
Translational	2.981	2.981	2.981
Rotational	2.981	2.981	2.981
Vibrational	19.092	29.415	17.227
Total	25.054	25.377	23.189

Parameters	HF/6-311++ (d, p)	B3LYP/6-31++(d, p)	B3LYP/6-311++G (d, p)
<b>Entropy</b>			
Translational	41.025	41.025	41.025
Rotational	31.426	31.426	31.074
Vibrational	15.540	15.594	15.589
Total	87.792	87.546	87.587
Dipole moment	39.4045	38.6462	38.6426

**Table 12.**

Theoretically computed zero point vibrational energy ( $\text{kcal mol}^{-1}$ ), rotational constants (GHz), rotational temperature (K), thermal energy ( $\text{kcal mol}^{-1}$ ), molar capacity at constant volume ( $\text{cal mol}^{-1} \text{K}^{-1}$ ) entropies ( $\text{cal mol}^{-1} \text{K}^{-1}$ ) and dipole moment (Debye) for ethylenediammonium chloride thiocyanate.

zero-point vibration energies, and the entropy. It can be seen that the total energies decrease with the increase of the size of the basic set. Changes in the total entropy of EDCT at room temperature and in different basic sets are only marginal.

## 4. Conclusions


The present document attempts to define the appropriate frequency assignments for the thiocyanate ethylenediammonium chloride compound from the FT-IR spectrum. Vibrational frequencies and infrared intensities are calculated and analyzed by the theoretical HF and DFT (B3LYP) levels, using the 6-31++G (d, p) and 6-311++G (d, p) base sets. The comparison between the calculated vibrational frequencies and the experimental values indicates that both methods can predict the FT-IR spectra of the title compound. The results of DFT-B3LYP method indicate better fit to experimental ones than ab initio HF upon evaluation of vibrational frequencies. Several thermodynamic parameters of the title molecule are comparatively discussed. The observed and the calculated wavenumbers are found to be in good agreement with majority modes.

## Author details

Sahel Karoui\* and Slaheddine Kamoun  
Laboratory of Material Engineering and Environment (LR11ES46),  
National School of Engineering, Sfax, Tunisia

\*Address all correspondence to: [karouisahel@yahoo.fr](mailto:karouisahel@yahoo.fr)

## IntechOpen

© 2019 The Author(s). Licensee IntechOpen. This chapter is distributed under the terms of the Creative Commons Attribution License (<http://creativecommons.org/licenses/by/3.0>), which permits unrestricted use, distribution, and reproduction in any medium, provided the original work is properly cited. 

## References

- [1] König JL, Antoon MK. Recent applications of FT-IR spectroscopy to polymer systems. *Applied Optics*. 1978;**17**:1374
- [2] Neumann T, Werner J, Jess I, Näther C. Poly[(1-1,3-thiocyanato-jN,S)(isonicotinato-jN,O)(ethanol-jO)-cadmium(II)]. *Acta Crystallographica*. 2012;**68**:1338
- [3] Wohler S, Jess I, Näther C. Crystal structure of di-aqua-bis-(2,6-di-methyl-pyrazine-κN)bis-(thio-cyanato-κN)cobalt(II) 2,5-di-methyl-pyrazine tris-olvate. *Acta Crystallographica*. 2013;**69**:195
- [4] Reinert T, Jess I, Näther C. Bis(3-tert-butylpyridine-jN)bis(4-tertbutylpyridine-jN)bis(thiocyanato-jN)-cadmium. *Acta Crystallographica*. 2012;**68**:1372
- [5] Werner J, Boeckmann J, Jess I, Näther C. Catena-Poly[[bis(3-acetylpyridine-jN)-cadmium]-di-l-selenocyanatoj2N:Se;j2Se:N]. *Acta Crystallographica*. 2012;**68**:704
- [6] Jan B, Näther C. Catena-Poly[[bis[[bis(3-aminopropyl)-amine-j3 N, N', N''] (thiocyanato-jN)-cadmium]-l4-sulfato-j4 O,O:O,O] methanol hemisolvate]. *Acta Crystallographica*. 2011;**67**:1201-1202
- [7] Karoui S, Kamoun S, Michaud F. Ethylenediammonium chloride thiocyanate. *Acta Crystallographica*. 2013;**69**:669
- [8] Jornet D, Bartovsky P, Domingo LR, Tormos R, Miranda MA. A characterization of the raman modes in a j-aggregate-forming dye: A comparison between theory and experiment. *The Journal of Physical Chemistry*. 2010;**114B**:11920
- [9] Bartlett HE, Jurriaanse A, De Haas K. Activity coefficients of aqueous thiocyanic acid solutions from electromotive force, transference number, and freezing-point depression measurements. *Canadian Journal of Chemistry*. 1969;**47**(16):2981-2986
- [10] Zhang J, Xiao HM. Computational studies on the infrared vibrational spectra, thermodynamic properties, detonation properties, and pyrolysis mechanism of octanitrocubane. *The Journal of Chemical Physics*. 2002;**116**:10674
- [11] Xu XJ, Xiao HM, Ju XH, Gong XD, Zhu WH. Computational studies on polynitrohexaazaadamantanes as potential high energy density materials. *The Journal of Physical Chemistry A*. 2006;**110**:5929
- [12] Chen ZX, Xiao JM, Xiao HM, Chiu YN. Studies on heats of formation for tetrazole derivatives with density functional theory B3LYP method. *The Journal of Physical Chemistry A*. 1999;**103**:8062
- [13] Basis sets density functional (DFT) methods. Gaussian 03 Program. Wallingford, CT: Gaussian Inc.; 2000
- [14] Frisch MJ, Nielsen AB, Holder AJ. Gauss View Users Manual. Pittsburgh, PA: Gaussian Inc; 2000
- [15] Kamoun S, Jouini A, Kamoun M, Daoud A. Structure of ethylenediammonium bis(dihydrogenmonophosphate). *Acta Crystallographica*. 1989;**C45**:481-482
- [16] Karoui S, Kamoun S, Jouini A. Synthesis, structural and electrical properties of  $[C_2H_{10}N_2][ (SnCl(NCS)_2)_2 ]$ . *Journal of Solid State Chemistry*. 2013;**197**:60-68

- [17] Kamoun S, Kamoun M, Daoud A. Etude par spectroscopie (IR et Raman) de l'hydrogène diammonium bis dihydrogène monophosphate  $\text{NH}_4(\text{CH}_2)_6\text{NH}_4(\text{H}_2\text{PO}_4)_2$ . *Spectrochimica Acta Part A*. 1991;**47**:1051-1059
- [18] Bhagavantam S, Venkatarayudu T. Raman effect in relation to crystal structure. *Proceedings of the Indiana Academy of Sciences*. 1939;**9**:224
- [19] Ouasri A, Jeghnou H, Rhandour A, Dhamelin court MC, Dhamelin court P, Mazzah A, et al. Structural phase transition in  $[\text{NH}_3(\text{CH}_2)_5\text{NH}_3]\text{BiCl}_5$ : Thermal and vibrational studies. *Journal of Raman Spectroscopy*. 2005;**36**:791-796
- [20] Jeghnou H, Ouasri A, Rhandour A, Dhamelin court MC, Dhamelin court P, Mazzah A, et al. Structural phase transition in  $(n\text{-C}_4\text{H}_9\text{NH}_3)_2\text{SiF}_6$ : DSC and Raman studies. *Journal of Raman Spectroscopy*. 2005;**36**:1023-1028
- [21] Durig JR, Panikar SS, Iwata T, Gounev TK. Conformational stability of ethylenediamine from temperature dependent infrared spectra of liquid xenon solutions,  $r_0$  structural parameters, ab initio calculations, and vibrational assignments. *Journal of Molecular Structure*. 2010;**984**:58-67
- [22] Oden LL, Decius JC. The infrared spectrum of ammonium thiocyanate from 90 to 300°K. *Spectrochimica Acta Part A*. 1964;**20**:667-874
- [23] Durig JR, Pate CB. *Spectrochimica Acta Part A*. 1972;**28**:1031-1038
- [24] Wickleder C, Larsen P.  $\text{Ca}(\text{SCN})_2$  and  $\text{Ca}(\text{SCN})_2 \cdot 2\text{H}_2\text{O}$ : Crystal structure, thermal behavior and vibrational spectroscopy. *Zeitschrift für Naturforschung*. 2002;**57**:1419-1426
- [25] Lieber E, Rao CNR, Ramachandran J. The infrared spectra of organic thiocyanates and isothiocyanates. *Spectrochimica Acta Part A*. 1959;**13**:296-299
- [26] Kniezo L, Kristian P. Synthesis, structure, and properties of  $\beta$ -styryl isothiocyanate. *Chemical Papers: Chemické Zvesti*. 1974;**28**:848-853
- [27] Kabesova M, Gazo J. Structure and classification of thiocyanates and the mutual influence of their ligands. *Chemical Papers: Chemické Zvesti*. 1980;**34**:800-841
- [28] Kohout J, Kabesova M, Gazo J. Synthesis and antiproliferative activity of cyclic arylidene ketones: A direct comparison of monobenzylidene and dibenzylidene derivatives. *Monatshefte für Chemie*. 1977;**108**:1011-1018
- [29] Palafox MA. Scaling factors for the prediction of vibrational spectra. I. Benzene molecule. *International Journal of Quantum Chemistry*. 2000;**77**:661



# Characterization of Whole and Fragmented Wild-Type Porcine IgG

*Claudia Nelson, Raymond Bacala, Baylie Gigolyk, Evelyn Ang, Haley Neustaeter, Emy Komatsu, Oleg Krokhin, Dave Hatcher and H el ene Perreault*

## Abstract

Glycoproteomic analyses of tryptic (glyco)peptides from wild-type (WT) porcine IgG were performed. In a first protocol, intact antibody was digested with trypsin, followed by glycopeptide enrichment and liquid chromatography-tandem MS (HPLC-MS/MS). This procedure allowed to detect *N*-glycopeptides observed previously (Lopez, P. G. et al., *Glycoconj. J.* 2016, 33 (1), 79), plus other non-reported *N*-glycopeptides. The method provided useful information but did not allow to discern between Fab (antigen-binding region) and Fc (constant region, fragment crystallizable) peptides/glycopeptides. In a second scheme, glycoproteomic analysis was attempted for Fab and Fc fragments obtained by papain and Fabulous™ hydrolysis. Usually employed for milligram amounts of antibodies, the papain and Fabulous™ protocols were adapted to 200 µg of WT IgG. Fab and Fc fragments were separated by size-exclusion (SEC) HPLC. Fractions collected were reanalyzed by gel electrophoresis (SDS-PAGE). Bands were excised, and fragments digested in-gel, followed by matrix-assisted laser desorption/ionization time-of-flight (MALDI-TOF) MS and HPLC/MS-MS. In the protocol no glycopeptide enrichment was involved, that is, whole tryptic digests were analyzed. Fc *N*-glycopeptides were identified, and greater numbers of non-glycosylated peptides were tabulated. Very few peptides overlapped between Fc and Fab, as most peptides were clearly from Fc or Fab. HPLC-MS/MS detected more sialylated glycoforms than MALDI-TOF-MS. Sections of Fab and Fc were assigned de novo, through a database search or manually.

**Keywords:** porcine IgG, papain, enzymatic fragmentation, Fabulous™, glycoproteomics

## 1. Introduction

There have been reports on the mass spectrometric (MS) analysis of pig immunoglobulins (IgG) in relationship with use in a xenotransplantation context [1–4]. These studies have explored the amino acid composition and glycosylation of pig IgG according to glycoproteomic [2, 3] and glycomic [1] workflows involving the enzymatic digestion of whole antibodies. Glycoproteomic workflows resulted in the

identification of many peptides that could be matched with the conserved gamma portion of the heavy chains of some of the 11 subtypes of pig IgG [5], including *N*-glycopeptides EEQFNSTYR and EAQFNSTYR [3]. No specific information was given on the variable portions of neither Fab nor Fc components, as most of such assignments would have had to be attributed *de novo*. The conserved Fc glycosylation site is often described as the only IgG site glycosylated at 100%, in spite of the fact that 10–15% of wild-type antibodies have glycosylation also in their variable region [6], and reports have shown that even higher glycosylation levels (up to 30–40%) can exist in the variable regions of polyclonal IgGs [7, 8].

For more specificity, the analysis of antibodies by MS can take great advantage of enzymatic fragmentation with papain [9, 10] or new enzymes produced by recombinant methods and available on the market [11]. This type of procedure has not been reported for the fragmentation of porcine IgG, to the authors' knowledge. For instance, procedures have been published for mouse [12, 13], chicken [14], rabbit [15], sheep [16], and human [17, 18] IgGs. The two groups of antibody fragments of primary interest are the antigen-binding fragments (Fab) and class-defining crystallizable fragments (Fc). The hinge region of immunoglobulins (IgGs) is readily accessible to proteolytic attack by enzymes [9, 10], and cleavage at that point produces F(ab')<sub>2</sub> or Fab fragments and the Fc fragment. Papain is a nonspecific thiol-endopeptidase and has a sulfhydryl group in its active site, which must be reduced for activity. When IgG molecules are incubated with papain in the presence of a reducing agent, one or more peptide bonds in the hinge region are split, producing three fragments of similar size: two Fab fragments and one Fc fragment [9, 10].

Fabulous™ enzyme is a recombinant cysteine protease that under reduced conditions digests in the hinge region of antibodies from many species and subclasses, including human, mouse, rat, and goat, yielding Fab and Fc fragments [11]. As a reducing agent is present during digestion, it is likely that interchain thiols will be reduced. Fabulous™ and papain have typically been used for the production of relatively large amounts of antibody fragments (10 mg of starting material), whereas methods adapted to MS require much less, about 50–200 µg. There is a need for downscaling these workflows, especially for porcine IgG, which has not been previously studied by fragmentation followed by MS.

Reports on post-fragmentation MS analyses of antibodies have demonstrated that detailed fragment characterization allows for the identification of more glycosylation sites than bottom-up approaches [19, 20]. It is also important to study amino acid sequences of the variable portions of IgG for therapeutic purposes [21], and the information obtained after fragmentation is much more specific than data generated through the tryptic digestion of whole intact antibodies.

The interest of the present study is to compare results from two main workflows aimed at characterizing wild-type porcine IgG's glycosylation and amino acid sequence features. In the first workflow, porcine IgG is digested with trypsin, followed by glycopeptide enrichment. Reversed-phase high-performance liquid chromatography (RPLC) coupled with electrospray ionization (ESI) MS and tandem MS (MS/MS) is used to characterize the glycopeptide-rich fraction. The second workflow involves subjecting porcine IgG to fragmentation by one of two enzymes, papain or Fabulous™. The steps necessary between fragmentation and MS included size-exclusion chromatography (SEC), sodium dodecyl sulfate polyacrylamide gel electrophoresis (SDS-PAGE), and tryptic digestion. This is the first attempt to characterize porcine IgGs in small amounts (sub-mg) using a combination of these methods. Two different MS techniques were used for the analysis of tryptic products of antibody fragments: matrix-assisted laser desorption/ionization time-of-flight (MALDI-TOF) MS and ESI/MS–MS coupled with RPLC.



As the tryptic digestion products of whole wild-type porcine IgG antibodies have been characterized by MALDI-MS [2, 3] and ESI-MS and MS/MS (new results presented in this report), data from these different workflows serve as comparative benchmarks between intact and fragmented IgG samples. Overlaps and differences allow to identify peptides and glycopeptides as originating from either the Fc or Fab portions, and database searches [22] can verify if these sequences are already available in the literature or need to be determined *de novo*. Porcine IgG is a complex mixture of subtypes, and the complementarity of MALDI- and LC/ESI-MS–MS brings a considerable amount of information to document the identification of these IgG components.

## 2. Experimental

### 2.1 Materials

Wild-type porcine IgGs were obtained from Université de Nantes (Dr. Jean-Paul Soullillou's Laboratory). Trypsin Ultra™ was purchased from Promega (Wisconsin, USA). The Fabulous™ enzyme was kindly provided by Genovis (Cambridge, MA). Dihydroxybenzoic acid (DHB), sinapinic acid, ammonium bicarbonate, dithiothreitol (DTT), L-cysteine, iodoacetamide (IAA), and trifluoroacetic acid (TFA) were purchased from Sigma-Aldrich (St. Louis, MO). Mini-Protean TGX precast gels (4–15%), Precision Plus™ protein standard, 2-mercaptoethanol, and 4x Laemmli sample buffer were obtained from Bio-Rad (Hercules, CA). Imperial™ protein stain, tris base (2-amino-2-(hydroxymethyl)-1,3-propanediol) and immobilized papain-cross linked and 6% in beaded agarose supplied as 50% glycerol in sodium acetate pH 4.5 were purchased from Thermo Scientific (Rockford, IL). Strata-X C-18 cartridges were obtained from Phenomenex (Torrance, CA). Acetonitrile (ACN) was purchased from EMD-Millipore (Darmstadt, Germany). Sodium phosphate dibasic anhydrous was purchased from McArthur Chemical Co. Ltd. (Montreal, Canada). Hydrochloric acid was purchased from Anachemia (Vancouver, Canada) and deionized water was obtained from an adapted filtration system (Millipore).

### 2.2 Tryptic digestion of whole porcine IgG

Porcine IgG (200 µg) was dissolved in 100 mM ammonium bicarbonate (pH~8) and vortexed. A DTT solution (10 mM) was added to the sample, which was then vortexed and left to react at 56°C for 40 min, then cooled to room temperature. After 500 mM IA was added, and the sample was left to react in the dark for 45 min. The excess of IA was quenched with the addition of 100 mM DTT, and the sample was left to react for 10 min in the dark. Trypsin was added and proteolysis took place at 37°C for ~18 h. To deactivate trypsin, the sample was frozen and dried under vacuum. Glycopeptide enrichment was then performed using a ProteoExtract™ glycopeptide enrichment kit (Millipore-Sigma, Etobicoke, ON) according to the manufacturer's procedure [23].

### 2.3 Papain digestion of porcine IgG

Just before use, 20 mM sodium phosphate digestion buffer was prepared with a 10 mM cysteine content, and the pH was adjusted to 7. Bead-immobilized papain slurry (20 µL, 50%) was added to an Eppendorf™ tube. The beads were washed twice with 160 µL of digestion buffer and then re-suspended in the buffer. Porcine IgG (200 µg) was dissolved in the digestion buffer. This was added to the tube containing the washed immobilized papain and digestion buffer. The sample was

incubated for ~24 h at 37°C. Constant mixing of the bead slurry was maintained during the whole incubation. The bead-immobilized enzyme was separated from the digest by centrifugation and 20 µL of 10 mM Tris–HCl, pH 7.5 was added before centrifugation. The supernatant, which contained the IgG fragments, was removed.

#### **2.4 Fabulous™ digestion for porcine IgG**

The IgG sample (200 µg) was added to 200 units of Fabulous™ enzyme in 200 µL of 10 mM Tris, 50 mM cysteine buffer. The sample was vortexed and incubated at 37°C for 1 h.

#### **2.5 Fractionation of IgG fragments by HPLC using a SEC column**

The digestion mixtures were injected into a preconditioned SEC-300 4.6 × 300 mm silica-based column (Phenomenex, Torrance, CA). The mixtures were eluted with a mobile phase of 0.1% TFA, 0.1% formic acid in 20% ACN at a flow rate of 0.3 mL/min (manufacturer's recommendation). The HPLC system used was a Waters 1525 binary pump equipped with a Waters 2707 autosampler and a Waters 2998 photodiode array detector (Milford, MA). Fractions were collected, dried, and re-suspended for MALDI-MS analysis.

#### **2.6 Separation of IgG fragments by SDS gel electrophoresis**

Once fractionated by SEC, Fab and Fc components were separated on a Mini-Protean™ Tetra cell system (Bio-Rad). Bio-Rad TGX™ gels used had 10 wells and a density gradient of 4–15%. Wells were washed individually four times with running buffer (10 × tris-glycine-SDS buffer diluted 1 × with water) prior to the loading samples. Each sample fraction containing Fab, Fc, or both Fab and Fc had its own lane on the gel. Each gel was loaded with 15 µL of each fraction (in water) in 11.3 µL of 4 × Laemmli sample buffer, without adding 2-mercapto-ethanol. Well 1 was loaded with 10 µL of Precision Plus Protein Kaleidoscope™ standard. Intact-reduced IgG (15 µL, ~14 µg) was loaded into well 2. IgG fragments (~14 µg) were loaded in other lanes. Running buffer was poured in the cell system and the voltage was set at 150 V. Samples were allowed to migrate for 40 min, until the dye front reached the bottom of the gel. The gel was removed from the cell and was rinsed four times with Millipore water, and sufficient Imperial™ protein stain was added. IgG fragments absorbed the stain overnight, and the stain was decanted and replaced with Millipore water until gel bands became visible.

#### **2.7 In-gel tryptic digest of IgG Fab and Fc fragments**

Non-reduced Fab and Fc bands were excised from the gel. Tryptic digestion was performed on each single cut out band. Bands were cut into small pieces and placed into 1.5 mL Eppendorf tubes. The digestion buffer was 50 mM ammonium bicarbonate in water. Each tube contained one lane worth of gel. Gel pieces were washed with wash buffer (1:1 digestion buffer-ethanol) until all protein stain was removed. They were then incubated in absolute ethanol for 10 min. Gel pieces were then rewashed with digestion buffer for 20 min and then incubated again in absolute ethanol for 20 min, which was removed from the gel by vacuum centrifugation. Trypsin solution was added and the tubes were placed on ice where the gel was allowed to swell. Thereafter, excess trypsin solution was discarded. Gel pieces

were covered with digestion buffer and incubated at 37°C for ~18 h. Glycopeptides and peptides were extracted on C<sub>18</sub> cartridges with buffer A, 0.5% acetic acid; extraction buffer B, 5:3 30%; ACN, 0.5% acetic acid; and extraction buffer C, 100% ACN. Samples were dried down for further analysis.

### **2.8 Peptide-N-glycosidase F (PNGase F) removal of glycans from trypsin digested Fab and Fc fragments**

A solution of PNGase F (4 µL, 10 units/µL) was added to a solution of tryptic glycopeptides. The sample was vortexed and set at 37°C for ~18 h. After the digest, glycans were separated from the de-glycosylated peptides on a C<sub>18</sub> cartridge. The cartridge was conditioned with 5 x 1 mL (ACN + 0.1% TFA), then 5 x 1 mL of (H<sub>2</sub>O + 0.1% TFA). The sample was loaded onto the cartridge and allowed to equilibrate for about 1–2 min. Glycans were eluted with 3 mL H<sub>2</sub>O + 0.1% TFA and collected in two fractions. Peptides were eluted with 1.5 mL of 50:50 ACN:H<sub>2</sub>O + 0.1% TFA. Solvent was evaporated from the fractions.

### **2.9 Preparation of samples for MALDI-MS analysis**

Glycopeptide fractions were mixed directly with 5 µL of DHB in 30:70 ACN: water. Samples (1 µL) were then spotted onto the stainless steel target and allowed to dry, for reflector positive mode MALDI-MS. For the Fab and Fc fragments from HPLC fractions, 5 µL of 0.1% TFA and 5 µL of sinapinic acid in 0.1% TFA, 30:70 ACN: water was added, and 1 µL was spotted onto the target already pre-spotted with 0.5 µL of sinapinic acid in ethanol. Spots were then allowed to dry for linear positive mode MALDI-MS.

### **2.10 MALDI-TOF-MS analysis**

These analyses were performed on an UltraFleXtreme™ mass spectrometer (Bruker, Billerica, MA) equipped with LID-LIFT™ technology for tandem MS experiments. For positive ionization mode, a nine-peptide calibration mixture with masses ranging from 500 to 5000 Da was used. In linear positive mode, the instrument was calibrated using tryptic peptides of cytochrome C, mass ranging from 10,000 Da to 160,000 Da.

### **2.11 Preparation of samples for HPLC-ESI-MS analysis**

For the Fab and Fc tryptic digest fragments, 100 µL of water was added to the pooled C<sub>18</sub> cartridge fractions of each Fab and Fc tryptic digests. Samples were sonicated and then ready for HPLC–MS analysis.

### **2.12 RPLC-MS/MS analysis of Fab and Fc tryptic digests**

Both digestion mixtures (50 µL) were in turn injected into a preconditioned Acquity BEH C<sub>18</sub> (1.7 µm, 2.1 x 50 m) silica-based, reverse phase column, on a Waters Acquity UPLC system (Waters, Mississauga, ON). The flow rate was 0.25 mL/min, and a linear increase from zero to 28% ACN in water with 0.1% formic acid was used. Mass spectrometric detection was performed on a Waters G2 Synapt ESI-MS instrument. Positive ionization mode was used. The analyzer mode was set to high resolution, with a capillary voltage of 3.00 kV and a cone voltage of 25 V. The Progenesis™ software was used to handle and search databases for these HPLC-MS/MS analyses.

### 2.13 Analysis of whole porcine IgG tryptic digest by RPLC-MS/MS

Separations were conducted on a LC Ultra system (Eksigent, Dublin, CA). A 100  $\mu\text{m} \times 200$  mm analytical column packed with 3  $\mu\text{m}$  Luna C18 (Phenomenex, Torrance, CA) was used, at 500 nL/min flow rate. A 300  $\mu\text{m} \times 5$  mm PepMap 100 trap-column (Thermo Fisher, San Jose, CA) was used to protect the analytical column. The elution gradient was as described above. A Triple TOF 5600 mass spectrometer (ABSciex, Concord, ON) was used in standard MS/MS data-dependent acquisition mode. Mass spectra (250 ms) were collected ( $m/z$  370–1250) and followed by up to 20 MS/MS measurements on the most abundant parent ions (400 counts/s threshold, +2 to +5 charge state,  $m/z$  100–1500 mass range for MS/MS, 100 ms each). Database search was performed using the Global Proteome Machine (GPM) proteomics data analysis system [24].

## 3. Results and discussion

### 3.1 Mass spectrometric analysis of tryptic digests of whole porcine IgG samples

In previous studies, wild-type porcine IgG was digested with trypsin, and glycopeptides/peptides were fractionated on a C18 cartridge. Glycopeptide fractions were analyzed by MALDI-MS/MS [2, 3, 30]. In a new separate experiment, the results of which are presented here, all tryptic products were then enriched for glycopeptides using an EMD-Millipore ProteoGlycan™ kit [23]. The glycopeptide-enriched fraction was injected into a RPLC-MS/MS system, using data-dependent MS/MS acquisition. **Figure 1a** shows the MS/MS total ion chromatogram (TIC) obtained from the elution, whereas **Figure 1b** represents the elution of peptides with  $m/z$  204

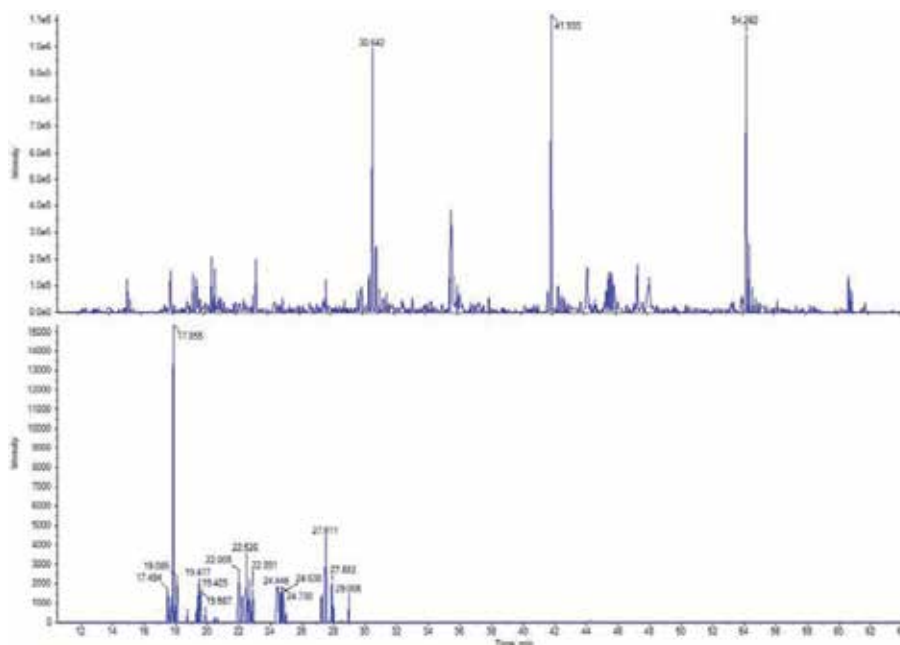


**Figure 1.** (a) Total HPLC/MS ion chromatogram obtained from the MS/MS spectra of porcine IgG tryptic peptides and glycopeptides after enrichment on EMD-Millipore Proteoglycan™. (b) Selected MS/MS fragment ion chromatogram at  $m/z$  204, indicating the elution times of glycopeptides [25].

ions as product in their MS/MS spectra, identified as glycopeptides [25]. Although enrichment was performed, there were still non-glycosylated peptides present in the sample. The  $m/z$  204 trace shows that glycosylated peptides eluted early in the analysis and that the most abundant compounds eluting in (a) were most probably non-glycosylated peptides.

A database search using GPM [24] helped to identify some non-glycosylated peptides, while for glycopeptides the extracted  $m/z$  204 chromatogram was used to manually identify as many glycopeptides as possible. **Table 1** gives a listing of all peptides detected and sequenced with GPM [24] or manually. For glycopeptide sequencing, MS/MS spectra were treated with CycloBranch [26] after removing abundant glycopeptide ions. As a few sequences are available in UniprotKB [22] for the Fc gamma portion of porcine IgG (K7ZLAZ, L8B180, L8B0S7, L8B0S2, L8B0Z4), and more are available [3] from previously published DNA sequences [5], some peptides show more than one identification source in **Table 1**. Only one entry was found for a porcine IgG Fab portion, P01846, which corresponds to the lambda ( $\lambda$ ) constant region. **Figure A1** compares the published porcine IgG Fc heavy chain sequences relating to **Table 1** assignments.

Points of interest arising from this table are (i) the presence of a large number of non-glycosylated, even after enrichment, from the Fab and Fc portions of the antibody and (ii) the detection of seven distinct glycosylated peptides, some with complex glycoforms and one with high-mannose glycoforms, thus of the *N*-type. Indeed, all MS/MS spectra of these glycopeptides showed characteristic fragment ions corresponding to the  $(M + H)^+$  ions of the bare peptides, next to the characteristic  $(M + H + 83)^+$  and  $(M + H + 203)^+$  ions [27], with the latter being predominant.

**Figure 2** shows four MS/MS spectra of glycopeptides, starting with two of the complex G0F forms of peptides of (a) constant region EAQFNSTYR [3] and (b) a variable region sequence partially determined as H<sub>2</sub>N-(300)-QNFSVFR by the CycloBranch software [26]. In these cases, the mass difference between the protonated precursors and  $(M + H)^+$  bare peptide fragments is 1444. The  $m/z$  204 and 366 fragment ions are predominant as glycopeptide signature. In **Figure 2c**, a sialylated complex glycoform is featured, the G1FS form of peptide EEQFNSTYR [3]. In previous studies of wild-type pig IgG, the presence of *N*-glycolyl neuraminic acid (NeuGc) is featured exclusively (i.e., no *N*-acetyl neuraminic acid (NeuAc)) has been reported [2, 3]. The fragmentation of NeuGc-containing species produces distinctive  $m/z$  308 and 290 fragments, as observed in (c). **Figure 2d** shows the fragmentation of a high-mannose glycoform of a peptide of undetermined sequence. The bare peptide  $(M + H)^+$  ions appear at  $m/z$  1069, with +83 ions ( $m/z$  1152) and +203 ions ( $m/z$  1272).

For known peptide sequences such as in **Figure 2a** and **c**, it is possible to find most bare peptide y and b ions, although they appear with very low abundance and are not accounted for by the search engine, due to the domination of all glycopeptide signature ions. There was an attempt by the authors to sequence all unknown glycopeptide sequences, with partial success, as indicated in red in **Table 1**.

Overall results suggest that *N*-glycosylation occurs in the Fc but also in the variable regions of the Fab and/or Fc domains of porcine IgG. Each glycosylated peptide detected indicated patterns linked to *N*-glycosylation, while there was no obvious detection of *O*-glycans. This may be due to the conditions used to enrich the glycopeptides with the EMD-Millipore Kit, which were optimized for *N*-glycosylated peptides [23, 28]. Results obtained with this first workflow will be compared with those generated with a more elaborated procedure involving fragmentation enzymes as discussed below.

Peptide sequence	$m/z$ (M + H) <sup>+</sup>	Error (ppm)	$m/z$ glycoform	Glycoform	Identification source <sup>a</sup>
Unknown	646.35				Unavailable
NFSTYR	787.37	0	2231.14 2392.28 2701.08 2863.10	G0F G1F G1FS G2FS	IgG1a-b, IgG2a-b, IgG4a-b, IgG5a-b, IgG6a-b, L8B0S7, L8B0S2, K7Z1A7, L8B180, L8B0Z4
LLVELIR	855.57	4.44			Unavailable
TVTSECA	864.38	3.8			P01846
FSGAISGNK	880.45	2.72			P01846
DLPAPTIR	882.5	-4.88			IgG2ba-b, IgG4a-b, IgG6a-b, L8B180, L8B0S7, L8B0Z4
LLLDLFR	889.55	-0.56			Unavailable
LLNGYRR	891.52	-4.6			Unavailable
AGGTTVTQVE	962.48	1.14			P01846
LIYQATNR	978.54	3.37			IPR 007110 (Ig C1-set)
VDPALPLEK	981.56	-1.58			Unavailable
NRPTGVFSR	983.54	-1.9			Unavailable
TISKATGPSR	1017.57	1.28			IgG3
LSSPATLNSR	1045.56	-3.44			Unavailable
Unknown	1069.55		2933.2	M9	Unavailable
FQQTGGQPPP	1096.54	-2.09			P01846
EAQFNSTYR	1115.49	-19.4	2414.05 2560.12 2722.15 2884.24 3029.35 3191.50	G0 G0F G1F G2F G1FS G3F	IgG6a, L8B180, L8B0Z4
Unknown	1154.53		2599.1	G0F	Unavailable

Peptide sequence	$m/z$ (M + H) <sup>+</sup>	Error (ppm)	$m/z$ glycoform	Glycoform	Identification source <sup>*</sup>
EEQFNSTYR	1173.5	-14.6	2471.01 2618.09 2634.07 2780.13 3087.23 2942.19 3104.23 3249.28 2833.04	G0 G0F G1 G1F G1FS G2F G3F G2FS M9-N	IgG1a-b,IgG2a-b,IgG4a-b,IgG5ab,IgG6b, L8B0S7,L8B0S2,K7ZLA7
TNNRPTGVPSR	1198.63				Unavailable
H2N-300-QNFSVFR	1212.13		2656.09 2819.14 2981.20	G0F G1F G2F	Unavailable
SYLALSADWK	1240.62	-0.64			P01846
DTNRPSGIPER	1241.62	-2.6			Unavailable
STNSRPTGVPSR	1258.65	0.16			P01846
FSGSGTDFLK	1303.62	2.74			Unavailable
SSSGFTQVTHE	1339.56	1.27			P01846
TAPSVYPLAPCGR	1388.71	7.85			IgG1a-b,IgG4b,IgG5b,IgG6b,L8B180,K7 ZLA7,L8B0Z4
LLGASVLGVGDHR	1406.81	1			Unavailable
Unknown	1415.62				Unavailable
Unknown	1467.28		2911.26 3073.31	G0F G1F	Unavailable
Unknown	1495.73				Unavailable
LVESGGGLVQPGSLR	1525.85	11			L8B0S2,L8B180,L8B0S7
QSNKYAASSYLAL	1529.76	0.39			P01846
AGGTTVTQVETTKPSK	1604.85	0.6			P01846
YAASSYLALSADWK	1632.79	0.24			P01846
VVSVLPQHQDWLK	1661.92	-10.4			IgG1a- b,IgG3,IgG6b,L8B180,K7ZLA7,L8B0Z4
QEYREDFLVTGK	1667.83	12.7			Unavailable
APASYFVQSVLTVSAK	1667.9	0			K7ZJF7

Peptide sequence	$m/z$ (M + H) <sup>+</sup>	Error (ppm)	$m/z$ glycoform	Glycoform	Identification source <sup>*</sup>
Unknown	1718.91				Unavailable
TVIYSTNSRPTGVPSR	1734.91	1.73			P01846
QLIYSTNNRPTGVPSR	1802.95	3.88			Unavailable
QLIYQINSRPTGVPSR	1816.97	1.98			IPR 007110 (Ig-like)
SSSGFTCQVTHEGTIVEK	1966.92	1.32			P01846
AAPTVINLPPSSEELGTNIK	1972	1.06			P01846
ASGVPRFRSGSGGTDFTLK	1985.96	1.86			Unavailable
FTDETLVSDLQPSLDRAR	2063.04	0.15			Unavailable
ATLVCLISDFYFGAVTVWK	2083.1	3.26			P01846
AGPLGWFERRPEPPGPPSK	2172.14	2.39			Unavailable
QSNNKYAAASSYLALSASDWK	2204.06	0.82			P01846
Unknown	2717.07				Unavailable
Unknown	2832.04				Unavailable

<sup>\*</sup>L8B180, L8B0Z4, L8B0S2, L8B0S7, K7ZLA7 porcine IgG heavy chain entries (Fc) [22]; P01846, porcine IgG lambda constant domain (Fab); K7ZJP7, IgM heavy chain; P01786, mouse IgG heavy chain; P01857, human IgG heavy chain; IgGs, from [3]; IPR, GPM entries.

**Table 1.**

Masses and sequences of peptides found in a glycopeptide-enriched fraction from porcine IgG (wild-type) tryptic digestion products. Red: Labeled manually; black: Sequenced and/or matched by GPM [24]. Glycopeptides,  $m/z$  values in bold not observed, only glycoforms.



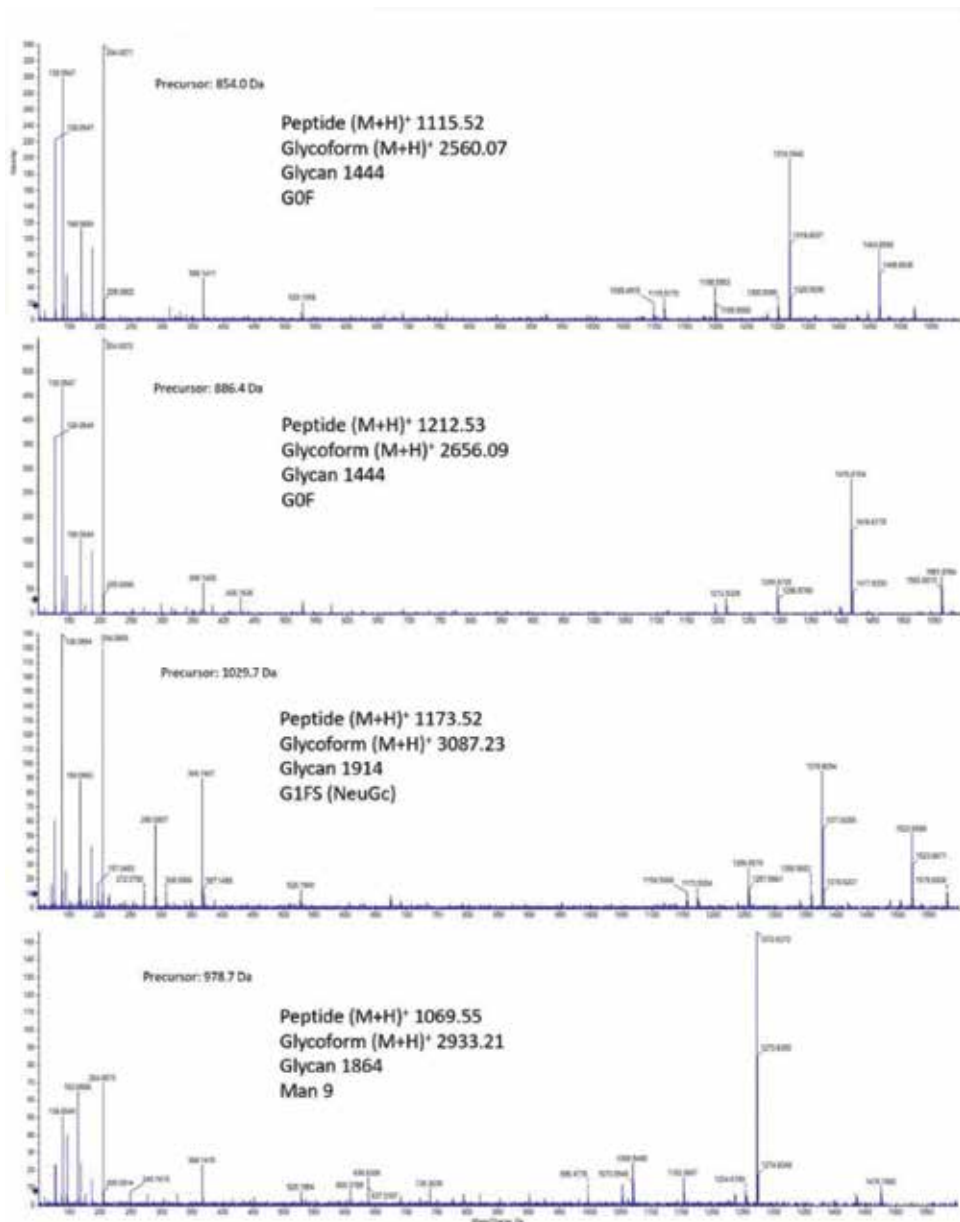


**Figure 2.** Tandem mass spectra of doubly or triply charged ions of glycopeptides enriched from the tryptic products of porcine wild-type IgG. (a) GoF glycoform of EAQFNSTYR, (b) GoF of undetermined peptide, (c) G1FS of EEQFNSTYR, (d) Man-9 of undetermined peptide.

### 3.2 Fragmentation of porcine wild-type IgG with papain and fabulous™ followed by SEC

Antibody samples were first fragmented on immobilized papain, and thus it is expected that only IgG-related products will be present in the mixture. As shown by **Figure 3a**, all antibody was fragmented (intact antibody would have appeared at ca. 4.5 min). In general, when IgG is incubated with papain with a reducing agent, one or more peptide bonds in the hinge region are split, producing three fragments of similar size: two Fab fragments and one Fc fragment. The Fc may remain intact

based on conditions and enzyme used [9, 10]. The cleavages occur at cysteines around position 271 (in **Figure A1**), about 10 amino acids from the IdeS cleavage site [29]. In human IgG subtypes (IgG1-4), there are on average of three cysteines in the range of hinge region positions 265–275 to make the numbers correspond with those of **Figure A1**, where papain cleavages can be initiated [29]. Porcine IgG has similar cysteine motifs in these positions; however, **Figure A1** shows different lengths of amino acid chains in the hinge region, which did not seem to prevent fragmentation. Interestingly in this papain-fragmentation experiment, the Fc did not remain intact, but the Fab did. **Figure 3a** shows significant separation although not at the baseline, but which still allowed the collection of Fab and Fc fractions.

In order to further isolate Fab and Fc segments, collected fractions were analyzed in turn by SDS-PAGE. This allowed identification by mass, with confirmation by linear mode MALDI-TOF-MS (not shown) and in-gel tryptic digestion of the bands (analyzed by reflector mode MALDI-TOF-MS and HPLC-MS, next section). The first major peak in **Figure 3a** was identified as originating from the Fab, and the second peak was identified as the Fc. The intact Fab fragment is larger and thus elutes prior to the split Fc, while the opposite is usually true in the case of human IgG [15].

Fabulous™ is a recombinant cysteine protease which under reducing conditions digests in the hinge region of antibodies from many species and subclasses, including human, mouse, rat, and rhesus monkey, yielding Fab and Fc fragments [11]. Some specific fragmentation site information is available for human IgG1, mouse IgG1, and rabbit IgG, but no information at all pertains to the fragmentation of porcine

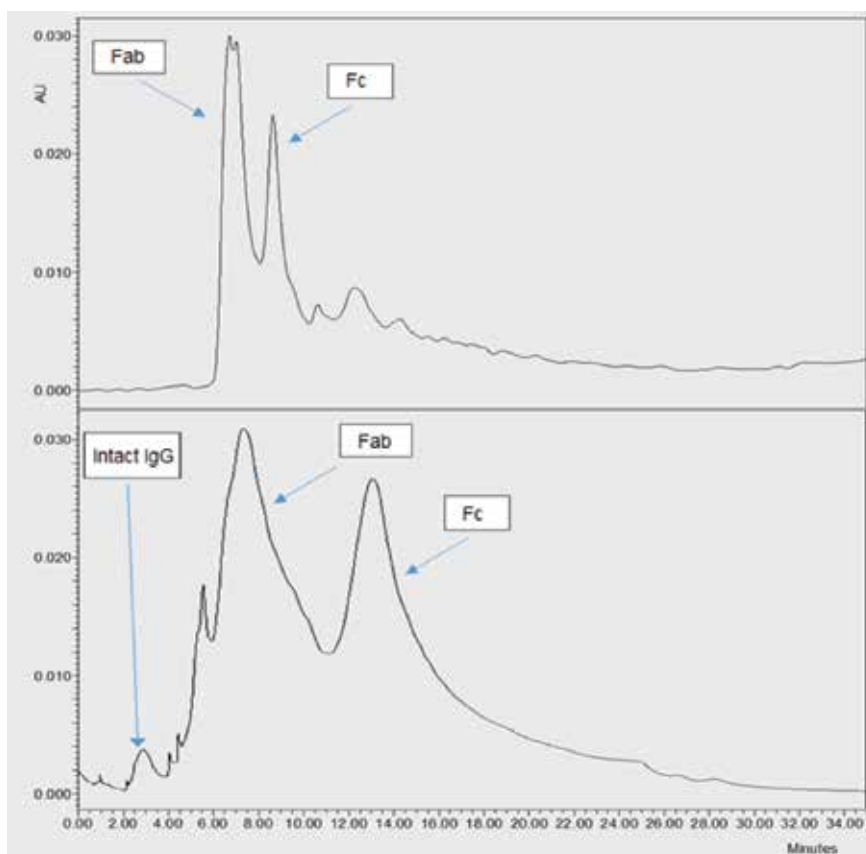


**Figure 3.** Size exclusion chromatograms obtained for 200  $\mu$ g of wild-type porcine IgG fragmented by (a) immobilized papain and (b) Fabulous™.

IgG. Looking at all porcine IgG subtype sequences (see alignment in **Figure A1**), they have a motif similar to that of rabbit IgG (KP<sup>270</sup>I/CP) [11], that is, with a potential fragmentation site between isoleucine I and cysteine C: CP<sup>270</sup>I/CPG or CP<sup>270</sup>I/CPA.

In general, when IgG molecules are incubated with Fabulous™ in the presence of a reducing agent, one or more peptide bonds in the hinge region are split next to a cysteine, producing two Fab fragments and one Fc. As the reducing agent is present during the digestion reaction, it is likely that all interchain thiols will be reduced.

In this experiment with Fabulous™ using 100 µg of pig IgG, a small portion of the antibody was not fragmented; otherwise the Fc was split into two halves and the Fab fragments remained intact. The HPLC-SEC chromatogram is shown in **Figure 3b**. The first major peak was indicative of the Fab fragment, and the second peak eluting after identified as the Fc, as verified later by SDS-PAGE and further tryptic digestion. As noticed in the chromatograms of **Figure 3**, elution times are different, that is, longer in portion b. This is due to gradual deterioration of the column, as both experiments depicted in a and b were performed several months apart.

The fact that Fabulous™ (28,724 Da [11]) was free in solution and not immobilized as in the case of papain involves that it would elute in the SEC chromatogram (**Figure 3b**), most probably in the second peak with the Fc. If this proprietary enzyme has a sequence similar to that of papain, subsequent proteolysis by trypsin is likely to occur extensively, as many lysine and arginine residues are present in papain's sequence [31].

### 3.3 SDS-PAGE separation of porcine IgG fragments

For papain-produced fragments, a nonreducing gel experiment was performed on the previously collected SEC fractions (**Figure 4a**). This experiment allowed confirming the identity of the fragments. A reducing SDS-PAGE experiment was also performed on intact pig IgG to serve as a control (**Figure 4b**). Bands were then excised from the gel, followed by in-gel tryptic digestion. This helped to single out heavy and light chains for differentiating between Fab and Fc according to their respective known glycopeptides and peptides [2, 3]. In **Figure 4a**, lanes 6–9 correspond to a fraction containing both Fab and Fc collected at the junction of SEC peaks in **Figure 3a**. A single 50 kDa Fab band and two 25 kDa bands were obtained. The Fab band is positioned just below the 50 kDa marker band and clearly below the Fc band in **Figure 4b**, and the Fab should have a lower molecular weight than intact Fc [32].

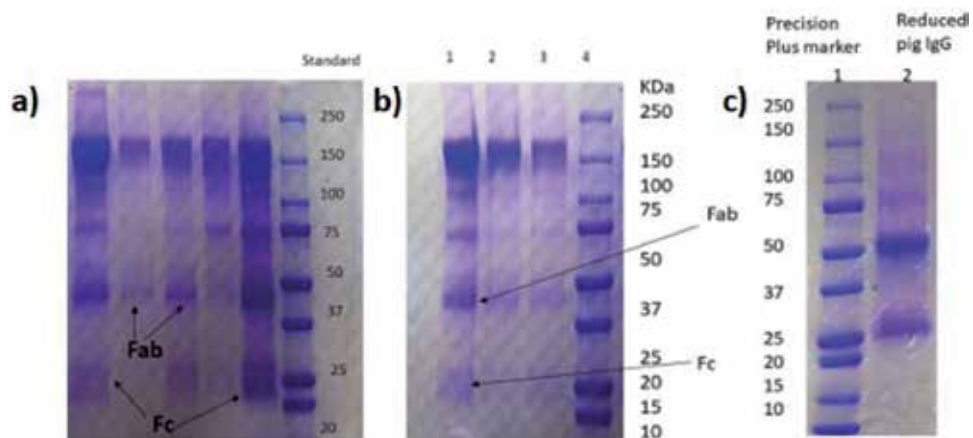


**Figure 4.** (a) Fab and Fc SEC fractions from papain-fragmented porcine IgG on nonreducing SDS-PAGE and (b) from Fabulous™-fragmented porcine IgG, (c) whole porcine IgG runs under reducing conditions.

Both bands appearing in the Fc region were digested independently with trypsin as denoted by “upper Fc band” and “lower Fc band.” It appears from further results that they belong to different IgG subtypes. For Fabulous™ fragments, the same experiment was conducted and results are shown in **Figure 4b**. According to gel separations, papain and Fabulous™ had very similar fragmentation effects on porcine IgG.

### 3.4 MALDI-MS of in-gel tryptic-digested Fc bands

**Figure 5a** shows the tryptic products for the upper Fc band (papain generated) in **Figure 4a**. The main glycopeptide observed has three main glycoforms at  $m/z$  2472, 2618, and 2780 as  $[M + H]^+$  ions. In **Figure 5b** (lower Fc band), two series of glycopeptides are observed, that is, the same as above and another one at  $m/z$  2414, 2560, and 2722. The amino acid sequences of these glycopeptides were verified by MALDI-MS/MS as EEQFNSTYR and EAQFNSTYR, respectively [2, 3], with glycoforms as indicated in the figure. PNGase de-glycosylation of these two samples led to the spectrum of **Figure 5c**, where peptides at  $m/z$  1117 (EAQFDSTYR) and 1175 (EEQFDSTYR) were detected, while the analysis of released glycans was not successful. Similar MALDI-MS and MS/MS results were obtained for the Fabulous™-generated porcine IgG that combined upper and lower Fc fragments digested with trypsin. Besides glycopeptides from the Fc region, other Fc  $\gamma$ -domain peptides were observed, as identified from the database [22] in **Table 2**.

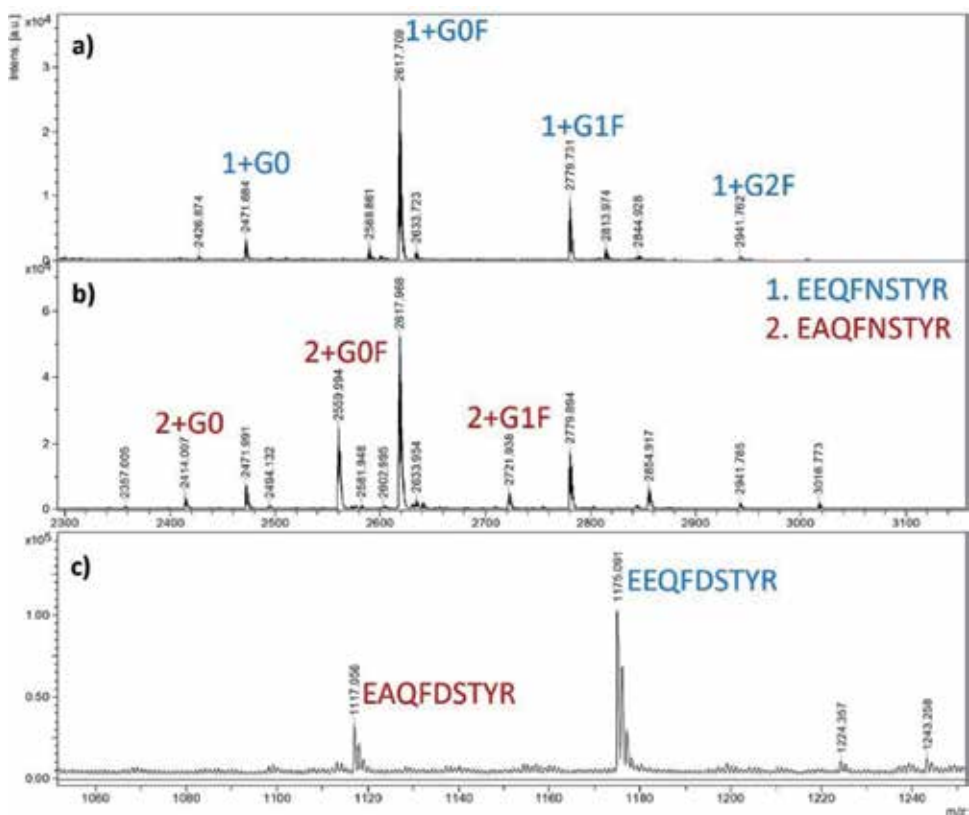


**Figure 5.** Reflector positive mode MALDI-TOF-MS spectra of (a) tryptic digestion products from pig IgG Fc fragment (higher 25 kDa band) and (b) lower Fc fragment. Both bands were excised from the gel run under non-reducing conditions shown in **Figure 4a**. (c) De-glycosylated peptides after removal of glycans to give peptides at  $m/z$  1117 and 1175.

Peptide sequence	$m/z$ (M + H) <sup>+</sup>	Error ppm	$m/z$ glyco-form	Glyco-form	Source*
Unknown	807.28				Unavailable
Unknown	842.38				Unavailable
Unknown	870.41				Unavailable
DLPAPIIR	882.5	-5.78			IgG2ba-b,IgG4a-b,IgG6a-b, L8B180, L8B0S7, L8B0Z4
Unknown	905.33				Unavailable
Unknown	951.33				Unavailable
Unknown	993.36				Unavailable
Unknown	1033.4				Unavailable
Unknown	1107.4				Unavailable
EAQFNSTYR	1115.5	-22.51	2560.39	G0F	IgG6a, L8B180, L8B0Z4
Unknown	1165.4				Unavailable
EEQFNSTYR	1173.50	-14.6	2471.60 2779.62 2779.63	G0 G0F G1F	IgG1a-b,IgG2a-b,IgG4a-b,IgG5a-b, IgG6b, L8B0S7, L8B0S2, K7ZLA7
Unknown	1209.5				Unavailable
Unknown	1261.4				Unavailable
VNNVDLPAPIIR	1308.6	-66.51			IgG1a-b, K7ZLA7
Unknown	1330.4				Unavailable
SNGQPEPEGNYR	1347.6	-1.48			IgG1a,IgG6a-b, L8B180, L8B0S2, K7ZLA7, L8B0Z4
Unknown	1374.4				Unavailable
Unknown	1392.2				Unavailable
Unknown	1427.6				Unavailable
Unknown	1475.6				Unavailable
Unknown	1503.4				Unavailable
LVESGGGLVQPGGSLR	1525.7	-74.23			L8B180, L8B0S7

Peptide sequence	$m/z$ (M + H) <sup>+</sup>	Error ppm	$m/z$ glyco-form	Glyco-form	Source*
VSSQNIQDFPSVLR	1589.8	42.9			K7ZJP7 (IgM HC const. region)
YAASSYLALSASDWK	1632.8	-24.5			P01846 UniproTKB (Ig $\lambda$ const. region)
VVSVLPQHQDWLK	1662	13.7			IgG1a-b, IgG3, IgG6b, L8B180, K7ZLA7, L8B0Z4
Unknown	1677.5				Unavailable
Unknown	1693.7				Unavailable
Unknown	1725.4				Unavailable
Unknown	1740.6				Unavailable
Unknown	1754.4				Unavailable
STGKPTLYNVSIVLSDT	1794.8	-60.4			K7ZJP7 (IgM HC const. region)
EPQVYTLSPSAEELSR	1805.8	-34.1			IgG6a-b, L8B180, L8B0Z4
EPQVYTLPPAEELSR	1825.9	2.9			IgG1a-b, K7ZLA7
EPQVYTLPPTEELSR	1855.9	-2.32			IgG4b
TTPPQQDVGTFFLYSK	1943.8	-50.7			IgG1a-b, K7ZLA7
TTPPQQDVGTYFLYSK	1959.9	-1.07			IgG2a-b, IgG3, IgG4a-b, IgG6a, L8B180, L8B0S7, L8B0Z4
AAPTVNLPPSSSELGTNK	1971.9	-36.6			P01846 UniproTKB (Ig $\lambda$ const. region)
Unknown	2135.8				Unavailable
Unknown	2162.9				Unavailable
Unknown	2211				Unavailable
GLEGLAVIGYGVITDYADSVK	2305.4	86.8			L8B180

\*L8B180, L8B0Z4, L8B0S2, L8B0S7, K7ZLA7, porcine IgG heavy chain entries (Fc) [22]; P01846, porcine IgG lambda constant domain (Fab); K7ZJP7, IgM heavy chain; P01786, mouse IgG heavy chain; P01857, human IgG heavy chain; IgGs, from [3]; IPR, GPM entries.

**Table 2.**

Masses and sequences of peptides found by MALDI-MS in porcine IgG (wild-type) tryptic digestion products of combined Fc bands obtained by papain and Fabulouso™ fragmentation. Peptides and glycopeptides in red were sequenced manually after MS/MS and/or tentatively identified by mass fingerprinting.

### 3.5 In-gel tryptic-digested fab bands analyzed by MALDI-MS

The bands just below 50 kDa from both papain and Fabulous™ digestion processes were excised from the gel and digested with trypsin. MALDI-MS spectra of the products were obtained, and display no obvious glycopeptides as found in the Fc. Some peaks could be identified as light and heavy chain Fab peptides. Fab peptide masses and sequences available are listed in **Table 3**.

Sequence	<i>m/z</i> ESI	<i>m/z</i> MALDI	Error ppm	Identification source
FSGAISGNK	880.45	880.39	-70.8	P01846 (Ig λ const. region)
Unknown	951.33	951.21		Unavailable
Unknown	993.36	993.56		Unavailable
Unknown		1052.22		Unavailable
Unknown		1119.29		Unavailable
Unknown		1141.26		Unavailable
Unknown	1209.48	1209.28		Unavailable
Unknown		1242.51		Unavailable
FSGSGSGTDFTLK	1303.62	1303.61	-4.91	Unavailable
Unknown		1339.55		Unavailable
Unknown		1374.27		Unavailable
Unknown		1383.95		Unavailable
Unknown		1419.30		Unavailable
Unknown		1476.02		Unavailable
Unknown	1503.39	1504.12		Unavailable
Unknown		1526.39		Unavailable
Unknown		1584.35		Unavailable
Unknown		1622.45		Unavailable
YAASSYLALSASDWK	1632.79	1632.85	36.7	P01846 (Ig λ const. region)
Unknown		1660.16		Unavailable
Unknown		1735.19		Unavailable
Unknown		1762.23		Unavailable
QLIYSTNNRPTGVPSR	1802.95	1803.00	27.73	Unavailable
Unknown		1826.41		Unavailable
Unknown		1866.38		Unavailable
Unknown		1910.24		Unavailable
Unknown		1942.26		Unavailable
AAPTVNLFPPSSEELGTNK	1972.00	1972.18	90.2	P01846 (Ig λ const. region)
Unknown		2034.37		Unavailable
FTDETLVSDLQPSLDRAR	2063.04	2063.17	62.9	Unavailable
Unknown	2135.81	2136.40		Unavailable
Unknown	2210.95	2211.46		Unavailable
Unknown		2338.64		Unavailable
Unknown		2377.63		Unavailable
Unknown		2408.38		Unavailable
VTLTCLVTGFYPPDIDVEWQR	2509.24	2509.39	58.5	IgG4a

Sequence	<i>m/z</i> ESI	<i>m/z</i> MALDI	Error ppm	Identification source
Unknown		2691.50		Unavailable
Unknown		2807.49		Unavailable

**Table 3.**

*Fab tryptic peptides from porcine IgG fragmented with papain and Fabulous™. Second column (*m/z* ESI): Already identified in **Table 1**. Error: Measured using the MALDI *m/z* values against calculated values. Sequences in red are assigned from mass only based on **Table 1**.*

Overall, MALDI-TOF-MS experiments allowed suggesting that efficient separation of Fab and Fc fragments from each other occurred, using the SEC/SDS-PAGE procedure. There was a minimal number of overlapping peptides between Fab and Fc MALDI spectra (**Tables 2** and **3**). In **Table 3**, peptides in red had already been sequenced and appeared in **Table 1**; peptides whose *m/z* values appear in the second column were also observed in **Table 1**, although not sequenced. Overlapping peptides between **Tables 2** and **3** are at *m/z* 2509 (unknown), 2884 (glycoform of *m/z* 1115), and *m/z* 1677 (IgM). The presence of IgM in the sample had been noticed in an earlier report [3].

### 3.6 Tryptic products of Fabulous™-fragmented porcine IgG analyzed by HPLC/MS

Each sample of digestion products from Fc and Fab bands were analyzed twice by HPLC/MS, and results are summarized in **Table 4**. In **Figure A2**, total ion chromatograms (TIC) of the pig Fab and Fc tryptic products showed differences in the retention times of some peaks as expected. Peaks observed at the same retention times (e.g., 4.41–4.46, 10.35, and 23.10 min) and common to all injections corresponded to singly charged ions of small compounds of *m/z* < 700 and were not considered in the analysis, as they probably were non-peptide contaminants. Peaks at 5.96 min also present in both chromatograms corresponded to a mass 1660 peptide from the Fab, AGGTTVTQVETTKPSK. Non-glycosylated peptides in **Table 4** were identified through MS/MS and database search, while glycopeptides were assigned by mass only in reference to entries in **Table 1**.

As Fabulous™ was possibly still present in the mixture at the time of tryptic digestion of the Fc gel band, analogous papain tryptic digestion products were sought for by *m/z*, but not found. Only one papain peptide with sequence YIDETNK (*m/z* 882.4203) could be present according to its nominal mass; however, the observed *m/z* 882.4998 peptide ions are closer to the calculated mass of IgG DLPAPITR, 882.4939. As seen in **Table 4**, many peptides remain un-sequenced/unidentified, and others are identified as either Fab or Fc peptides of porcine IgG. Interestingly, there were some very good matches with human and mouse IgG, which is not surprising given relatively high levels of homology between mammal species in general. However even with all the heavy chain sequences available in the literature for porcine IgG (see footnote of **Table 4** and **Figure A1**), none of them contained the human- and murine-assigned peptides. It is also interesting to observe that most peptides are predominant in either the Fab or Fc injections and that overlapping peptides are clearly more present in one sample than in the other. Accordingly, all Fab P01846 peptides (*m/z* 880, 1175, 1274, 1375, 1533, 1590, and 1661) were more abundant in the Fab than the Fc sample, although all these peptides showed some level of overlap. The same reasoning is applicable to Fc peptides, including the *N*-glycoforms of EAQFNSTYR and EEQFNSTYR. It is also possible to know the origin of most unidentified peptides in **Table 4** by comparing their normalized abundances. Other *N*-glycopeptides reported in **Table 1** were not detected in these Fab and Fc RPLC/MS experiments, possibly due to the lack of glycopeptide enrichment and to sample loss during the SEC and SDS-PAGE procedures.



Mass (calc.)	$m/z$ (M + H) + (exp.)	$m/z$ error (ppm)	PigFabwt (avg)	PigFwwt (avg)	Normalized abundance	Sequence	Sources of identification*
516.301	517.309	0.00	0.0	23.9		VDKR	IgG1a-b,IgG2a-b,IgG3,IgG4a-b
585.322	586.330	-1.97	76.1	1972.6		PGSILR	P01786
712.372	713.380	-4.25	8.0	891.4		LVESGGGL	P01786
768.412	769.420		0.0	9.4			
806.345	807.353		652.0	22.4			
811.439	812.447	-5.63	6.1	424.4		LVESGGGLV	P01786
816.416	817.424		0.0	78.4			
824.372	825.380		0.0	9.1			
826.434	827.442		749.4	1176.6			
827.511	828.519		478.3	166.0			
834.421	835.429		0.0	65.1			
837.492	838.500	-5.12	14.2	0.0		ALPAPIEK	P01857
841.502	842.510		977.9	1260.9			
844.291	845.299		264.0	0.0			
850.418	851.426		0.0	42.4			
861.432	862.440		220.3	52.3			
872.373	873.381		0.0	74.7			
872.397	873.405		0.0	15.5			
879.445	880.453	-0.45	1559.7	479.8		FSGAISGNK	P01846
881.492	882.500	-5.78	0.0	410.6		DLPAPITR	IgG2ba-b,IgG4a-b, IgG6a-b,L8B180,L8B057,L8B074

Mass (calc.)	$m/z$ (M + H) <sup>+</sup> (exp.)	$m/z$ error (ppm)	Pig Fab wt (avg)	Pig Fc wt (avg)	Normalized abundance	Sequence	Sources of identification <sup>*</sup>
888.366	889.374		0.0	44.9			
917.391	918.399		254.9	54.6			
919.450	920.458		17.9	135.1			
935.856	936.864		2502.6	2690.0			
939.510	940.518	7.61	86.4	407.8	LVESGGGLVQ	P01786	
990.341	991.349		264.4	5.6			
994.506	995.513		13.2	518.7			
994.512	995.520		7.6	311.7			
1043.899	1044.907		1589.5	1690.0			
1044.554	1045.562	-2.30	5106.9	6511.7	LSSPATLNSR	Unavailable	
1057.831	1058.839		1179.7	1190.5			
1066.539	1067.547	-1.47	0.0	8.5	VDGVEVHNAK	P01857	
1103.601	1104.609		0.0	17.0			
1164.577	1165.585		66.4	199.4			
1174.613	1175.621	-5.01	468.4	169.5	TQGVETTKPSK	P01846	
1208.640	1209.648		0.0	790.8			
1238.648	1239.656		1.6	343.5			
1259.553	1260.561		3.7	480.5			
1260.536	1261.544		15.5	1386.4			
1273.685	1274.693	-1.89	324.0	104.5	VTQGVETTKPSK	P01846	
1296.678	1297.686		9.3	727.0			
1298.485	1299.493		30.8	263.2			
1302.609	1303.617	0.00	2446.2	908.9	FSGSGGTFDTLTK	Unavailable	

Mass (calc.)	$m/z$ (M + H) + (exp.)	$m/z$ error (ppm)	Pig Fab wt (avg)	Pig Fc wt (avg)	Normalized abundance	Sequence	Sources of identification*
1307718	1308.726	-1.30	139.6	13772.8		VNNVDLPAPITR	IgG1a-b,K7ZLA7
1308.702	1309.710		13.2	3997.2			
1312.672	1313.680	-1.22	2.4	306.7		ESGGGLVQGGSLR	P01786
1316.625	1317.633		896.9	223.7			
1329.687	1330.695		20.3	434.9			
1330.670	1331.678		87.9	1324.0			
1334.648	1335.656		23.1	374.1			
1340.548	1341.556		131.8	45.0			
1345.666	1346.674		5.8	2149.3			
1346.587	1347.595	1.41	47.2	658.2		SNGQPEPEGNYS	IgG1a, IgG5b, IgG6b, L8B180K7ZLA7, L8B0Z4
1347.568	1348.576		50.8	1702.0			
1350.620	1351.628		7.9	512.8			
1368.616	1369.624		16.4	484.9			
1374.732	1375.740	-2.30	742.1	219.7		TVTQGVETTKPSK	P01846
1376.558	1377.566		457.8	61.0			
1390.608	1391.616		3.4	308.0			
1391.593	1392.601		6.6	898.0			
1399.808	1400.816		1434.9	1503.7			
1433.682	1434.690		8.5	226.8			
1449.688	1450.696		17.8	958.3			

Mass (calc.)	$m/z$ (M + H) <sup>+</sup> (exp.)	$m/z$ error (ppm)	Pig Fab wt (avg)	Pig Fc wt (avg)	Normalized abundance	Sequence	Sources of identification*
1514.667	1515.675		100.8	1436.0			
1524.822	1525.830	-2.62	1005.8	20216.6		LVESGGGLVQPGGSLR	L8B180, L8B0S7
1530.664	1531.672		0.3	599.0			
1532.803	1533.811	-0.91	646.1	171.1		GTTVTQGVETTKPSK	P01846
1546.798	1547.806		64.1	2405.4			
1562.772	1563.780		192.8	4750.7			
1578.744	1579.752	4770	4.7	439.3		ERQFNSTYR +2GlcNAc	IgG1a-b,IgG2a-b,IgG4a-b,IgG5a-b,IgG6b,L8B0S7,L8B0S2,K7ZLA7
1589.823	1590.831	-1.93	647.8	181.7		GTTVTQGVETTKPSK	P01846
1624.841	1625.849		321.8	72.8			
1642.851	1643.859	-0.92	1827.2	614.7		AGTTVTQGVETTKPSK	[C-term] neutral loss
1660.864	1661.872	0.26	11688.6	4028.5		AGTTVTQGVETTKPSK	P01846
1682.829	1683.837		346.8	77.9			
1698.811	1699.819		1146.9	308.5			
1719.703	1720.711		10.5	471.9			
1735.702	1736.710		0.0	480.4			
1753.805	1754.813		2.7	493.2			
1769.797	1770.805		4.8	723.1			

Mass (calc.)	$m/z$ (M + H) <sup>+</sup> (exp.)	$m/z$ error (ppm)	Pig Fab wt (avg)	Pig Fc wt (avg)	Normalized abundance	Sequence	Sources of identification*
1801.950	1802.958	3.60	191.0	99.2	99.2	QLIYSTNNRPTGVPSR	Unavailable
1807.752	1808.760		4.8		287.3		
1824.931	1825.939	2.90	4.0	670.0	670.0	EPQYYTLPPEAELSR	IgG1a-b,K7ZLA7
1854.932	1855.940	-2.32	0.0	1499.6	1499.6	EPQYYTLPPEEELSR	IgG4b
1862.867	1863.875		0.0	695.8	695.8		
1919.930	1920.938		1.8	0.0	0.0		
1958.924	1959.932	-1.07	3.4	2082.2	2082.2	TTPPQQDVGTYFLYSK	IgG4a-b, IgG6a, L8B180, L8B0S7, IgG2a, IgG2b, IgG3
2092.889	2093.897		649.7		14.8		
2251.915	2252.923		0.0	750.1	750.1		
2267.910	2268.918		0.0	356.8	356.8		
2289.908	2290.916		0.0	72.8	72.8		
2355.931	2356.939		0.0	62.0	62.0		
2413.960	2414.968	-11.42	0.0	2793.9	2793.9	G0 of EAQFNSTYR	IgG6a, L8B180, L8B0Z4
2435.939	2436.947		0.0	86.5	86.5		
2451.911	2452.919		0.0	90.0	90.0		
2558.988	2559.995	-19.69	0.0	25.6	25.6	G0F EAQFNSTYR	IgG6a, L8B180, L8B0Z4
2576.008	2577.016		0.0	439.0	439.0		
2617.036	2618.044	-2.66	3.5	1257.9	1257.9	G0F EEQFNSTYR	IgG1a-b, IgG2a-b, IgG4a-b, IgG5a-b, IgG6b, L8B0S7, L8B0S2, K7ZLA7

Mass (calc.)	$m/z$ (M + H) + (exp.)	$m/z$ error (ppm)	Pig Fab wt (avg)	Pig Fc wt (avg)	Normalized abundance	Sequence	Sources of identification*
2639.006	2640.014		0.0	706.3			
2654.984	2655.992		2.5	1048.1			
2670.955	2671.963		0.0	200.5			
2692.958	2693.966		0.0	49.2			
2779.092	2780.100	-1.36	0.0	1327.0		G1F EEQFNSTYR	IgG1a-b,IgG2a-b,IgG4a-b,IgG5a-b,IgG6b,L8B0S7,L8B0S2,K7ZLA7
2801.070	2802.078		2.8	244.1			
2817.033	2818.041		0.0	380.8			
2941.166	2942.174	5.90	0.0	266.4		G2F EEQFNSTYR	IgG1a-b,IgG2a-b,IgG4a-b,IgG5a-b,IgG6b,L8B0S7,L8B0S2,K7ZLA7
3004.216	3005.224		0.0	68.7			
3086.182	3087.190	-1.33	0.0	159.4		G1FS EEQFNSTYR	IgG1a-b,IgG2a-b,IgG4a-b,IgG5a-b,IgG6b,L8B0S7,L8B0S2,K7ZLA7

\*L8B180,L8B0Z4,L8B0S2,L8B0S7,K7ZLA7, porcine IgG heavy chain entries (Fc) [22]; P01846, porcine IgG lambda constant domain (Fab); K7ZLP7, IgM heavy chain; P01786, mouse IgG heavy chain; P01857, human IgG heavy chain; IgGs, from [3]; IPR, GPM entries.

**Table 4.**  
Tryptic peptides from pig IgG Fab and Fc fragment analyzed by HPLC-MS/MS.

### 3.7 Comparative aspects of both workflows

The initial RPLC-MS/MS experiment on the enriched whole IgG digest produced the most useful information in terms of glycopeptides. Besides the latter, many peptides were identified as originating from the Fc or Fab portion, while for other peptides origin remained unknown. This first workflow allowed detecting *N*-glycopeptides from the Fab portion of the antibody, although their sequences could not be completely assigned. The second workflow necessitated more intensive work than the first one. Size-exclusion chromatography or SDS-PAGE was not sufficient on its own to properly separate Fab and Fc, and a combination of both was preferable. Even then, RPLC/MS results show partial overlaps for many peptides, although most peptides were much more abundant in one sample (Fc or Fab) than in the other. In terms of ionization modes used in the second workflow, ESI yielded more details on sialylated glycopeptides, but did not allow the observation of Fab *N*-glycopeptides. As analyses by MALDI were the result of depositing all tryptic products of a gel band onto one target spot, it is probable that the signals of sialylated glycopeptides or low concentration Fab glycopeptides were overtaken competitively by peptides that are more abundant.

## 4. Conclusions

Porcine immunoglobulins constitute a complex ensemble of biomolecules, with several subtypes whose amino acid sequences are not clearly assigned and described in the literature (see **Figure A1**). In this study, three state-of-the-art mass spectrometers were used to characterize tryptic peptides, offering a considerable amount of complementary information owing to the great sensitivities of these instruments, given the small amounts of IgGs used. Indeed, fragmentation of porcine IgG into its Fc and Fab portions was achieved for the first time using papain and Fabulous™ on 200 µg or less of antibody. Fragments needed separation by both SEC and SDS-PAGE before analysis by MALDI-TOF-MS and HPLC/MS. These separation procedures did not eliminate the overlapping of Fab and Fc tryptic peptides entirely; however, there was a significant level of discrimination. This workflow resulted in better knowledge about the origin of tryptic peptides from IgG.

During the course of this work, the several sources of sequence information on porcine IgG found in **Figure A1** were used to verify HPLC-MS/MS, MALDI-TOF-MS, and HPLC-MS data. Most Fc peptides were from the gamma constant region, where some Fab peptides were identified as belonging to the constant portion of the lambda chain. The HPLC-MS/MS method of tryptic peptide without previous Fab-Fc fragmentation was the most efficient in terms of useful data generated per amount of sample used, although many peptides could not be related to either Fc or Fab. This study highlights the need for detailed pertinent sequence information for porcine IgG, which is not a commonly studied set of biomolecules. Future work will involve the quantification of IgG subtypes according to unique peptide sequences that are already known in each subtype.

## Acknowledgements

The authors thank Dr. Jean-Paul Soulillou and his team at the Université de Nantes, France, for providing pig IgG samples. Thanks to Genovis for donating Fabulous™ enzyme.

## Conflict of interest

None of the authors has a conflict of interest.

## A. Appendix: supplementary materials

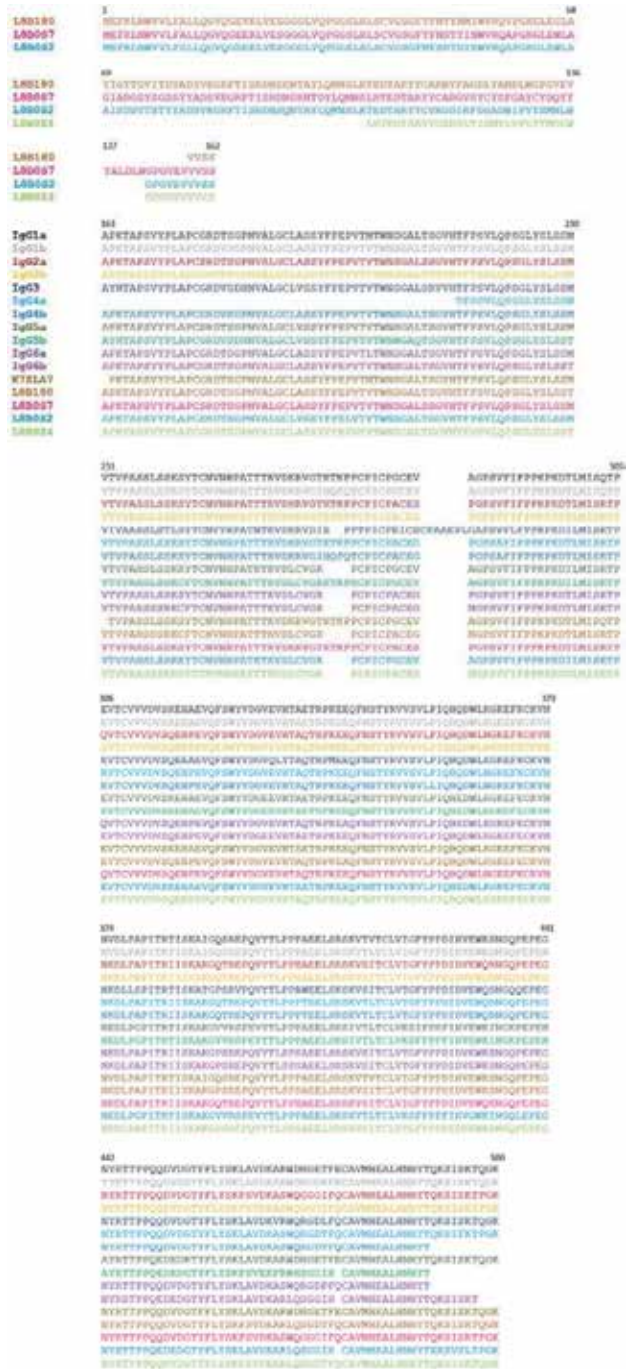


**Figure A1.** Alignment of sequences available in the literature for the porcine IgG heavy chains. IgGn: from Ref. [3]. Others: UniprotKB [22].



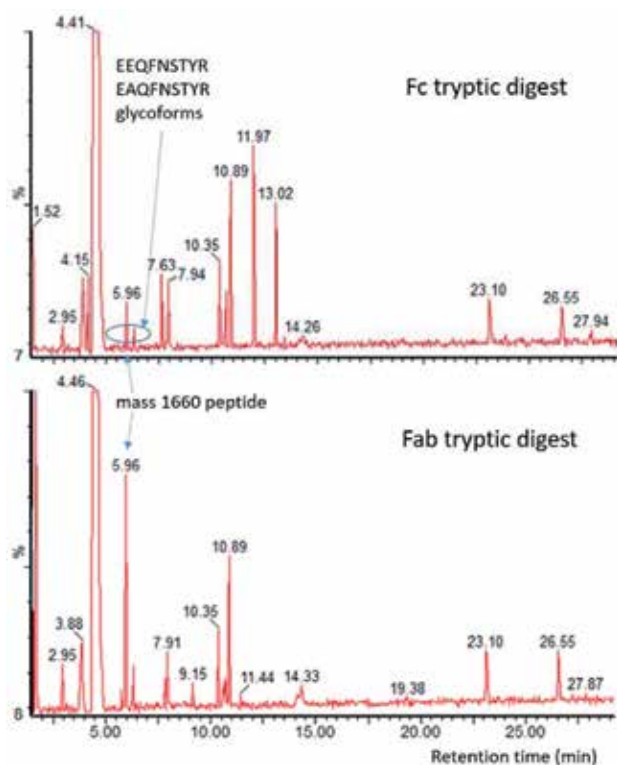


**Figure A2.** HPLC/MS total ion chromatograms obtained for the tryptic products of wild-type porcine IgG Fabulous™ fragments, (a) Fc and (b) Fab.

## Author details

Claudia Nelson<sup>1</sup>, Raymond Bacala<sup>2</sup>, Baylie Gigolyk<sup>1</sup>, Evelyn Ang<sup>3</sup>,  
Haley Neustaeter<sup>3</sup>, Emy Komatsu<sup>1</sup>, Oleg Krokhin<sup>3</sup>, Dave Hatcher<sup>4</sup>  
and H el ene Perreault<sup>1\*</sup>

1 Chemistry Department, University of Manitoba, Winnipeg, MB, Canada


2 Chemistry Department, University of Manitoba and  
Canadian Grain Commission, Government of Canada, Winnipeg, MB, Canada

3 Chemistry Department and Department of Internal Medicine,  
University of Manitoba, Winnipeg, MB, Canada

4 Canadian Grain Commission, Government of Canada, Winnipeg, MB, Canada

\*Address all correspondence to: [helene.perreault@umanitoba.ca](mailto:helene.perreault@umanitoba.ca)

## IntechOpen

  2019 The Author(s). Licensee IntechOpen. This chapter is distributed under the terms of the Creative Commons Attribution License (<http://creativecommons.org/licenses/by/3.0>), which permits unrestricted use, distribution, and reproduction in any medium, provided the original work is properly cited. 

## References

- [1] Burlak C et al. N-linked glycan profiling of GGTA1/ CMAH knockout pigs identifies new potential carbohydrate xenoantigens. *Xenotransplantation*. 2013;**20**(5):277-291
- [2] Buist M et al. Features of N-glycosylation of immunoglobulins from knockout pig models. *Journal of Analytical and Bioanalytical Techniques*. 2016;**7**:333-342
- [3] Lopez PG et al. Characterization of N-glycosylation and amino acid sequence features of immunoglobulins from swine. *Glycoconjugate Journal*. 2016;**33**(1):79-91
- [4] Reynard O et al. Anti-EBOV GP IgGs lacking  $\alpha$ 1-3-Galactose and Neu5Gc prolong survival and decrease blood viral load in EBOV-infected Guinea pigs. *PLoS One*. 2016;**11**:e0156775. Accepted, in revision. (Accepted, in revision)
- [5] Butler JE et al. Porcine IgG: Structure, genetics, and evolution. *Immunogenetics*. 2009;**61**(3):209-230
- [6] Vidarsson G, Dekkers G, Rispens T. IgG subclasses and allotypes: From structure to effector functions. *Frontiers in Immunology*. 2014;**5**:520
- [7] Dwek RA, Lellouch AC, Wormald MR. Glycobiology: 'The function of sugar in the IgG molecule'. *Journal of Anatomy*. 1995;**187**(Pt 2):279-292
- [8] Wormald MR et al. Variations in oligosaccharide-protein interactions in immunoglobulin G determine the site-specific glycosylation profiles and modulate the dynamic motion of the Fc oligosaccharides. *Biochemistry*. 1997;**36**(6):1370-1380
- [9] Andrew SM, Titus JA. Fragmentation of immunoglobulin G. *Current Protocols in Immunology*. 2001;**Chapter 2**:Unit 2.8
- [10] Andrew SM, Titus JA. Fragmentation of immunoglobulin G. *Current Protocols in Cell Biology*. 2003;**Chapter 16**:Unit 16.4
- [11] Application Site for Fabulous™ Enzyme, on Genovis Inc. Web Site [Internet]. Available from: <https://www.genovis.com/products/igg-proteases/fabulous/> [Accession Date: 20-08-2018]
- [12] Demignot S, Garnett MC, Baldwin RW. Mouse IgG2b monoclonal antibody fragmentation. Preparation and purification of Fab, Fc and Fab/c fragments. *Journal of Immunological Methods*. 1989;**121**(2):209-217
- [13] Adamczyk M, Gebler JC, Wu J. Papain digestion of different mouse IgG subclasses as studied by electrospray mass spectrometry. *Journal of Immunological Methods*. 2000;**237**(1-2):95-104
- [14] Suzuki N, Lee YC. Site-specific N-glycosylation of chicken serum IgG. *Glycobiology*. 2004;**14**(3):275-292
- [15] Antibody Fragmentation Methods Explained on the Thermo-Fisher Inc. Web Site [Internet]. Available from: <https://www.thermofisher.com/ca/en/home/life-science/protein-biology/protein-biology-learning-center/protein-biology-resource-library/pierce-protein-methods/antibody-fragmentation.html> [Accession Date: 10-08-2018]
- [16] Al-Abdulla I, Casewell NR, Landon J. Single-reagent one-step procedures for the purification of ovine IgG, F(ab')<sub>2</sub> and Fab antivenoms by caprylic acid. *Journal of Immunological Methods*. 2014;**402**(1-2):15-22
- [17] Yu D, Ghosh R. Membrane bioreactor separator system for integrated IgG fragmentation and Fab purification. *Journal of Immunological Methods*. 2010;**359**(1-2):37-41

- [18] Yu D, Ghosh R. Integrated fragmentation of human IgG and purification of Fab using a reactant adsorptive membrane bioreactor separator system. *Biotechnology and Bioengineering*. 2009;**104**(1):152-161
- [19] Bondt A et al. Immunoglobulin G (IgG) Fab glycosylation analysis using a new mass spectrometric high-throughput profiling method reveals pregnancy-associated changes. *Molecular & Cellular Proteomics*. 2014;**13**(11):3029-3039
- [20] Hafkenscheid L et al. Structural analysis of variable domain glycosylation of anti-citrullinated protein antibodies in rheumatoid arthritis reveals the presence of highly sialylated glycans. *Molecular & Cellular Proteomics*. 2017;**16**(2):278-287
- [21] Schmelter C et al. Peptides of the variable IgG domain as potential biomarker candidates in primary open-angle glaucoma (POAG). *Human Molecular Genetics*. 2017;**26**(22):4451-4464
- [22] Protein Database, Uniprotkb [Internet]. Available from: [www.uniprotkb.com](http://www.uniprotkb.com) [Accession date: 01-11-2018]
- [23] Product Application Site for Glycopeptide Enrichment Kits, on Millipore Inc. Web Site [Internet]. Available from: <http://www.emdmillipore.com/CA/en/product/ProteoExtract-Glycopeptide-Enrichment-Kit> [Accession Date: 15-07-2018]
- [24] The Global Proteome Machine Proteomics Data Analysis, Reuse and Validation for Biological and Biomedical Research [Internet]. Available from: <http://www.thegpm.org/> [Accession Date: 21-11-2018]
- [25] Pompach P et al. Semi-automated identification of N-Glycopeptides by hydrophilic interaction chromatography, nano-reverse-phase LC-MS/MS, and glycan database search. *Journal of Proteome Research*. 2012;**11**(3):1728-1740
- [26] Novak J et al. CycloBranch: De novo sequencing of nonribosomal peptides from accurate product ion mass spectra. *Journal of the American Society for Mass Spectrometry*. 2015;**26**(10):1780-1786
- [27] Krokhin O et al. Site-specific N-glycosylation analysis: Matrix-assisted laser desorption/ionization quadrupole-quadrupole time-of-flight tandem mass spectral signatures for recognition and identification of glycopeptides. *Rapid Communications in Mass Spectrometry*. 2004;**18**(18):2020-2030
- [28] Komatsu E et al. Characterization of immunoglobulins through analysis of N-glycopeptides by MALDI-TOF MS. *Methods*. 2016;**104**:170-181
- [29] Wenig K et al. Structure of the streptococcal endopeptidase IdeS, a cysteine proteinase with strict specificity for IgG. *Proceedings of the National Academy of Sciences of the United States of America*. 2004;**101**(50):17371-17376
- [30] Bodnar E et al. An integrated approach to analyze EG2-hFc monoclonal antibody N-glycosylation by MALDI-MS. *Canadian Journal of Chemistry*. 2015;**93**(7):754-763
- [31] Specific Accession Number for Papain on Uniprotkb Protein Database [Internet]. Available from: <https://www.uniprot.org/uniprot/P00784> [Accession Date: 10-08-2018]
- [32] Janeway CA, Travers P, Walport M. The structure of a typical antibody molecule. In: *Immunobiology: The Immune System in Health and Disease*. 5th ed. New York: Garland Science; 2001



---

Section 3

Separation Approaches  
and Validation

---



# Bioanalytical Method Development and Validation: A Review

*Mahesh Mukund Deshpande, Veena Sanjay Kasture, Mahalaxmi Mohan and Macchindra J. Chavan*

## Abstract

For various types of drug approval processes like INDs, NDAs, ANDAs, veterinary drug approval, the data related to bioanalytical method development and validation is needed to sponsors. Various agencies namely US FDA, American association of pharmaceutical scientists (AAPS), Health protection Branch (HPB), Association of analytical chemists (AOAC), Center for Veterinary Medicine (CVM), U.S. Department of Health and Human Services Food and drug Administration, Center for Drug Evaluation and Research (CDER), European Medicine Agency (EMA), China Food and Drug administration (CFDA), European Bioanalytical Forum (EBF), Global CRO council (GCC), ANVISA (Brazil), Japan Bioanalytical Forum (JBF) had done collective efforts at different timings to regulate and harmonize bioanalytical method development and validation.

Regulatory guidance documents are available as a result of the involvement of various official agencies. Bioanalytical method development and validation can be performed with various validation parameters by using LC-MS/MS and other analytical techniques. Also, there are various stability guidelines and procedures were set which are useful for bioanalysis.

The present review is having a special concern on regulatory and practical perspectives to researchers for development and validation of the bioanalytical method.

**Keywords:** bioanalytical method development and validation, validation parameters, sample extraction technique, stability, good laboratory technique, recent trends

## 1. Introduction and history

When we draw attention on bioanalytical method development and validation, from last three decades, there was major progress in this field. Various agencies namely US Food and drug administration (US FDA), American association of pharmaceutical scientists (AAPS), Health protection Branch (HPB), Association of analytical chemists (AOAC), Center for Veterinary Medicine (CVM), U. S. Department of Health and Human Services Food and drug Administration, Center for Drug Evaluation and Research (CDER), European Medicine Agency (EMA), China Food and Drug Administration (CFDA), European Bioanalytical forum (EBF), Global CRO Council (GCC), ANVISA (Brazil) had done collective efforts at different timings to regulate and harmonize bioanalytical method development and validation. The

very first workshop was held in Arlington, VA, December 3–5, 1990 which was collectively organized by AAPS, U.S. Food and Drug Administration, the International Pharmaceutical Federation (FIP), the HPB, and the AOAC and the report of that was published in *Pharmaceutical research* and four other journals. This workshop clearly points out two important phases of bioanalytical method development and validation that are, an analytical method development in which all parameters of the bioanalytical method should be developed including assay definition, and actual application of a bioanalytical method for Bioavailability, Bioequivalence and Pharmacokinetics studies. Draft guidance on bioanalytical methods validation was issued by the FDA in January 1999. The second AAPS/FDA bioanalytical workshop was held in January 2000. The workshop has resulted in a report 'Bioanalytical method validation—A revisit with a Decade of Progress'. This workshop also forms the basis of FDA guidance on bioanalytical method development and validation, in May 2001. A separate workshop was held 2000 to discuss validation principles for macromolecules. To address the need for guiding principles for the validation of bioanalytical methods for macromolecules, the AAPS Ligand—Binding Assay, Bioanalytical focus group developed and published recommendations for the development and validation of ligand-binding assays in 2003. Current FDA guidance and bioanalytical methods validation workshop white paper was published in 2006. The third AAPS-FDA bioanalytical workshop was held on May 1–3, 2006, in Arlington, VA, concluded with several recommendations to achieve the above goals and objectives related to bioanalytical method development and validation. There was EMA Draft guidance on validation of bioanalytical methods held on April 15–16, 2010. GCC, EBF, CFDA, ANVISA had taken the wide range of efforts to discuss various practical problems of bioanalysis in this decade along with the industry. The regular workshops, conferences of these organizations create interest and improve knowledge in bioanalysis field.

In May 2018, U.S. Department of Health and Human Services, Food and drug administration, Center for Drug Evaluation and Research (CDER) and Center for Veterinary Medicine (CVM) were published guidance for industry regarding bioanalytical method development and validation [1].

## **2. Need of bioanalytical method development and validation**

Sponsors are applying for investigational new drug application (IND), new drug application (NDA), Abbreviated new drug application (ANDA) to FDA. To fulfill the formalities, they have to submit human clinical pharmacology, bioavailability (BA), and bioequivalence (BE) studies, requiring pharmacokinetic (PK) evaluation including non-human pharmacology and toxicology studies and preclinical studies, for this purpose there is a need to develop and validate bioanalytical method. Generally, for industrial use, the bioanalytical methods are developed in biological matrices such as blood, serum, plasma, or urine [2]. The new guidance was having influence of chromatographic assays (CCs) and ligand binding assays (LBAs), as these types of assays can quantitatively determine the drugs and their metabolites, therapeutic proteins and biomarkers in biological matrices such as blood, serum, plasma, urine and tissues. The guidance document also includes the public comments on the revised draft published in 2013. It also provides recommendations for the development, validation and in-study use of bioanalytical methods. The recommendations can be modified with proper supporting documents according to the specific type of bioanalytical method. The advances in scientific and technical factors were included in the guidance. For the successful conduct of nonclinical, biopharmaceutics and clinical studies, the validated analytical methods which provide quantitative data of analytes including drugs and biological products and



biomarkers in given biological matrix are critical ones. These validated methods provide important data related to safety and effectiveness of drugs and biological products. The validated method addresses the key questions related to specificity, accuracy and precision, sensitivity, sample collection, handling, storage of analyte. There is need for partial or cross validation when there are changes to a validated method. The level of validation should be proper for intended purpose of the study which is stated by fit-for-purpose. The most crucial studies submitted in an NDA, BLA or ANDA which helps in regulatory decision making for approval, safety such as BE or pharmacokinetic studies should contain validated bioanalytical methods. The analytical laboratory, which is involved in conducting toxicology studies for regulatory submissions, should follow 21 CFR 58 and GLP [2].

### **3. Instrumentation for bioanalytical method development and validation**

Gas chromatography, high-pressure liquid chromatography, LC and GC, combined with mass spectrometric (MS) procedures such as LC-MS, LC-MS-MS, GC-MS, and GC-MS-MS are used for quantitative analysis. For the quantification of conventional, low molecular weight drugs in biological fluids has shifted dramatically in favor of mass spectrometry-based methods, particularly LC-MS and LC-MS-MS. In the years of 90's there have been tremendous advancements in the field of mass spectrometry with the development of new interfaces, ionization and detection techniques. These advancements resulted in the rapid emergence and widespread commercial use of hyphenated mass spectrometry-based assays, which have largely replaced conventional HPLC, GC, and GC-MS assays [2].

### **4. Validation and acceptance criteria**

#### **4.1 Background**

The main purpose of bioanalytical method development is to clearly define the design, operating conditions, limitations and suitability of the method for its intended purpose. It also ensures that the method is optimized for validation. Before starting development of bioanalytical method, the sponsor should perform the detail study of analyte including physicochemical properties, in vitro and in vivo metabolism and protein binding etc.

The procedures related to extracting the analyte from biological matrix and its detection are the important tasks in method development.

Following are the parameters for method development:

- Reference standards
- Critical reagents
- Calibration curve
- Quality control samples(QCs)
- Selectivity and specificity
- Sensitivity

- Accuracy
- Precision
- Recovery
- Stability of the analyte in the matrix

The developed method should be suitable for analysis of study sample and that is proved on the basis of bioanalytical method validation results. In case if there is new drug entity, its metabolites or biomarkers or any revisions to existing method, the full validation is necessary. The detailed written description like protocol, SOP's should be established. The detailed description of parameters, environment, matrix, collection of sample should be included. Any parameter and results draws any conclusion should be documented and presented in detailed report. Each analyte should be validated in biological matrix [1].

Three types of validation are full validation, partial validation, cross validation. When there is completely new drug entity under investigation, bioanalytical method is developing for the very first time, any small change in laboratories, instrument, software, matrix, (from rat plasma to mouse plasma or matrix within species like human plasma to human urine) in that case validation can range from as little as one assay accuracy and precision determination to a nearly, full validation. In Cross validation, comparison is done in between two bioanalytical methods. For example, data generated using different analytical techniques like LC-MS-MS vs. ELISA in different studies are included in a regulatory submission [3, 4].

#### *4.1.1 Validation parameters*

According to FDA guidance following are common method validation terms.

##### *4.1.1.1 Reference standards and critical reagents*

The reference standard should be authenticated with known identity and purity to prepare the known concentrations. The reference standard should be identical to the analyte under study but if not possible then the established chemical form like free base, free acid or salt with known purity can be used. For commercially available reference standards, they should be with certificate of analyses (CoA) as per requirement of USP standards. In certain cases, if there is no CoA for internally or externally generated standards, then detail information and evidences regarding purity, source, and lot number should be provided. If expired reference standards are available in that case CoA is necessary or there should be regeneration of identity and purity standards. In case of internal standards, there is no need of CoA, if it is not interfering with analyte. The critical reagents should be properly characterized and documented for identity, purity and stability. These critical reagents include antibiotics, labeled analytes and matrices.

In case there is change in critical reagent like lot-to-lot change or switches to another reagent then there is need of assay validation [1].

##### *4.1.1.2 Calibration curve*

The proper quantitation range should be selected for assay and calibration standards based on expected concentration range in the particular type of

study. While studying Ligand Binding Assays (LBAs) there should be anchor points outside the range of quantification in addition to calibration standards. However, these anchor points should not be the part of the acceptance criteria. In most of the LBAs the calibration curves are nonlinear therefore more calibration standards are needed to finalize the calibration range for LBAs than for Chromatographic assays (CCs).

The response-error relationship for LBA standard curves is variable function of the mean response. The concentration-response relationship should be explained with simple model including weighting scheme and regression equation. The reproducible calibration curve should be obtained. The biological matrix should be same throughout the study. The calibration curve should be generated for each analyte if sample contains more than one analyte. In case of surrogate matrices, there should be proper justification and validation of the calibration curves [1].

#### *4.1.1.3 Quality control samples*

For determining precision and accuracy as well as stability, the quality control samples should be used. During method development stage, freshly prepared QCs are recommended. For evaluation of performance of method and stability of analyte, QCs are helpful. While determining the precision and accuracy of the method, the performance QCs are included. The stability QCs are useful to determine stability under stress condition. The calibration standards and QCs are prepared from separately. The calibrators and QCs should be prepared in lots of blank matrix that is free of interference or matrix effects [1].

#### *4.1.1.4 Accuracy*

The degree of closeness of the observed concentration to the nominal or known true concentration. It is typically measured as relative error (% RE) [5, 6].

#### *4.1.1.5 Precision*

Measurement of scattering for the concentrations obtained for the replicate sampling of a homogeneous sample. It is typically measured as coefficient of variation (%CV) [5, 6].

#### *4.1.1.6 Selectivity*

The ability of the bioanalytical method to measure and differentiate the analyte in the presence of components that may be expected to be present. These could include metabolites, impurities, degradants or matrix components [5, 6].

#### *4.1.1.7 Sensitivity (LLOQ, Lower limit of quantitation)*

The lowest concentration of an analyte in a sample that can be quantitatively determined with an acceptable precision and accuracy [5, 6].

#### *4.1.1.8 Standard curve*

The relationship between the experimental response value and the analytical concentration [5, 6].

#### *4.1.1.9 Linearity*

The ability of the bioanalytical procedure to obtain test results that are directly proportional to the concentration of an analyte in the sample within the range of the standard curve [5, 6].

#### *4.1.1.10 Quantification range*

The range of concentration, including the LLOQ and ULOQ (Upper limit of Quantitation) that can be reliably and reproducibly quantified with suitable accuracy and precision by a concentration-response relationship [5, 6].

#### *4.1.1.11 Recovery*

The extraction efficiency of an analytical process, reported as a percentage of the known amount of an analyte carried through the sample extraction and processing steps of the method [5, 6].

#### *4.1.1.12 Matrix factor*

A quantitative measure of the matrix effects due to suppression or enhancement of ionization in a mass spectrometric detector [5, 6].

#### *4.1.1.13 Stability*

The chemical or physical stability of an analyte in a given matrix under specific conditions for given time intervals [5, 6].

#### *4.1.1.14 Reproducibility*

Ability of the method to yield similar concentration for a sample when measured on different occasions [5, 6].

### *4.1.2 Stability study*

Special focus is given on stability study. Various stability parameters can be explained as below [5, 6].

#### *4.1.2.1 Stock solution stability*

The stock solution stability of drug sample and internal standard should be evaluated at room temperature for minimum of 6 h. The stock solutions are kept at frozen or refrigerated over the period. Then these stock solutions are evaluated by comparing with the response of freshly prepared stock solutions. The stock solution stability should be performed at least for one concentration in duplicate.

#### *4.1.2.2 Post preparative (extracted samples or autosampler tray) stability*

This stability is determined for extracted samples. To cover expected run time for the analytical batch and to allow delayed injection due to some instrument malfunctioning or long term storage of the samples, this stability is determined for

~48 to 96 h. This stability is determined on QC samples which are kept for measurable time at the autosampler tray. These samples are analyzed with fresh standards.

#### *4.1.2.3 Benchtop stability*

The QC samples at minimum of two concentration levels are kept at room temperature for 4–24 h. It covers the time to extract the samples. The concentrations are analyzed by comparing with their nominal values. The samples are analyzed in replicates generally in triplicate.

#### *4.1.2.4 Freeze-thaw stability*

This stability is determined at a minimum of two concentration levels. The samples are frozen overnight for –20 or –70°C. Then it is removed and thawed at room temperature. After that, the samples are frozen again at the same temperature for 12–24 h and again thawed. This freeze thaw cycle is repeated for two more times. After completion of third cycle the samples are analyzed. If more degradation is observed than normal values then the first and second freeze-thaw cycle is repeated and the step in which instability occurred is determined. The freeze-thaw cycle can be extended as per requirement.

#### *4.1.2.5 Freezer storage stability*

The freezer storage stability should be carried out at nominal freezer storage temperature during the validation process. The long term stability should be carried out and properly documented as per the procedure discussed below.

#### *4.1.2.6 Postvalidation long-term stability*

This stability is performed after validation. The two QC samples in the matrix low and high concentration level are analyzed by keeping at long-term storage temperature and analyzed in triplicate. The postvalidation long-term stability should be performed in regular intervals starting from 1, 3, 6, 9 and 12 months in accordance with the length of stability required. The long-term stability of incurred samples at storage data should be assessed with stored in vivo samples. The results should be incorporated in the original report or separate report should be prepared.

#### *4.1.2.7 Matrix stability*

At lower temperature, there may be denaturation of matrix proteins. Therefore matrix stability should be validated. For that purpose, additional stability should be carried out at lower temperatures for sample matrix [7].

#### *4.1.2.8 Bioanalysis of hemolyzed samples*

As per 2009 EMA draft guidance and the 2003 ANVISA guideline hemolyzed samples should be analyzed during method validation but practically that will difficult at the time of method validation, therefore, it was recommended to perform at the time of method development. Data reliability and reproducibility should be monitored according to an internal standard (IS) and incurred sample reproducibility (ISR) response. Also one can apply standard addition or standard dilution for further investigation of data reporting. However, the final recommendation about

hemolyzed sample is that there is no standard approach for testing of these types of samples, so there should be the least impact on method development or validation.

#### *4.1.2.9 Whole blood stability evaluation*

The immediate spinning down of aliquot of whole blood containing the drug taken immediately following preparation (time zero) followed by the spinning down of another aliquot following the stability period. The whole blood stability should be performed during method validation. However, there are various approaches for determination of whole blood stability. In case of large molecule, it is not applicable [7].

#### *4.1.2.10 Dilution effects*

The integrity of the dilution should be monitored during validation by QC samples above the ULOQ with like matrix to bring to within quantitation range, if the method measures the diluted samples. There should be proper demonstration of accuracy and precision of these diluted QCs [1].

## **5. Sample collection, stability, storage, sample transport**

For analysis purpose, some processing is required after collection from an animal or human subject. Harvesting of plasma or serum can be done by centrifugation process and it is kept in frozen condition. The conditions like temperature, centrifugation time and force, maximum from sampling to freezing sample are specified and maintained for proper development of the method. If an analyte is less stable in whole blood than plasma, any delay in processing the sample or poor temperature control could result in analyte loss; in such case, one can apply stabilizers or other special sample handling conditions. The stability of analyte in biomatrix should be defined during validation and analyzed during that period only. To obtain Short-term stability, freeze-thaw stability, long-term stability in bio-matrix (typically at  $-20$  or  $-70^{\circ}\text{C}$ ), there is need to maintain all parameters like backup capacity of freezer, alarm system for staff, freezer and also all related document, to track sample during collection, storage and stability. Bio-matrix samples are usually frozen in insulated containers with dry ice. The main concern is ensuring that the shipment is still frozen upon arrival. Shipments are usually packed with sufficient dry ice to last for a significantly greater period than the anticipated shipment time. Samples are split into two aliquots at the collection site, for additional security; a set of reserve aliquots can then be safely stored until the first set is received for analysis [8–14].

## **6. Sample extraction techniques**

Sample preparation is most important and critical step in bioanalytical method development and validation. The main task is to remove interferences present in the sample and to make the sample with the higher concentration of analyte, which contributes to the sensitivity of the method [6].

There are various methods of extraction as follows.

### **6.1 Liquid-liquid extraction**

In liquid-liquid extraction, the analyte gets partitioned in between two immiscible phases. Generally, selective partitioning of an analyte of interest is occurring

in between two immiscible solvents and proper extracting solvents plays important role in this step. In LLE, the analyte gets distributed in one immiscible phase and this partitioning also helps to separate interferences. The analyte is dissolved in a suitable solvent. Then the second solvent is added which should be immiscible with the first solvent. The contents in the sample tube are mixed thoroughly and the two immiscible solvents are allowed to separate into two layers. The less dense solvent will be upper layer, while the more dense solvent will be the lower layer. The analyte mixture will be get separated or distribute in two immiscible solvents according to their partition coefficient. The extent of partition of analyte is depends upon the solubility characteristics of the components of analyte in mixture. As there is the partitioning of analyte in between two immiscible layers, the analyte which is soluble in less dense solvent will be at the upper layer and which one more soluble in the denser solvent will be in the lower layer. These two immiscible layers are separated and after separation, the respective analyte is isolated. The hydrophilic compounds are getting soluble in polar aqueous phase and hydrophobic compounds are in the organic solvent. Generally, by evaporation, the analyte in the organic phase is recovered and diluted with mobile phase and then injected into the column while aqueous phase may directly be injected [6].

In LLE analyte is brought in the organic phase, and for that, the required conditions are maintained. In this, there is a direct extraction of biological material with the water-immiscible solvent. The important task is partitioning of analyte in to the organic phase in which aqueous phase is also present [7].

## **6.2 Solid phase extraction**

In Solid Phase Extraction, the partitioning is occurring in between liquid and solid phase. The main advantage of SPE is removing impurities present in analyte, which helps in increasing the sensitivity of the method. The removal of particulate matter from analyte is major output of SPE. In SPE, multiple sampling generally 12–24 with a lower quantity of solvent with automation are major contributing factors. In SPE the recovery of the sample is higher. Small disposable column or cartridge is employed for partitioning. The SPE consists of the medical syringe which is packed with 0.1–0.5 g of sorbent generally C18 silica. Liquid samples are added to the cartridge and wash solvent is selected to either strongly retain or unretain the analyte. To minimize the presence of interferences, this method is advantageous. Even though analyte get retained on the cartridge, the interferences can be eluted or washed, that results in the analyte-free from interferences. Then the analyte is eluted with elution solvent and either directly injected in or evaporated to dryness followed by dilution with the HPLC mobile phase [15, 16].

## **6.3 Protein precipitation**

Protein precipitation is one of the methods to make the matrix interference free. This can be achieved by denaturation and precipitation. Trichloroacetic acid and perchloric acid has a wide choice as a precipitating agent. Various organic solvents like methanol, acetonitrile, acetone, and ethanol are the wide choice for removing plasma proteins and possess compatibility with high performance liquid chromatography (HPLC) as a mobile phase. One part of sample matrix is diluted with three–four parts of the precipitating agent then vortex mixing is carried out. After that centrifugation, filtration is done to remove the protein mass. The supernatant liquid or filtrate obtained is directly analyzed for the analyte of interest. For quantitative analysis, the supernatant can be isolated, evaporated to dryness and then reconstituted with a suitable solvent before analysis [8]. In protein precipitation

method, the analyte should be freely soluble into the reconstituting solvent. Either by converting soluble protein to a nonsoluble state that salting out or by the addition of water miscible precipitation solvent or organic solvents such as acetone, ethanol, acetonitrile or methanol, this technique can be achieved [10, 15].

#### **6.4 Solid phase microextraction**

Solid Phase Microextraction involves the sampling, extraction, concentration and sample introduction single step which is solvent-free step. The bonded phase which is fused silica fiber coated with polyacrylate, polydimethylsiloxane, carbowax is kept in contact with the sample and exposed to the vapor, also it can be placed in the stream of a gaseous sample to isolate the analyte and concentrate analyte into a range of coating materials. Lastly, the fibers are transferred to analytical instruments like gas chromatography (GC) and GC/mass spectrometry (GC/MS) for separation and quantification of the target analyte with the help of syringe. For routine analysis of volatile and semi-volatile compounds, SPME can be implemented. Exposed fiber has the ability to extract and sample delivery is a key aspect of this method [8–14]. The SPME apparatus is a very simple device. It looks like modified syringe consisting of a fiber holder and a fiber assembly, the latter containing a 1–2 cm long retractable SPME fiber. Analyte in the sample is directly extracted and concentrated to the extraction fiber. The method saves preparation time and disposal costs and can improve detection limits. SPME was also introduced for direct coupling with high-performance liquid chromatography (HPLC) and HPLC-MS in order to analyze weakly volatile or thermally labile compounds not amenable to GC or GC-MS [12].

#### **6.5 Matrix solid-phase dispersion**

In Matrix solid-phase dispersion technique solid matrices are used for sample preparation. It is advantageous as the sample requirement is less than 1 g with low solvent, which is why it is also termed as microscale extraction technique. Near about 98% solvent use is reduced and giving 90% sample turnaround time. In the Conventional extraction of an organic analyte from tissue, the homogenization of small amount of sample tissue with bulk bonded silica-based sorbent has to perform, this can be achieved in mortar and pestle. The structure of tissue is getting disturbed due to mechanical shearing. The sample gets dispersed on the surface of support sorbent, for this, hydrophilic and hydrophobic interaction plays a role which causes the mixture to become semi-dry and free-flowing homogeneous blend of the sample. The sample disruption will be performed due to bound solvent in the sorbent. The sample disperses over the surface of the bonded phase support material to provide a new mixed-phase for isolating analytes from various sample matrices. The interferences and analyte are eluted by transferring in to a pre-fitted SPE cartridge. This technique has recently been applied, using acid alumina, to extract the organic analyte. The two important lacunas with the method are longer analytical time and having a limited limit of determination (LOD) [15, 20, 21].

#### **6.6 Supercritical fluid extraction**

Supercritical fluid extraction is generally used for removing nonpolar to moderately polar analyte from the matrix. As per regulatory point of view, there should be need to replace organic solvents and it is advantageous in the sense of environment. The density of the supercritical fluid is like liquid while its viscosity and diffusivity is in the gas and liquid values. By reducing the pressure and by the evaporation, the recovery of supercritical solvent can be obtained. Even though there is increase in the



pressure, if the temperature is maintained above the critical temperature, the liquid phase will not be appeared. To obtain more efficient extraction the density of supercritical fluid should be like liquid which can be obtained by increasing pressure and this step is more advantageous than that of organic solvents. Carbon dioxide dissolves many volatile polar compounds, acting as a good supercritical solvent. This work can be achieved in the presence of trace amounts of polar co-solvents like water and short-chain alcohols. Supercritical fluids can be used to extract analyte from samples [15, 17]. The SFE is a fast process. The rate of diffusion of a species in the fluid and viscosity of the fluid determines the rate of mass transfer between a sample matrix and an extraction fluid. The greater the diffusion rate and the lower the viscosity, the greater will be the rate of mass transfer. The SFE can generally be completed in 10–60 min. The solvent strength of a supercritical fluid can be varied by changes in the pressure and to a lesser extent in temperature. Many supercritical fluids are gases at ambient conditions. Thus recovery of analyte becomes simple compared to organic liquids. Some supercritical fluids are cheap, inert and nontoxic. Thus they are readily disposed-off after an extraction is completed by allowing them to evaporate into the atmosphere [11].

### **6.7 Column switching**

The broad definition of 2D (or multidimensional) chromatography is a ‘Selective transfer of analyte of interest from a first column to the second column. (By means of switching valve)’ [12]. Column switching is one of the interesting techniques for sample preparation. In this technique, the analyte of interest is retained and separated on HPLC stationary phase while the unretained components are eliminated from the column. In this technique, the component of interest separated at lower retention time is cut and transferred onto another HPLC column for further separation. The important advantage is that the process is automated and whatever transfer of analyte occurs can be determined quantitatively. The analyte gets transferred quantitatively without any loss in concern with the adsorption or degradation [15, 18, 19].

## **7. Acceptance criteria for method validation**

One care must be taken while preparing standard and QC samples, which they should be prepared from same stock solution, also the stability and accuracy of both should be verified before proceeding for actual practical. The selectivity of sample matrix should be verified, can be used throughout the experiment. Standard curve samples can be inserted at any sight in the run.

### **7.1 Matrix-based standard calibration samples**

75% or a minimum of 6 standards, when back-calculated (including ULOQ) should fall within  $\pm 15\%$  of nominal, except for LLOQ when it should be within  $\pm 20\%$  of the nominal value.

### **7.2 Quality-control samples**

At least five replicates, at a minimum of three concentration levels that are LLOQ, MQC and HQC should be inserted into each run. The results obtained for QC samples are the basis of acceptance or rejection of the run. At least 67% (4/6) of the QC samples must be within 15% of their respective nominal (theoretical) values; 33% of the QC samples (not all replicates at the same concentration) may be outside the  $\pm 15\%$  of the nominal value [3].

### **7.3 Selectivity**

For chromatographic assays, the peak response in the blank matrix at the retention time of analyte(s) should be no more than 20% of the response for the lower limit of quantitation (LLOQ) sample [5, 6].

### **7.4 Sensitivity**

Sensitivity of the method is defined as the lowest concentration that can be measured with an acceptable limit of accuracy and precision. By analyzing at least five replicates of the sample at the LLOQ on one of the validation days should be performed for determining the accuracy and precision. The samples used should be different from that of calibration curve samples. The accuracy as determined by the relative error (RE %) at this concentration should be within  $\pm 20\%$  and the CV should be less than 20% [5, 6].

### **7.5 Accuracy and precision**

Accuracy and precision should be determined for both intra- and inter-runs. They are determined at three concentration levels, which are representing entire calibration range. The mean and CV of observed QC concentrations should be determined to obtain intra-run accuracy and precision. The mean of the observed concentrations should be within  $\pm 15\%$  of the nominal at all concentrations of the QC samples. Coefficients of variation (indicating precision) around the mean observed concentration should not exceed 15% at all concentrations. For both intra and inter-run, all QC samples should be considered for calculation including the samples that are failed [5, 6].

### **7.6 Extraction efficiency**

The ratio of the results obtained for analyte from an extracted sample to the results obtained by analyzing unextracted samples. In both cases samples should contain same amount of analyte. The extraction efficiency need not be very high, but it should be consistent, precise and reproducible. One can also determine the extraction efficiency of IS. The ratio of the extraction efficiencies of the analyte and IS provide an IS-normalized extraction efficiency [5, 6].

### **7.7 Matrix effect**

The Matrix effect is the suppression or enhancement of ionization of analyte by the presence of matrix components in the biological samples. The quantitative measure of matrix effect is matrix factor. Matrix factor = peak response in presence of matrix ions/peak response in absence of matrix ions [22]. For determining matrix effect standard curve should be compared with the standard in the buffer to detect matrix effects. Parallelism of diluted study samples should be evaluated with the diluted standard to detect matrix effects [9]. Due to disease conditions, there may be variations in lipid or specific or total protein that should be considered while determining matrix effect. During method development, the impact of hemolyzed and lipemic samples may be assessed. At the time of validation, suppression/enhancement (matrix effect), should be assessed instead of matrix factor [21].

## 7.8 Recovery

The recovery of analyte should be consistent and reproducible. It is not expected that it should be 100%. The recovery should be determined at three concentrations that are low, medium, and high by comparing analyte results of extracted samples with those of spiked control extracts [21].

## 8. Good laboratory practices: an important part of regulatory acceptance

The workshop on EMA draft guideline on validation of bioanalytical methods held on April 15–16, 2010 in Brussels that was jointly organized by the European bioanalysis forum (EBF) and the European federation of pharmaceutical Sciences (EUFEPS). The draft guideline explains how Good Laboratory Practices are essential for bioanalytical method development and validation. For regulatory acceptance of method, the GLP should be followed. The word that is “regulated bioanalysis” should be implemented while practicing the bioanalysis. The internal quality assurance units are responsible for proper procedures, documentation of data and review of all processes. This should be performed in a transparent environment. In addition, the fundamentals of GLP should be strictly and interestingly supported by both bioanalytical chemist and regulators that contribute in the reliability of bioanalytical results. When there is any new or literature based method, complete validation should be performed. In case there is a change in the matrix, partial validation should be performed. For QC samples, which are separated in two aliquots in such case, cross validation is to perform. Selectivity should be confirmed by using at least six sources of the appropriate blank matrix. In the case of matrix effect at three times LLOQ and additional determinations of at medium and high QC were recommended. Stability should be performed at every stage. The between-run accuracy of QC samples should be within 15% of the nominal value and between-run precision should not exceed 15% [8]. SOPs should be readily available for various activities of bioanalytical method development and validation. Study director or principal investigator should have overall responsibility of the bioanalytical method. In addition, all protocols should be generated according to GLP and any alteration in protocol can be done by issuing amendment [8–14].

## 9. Recent trends of bioanalytical method development and validation

As per second China bioanalysis forum (CBF), all approved clinical trials that are BE and pharmacokinetic (phase I–IV trials) should be registered and published on CFDA website [eng.sfda.gov.cn](http://eng.sfda.gov.cn). CBF expert committee (EC) participated in the first independent BMV draft guidance of the Chinese pharmacopeia [14].

European bioanalytical forum was established in 2006 to focus on the issues on ISR, matrix suppression and metabolite quantification. The EBF-IGM also focuses on Ligand-binding assays (LBAs) and immunogenicity assessment. There were certain observations of the industry as well as FDA during audits creates interest in ISR (Incurred sample reproducibility). It should be included in bioanalytical support. Because there were, different observations and readings were found while performing repeat analysis. In bioanalytical method validation, human methods are considered validated without ever applying to study samples which are the major drawback of FDAs guidance. The EBF provides additional clarification and

recommendations with a view to achieving uniformity in quantitative bioanalytical estimations of various molecules. The ISR reinforces confidence that a method is valid and reproducible. The few important recommendations related to acceptance of ISR suggest that it does not accept or reject a study. Failed ISR should lead to investigation and follow-up. For small molecules, two-thirds of repeats agree within 20%, large molecules within 30%. Incurred sample reproducibility enforces the confidence that a method is valid and reproducible for intended purpose. ISR should be part of method validation in addition to various parameters. It is important to document robustness and repeatability of the method. It is part of regular process check on laboratory procedures like SOPs and analysis protocols. Whenever the first time in a new matrix whether animal or human, in new population, first patient study, disease state changes in patient population, any major method change, existing method in new laboratory, whenever scientific reasons require retesting of ISR, process check, all BE studies, incidental check in any studies collectively both clinical and nonclinical studies, there is recommendation of ISR by EBF [23].

The 5th Global CRO Council was held on 13 November 2011 in which European medicines Agency (EMA) guidelines were the main issue of discussion. The GCC recommends three major recommendations on incurred sample reproducibility, consultants, and good clinical practice. The ISR should be carried out in separate batches from that of study samples in a very short period finalized on the priority basis of knowledge related to the stability of the analyte and the matrix. The mean of two results that are of original and ISR results and their difference should be determined. They also recommend good clinical practices with respect to method validation, ISR, repeat analysis, Data recording, reporting and retention of data, facilities and equipment maintenance, computerized systems, QA and QC, SOPs and policies [24]. The European medicine agency (EMA) suggests about the stability of sample in the matrix containing all the analyte. Accordingly, Global CRO council recommends stability validation experiments in presence of co-administered compounds for fixed-dose drug combination studies including patient studies [25]. The 2nd Global CRO Council (GCC) for bioanalysis closed forum was held on 15 April 2011 in Montreal, Canada. In this forum they have suggested 10 recommendations on internal standard response, analyte stability, stability of light-sensitive compounds, Incurred sample reanalysis, incurred sample accuracy, whole blood stability evaluation, stability of the Co-administered compounds, rejected evaluations of validation reports, stock solutions used for calibrates and quality control sample preparation, carryover control, which are essential while developing bioanalytical method [26]. The GCC also recommends 20 recommendations on new EMA guidelines on issues like certificate of analysis, internal standard, calibration curve, accuracy, stability, sample stability, matrix effect, presence of excipients, matrix obtained from special populations, study samples, calibration standard and QC samples, acceptance criteria, chromatogram integration, sample reanalysis, reference standards, matrix effect, matrix selection, parallelism, stability, reagents [27].

The 5th Workshop on Recent Issues in Bioanalysis (WRIB) was held in Montreal, Canada, on 13 and 14 April 2011 which was organized by Calibration and Validation Group (CVG). This workshop gives 17 recommendations on various points like alternate detectors, tissue analysis, whole-blood stability evaluation, chromatographic peak integration, Systems cross-validation, stability issues in bioanalytical method validation and the definition of fresh, fit-for—purpose validations, interpretation of guidelines between different auditors, batch failure, effect of anticoagulant counter ions, differences in slopes of the calibration curves on different LC-MS/MS systems, variability of the IS response in analytical results, reinjection versus reanalysis versus nonreportable values, matrix stability for co-formulated and

co-administered drugs, Hemolysis of samples, method transfers and cross-validations, method development data. These recommendations should be studied and implemented for proper regulatory acceptance of bioanalytical methods [28]. The new draft guidance ANVISA (Brazil) was put forth in 2011. Japan bioanalysis forum (JBF) was also put forth in 2011, which has participated for MHLW bioanalytical study group to draft Japanese guidelines for bioanalytical method development. Both ANVISA and JBF guidelines are having the impact of EMA guidelines with no any remarkable difference [29]. In September 2013, FDA released a draft guidance, which includes number of changes in bioanalysis and addition of biomarker assays [30]. In December 2013 there was 8th GCC closed forum to discuss 2013 revised FDA draft guidance. It was recommended that there should be minimum requirements for biomarker assays. It should be extended to validated, qualified or screening assays. In case of full validation, the pharmacokinetic assay approach can be implemented but there will be certain limitations as biomarker kit are involved [31].

## 10. Conclusion

To evaluate and interpret bioavailability, bioequivalence, pharmacokinetic and toxicokinetic study data, bioanalytical method validation plays an important role. In this, the quantitative estimation of drug and its metabolites in the biological fluid can be performed. There is a need to discuss issues related to bioanalytical method development and validation and need to follow the guidelines, regulatory aspects that are formed during the tenure of last three decades. Nowadays LC-MS/MS plays important role in developing bioanalytical methods including GC-MS and other techniques which are useful for these types of tasks. Various related authorities are having a keen focus on different aspects of bioanalytical method development and validation. If researchers applied all practical aspects of bioanalytical method development and validation for determination of API or certain chemical entity, that is advantageous for regulatory submissions of particular drug component. While developing the bioanalytical method there should be complete clarity about the nature of the analyte, that whether it is a small molecule or macromolecule. There certain differences in principles of bioanalysis for these types of an analyte. For small molecules generally LC-MS and for macromolecules, Ligand-binding assays should be performed. Recent trends related to bioanalytical method development and validation should be followed with GLP requirements for regulatory acceptance of method. There are continuous conferences; workshops are arranged at different sights of the world by CBF, GCC, and other related agencies to discuss, to solve and to improve practical difficulties and additions in the field of bioanalysis.

## List of abbreviations

AAPS	American Association of pharmaceutical Scientist
HPB	health protection branch
AOAC	Association of Analytical Chemist
CVM	Center for Veterinary Medicine
CDER	Center for Drug Evaluation and Research
EMA	European Medicine Agency
CFDA	China Food and Drug Administration
EBF	European Bioanalytical Forum
GCC	Global CRO Council
BA	bioanalytical

BE	bioequivalence
LC	liquid chromatography
GC	gas chromatography
MS	mass spectrometry
CBF	China Bioanalytical Forum
JBF	Japanese Bioanalytical Forum
CoA	certificate of analyses
LBA <sub>s</sub>	ligand binding assays
CC <sub>s</sub>	chromatographic assays
ISR	incurred sample analysis
IS	internal standard
SOP	standard operating procedure
GLP	good laboratory practices
LLOQ	lower limit of quantitation
ULOQ	upper limit of quantitation
QC	quality control
MQC	middle quality control
HQC	high quality control
QA	quality assurance
SOP'S	standard operating procedure
CV	coefficient of variance
FDA	Food and Drug administration

## Author details

Mahesh Mukund Deshpande<sup>1,2\*</sup>, Veena Sanjay Kasture<sup>3</sup>, Mahalaxmi Mohan<sup>4</sup> and Macchindra J. Chavan<sup>2</sup>

1 Jawaharlal Nehru Technological University, Hyderabad, India


2 Amrutvahini College of Pharmacy, Sangamner, India

3 Pinnacle Biomedical Research Institute, Bhopal, India

4 MGV'S Pharmacy College, Nashik, India

\*Address all correspondence to: mahesh\_deshpande11@rediffmail.com

## IntechOpen

© 2019 The Author(s). Licensee IntechOpen. This chapter is distributed under the terms of the Creative Commons Attribution License (<http://creativecommons.org/licenses/by/3.0>), which permits unrestricted use, distribution, and reproduction in any medium, provided the original work is properly cited. 

## References

- [1] Bioanalytical Method Development and Validation Guidance for Industry U.S. Department of Health and Human Services, Food and Drug Administration Center for Drug Evaluation and Research (CDER), Center for Veterinary Medicine (CVM). May 2018
- [2] Shah VP, Midha KK, Findlay JWA, Hill HM, Hulse JD, McGilveray LJ, et al. Bioanalytical Method Validation—A Revisit with a Decade of Progress, Synthesis of Conference held in Arlington, VA; December 3-5, 1990 and report published in pharmaceutical research 1992;9:588-592. *Pharmaceutical Research* 2000;17(12):1551-1557
- [3] Shah VP. The history of bioanalytical method validation and regulation: Evolution of a guidance document on bioanalytical methods validation. *The AAPS Journal*. 2007;9(1):E43-E47. Article 5
- [4] Food and Drug Administration. Draft Guidance for Industry: Bioanalytical Method Validation. Rockville, MD: US Food and Drug Administration; 1999
- [5] Bansal S, DeStefano A. Key elements of bioanalytical method validation for small molecules. *The AAPS Journal*. 2007;9(1):E109-E114. Article 11
- [6] Food and Drug Administration (FDA). Guidance for Industry: Bioanalytical Method Validation. Rockville, MD: US Department of Health and Human Services, Food and Drug Administration, Center for Drug Evaluation and Research; 2001
- [7] James CA, Hill HM. Procedural elements involved in maintaining bioanalytical data integrity for good laboratory practices studies and regulated clinical studies. *The AAPS Journal*. 2007;9(2):E123-E127. Article 14
- [8] Singh UK, Pandey S, Keshri PK, Wal P. Bioanalytical Method Development and Validation. Available from: <http://pharma.financialexpress.com/20081232/research02.shtml>
- [9] Blume H, Brendel E, Brudny-Kloppel M, Grebe S, Lausecker B, Rohde G, et al. Workshop/Conference report on EMA draft guideline on validation of bioanalytical methods. *European Journal of Pharmaceutical Sciences*. 2011;42:300-305
- [10] Guidance for industry bioanalytical method validation U.S. Department of Health and Human Services food and drug administration center for drug evaluation and research (CDER) Center for Veterinary medicine (CVM). May 2001
- [11] Skoog DA, Holler FJ, Timonthy A. Nieman Principles of Instrumental Analysis. 5th ed. Singapore Thomson Asia Pte Ltd; 2003
- [12] Vas G, Vekey K. Solid-phase microextraction: A powerful sample preparation tool prior to mass spectrometric analysis. *Journal of Mass Spectrometry*. 2004;39:233-254
- [13] Rogatsky E. 2D or not 2D column-switching techniques, multidimensional separations and chromatography: Approaches and definitions. *Journal of Chromatography and Separation Techniques*. 2012;3:8
- [14] Tang D, Zhong D, Dong K. The 2nd China bioanalysis forum annual conference: Clinical bioanalysis and large molecule bioanalysis. *Bioanalysis*. 2014;6(20):2709-2712
- [15] Lakshmana PS, Supriyaprakash TNK. Extraction of drug from the biological matrix: A review. In: Naik GR, editor. *Applied Biological Engineering—Principles and Practice*.

Intech. pp. 479-506. Available from: <http://www.intechopen.com/looks/applied-biological-engineering-principles-and-practice/extraction-of-the-drug-from-the-biological-matrix>. ISBN: 978-953-51-412-4

[16] Font G, Manes J, Moltoj C. Solid-phase extraction in multi-residue pesticide analysis of water. *Journal of Chromatography A*. 1993;**642**:135-161

[17] Mohamed RS, Mansoori G. *The Use of Supercritical Fluid Extraction Technology in Food Processing*. London, UK: The World Market Research Centre; 2002

[18] Falco PC, Hernandez RH, Cabeza AS. Column-switching techniques for screening of diuretics and probenecid in urine samples. *Analytical Chemistry*. 1994;**66**(2):244-248

[19] Falco PC, Hernandez RH, Cabeza AS. Column-switching techniques for high performance liquid chromatography of drugs in biological samples. *Journal of Chromatography: Biomedical Applications*. 1993;**619**(2):177-190

[20] Backes D. Strategy for the development of quantitative analytical procedures. In: Venn RF, editor. *Principles and Practice of Bioanalysis*. New York: Taylor & Francis; 2000. pp. 342-358

[21] Barker SA, Long AR, Short CR. Isolation of drug residues from tissues by solid phase dispersion. *Journal of Chromatography*. 1989;**475**:353-361

[22] Vishwanathan CT, Bansal S, Booth B, DeStefano AJ, Rose MJ, Sailstad J, et al. Workshop/Conference Report—Quantitative bioanalytical methods validation and implementation: Best practices for chromatographic and ligand binding assays. *The AAPS Journal*. 2007;**9**(1):E30-E39. Article 4

[23] Timmerman P, Luedtke S, van Amsterdam P, Brudny-Kloppel M, Lausecker B. Incurred sample reproducibility: Views and recommendations by the European Bioanalysis Forum. *Bioanalysis*. 2009;**1**(1):1049-1056

[24] Sangster T et al. Recommendation on ISR in multi-analyte assays, QA/bioanalytical consultants and GCP by global CRO council for bioanalysis (GCC). *Bioanalysis*. 2012;**4**(14):1723-1730

[25] Lowes S et al. Recommendations on bioanalytical method stability implications of co-formulated drugs by global CRO council for bioanalysis (GCC). *Bioanalysis*. 2012;**4**(17):2117-2126

[26] Lowes S et al. Recommendations on: Internal standard criteria, stability, incurred sample reanalysis and recent 483s by global CRO council for bioanalysis. *Bioanalysis*. 2011;**3**(12):1323-1332

[27] Boterman M et al. Recommendation on the interpretation of the new European medicines agency guideline on bioanalytical method validation by global CRO for bioanalysis (GCC). *Bioanalysis*. 2012;**4**(6):651-660

[28] Garofolo F et al. White paper on recent issues in bioanalysis and regulatory findings from audits and inspections. *Bioanalysis*. 2011;**3**(18):2081-2096

[29] Garofolo F. *Updates on Global Harmonization of Bioanalytical Guidance/Guidelines*. Laval (Montreal), Canada: Algorithm Pharma

[30] Booth B et al. Workshop report: Crystal city V-quantitative bioanalytical method validation and implementation: The 2013 revised FDA guidance. *The AAPS Journal*. 2015;**17**(2):277-288



[31] Bower J et al. 8th GCC: Consolidated feedback to US FDA on the 2013 draft FDA guidance on bioanalytical method validation. *Bioanalysis*. 2014;**6**(22):2957-2963



---

Section 4

Recent Developments and  
Applications in Analytical  
Chemistry

---



# Aptamers for Diagnostics with Applications for Infectious Diseases

*Muslum Ilgu, Rezzan Fazlioglu, Meric Ozturk, Yasemin Ozsurekci and Marit Nilsen-Hamilton*

## Abstract

Aptamers are in vitro selected oligonucleotides (DNA, RNA, oligos with modified nucleotides) that can have high affinity and specificity for a broad range of potential targets with high affinity and specificity. Here we focus on their applications as biosensors in the diagnostic field, although they can also be used as therapeutic agents. A small number of peptide aptamers have also been identified. In analytical settings, aptamers have the potential to extend the limit of current techniques as they offer many advantages over antibodies and can be used for real-time biomarker detection, cancer clinical testing, and detection of infectious microorganisms and viruses. Once optimized and validated, aptasensor technologies are expected to be highly beneficial to clinicians by providing a larger range and more rapid output of diagnostic readings than current technologies and support personalized medicine and faster implementation of optimal treatments.

**Keywords:** aptamer, SELEX, biosensors, aptasensors, diagnostics, infectious diseases

## 1. Introduction

In 1868, a young Swiss physician Friedrich Miescher isolated a new biological compound from nuclei of white blood cells, which had not been described before. He named it “nuclein” [1]. Today, it is known as “deoxyribonucleic acid (DNA)” which is nucleic acid in nature and carries heritable information for biological organisms. However, with advancements in the molecular genetics field, scientists started to discover new functions of nucleic acids other than storing and transferring genetic information [2].

In the 1980s, research on human immunodeficiency virus (HIV) and adenoviruses revealed a new understanding of the importance of selective interactions between nucleic acids and proteins. These studies demonstrated that viruses express small RNAs, which bind to cellular or viral proteins with high specificity. In parallel with these discoveries, scientists focused on deciphering fundamental features of short RNAs that can fold into unique three-dimensional structures [3]. In 1990, three separate groups [4–6] invented the systematic evolution of ligands by exponential enrichment (SELEX) method by which they obtained nucleic acid molecules, similar to naturally occurring nucleic acids, which have high specificities and affinities toward their targets. They named these in vitro selected molecules “aptamers.” Since then, researchers have selected numerous aptamers against targets varying from small molecules to cells using SELEX [3].

## 1.1 Systematic evolution of ligands by exponential enrichment

SELEX is a technique to isolate an aptamer that is specific for the desired target from a randomized oligonucleotide (oligo) library by simulating evolution (systematic evolution of ligands). This *in vitro* technique includes a number of selection rounds (between 5 and 20) alternated with exponential amplification of the fittest oligonucleotides by PCR for DNA libraries or RT-PCR for RNA libraries (exponential enrichment).

In a typical SELEX experiment, the starting pool contains up to  $10^{15}$  random oligonucleotide sequences. These sequences in the pool have a unique three-dimensional (3D) structure defined by the combination of interactions that include base pairing, stacking, sugar packing, and noncanonical intramolecular interactions. This structural complexity in the pool establishes a high probability of selecting an oligo that can interact avidly and specifically with the target of interest (aptamer). The intermolecular interaction between aptamer and target may include hydrogen bonds, salt bridges, van der Waals, and hydrophobic and electrostatic interactions.

Traditionally, SELEX is comprised of three main steps: incubation, separation, and amplification. The process involves incubating a “library” of oligos with randomized internal sequences of 20–60 nt with target molecules for a chosen period of time. Removal of unbound oligos from this mixture completes this initial step. Oligos that remain bound to the target are separated and amplified either by PCR or RT-PCR depending on the oligo type, DNA, or RNA. For DNA SELEX, biotin-labeled primers can be used in PCR, and the resulting double-stranded forms are separated using methods such as streptavidin bead capture. For RNA, T7 RNA polymerase promoter-containing primers are used in RT-PCR after which RNA libraries are amplified by *in vitro* transcription. The protocol follows the same amplification steps for several rounds (4–20) as for DNA SELEX (**Figure 1**). Negative selection can be included in either RNA or DNA SELEX protocols, which is achieved by passing the nucleic acid pool over a supporting matrix in the absence of the target. This step aims at eliminating the oligos that bind the matrix in a target-independent manner. Analogs of the target can also be included during selection rounds as competitors of binding if there is a means of separating the target from the analog competitors. This competition is expected to result in aptamers with higher specificity for the target over the analogs.

Two alternative protocols are followed after these rounds to complete the SELEX. The selected oligos from the final round are cloned and sequenced for aptamer identification. Alternatively, high-throughput sequencing (or next-generation sequencing) can be employed to obtain sequence data from oligos present in the pool after different rounds of selection. Comparative sequence analysis allows pinpointing



**Figure 1.** Schematic representation of SELEX protocol.

consensus sites that are potentially involved in target recognition [7, 8]. The most promising sequences are synthesized and characterized further, among which aptamers with nanomolar dissociation constants are frequently identified. In some instances, aptamers have also been isolated with picomolar dissociation constants.

In vitro selection can take months. To shorten the time for selecting high affinity aptamers, Golden et al. suggested a new method for SELEX: photochemical SELEX (PhotoSELEX) [9]. The technique involves the evolution of modified DNA aptamers, which are capable of forming a photoinduced covalent bond with their targets. Thus, these aptamers have greater specificity, and fewer selection rounds are required to select aptamers compared with the traditional SELEX methodologies.

## 1.2 Aptamer structure

Aptamer selection directly depends on environmental components during SELEX. This is because the ionic components and pH of the environment can dictate the predominant structures of oligos in the pool. Nucleic acids are negatively charged molecules that create an “ionic atmosphere” for ion-nucleic acid interactions, a freely joined sheath of ions surrounding the nucleic acids. These electrostatic interactions directly affect the structure of nucleic acids and thus the target binding by changing charge distribution. For specific ligand binding, it is crucial that the aptamer reliably forms the appropriate three-dimensional (3D) structure. However, structures of short oligonucleotides like aptamers are affected by the incubation temperature and the components of the operating buffer system such as the specific ions, ionic strength, and pH. Therefore, the affinities and future performance of aptamers depend on the buffers used during aptamer selection, and the choice of buffer present during selection requires attention when developing a SELEX protocol [10–13].

Some factors present in the samples to be analyzed may have a negative impact on aptamer performance. For example, aptamers are susceptible to nucleases that are present in many biological samples. This is particularly true for RNA, having the 2'OH group, which can electrophilically attack the phosphate of the nucleic acid backbone. Nucleases promote this chemical property to catalyze hydrolysis of RNA, and this property also makes RNA more chemically labile to high pH and temperature compared with DNA. To counter this susceptibility to hydrolysis and to stabilize nucleic acids, many post-selection chemical modifications can be made. However, incorporating these modifications into the aptamer after its selection carries a large risk of altering the aptamer structure with a resulting loss of affinity for the target analyte. Alternatively, the less risky approach is to use chemically substituted nucleotide analogs during SELEX.

Secondary motifs in the tertiary structures of aptamers are diverse. Such motifs include the “stem-loop,” “hairpin structure,” “pseudoknot,” “internal bulge,” “kissing loop,” “three-way junction,” and “the G-quadruplex.” To understand these structures in detail, X-ray crystallography or nuclear magnetic resonance spectroscopy is utilized. But these techniques are laborious and expensive. To ease the process, computer algorithms have been developed to estimate the lowest free-energy structures using sequence-based modeling [14]. This makes it possible to quickly predict the secondary structure of oligonucleotides without needing many resources. However, computational approaches to obtaining 3D models of nucleic acid structures by modeling from primary sequence are still in the development phase, and the results are not as reliable as experimental methods [15–17].

Aptamers have a significant advantage over antibodies as components of sensing units. One advantage is that nucleic acid structures can be regenerated several times with little activity loss, whereas protein-based antibodies can only be used once or a few times before their functionality is lost. In contrast to antibodies or enzymes,

Features	Aptamers	Antibodies
Target Molecules	Any molecule and cell	Limited to immune response producing targets
Molecular Structure	Nucleic acid or peptide	Protein
Size	Small (<30 kDa)	Large (>75 kDa)
Stability	Reversible after rounds of denaturation	Easily lose function after denaturation
Chemical Functionality	Easy to modify chemical structure	Hard to modify chemical structure
Immunogenicity	Non-immunogenic	Immunogenic
Affinity & Specificity	High	High
Generation Time	Several Weeks	Several Months
Cost	<\$50 / gram	~\$300 / gram
Storage	Stable at room temperature; No need to freeze	Easily denaturated; Need to freeze
Shelf Life	Several years (if frozen or dried )	~6 months

**Table 1.**  
*Comparison of aptamers with antibodies.*

nucleic acid aptamers are often highly stable and can be inexpensively synthesized with high reproducibility and purity. Like antibodies, they bind their targets with high affinity and specificity (**Table 1**). These properties are motivating the current flood of reports of aptamer-based biosensors employing a wide range of technologies.

### 1.3 Aptamers for diagnostic and therapeutic applications

Development of novel biosensors for various clinical diseases has become essential as new health issues emerged. To meet this goal, antibodies have been used extensively; however, more recently, aptamers have been recognized as promising alternatives for developing diagnostic devices.

A biosensor is a tool with the ability to provide a measurable signal as a result of biomolecular interactions. Biosensors generally consist of two components: a bioreceptor and a transducer. The bioreceptor binds specifically to the molecule of interest, and the transducer turns information from the binding event into a detectable signal. The components of the transducer include a detector and a reporter, which acts as a bridge between the bioreceptor and the detector.

The most critical part of the biosensor is the bioreceptor (or bio-recognition element). The success of the sensor directly depends on its high affinity and specificity. Because of their more flexible structures, aptamers can provide a substantial signal in combination with a larger number of detection methods than possible for antibodies. Aptamers are preferred over antibodies for biosensor applications because of their cost, stability, and reusability as well as the aforementioned advantages (see **Table 1**). Biosensors, called “aptasensors,” have been developed with many detectors including electrochemical, optical, microcantilever, and acoustic detectors [10].

Aptamers are also used in therapeutic applications, which will not be extensively discussed in this chapter. For discussions of therapeutic applications, the reader is directed to reviews that focus on this topic [18–21]. The majority of therapeutic aptamers inhibit their target molecules, and some act as receptor agonists. Potential therapeutic aptamers against proteins including nucleolin, chemokine ligand 12, or thrombin have been described. Several RNA and DNA aptamers are undergoing clinical trials, yet only pegaptanib against vascular endothelial growth factor has so far been in the USA by the FDA for the treatment of vascular ocular disease [3].

To advance therapeutic applications, drug delivery systems with aptamers have been developed. For such applications, aptamers are needed that recognize cell surface proteins, which can be challenging to select because these proteins are difficult to purify in their natural conformations. The development of cell-based selection techniques has enabled aptamer selection against proteins in their native form while they are on the cell surface. These selections are performed against single-cell types [22]



to obtain aptamers with the ability to bind cell surface proteins specifically expressed on the surface of the cell type used for selection. Delivery systems with these aptamers can carry a variety of cargos into cells by taking advantage of the surface protein internalization in response to aptamer-receptor binding.

## 2. Aptamer use in diagnostics

Diagnostics is one of the most dynamic fields in biosensor research. To support early diagnosis and individualized medicine, researchers seek to develop methods to detect identified biomarkers by more sensitive, time-saving, and cheaper methods. The perfect sensor for medical diagnostics should also be specific, reusable, easy to monitor, nonreactive, and stable with various biological samples. Aptamers can be developed to meet all these requirements. With their wide spectrum of possible targets, sensitive detection of virtually all toxins, drugs, peptides, proteins, metabolites, biomarkers, and cells is possible with aptamers.

Several types of aptasensors have been developed based on electrochemical, optical, mechanical, and acoustic approaches. An early use of aptamers as bio-recognition elements in aptasensors was reported in 1996 with an optical biosensor that utilized fluorescently labeled aptamers in a homogenous assay [23]. Later, aptamers were integrated onto solid supports, which provided an opportunity for real-time analyte detection. Most of these studies have been at the proof-of-principle level, and the majority of studies have been performed with the thrombin aptamer (TA), which has the advantage of a stable target and aptamer. Thrombin aptamer self-assembles into a highly stable G-quadruplex structure, and thrombin is a structurally stable globular protein found in blood. Future studies to optimize other aptasensors with less stable aptamers and analytes in complex matrices are likely to be challenging.

Aptamers fold their flexible, single-stranded chains into 3D structures, which may change upon binding to their cognate target molecules. This structure-switching characteristic has been capitalized on in many aptamer applications. An early example used electrochemical sensing with aptamers immobilized on an electrode surface, and target binding is observed by measuring electrochemical current variations. This system utilized an amperometric sandwich assay combining TA on a gold electrode which was used to capture the TA-labeled glucose dehydrogenase (GDH) [24].

Several types of aptasensors have been developed based on electrochemical, optical, mechanical, and acoustic approaches, which are discussed in the following sections.

### 2.1 Electrochemical aptasensors

Electrochemical aptasensors are constructed by attaching an aptamer that carries a redox-active moiety to an electrode surface. Such aptasensors can make use of voltammetric (amperometric), potentiometric, conductometric, or impedimetric assays for analyte detection. In some formats, the aptamer is labeled with an electroactive group and a structural change in the aptamer upon binding to the target analyte and changes the distance of the electroactive group from the electrode surface, resulting in the switching “on/off” of the electrochemical signal. Measurement of changes in electrochemical features after target binding has been used to determine target concentration [24]. So far, electrochemical aptasensors have been reported for a wide range of targets including PDGF, thrombin and immunoglobulin E (IgE), cocaine, theophylline, adenosine, aminoglycosides, and adenosine triphosphate (ATP) and inorganic ions such as potassium ( $K^+$ ) [10].

In addition to their innate structural changes on binding their target molecules, other structural constraints can be applied to aptamers that result in signals for detection by electrochemical approaches. The most commonly used additional constraint is an oligonucleotide (either connected with the aptamer or separate) that is complementary to part of the aptamer and, upon hybridizing with the aptamer, constrains its structure to an inactive form. For example, a biotin-tagged DNA aptamer for zeatin was hybridized with a complimentary “assist DNA” to form a Y-type DNA structure. Avidin-modified alkaline phosphatase (ALP) was attached to this structure with two biotins at the terminals of DNA aptamer. In the presence of zeatin, this complex was disrupted which leads to a decrease in the oxidation signal from p-nitrophenol (PNP) produced by the catalytic effect of ALP. From this, zeatin concentration in the range of 50 pM–50 nM was selectively measured with a detection limit of 16.6 pM [25].

Redox-active methylene blue (MB) has been used as an aptamer label and electrotransfer communication agent with the electrode. Methylene blue enables the detection of changes in aptamer conformation upon target binding. For example, an MB-labeled TA was used to construct an aptasensor by its immobilization on an electrode. The flexible conformation of the aptamer enabled the electrotransfer from MB to the electrode. The structural change upon analyte binding shielded MB in a “signal-off” mode. However, this mode is a disadvantage for diagnostics because the amperometric response decreases as a result of the association of the target thrombin with the aptamer.

Several approaches have been taken to develop aptasensors that operate in a “signal-on” mode. As an example, the TA was modified with an electroactive ferrocene group as the redox label at one end and a thiol group at the other end. The electrical contact of the electrode with the ferrocene label was affected by the long, flexible aptamer chain. Thrombin binding stabilizes the aptamer’s G-quadruplex conformation, which brings the ferrocene group closer to the electrode. This close proximity enables electron transfer between the electro-active ferrocene units and the electrode, thus producing a positive signal in the presence of thrombin. A similar approach to creating signal-on electrochemical aptasensors utilized the conformational change in the cocaine aptamer that occurs on binding its target. In the absence of the target, the aptamer on the solid surface stays in a partially folded form as a three-way junction. Cocaine binding decreases the distance for electron transfer and thus increases the signal [26].

Demirkol et al. generated an electrochemical aptasensor to detect *E. coli* O157:H7. The electrode surfaces were modified by cysteamine via self-assembled monolayer formation. The carboxyl-functionalized quantum dots and aptamers were conjugated to cysteamine-modified gold electrodes [27]. Ge et al. reported an affinity-mediated homogeneous electrochemical aptasensor using graphene-modified glassy carbon electrode (GCE) as the sensing platform. In this approach, the aptamer-target recognition is converted into an ultrasensitive electrochemical signal output with the aid of a novel T7 exonuclease (T7Exo)-assisted target-analog recycling amplification strategy, in which ingeniously designed methylene blue (MB)-labeled hairpin DNA reporters are digested in the presence of target and, then, converted to numerous MB-labeled long ssDNAs. The distinct difference in differential pulse voltammetry response between the designed hairpin reporters and the generated long ssDNAs on the graphene/GCE allows ultrasensitive detection of target biomolecules [28]. Lai et al. proposed a renewable electrochemical aptasensor for super sensitive  $\text{Hg}^{2+}$  determination [29]. The novel aptasensor, based on sulfur-nitrogen co-doped ordered mesoporous carbon (SN-OMC) and a thymine- $\text{Hg}^{2+}$ -thymine (T- $\text{Hg}^{2+}$ -T) mismatch structure, used ferrocene as signal molecules to achieve the conversion of signal to current. In the absence of  $\text{Hg}^{2+}$ ,

the thiol-modified T-rich probe 1 spontaneously formed a hairpin structure by base pairing. After hybridizing with the ferrocene-labeled probe 2 in the presence of  $\text{Hg}^{2+}$ , the hairpin structure of probe 1 was opened due to the preferential formation of the T- $\text{Hg}^{2+}$ -T mismatch structure, and the ferrocene signal molecules approached the modified electrode surface. Sulfur-nitrogen co-doped ordered mesoporous carbon with high specific surface area and ample active sites acted as a signal amplification element in electrochemical sensing. The sensitive determination of  $\text{Hg}^{2+}$  can be actualized by analyzing the relationship between the change of oxidation current caused by ferrocene and the  $\text{Hg}^{2+}$  concentrations [29]. Finally, Wang et al. combined the strengths of advanced aptamer technology, DNA-based nanostructure, and portable electrochemical devices to develop a nanotetrahedron (NTH)-assisted aptasensor for direct capture and detection of hepatocellular exosomes. The oriented immobilization of aptamers significantly improved their accessibility to suspended exosomes, and the NTH-assisted aptasensor could detect exosomes with 100-fold higher sensitivity when compared to the single-stranded aptamer-functionalized aptasensor [30].

Recently, nanoporous metal surfaces have been found as good sensor platforms for aptamers. Nanoporous gold [31, 32]-based sensors have been used with the TA and ATP aptamers and a redox probe to provide the electrons to the gold surface for sensitive detection of analyte by electrochemical impedance spectroscopy (EIS). The ATP aptamer was in a split format with the second half of the aptamer covalently linked with 3,4-diaminobenzoic acid (DABA), which created the EIS signal by its oxidation at the gold interface. For an analyte that can undergo redox reactions, such as bisphenol A (BPA), this property can be used to provide a signal [33]. Other nanoporous surfaces such as graphene oxide/Au composites and porous PtFe or PtTiAl ternary alloys have also been employed to measure breast cancer cells using the MUC-1 aptamer linked with the electroactive label thionine [34] or kanamycin with  $[\text{Fe}(\text{CN})_6]^{3-/4-}$  [35]. The ability of aptamers to hybridize with other oligonucleotides was employed to create molecular gates over the pores in nanoporous gold surfaces. The gate, created with an aptamer highly specific for the avian influenza viruses (AIV) H5N1 hybridized to oligos linked to the nanoporous gold surface, was closed in the absence of AIV H5N1 but open when the virus bound and released the aptamer. The open pores allowed the entry of substrate and cofactor for lactate dehydrogenase, layered on a glassy electrode below the nanoporous gold. Cyclic voltammetry was used to detect the gold-catalyzed oxidation of the NADH produced as a result of LDH activity [34].

Nanoporous anodized aluminum oxide surfaces have more recently been used for providing a nanoporous surface through which electron movement can be controlled by aptamer-analyte binding. In these aptasensors, the aptamers are attached to a gold surface, which is provided by 2 nm gold nanoparticles [36] or by a surface coating created by sputtering [37]. The structural change in the aptamer due to binding of the analyte reduces access of  $[\text{Fe}(\text{CN})_6]^{3-/4-}$  to the gold surface [36], which can be measured by EIS. Even in the absence of a redox probe, a good EIS signal can be obtained due to a combination of steric hindrance and change in electrical conductance around the pores resulting from the structural changes that occur in the highly negatively charged aptamers upon binding their targets [37].

## 2.2 Optical aptasensors

Another type of biosensor that utilizes aptamers as bio-recognition elements is the optical sensor, for which fluorescent and colorimetric assays are the two widely used formats. In general, fluorescent detection is preferred due to its suitability for real-time detection and because there are many available labeling options as fluorophores and quenchers, which can easily be incorporated during aptamer synthesis.

To convert aptamers into fluorescent signaling probes, several strategies have been developed. A frequently used format places an aptamer sequence in a molecular beacon-like, hairpin structure in which ends are labeled either with two fluorophores or a fluorophore and a quencher. This system utilizes Förster resonance energy transfer (FRET), which relies on the energy transfer between donor and acceptor. Upon target binding, the structure is disrupted by separating the two ends, thus leading to a fluorescence signal. In this format, the use of organic fluorescent dyes or quantum dots (QDs) improved the assay performance and could also be used to detect drug delivery in cells. Another format places a fluorophore-labeled aptamer in a duplex structure with a complementary DNA sequence labeled with a quencher. The aptamer target successfully competes with the complementary DNA resulting in departure of the complementary strand from the aptamer and an accompanying increase in the fluorescence signal [26].

In optical analysis, simultaneous detection of several analytes is readily achieved by multiplexing. In one of the earliest examples, fluorescently labeled aptamers were immobilized on a glass surface. In this system, detection of thrombin and three cancer-biomarker proteins, inosine monophosphate dehydrogenase, vascular endothelial growth factor, and basic fibroblast growth factor, was achieved by fluorescence polarization even in the presence of human serum and *E. coli* cell lysates [10]. The use of aptamer-linked beads in a microarray setting brought a further sophistication of an “electronic tongue” that consists of a fluid delivery system and a fluorescence microscope attached to a digital camera for quantification [10].

Graphene oxide-based aptasensors can also be readily multiplexed [10]. As an example, a novel label-free fluorescent approach was constructed for H1N1 detection based on graphene-oxide and strand displacement reaction, using SYBR Green I (SGI) for signal amplification [38]. Another example is an assay for detection of the pathogenic bacterium, *Pseudomonas aeruginosa*. This assay was enabled by highly specific aptamers conjugated with photoluminescent carbon dots as the fluorescent probe and graphene oxide as the quencher, and it allowed detection of as low as 9 CFU mL<sup>-1</sup> *P. aeruginosa* [39]. Electrochemiluminescence is another output option for aptasensors [40].

### 2.3 Microcantilever aptasensors

Incorporating aptamers into microcantilever sensors offers the possibility of label-free target detection, low noise, high scalability, and small testing volumes [10]. Microcantilever-based sensing has been incorporated into several experimental chemical and biological sensing systems due to its small size, low cost, low sample volume, label-free detection, and ease of integration with microfluidic devices [41]. High-throughput analysis is achievable via microcantilever arrays for parallel processing, although they cannot easily be extensively multiplexed. Microcantilever aptasensors can be operated in either static or dynamic mode. In a liquid environment, the static mode can be more sensitive compared to the dynamic mode. In the static mode, one side of the microcantilever is functionalized with aptamers for analyte detection. Surface stress is generated when target analyte adsorbs onto the functionalized surface. The difference in surface stress between the top and bottom surface results in microcantilever bending, which can be upward (positive) or downward (negative) depending on the type of molecular interactions involved. Displacement of the beam can be detected by using readout techniques such as optical, piezoresistive, and capacitive. The optical technique is the most popular approach because it has high resolution and linear response and produces absolute displacement measurement. Detection of proteins and small molecule analytes, with an aptamer-decorated cantilever, can be achieved with many sensing means including interferometry [42–44] and piezoresistivity [45, 46]. Further

development of microcantilever devices will require solutions to their sensitivity to vibration and the limits to which they can be multiplexed.

## 2.4 Acoustic aptasensors

Early work on acoustic aptasensors included the modification of gold-coated quartz crystals with aptamers. Target binding changes the frequency or phase shift which can be detected as a change in the input and output light. For example, the IgE DNA aptamer on a quartz crystal microbalance (QCM) format provided a detection limit of  $3.3 \text{ ng.cm}^{-2}$  of IgE [47].

Label-free and real-time quantification of proteins were also measured by the propagation of the acoustic wave in a surface acoustic wave (SAW) biosensor, which included an array of five sensor elements to detect human  $\alpha$ -thrombin or HIV-1 Rev peptide. This system had a detection limit of  $75 \text{ pg.cm}^{-2}$  for both  $\alpha$ -thrombin and HIV-1 Rev peptide as analytes [48]. The aptamers demonstrated a better linear response, stability, and reusability when compared with antibodies specific for IgE.

Surface plasmon resonance (SPR) sensors, similar to QCM and SAW aptasensors, rely on a change in refractive index due to target binding. Quartz crystal microbalance and surface plasmon resonance aptasensors for detection of HIV-1 Tat protein were found to have similar high specificities with the SPR sensor having a wider linear range [49]. The SPR aptasensor for retinol binding protein-4 was found more sensitive than an ELISA [50]. In developing SPR aptasensors, combined approaches resulted in a microfluidic device with interdigitated transducer creating high-frequency acoustic waves for target separation [51]. Biotinylated-thrombin aptamers were captured by streptavidin-functionalized polystyrene, which was pumped in the microchannel after incubating with sample. In the microfluidic device, SAW exposure leads to separation of thrombin captured in the polystyrene by its aptamer from the nontarget serum proteins.

Gold nanoparticles (AuNPs) have also been utilized in developing SPR aptasensors. A U-shaped fiber-optic SPR biosensor was developed for the rapid detection of BPA [52]. Incubation of bare AuNPs with BPA aptamer resulted in AuNPs/ssDNA complexes which are stable in high salt. Bisphenol A binding disrupted this complex, which resulted in the aggregation of AuNPs and enhanced refractive index of the solution in the fiber-optic SPR sensor. This system had a detection limit of  $3.7 \text{ pg.mL}^{-1}$ , and linear range was  $0.01\text{--}50 \text{ ng.mL}^{-1}$ .

Neves et al. generated two sensitive cocaine aptasensors that rely on an electromagnetic piezoelectric acoustic sensor (EMPAS) platform as the basis of ultra-high frequency with tuned signal-to-noise ratio [53]. The sensing interface consists of a S-(11-trichlorosilyl-undecanyl) benzenethiosulfonate (BTS) adlayer-coated quartz disc onto which a structure-switching cocaine aptamer was immobilized, completing the preparation of the MN4 cocaine aptamer with an apparent  $K_d$  of  $45 \pm 12 \text{ }\mu\text{M}$  and limit of detection of  $0.9 \text{ }\mu\text{M}$ . The same group developed an MN6 cocaine aptasensor using an EMPAS platform that had apparent  $K_d$  of  $27 \pm 6$  and a  $0.3 \text{ }\mu\text{M}$  detection limit [54].

Detection of cells using SPRs has some limitations that have been creatively overcome. The first limitation includes nonselective binding that causes the refractive index changes, which can be circumvented by reference flow cells to offset this effect [55]. Second is the sensing range, which is typically around  $200 \text{ nm}$  compared with cell dimensions that are in the micron range. Using long-range SPR, the depth was increased over  $800 \text{ nm}$ , which increased the sensitivity for cell detection [56]. Another drawback is its low-throughput, which has been resolved by SPR imaging technology.

### 3. Clinical perspective

As discussed throughout this chapter, aptamers can be evolved to have high affinity and specificity for a range of target molecules that includes small organics, peptides, protein, sugar, viruses, bacteria, parasites, live cell, and tissue (**Tables 2 and 3**). This characteristic paves the way for aptamers to have applications in various disciplines including sensing, medicine, pharmacology, and microbiology. Aptamer-based sensors have great promise as effective tools in the areas of diagnostics and therapeutics for clinical use [164, 165].

#### 3.1 Clinical diagnostics

In clinical practice, the quantification of single biomarkers is frequently not sufficient to support a confident diagnosis. Thus, multiple analyses are required for each diagnosis, many of which might rely on antibodies, the current workhorses of the diagnostic world. Although many antibodies are highly sensitive and specific for their antigen targets, they often suffer from batch-to-batch variation. ELISA assays, which are the main diagnostic platform for antibodies, have been improved with protocols that increase their efficiency and the specificity of their output. However, ELISA assays cannot be readily multiplexed to measure simultaneously the many biomarkers required for a confident diagnosis. A strength of aptamer biosensors is their ability to be multiplexed. Another strength is the range of technologies that can be applied to produce operating aptasensors [166–168]. With these strengths to drive it, aptasensor technology is one of the fastest growing biotechnology areas in diagnostics with an expectation of reaching about \$250 million by 2020 [169, 170].

Aptamers can provide new opportunities for medical diagnostics beyond what is available with antibodies [18, 171]. For example, aptamers can be selected against non-immunogenic and toxic targets, to which antibodies cannot be elicited. These short, single-stranded oligonucleotides can be synthesized via simple chemical synthesis, making them easier and less costly to produce than antibodies [172]. When synthesized in cells containing DNAs encoding RNA aptamers, they can fold appropriately and recognize intracellular targets [173–175].

A limited number of aptasensors are in the pipeline to be used in the areas such as biomarker and microorganism detection and cancer clinical testing. The available aptasensors include (1) OTA-Sense for detection of Ochratoxin A (OTA), a toxin produced by fungi [165, 176]; (2) AflaSense for detection of aflatoxins [95, 177–179]; (3) AptoCyto for flow cytometry applications [165]; (4) AptoPrep as a kit including conjugated aptamers specific to CD-31, EGFR, HGFR, and ICAM-2 [165]; (5) SOMAscan as a platform with the ability to detect >1300 proteins from small volumes [180–184]; (6) an aptamer-based proteomics technology developed by Jung et al. for detecting non-small cell lung cancer [165]; and (7) OLIGOBIND for measuring the thrombin level in blood [185].

Highly sensitive tests are required to specifically detect cancer cells in body fluids over all others. Success in this effort requires the identification of biomarkers that are found only on tumor cells. Some aptamers have been identified that might be applied to detecting tumor cells in the blood. For example, cancer cells and normal cells have been distinguished by using electrochemical sensors, a SERS active bimetallic core-satellite nanostructure, porphyrin-based covalent organic framework based aptasensor [186], and a deterministic lateral displacement (DLD) pattern-based aptamer-tailed octopus chip [187]. Recently, some aptasensors have been tested in cancer studies. Prostate-specific antigen (PSA), mucin 1 (MUC1), PDGF-BB, and vascular endothelial growth factor (VEGF) are detected as cancer biomarkers in cancer cell lines [165, 188].

Organism	Target	Aptamer	Backbone	Binding affinity (Kd)	Reference
<i>M. tb</i> Beijing strain	ManLAM	T9	DNA	668 ± 59 nM	[57]
<i>M. tb</i> H37Rv	CE protein	CE24	DNA	0.375 μM	[58]
	CE protein	CE15	DNA	0.16 μM	
<i>M. tb</i>	CE protein	CSIR 2.11	DNA		[59]
	MPT64	MPT64-A1	DNA		[60, 61]
	EsxG protein	G43	RNA	8.04 ± 1.90 nM	[62]
	EsxG protein	G78	RNA	78.85 ± 9.40 nM	
	Whole bacterium	MA1	DNA	12.02 nM	[63]
	Whole bacterium	Aptamer 1	DNA	37 ± 4 nM	[64]
<i>S. typhimurium</i>	Outer membrane proteins	Aptamers 33 and 45	DNA		[65, 66]
	OmpC protein	I-2	RNA	20 nM	[67]
	Whole bacterium	C4	DNA		[68]
	Whole bacterium	ST2P	DNA	6.33 ± 0.58 nM	[69]
	Whole bacterium	SAL 26	DNA	123 ± 23 nM	[70]
<i>Salmonella</i> Paratyphi A	Whole bacterium	Apt22	DNA	47 ± 3 nM	[71]
<i>S. enteritidis</i>	Mixtures of 10 strains of <i>S. enteritidis</i>	S25	RNA		[72]
	Whole bacterium	crn1	DNA	0.971 μM	[73]
	Whole bacterium	crn2	DNA	0.309 μM	
<i>S. aureus</i>	S. Endotoxin B	APT <sup>SEB</sup> 1	DNA		[74]
	S. Endotoxin C1	C10	DNA	65.14 ± 11.64 nM.L <sup>-1</sup>	[75]
	Alpha toxin	R12.06	DNA	93.7 ± 7.0 nM	[76]
	Peptidoglycan	Antibac1	DNA	0.415 ± 0.047 μM	[77]
	Peptidoglycan	Antibac2	DNA	1.261 ± 0.280 μM	
	Protein A	PA#2/8	DNA	172 ± 14 nM for the recombinant Protein A and 84 ± 5 nM for the native Protein A	[78]
	Whole bacterium	SA20	DNA	70.68 ± 39.22 nM	[79, 80]
	Whole bacterium	SA23	DNA	61.50 ± 22.43 nM	
	Whole bacterium	SA31	DNA	82.86 ± 33.20 nM	
	Whole bacterium	SA34	DNA	72.42 ± 35.23 nM	
	Whole bacterium	SA43	DNA	210.70 ± 135.91 nM	
Whole bacterium	SA17	DNA	35 nM	[81]	
Whole bacterium	SA61	DNA	129 nM		
<i>L. monocytogenes</i>	Internalin A	A8	DNA		[82]
	Listeriolysin O	LLO-3	DNA		[83]
	Whole bacterium	Lbi-17	DNA		[84]
	Whole bacterium	LMCA2	DNA	2.01x10 <sup>-12</sup> M	[85]
	Whole bacterium	LMCA26	DNA	1.56x10 <sup>-10</sup> M	
<i>E. coli</i> 0157	LPS	E-5, E-11, E-12, E-16 to E-19	DNA		[86]
<i>E. coli</i> 0158	Whole bacterium	AM-6	DNA	1076 ± 678 pmol	[87]
<i>E. coli</i> K88	Whole bacterium	Apt B12	DNA	15 ± 4 nM	[88]

Organism	Target	Aptamer	Backbone	Binding affinity (Kd)	Reference
<i>E. coli</i> KCTC 2571	Whole bacterium	E1	DNA	12.4 nM	[35, 89]
	Whole bacterium	E2	DNA	25.2 nM	
	Whole bacterium	E10	DNA	14.2 nM	
	Whole bacterium	E12	DNA	16.8 nM	
<i>E. coli</i> DH5 $\alpha$	Whole cell	Ec3(31)	RNA	225 nM	[90]
	Whole cell	8.28A	DNA	27.4 $\pm$ 18.7 nM	[91]
<i>M. tb</i> H37Rv	Whole bacterium	NK2	DNA		[92]
	ManLAM	ZXL1	DNA	436.3 $\pm$ 37.84 nM	[93]
BCG	ManLAM	BM2	DNA	8.59 $\pm$ 1.23 nM	[94]
<i>M. tb</i>	Acetohydroxyacid synthase	Mtb-Apt1	DNA	1.06 $\pm$ 0.10 $\mu$ M	[95]
	Acetohydroxyacid synthase	Mtb-Apt6	DNA	0.210 $\pm$ 0.05 $\mu$ M	
<i>S. typhi</i>	Type IVB pili	S-PS8.4	RNA	8.56 nM	[96, 97]
<i>S. aureus</i>	SEA	S3	DNA	36.93 $\pm$ 7.29 nM	[98]
	$\alpha$ -toxin	AT-33	DNA		[99]
	$\alpha$ -toxin	AT-36	DNA		

**Table 2.**  
Aptamers selected against bacteria.

Organism	Target	Aptamer	Backbone	Binding affinity (Kd)	Reference
HIV-1	Tat	RNA <sup>Tat</sup>	RNA	120 $\pm$ 13 pM	[49, 100, 101]
HCV	E2 protein	ZE2	DNA	1.05 $\pm$ 1 nM	[102]
	Core protein	9–14	RNA	142 nM	[103]
	Core protein	9–15	RNA	224 nM	
	Core protein	C4	DNA		[104, 105]
Influenza A virus (H3N2)	HA(91–261)	A22	DNA		[106]
	HA	Clone B	RNA	200 pM	[107]
	Whole virus	P30-10-16	RNA	188 pM	[108]
Influenza A virus (H5N1)	HA	A10	DNA		[109]
Influenza A virus (H9N2)	HA(101–257)	C7	DNA		[110]
Influenza A virus (H5N1)	HA	HAS15–5	RNA		[111]
Influenza A virus (H1N1)	HA	D-26	RNA	67 fM	[112]
Influenza A virus (H3N2)	HA	HA68	DNA	7.1 nM	[113]
Influenza A virus (H5N1) and (H7N7)	HAs from H5N1 and H7N7	8-3	RNA	170 fM	[114]
Influenza A virus	HA1 subunit	ApI	DNA	64.76 $\pm$ 18.24 nM	[115]
Influenza A virus	HA1 subunit	ApII	DNA	69.06 $\pm$ 12.34 nM	
Influenza A virus	HA1 subunit	ApIII	DNA	50.32 $\pm$ 14.07 nM	



Organism	Target	Aptamer	Backbone	Binding affinity (Kd)	Reference
Influenza A virus (H9N2)	HA	A9	DNA	46.23 ± 5.46 nM	[116]
Influenza A virus (H9N2)	HA	B4	DNA	738 ± 1.09 nM	[117]
Influenza A virus (H5N1) and (H5N8)	Whole virus	IF22 and IF23	DNA		[118]
HBV	Surface antigen	HBs-A22	RNA		[119]
HPV 16	E7 protein	G5α3N.4	RNA	1.9 μM	[120]
HIV-1	Gp120	B40	RNA	21 ± 2 nM	[121]
	Gp120	B40t77	RNA	31 ± 2 nM	
	Gp120	A-1	RNA	52 nM	[122]
	Gp120	BclON-mut	DNA	143 ± 79 nM	[123]
	Gp120	F-thio-BclON	DNA	86 ± 17 nM	
	RT	1.1RNA	RNA	5 nM	[124]
	RT	RT1t49	DNA	1 nM	[125]
	RT	4.20	DNA	180 ± 70 pM	[126]
	RT	R12-2	DNA	70 nM	[127]
	RT	37NT	DNA	660 pM	[128]
	RT	FA1	FANA aptamer	Low pM range	[129]
	5'-UTR of HIV-1 genome	RNApt16	RNA	280 ± 60 nM	[130]
	TAR RNA element	IV04	DNA	20 nM	[131]
	Integrase	T30695	DNA	0.5 ± 0.2 μM	[132, 133]
	Integrase	93del	DNA		[56, 134, 135]
Nucleocapsid protein	8-6	RNA	1.4x10 <sup>-9</sup> M	[136]	
Gag protein	DP6-22	RNA	100 ± 3.4 nM	[137]	
Rev protein	RBE(apt)	RNA		[138]	
Integrase	S3R3	RNA	47 ± 3 nM	[139]	
HCV	NS3 protein	G6-16	RNA	238 nM	[140]
	Truncated protease domain of NS3 protein	G9-I	RNA	10 nM	[141]
	Helicase domain of NS3	G5	RNA	25 nM	[142]
	IRES domains III-IV	3-07	RNA	9 nM	[143]
	IRES	AP50	RNA	5 nM	[144, 145]
	IRES domain IIIf and IV	HH-11	RNA		[146]
	NSSB	27v	DNA	132.3 ± 20 nM	[147, 148]
	NSSB	r10/43	RNA	1.3 ± 0.3 nM	[149]
	NSSB	r10/47	RNA	23.5 ± 6.7 nM	
	NSSB	R-F t2	RNA	2.62 ± 0.90 nM	[85, 150]

Organism	Target	Aptamer	Backbone	Binding affinity (Kd)	Reference
Influenza A virus (H5N2)	Glycosylated HA	HA12-16	RNA		[151]
Influenza A virus (H1N1, H5N1, H7N7 and H7N9)	Residues in the N-terminal of the PA <sub>N</sub> of the influenza A virus polymerase	PAN-2	DNA	247 ± 11 nM	[152]
HBV	Truncated P protein	S9	RNA		[153]
	Core protein	Apt.No.28	DNA		[154]
	Capsid	AO-01	DNA	180 ± 82 nM	[155]
HPV 16	E7 protein	A2	RNA	107 nM	[156, 157]
	E6 protein	F2	RNA		[158]
SARS-CoV	Helicase	NG8	DNA	5 nM	[159]
DENV-2	Envelope protein domain III	S15	DNA	200 nM	[160]
RABV	Glycoprotein	GE54	DNA	307 nM	[161]
EBOV	EBOV sGP	39SGP1A	RNA	27 nM	[162]
Zika	NS1 protein	Clone 2	DNA	24 pM	[163]
	NS1 protein	Clone 10	DNA	134 nM	

**Table 3.**  
Aptamers selected against viruses.

Many conventional diagnostic technologies for detecting virus and bacteria, including serologic-, nucleic acid-, and culture-based tests, are either time-consuming or expensive on account of the need for sophisticated equipment [188]. For example, the gold standard for laboratory diagnosis of acute viral infections is isolation and characterization of the virus or bacterium. Isolation and long replication times for some viruses and bacterial strains can delay confirmation of the initial diagnosis for more than a week. The most commonly used alternative method is the ELISA. However, cross-reactive antibodies against viruses, particularly when they are part of the same virus family, may confound the results of serologic tests and may lead to misinterpretation during the epidemiologic assessment in regions of the world where they are co-endemic [189]. For instance, among the flaviviruses, serological cross-reactivity between Zika virus and dengue virus confounds diagnosis of Zika virus infections in pregnant woman in regions where Dengue virus is also endemic [190]. Additionally, ELISA-detecting antibodies (IgG and IgM) that were produced against the virus do not identify the active infection or the virus particles. Because they can interact with different regions of the protein compared with antibodies, aptamers might be capable of distinguishing viruses that cannot be distinguished serologically [162]. Aptamers that have been reported to specifically bind flaviviruses and their protein products including Ebola [162], Zika [163], and dengue virus [160] should be tested for their abilities to distinguish these viruses.

The abilities to detect, identify, and quantify microbes and viruses and to identify virally infected cells are essential for their early diagnosis. An increasing number of aptamers have been isolated that bind specific microbes such as *Escherichia coli*, *Bacillus thuringiensis*, *Campylobacter jejuni*, and *Campylobacter coli* [191], various salmonella species, including *S. enteritidis* [72] and *S. enterica* [65], and staphylococcus species including *S. aureus* [79], *S. typhimurium* [67], and *S.*

*enteritidis* [192] (**Table 2**). In addition to the aptamers recognizing flaviviruses discussed in the previous paragraph, there are also aptamers that bind HIV-1 and hepatitis C virus (HCV) [188], among others (**Table 3**).

Aptasensors that have been developed using a number of the aptamers just mentioned hold the promise of prompt management of infections with a decreasing incidence of morbidity. Another possible application of aptasensors is in vaccine development. The costs and extended time associated with the assessment of vaccine concentrations by ELISA might be overcome by the application of aptasensors [193].

### 3.2 Future directions in clinics

Application of aptamer technology in the clinic has the potential of solving some stubborn diagnostic problems. Here we discuss some examples.

Tuberculosis (TB) is caused by *Mycobacterium tuberculosis* and is one of the top ten causes of death worldwide [194]. The incidence of childhood TB is reported as a half a million cases with 74,000 deaths annually by the World Health Organization [195]. The most commonly used diagnostic tool for tuberculosis is the TB skin test. However, a false-positive test result in people vaccinated with the bacillus Calmette-Guerin (BCG) vaccine can be a confounding factor for diagnosis. Thus, the distinction of infection from disease, particularly in children, is still unclear. Additionally, microbiologic confirmation of bacteria in body fluids in childhood is difficult because of the poor bacillary count [195–197].

Cytomegalovirus (CMV) causes life-threatening infections in patients with solid organ transplantation, hematopoietic stem cell transplantation, and AIDS. Cytomegalovirus causes acute and latent infections and reactivates in immunosuppressed patients. Isolation and infection control procedures as well as proper management of VHF commonly depend on an accurate diagnosis [198]. Current diagnostic tests targeting CMV DNA and CMV antigens are insufficient for discriminating acute and latent infections and detecting organ involvement. As a result, the results of these tests are frequently misinterpreted [199–201]. Viral hemorrhagic fevers (VHFs) are caused by a couple of viruses including *Arenaviridae*, *Bunyaviridae*, *Filoviridae*, and *Flaviviridae*. Fulminant and fatal disease processes are the common features of the VHFs and diagnosing and distinguishing of VHF from other tropical diseases may be problematic because of the indiscriminatory symptoms [202].

An accurate and reliable diagnosis of these and other infections will provide for appropriate management and will decrease morbidity and mortality. Thus, development of fast microorganism-focused tests will provide rapid accurate diagnosis of infection and organ involvements. It seems inevitable that, in the near future, many aptamer-based methods/tools will provide for early diagnosis that will enable rapid initiation of optimal treatment regimens for viral and bacterial diseases.

## 4. Future perspective

First identified in 1890 [203], antibodies and their means of interaction with their antigens were already being extensively studied in the early twentieth century, and their structures were reported in the 1960s by Gerald Edelman [204]. Continuing studies of antibodies and the means of eliciting them have resulted in a detailed understanding of how they interact with their antigens. This knowledge combined with an expansive array of available antibodies motivates scientists to incorporate them into new diagnostic tools. Thus, antibody use dominates the 45 billion dollars global diagnostics market.

The more recently discovered aptamers are generally compared with antibodies due to their functional similarity. Since the discovery of aptamers in the 1990s, over a thousand studies have been conducted on applications of aptamers for diagnostics. Aptamers that specifically target biomarkers and bacterial or viral virulence factors such as surface glycoproteins or secreted proteins have been generated. These studies have demonstrated the range of targets that can be recognized by aptamers and the number of sensor platforms into which aptamers can be incorporated, many of which have been discussed in this chapter. However, the more structurally flexible aptamers are not as readily plugged into standard diagnostic assays as antibodies. In this burgeoning and yet immature field of aptasensors, there is still much to be learned about how to control aptamer behavior.

More systematic studies are needed to optimize selection methods, and more aptamers need to be characterized structurally. The biological matrix in which the analyte will be measured in the final application platform should be considered at the beginning of the selection so as to use buffer and ionic compositions during SELEX that resemble the target matrix. Maturation of aptamers to increase specificity for their target analyte in the appropriate matrix and for effective performance in the chosen reporter platform is also extremely important.

Aptamers offer the allure of easier production, ease of chemical modification, smaller size, reusability, stability even at high temperatures, low cost, and a long shelf life. A variety of chemical modifications further enhance aptamer stability. A significant advantage over antibody-based assays is that aptamers can be reused for many cycles without losing potency with the analyte being removed between each cycle by heating or other means. These features hold promise for the continued incorporation of aptamers into various sensor platforms and for the further development and eventual commercial application of aptasensors for diagnostics.

## **Acknowledgements**

Authors are thankful to the administrative staff members at IntechOpen for their invaluable help.

## **Conflict of interest**

MNH is the owner of Aptalogic Inc. located in Ames, IA, USA.

## Author details

Muslum Ilgu<sup>1\*</sup>, Rezzan Fazlioglu<sup>1</sup>, Meric Ozturk<sup>1</sup>, Yasemin Ozsurekci<sup>2</sup>  
and Marit Nilsen-Hamilton<sup>3</sup>

1 Department of Biological Sciences, Middle East Technical University, Ankara, Turkey


2 Department of Pediatric Infectious Diseases, Hacettepe University, Ankara, Turkey

3 Roy J. Carver Department of Biochemistry, Biophysics and Molecular Biology, Iowa State University, Ames, IA, USA

\*Address all correspondence to: [ilgu@metu.edu.tr](mailto:ilgu@metu.edu.tr)

## IntechOpen

---

© 2019 The Author(s). Licensee IntechOpen. This chapter is distributed under the terms of the Creative Commons Attribution License (<http://creativecommons.org/licenses/by/3.0>), which permits unrestricted use, distribution, and reproduction in any medium, provided the original work is properly cited. 

## References

- [1] Dahm R. Friedrich Miescher and the discovery of DNA. *Developmental Biology*. 2005;**278**(2):274-288. DOI: 10.1016/j.ydbio.2004.11.028
- [2] Lipfert J, Doniach S, Das R, Herschlag D. Understanding nucleic acid-ion interactions. *Annual Review of Biochemistry*. 2014;**83**:813-841. DOI: 10.1146/annurev-biochem-060409-092720
- [3] Song KM, Lee S, Ban C. Aptamers and their biological applications. *Sensors*. 2012;**12**(1):612-631. DOI: 10.3390/s120100612
- [4] Tuerk C, Gold L. Systematic evolution of ligands by exponential enrichment: RNA ligands to bacteriophage T4 DNA polymerase. *Science*. 1990;**249**(4968): 505-510. DOI: 10.1126/science.2200121
- [5] Ellington AD, Szostak JW. In vitro selection of RNA molecules that bind specific ligands. *Nature*. 1990;**346**: 818-822. DOI: 10.1038/346818a0
- [6] Robertson DL, Joyce GF. Selection in vitro of an RNA enzyme that specifically cleaves single-stranded DNA. *Nature*. 1990;**344**(6265):467-468. DOI: 10.1038/344467a0
- [7] Hoinka J, Zotenko E, Friedman A, Sauna ZE, Przytycka TM. Identification of sequence-structure RNA binding motifs for SELEX-derived aptamers. *Bioinformatics*. 2012;**28**(12):i215-223. DOI: 10.1093/bioinformatics/bts210
- [8] Hoinka J, Berezhnoy A, Sauna ZE, Gilboa E, Przytycka TM. AptaCluster—A method to cluster HT-SELEX aptamer pools and lessons from its application. *Lecture Notes in Computer Science*. 2014;**8394**(LNBI):115-128. DOI: 10.1007/978-3-319-05269-4\_9
- [9] Tombelli S, Minunni M, Mascini M. Analytical applications of aptamers. *Biosensors & Bioelectronics*. 2005;**20**(12):2424-2434. DOI: 10.1016/j.bios.2004.11.006
- [10] Ilgu M, Nilsen-Hamilton M. Aptamers in analytics. *The Analyst*. 2016;**141**(5):1551-1568. DOI: 10.1039/c5an01824b
- [11] Yu Q, Dai Z, Wu W, Zhu H, Ji L. Effects of different buffers on the construction of aptamer sensors. *IOP Conference Series: Materials Science and Engineering*. 2017;**274**(1):012117. DOI: 10.1088/1757-899X/274/1/012117
- [12] Bruno JG, Sivils JC. Studies of DNA aptamer oligonucleotide and picogreen fluorescence interactions in buffer and serum. *Journal of Fluorescence*. 2016;**26**(4):1479-1487. DOI: 10.1007/s10895-016-1840-1
- [13] Baaske P, Wienken CJ, Reineck P, Duhr S, Braun D. Optical thermophoresis for quantifying the buffer dependence of aptamer binding. *Angewandte Chemie International Edition*. 2010;**49**(12):2238-2241. DOI: 10.1002/anie.200903998
- [14] Radom F, Jurek PM, Mazurek MP, Otlewski J, Jeleń F. Aptamers: Molecules of great potential. *Biotechnology Advances*. 2013;**31**(8):1260-1274. DOI: 10.1016/j.biotechadv.2013.04.007
- [15] Parisien M, Major F. The MC-Fold and MC-Sym pipeline infers RNA structure from sequence data. *Nature*. 2008;**452**(7183):51-55. DOI: 10.1038/nature06684
- [16] Lu XJ, Bussemaker HJ, Olson WK. DSSR: An integrated software tool for dissecting the spatial structure of RNA. *Nucleic Acids Research*. 2015;**43**(21):e142. DOI: 10.1093/nar/gkv716
- [17] Chojnowski G, Waleń T, Bujnicki JM. RNA bricks—A database of RNA 3D

- motifs and their interactions. *Nucleic Acids Research*. 2014;**42**(Database issue): D123-D131. DOI: 10.1093/nar/gkt1084
- [18] Banerjee J, Nilsen-Hamilton M. Aptamers: Multifunctional molecules for biomedical research. *Journal of Molecular Medicine*. 2013;**91**(12):1333-1342. DOI: 10.1007/s00109-013-1085-2
- [19] Zhou G, Latchoumanin O, Bagdesar M, Hebbard L, Duan W, Liddle C, et al. Aptamer-based therapeutic approaches to target cancer stem cells. *Theranostics*. 2017;**7**(16):3948-3961. DOI: 10.7150/thno.20725
- [20] Esposito CL, Catuogno S, Condorelli G, Ungaro P, De Francis V. Aptamer chimeras for therapeutic delivery: The challenging perspectives. *Genes (Basel)*. 2018;**9**(11):529. DOI: 10.3390/genes9110529
- [21] Ismail SI, Alshaer W. Therapeutic aptamers in discovery, preclinical and clinical stages. *Advanced Drug Delivery Reviews*. 2018;**134**:51-64. DOI: 10.1016/j.addr.2018.08.006
- [22] Chen M, Yu Y, Jiang F, Zhou J, Li Y, Liang C, et al. Development of cell-SELEX technology and its application in cancer diagnosis and therapy. *International Journal of Molecular Sciences*. 2016;**17**(12):2079. DOI: 10.3390/ijms17122079
- [23] Drolet DW, Moon-McDermott L, Romig TS. An enzyme-linked oligonucleotide assay. *Nature Biotechnology*. 1996;**14**(8):1021-1025. DOI: 10.1038/nbt0896-1021
- [24] Ikebukuro K, Kiyohara C, Sode K. Electrochemical detection of protein using a double aptamer sandwich. *Analytical Letters*. 2004;**37**(14):2901-2909. DOI: 10.1081/AL-200035778
- [25] Zhou Y, Yin H, Wang Y, Sui C, Wang M, Ai S. Electrochemical aptasensors for zeatin detection based on MoS<sub>2</sub> nanosheets and enzymatic signal amplification. *The Analyst*. 2018;**143**(21):5185-5190. DOI: 10.1039/C8AN01356J
- [26] Song S, Wang L, Li J, Fan C, Zhao J. Aptamer-based biosensors. *Trends in Analytical Chemistry*. 2008;**27**(2):108-117. DOI: 10.1016/j.trac.2007.12.004
- [27] Odacı-Demirkol D, Güleç K. Electrochemical sensing and fluorescence imaging of *E. coli* O157:H7 based on aptamer-conjugated semiconducting nanoparticles. *Süleyman Demirel Üniversitesi Fen Bilimleri Enstitüsü Dergisi*. 2018;**22**:421-426
- [28] Ge L, Wang W, Sun X, Hou T, Li F. Affinity-mediated homogeneous electrochemical aptasensor on a graphene platform for ultrasensitive biomolecule detection via exonuclease-assisted target-analog recycling amplification. *Analytical Chemistry*. 2016;**88**(4):2212-2219. DOI: 10.1021/acs.analchem.5b03844
- [29] Lai C, Liu S, Zhang C, Zeng G, Huang D, Qin L, et al. An electrochemical aptasensor based on sulfur-nitrogen Co-doped ordered mesoporous carbon and thymine-Hg<sup>2+</sup>-thymine mismatch structure for Hg<sup>2+</sup> detection. *ACS Sensors*. 2018;**3**(12):2566-2573. DOI: 10.1021/acssensors.8b00926
- [30] Wang S, Zhang L, Wan S, Cansiz S, Cui C, Liu Y, et al. Aptasensor with expanded nucleotide using DNA nanotetrahedra for electrochemical detection of cancerous exosomes. *ACS Nano*. 2017;**11**(4):3943-3949. DOI: 10.1021/acsnano.7b00373
- [31] Qiu H, Sun Y, Huang X, Qu Y. A sensitive nanoporous gold-based electrochemical aptasensor for thrombin detection. *Colloids Surfaces B Biointerfaces*. 2010;**79**(1):304-308. DOI: 10.1016/j.colsurfb.2010.04.017
- [32] Kashefi-Kheyraadi L, Mehrgardi MA. Aptamer-based electrochemical

- biosensor for detection of adenosine triphosphate using a nanoporous gold platform. *Bioelectrochemistry*. 2013;**94**:47-52. DOI: 10.1016/j.bioelechem.2013.05.005
- [33] Zhu B, Alsager OA, Kumar S, Hodgkiss JM, Travas-Sejdic J. Label-free electrochemical aptasensor for femtomolar detection of 17 $\beta$ -estradiol. *Biosensors & Bioelectronics*. 2015;**70**:398-403. DOI: 10.1016/j.bios.2015.03.050
- [34] Yan M, Sun G, Liu F, Lu J, Jinghua Yu XS. Investigations on the interface of nucleic acid aptamers and binding targets. *Analytica Chimica Acta*. 2013;**798**:33-39. DOI: 10.1039/C8AN01467A
- [35] Guo Y, Wang Y, Liu S, Yu J, Wang H, Wang Y, et al. Label-free and highly sensitive electrochemical detection of *E. coli* based on rolling circle amplifications coupled peroxidase-mimicking DNAAzyme amplification. *Biosensors & Bioelectronics*. 2016;**75**:315-319. DOI: 10.1016/j.bios.2015.08.031
- [36] Peinetti AS, Ceretti H, Mizrahi M, González GA, Ramírez SA, Requejo FG, et al. Confined gold nanoparticles enhance the detection of small molecules in label-free impedance aptasensors. *Nanoscale*. 2015;**7**(17):7763-7769. DOI: 10.1039/c5nr01429h
- [37] Gosai A, Hau Yeah BS, Nilsen-Hamilton M, Shrotriya P. Label free thrombin detection in presence of high concentration of albumin using an aptamer-functionalized nanoporous membrane. *Biosensors & Bioelectronics*. 2019;**126**:88-95. DOI: 10.1016/j.bios.2018.10.010
- [38] Feng X, Liu K, Ning Y, Chen L, Deng L. A label-free aptasensor for rapid detection of H1N1 virus based on graphene oxide and polymerase-aided signal amplification. *Nanomedicine and Nanotechnology*. 2015;**6**(3):288. DOI: 10.4172/2157-7439.1000288
- [39] Sadeghi AS, Ansari N, Ramezani M, Abnous K, Mohsenzadeh M, Taghdisi SM, et al. Optical and electrochemical aptasensors for the detection of amphenicols. *Biosensors & Bioelectronics*. 2018;**118**:137-152. DOI: 10.1016/j.bios.2018.07.045
- [40] Du X, Jiang D, Hao N, Qian J, Dai L, Zhou L, et al. Building a three-dimensional nano-bio interface for aptasensing: An analytical methodology based on steric hindrance initiated signal amplification effect. *Analytical Chemistry*. 2016;**88**(19):9622-9629. DOI: 10.1021/acs.analchem.6b02368
- [41] Luka G, Ahmadi A, Najjaran H, Alocilja E, Derosa M, Wolthers K, et al. Microfluidics integrated biosensors: A leading technology towards lab-on-A-chip and sensing applications. *Sensors (Basel)*. 2015;**15**(12):30011-30031. DOI: 10.3390/s151229783
- [42] Kang K, Sachan A, Nilsen-Hamilton M, Shrotriya P. Aptamer functionalized microcantilever sensors for cocaine detection. *Langmuir*. 2011;**27**(23):14696-14702. DOI: 10.1021/la202067y
- [43] Kang K, Nilsen-Hamilton M, Shrotriya P. Differential surface stress sensor for detection of chemical and biological species. *Applied Physics Letters*. 2008;**93**(14):14-17. DOI: 10.1063/1.2996411
- [44] Zhai L, Wang T, Kang K, Zhao Y, Shrotriya P, Nilsen-Hamilton M. An RNA aptamer-based microcantilever sensor to detect the inflammatory marker, mouse lipocalin-2. *Analytical Chemistry*. 2012;**84**(20):8763-8770. DOI: 10.1021/ac3020643
- [45] Lim YC, Kouzani AZ, Duan W, Dai XJ, Kaynak, A, Mair D. Design and evaluation of a microcantilever aptasensor. In: *ISCAS*



- 2014; Proceedings of the 2014 IEEE International Symposium on Circuits and Systems, IEEE, Piscataway, NJ. 2014. pp. 221-224. DOI: 10.1109/ISCAS.2014.6865105
- [46] Zhao Y, Schagerl M, Viechtbauer C, Loh KJ. Characterizing the conductivity and enhancing the Piezoresistivity of carbon nanotube-polymeric thin films. *Materials (Basel)*. 2017;**10**(7):724. DOI: 10.3390/ma10070724
- [47] Liss M, Petersen B, Wolf H, Prohaska E. An aptamer-based quartz crystal protein biosensor. *Analytical Chemistry*. 2002;**74**(17):4488-4495. DOI: 10.1021/ac011294p
- [48] Schlenso MD, Gronewold TMA, Tewes M, Famulok M, Quandt E. A love-wave biosensor using nucleic acids as ligands. *Sensors & Actuators, B: Chemical*. 2004;**101**(3):308-315. DOI: 10.1016/j.snb.2004.03.015
- [49] Tombelli S, Minunni M, Luzi E, Mascini M. Aptamer-based biosensors for the detection of HIV-1 Tat protein. *Bioelectrochemistry*. 2005;**67**(2 Spec Issue):135-141. DOI: 10.1016/j.bioelechem.2004.04.011
- [50] Wilson R, Cossins A, Nicolau DV, Missailidis S. The selection of DNA aptamers for two different epitopes of thrombin was not due to different partitioning methods. *Nucleic Acid Therapeutics*. 2013;**23**(1):88-92. DOI: 10.1089/nat.2012.0386
- [51] Ahmad Raston NH, Nguyen VT, Gu MB. A new lateral flow strip assay (LFSA) using a pair of aptamers for the detection of vaspin. *Biosensors & Bioelectronics*. 2017;**93**:21-25. DOI: 10.1016/j.bios.2016.11.061
- [52] Luo Z, Zhang J, Wang Y, Chen J, Li Y, Duan Y. An aptamer based method for small molecules detection through monitoring salt-induced AuNPs aggregation and surface plasmon resonance (SPR) detection. *Sensors & Actuators, B: Chemical*. 2016;**236**:474-479. DOI: 10.1016/j.snb.2016.06.035
- [53] Neves MADD, Blaszykowski C, Bokhari S, Thompson M. Ultra-high frequency piezoelectric aptasensor for the label-free detection of cocaine. *Biosensors & Bioelectronics*. 2015;**72**:383-392. DOI: 10.1016/j.bios.2015.05.038
- [54] Neves MAD, Blaszykowski C, Thompson M. Utilizing a key aptamer structure-switching mechanism for the ultrahigh frequency detection of cocaine. *Analytical Chemistry*. 2016;**88**(6):3098-3106. DOI: 10.1021/acs.analchem.5b04010
- [55] Cai S, Yan J, Xiong H, Liu Y, Peng D, Liu Z. Investigations on the interface of nucleic acid aptamers and binding targets. *The Analyst*. 2018;**143**(22):5317-5338. DOI: 10.1039/c8an01467a
- [56] Faure-Perraud A, Métifiot M, Reigadas S, Recordon-Pinson P, Parissi V, Ventura M, et al. The guanine-quadruplex aptamer 93del inhibits HIV-1 replication ex vivo by interfering with viral entry, reverse transcription and integration. *Antiviral Therapy*. 2011;**16**(3):383-394. DOI: 10.3851/IMP1756
- [57] Tang XL, Wu SM, Xie Y, Song N, Guan Q, Yuan C, et al. Generation and application of ssDNA aptamers against glycolipid antigen ManLAM of *Mycobacterium tuberculosis* for TB diagnosis. *The Journal of Infection*. 2016;**72**(5):573-586. DOI: 10.1016/j.jinf.2016.01.014
- [58] Tang XL, Zhou YX, Wu SM, Pan Q, Xia B, Zhang XL. CFP10 and ESAT6 aptamers as effective mycobacterial antigen diagnostic reagents. *The Journal of Infection*. 2014;**69**(6):569-580. DOI: 10.1016/j.jinf.2014.05.015
- [59] Rotherham LS, Maserumule C, Dheda K, Theron J, Khati M. Selection and application of ssDNA aptamers to

- detect active TB from sputum samples. PLoS One. 2012;7(10):e46862. DOI: 10.1371/journal.pone.0046862
- [60] Qin L, Zheng R, Ma Z, Feng Y, Liu Z, Yang H, et al. The selection and application of ssDNA aptamers against MPT64 protein in *Mycobacterium tuberculosis*. Clinical Chemistry and Laboratory Medicine. 2009;47(4):405-411. DOI: 10.1515/CCLM.2009.097
- [61] Zhu C, Liu J, Ling Y, Yang H, Liu Z, Zheng R, et al. Evaluation of the clinical value of ELISA based on MPT64 antibody aptamer for serological diagnosis of pulmonary tuberculosis. BMC Infectious Diseases. 2012;12:96. DOI: 10.1186/1471-2334-12-96
- [62] Ngubane NAC, Gresh L, Pym A, Rubin EJ, Khati M. Selection of RNA aptamers against the M. tuberculosis EsxG protein using surface plasmon resonance-based SELEX. Biochemical and Biophysical Research Communications. 2014;449(1):114-119. DOI: 10.1016/j.bbrc.2014.04.163
- [63] Aimaiti R, Qin L, Cao T, Yang H, Wang J, Lu J, et al. Identification and application of ssDNA aptamers against H37Rv in the detection of *Mycobacterium tuberculosis*. Applied Microbiology and Biotechnology. 2015;99(21):9073-9083. DOI: 10.1007/s00253-015-6815-7
- [64] Zhang XQ, Feng Y, Yao QQ, He F. Selection of a new *Mycobacterium tuberculosis* H37Rv aptamer and its application in the construction of a SWCNT/aptamer/Au-IDE MSPQC H37Rv sensor. Biosensors & Bioelectronics. 2017;98:261-266. DOI: 10.1016/j.bios.2017.05.043
- [65] Joshi R, Janagama H, Dwivedi HP, Senthil Kumar TMA, Jaykus LA, Schefers J, et al. Selection, characterization, and application of DNA aptamers for the capture and detection of *Salmonella enterica* serovars. Molecular and Cellular Probes. 2009;23(1):20-28. DOI: 10.1016/j.mcp.2008.10.006
- [66] Ma X, Jiang Y, Jia F, Yu Y, Chen J, Wang Z. An aptamer-based electrochemical biosensor for the detection of *Salmonella*. Journal of Microbiological Methods. 2014;98(1):94-98. DOI: 10.1016/j.mimet.2014.01.003
- [67] Han SR, Lee SW. In vitro selection of RNA aptamer specific to *Salmonella Typhimurium*. Journal of Microbiology and Biotechnology. 2013;23(6):878-884. DOI: 10.4014/jmb.1212.12033
- [68] Moon J, Kim G, Lee S, Park S. Identification of *Salmonella typhimurium*-specific DNA aptamers developed using whole-cell SELEX and FACS analysis. Journal of Microbiological Methods. 2013;95(2):162-166. DOI: 10.1016/j.mimet.2013.08.005
- [69] Duan N, Wu S, Chen X, Huang Y, Xia Y, Ma X, et al. Selection and characterization of aptamers against *Salmonella typhimurium* using whole-bacterium systemic evolution of ligands by exponential enrichment (SELEX). Journal of Agricultural and Food Chemistry. 2013;61(13):3229-3234. DOI: 10.1021/jf400767d
- [70] Lavu PSR, Mondal B, Ramlal S, Murali HS, Batra HV. Selection and characterization of aptamers using a modified whole cell bacterium SELEX for the detection of *Salmonella enterica* Serovar *Typhimurium*. ACS Combinatorial Science. 2016;18(6):292-301. DOI: 10.1021/acscombsci.5b00123
- [71] Yang M, Peng Z, Ning Y, Chen Y, Zhou Q, Deng L. Highly specific and cost-efficient detection of *Salmonella paratyphi* A combining aptamers with single-walled carbon nanotubes.

- Sensors (Switzerland). 2013;**13**(5):6865-6881. DOI: 10.3390/s130506865
- [72] Hyeon JY, Chon JW, Choi IS, Park C, Kim DE, Seo KH. Development of RNA aptamers for detection of *Salmonella enteritidis*. Journal of Microbiological Methods. 2012;**89**(1):79-82. DOI: 10.1016/j.mimet.2012.01.014
- [73] Bayraç C, Eyidoğan F, Avni Öktem H. DNA aptamer-based colorimetric detection platform for *Salmonella enteritidis*. Biosensors & Bioelectronics. 2017;**98**:22-28. DOI: 10.1016/j.bios.2017.06.029
- [74] DeGrasse JA. A single-stranded DNA aptamer that selectively binds to *Staphylococcus aureus* enterotoxin B. PLoS One. 2012;**7**(3):e33410. DOI: 10.1371/journal.pone.0033410
- [75] Huang Y, Chen X, Duan N, Wu S, Wang Z, Wei X, et al. Selection and characterization of DNA aptamers against *Staphylococcus aureus* enterotoxin C1. Food Chemistry. 2015;**166**:623-629. DOI: 10.1016/j.foodchem.2014.06.039
- [76] Hong KL, Battistella L, Salva AD, Williams RM, Sooter LJ. In vitro selection of single-stranded DNA molecular recognition elements against *S. Aureus* alpha toxin and sensitive detection in human serum. International Journal of Molecular Sciences. 2015;**16**(2):2794-2809. DOI: 10.3390/ijms16022794
- [77] Ferreira IM, de Souza Lacerda CM, de Faria LS, Corrêa CR, de Andrade ASR. Selection of peptidoglycan-specific aptamers for bacterial cells identification. Applied Biochemistry and Biotechnology. 2014;**174**(7):2548-2556. DOI: 10.1007/s12010-014-1206-6
- [78] Stoltenburg R, Schubert T, Strehlitz B. In vitro selection and interaction studies of a DNA aptamer targeting Protein A. PLoS One. 2015;**10**(7):e0134403. DOI: 10.1371/journal.pone.0134403
- [79] Cao X, Li S, Chen L, Ding H, Xu H, Huang Y, et al. Combining use of a panel of ssDNA aptamers in the detection of *Staphylococcus aureus*. Nucleic Acids Research. 2009;**37**(14):4621-4628. DOI: 10.1093/nar/gkp489
- [80] Borsa BA, Tuna BG, Hernandez FJ, Hernandez LI, Bayramoglu G, Arica MY, et al. *Staphylococcus aureus* detection in blood samples by silica nanoparticle-oligonucleotides conjugates. Biosensors & Bioelectronics. 2016;**86**:27-32. DOI: 10.1016/j.bios.2016.06.023
- [81] Chang YC, Yang CY, Sun RL, Cheng YF, Kao WC, Yang PC. Rapid single cell detection of *Staphylococcus aureus* by aptamer-conjugated gold nanoparticles. Scientific Reports. 2013;**3**:1863. DOI: 10.1038/srep01863
- [82] Ohk SH, Koo OK, Sen T, Yamamoto CM, Bhunia AK. Antibody-aptamer functionalized fibre-optic biosensor for specific detection of *Listeria monocytogenes* from food. Journal of Applied Microbiology. 2010;**109**(3):808-817. DOI: 10.1111/j.1365-2672.2010.04709.x
- [83] Bruno JG, Phillips T, Montez T, Garcia A, Sivils JC, Mayo MW, et al. Development of a fluorescent enzyme-linked DNA aptamer-magnetic bead sandwich assay and portable fluorometer for sensitive and rapid listeria detection. Journal of Fluorescence. 2015;**25**(1):173-183. DOI: 10.1007/s10895-014-1495-8
- [84] Suh SH, Jaykus LA. Nucleic acid aptamers for capture and detection of *Listeria* spp. Journal of Biotechnology. 2013;**167**(4):454-461. DOI: 10.1016/j.jbiotec.2013.07.027
- [85] Lee SH, Ahn JY, Lee KA, Um HJ, Sekhon SS, Sun Park T, et al. Analytical bioconjugates, aptamers, enable specific quantitative detection of *Listeria monocytogenes*. Biosensors &

- Bioelectronics. 2015;**68**:272-280. DOI: 10.1016/j.bios.2015.01.009
- [86] Bruno JG, Phillips T, Carrillo MP, Crowell R. Plastic-adherent DNA aptamer-magnetic bead and quantum dot sandwich assay for campylobacter detection. *Journal of Fluorescence*. 2009;**19**(3):427-435. DOI: 10.1007/s10895-008-0429-8
- [87] Amraee M, Oloomi M, Yavari A, Bouzari S. DNA aptamer identification and characterization for *E. coli* O157 detection using cell based SELEX method. *Analytical Biochemistry*. 2017;**536**:36-44. DOI: 10.1016/j.ab.2017.08.005
- [88] Peng Z, Ling M, Ning Y, Deng L. Rapid fluorescent detection of *Escherichia coli* K88 based on DNA aptamer library as direct and specific reporter combined with immuno-magnetic separation. *Journal of Fluorescence*. 2014;**24**(4):1159-1168. DOI: 10.1007/s10895-014-1396-x
- [89] Kim YS, Song MY, Jurng J, Kim BC. Isolation and characterization of DNA aptamers against *Escherichia coli* using a bacterial cell-systematic evolution of ligands by exponential enrichment approach. *Analytical Biochemistry*. 2013;**436**(1):22-28. DOI: 10.1016/j.ab.2013.01.014
- [90] Dua P, Ren S, Lee SW, Kim J, Shin H, Jeong O, et al. Cell-SELEX based identification of an RNA aptamer for *Escherichia coli* and Its use in various detection formats. *Molecules and Cells*. 2016;**39**(11):807-813. DOI: 10.1111/j.1369-7625.2012.00810.x
- [91] Renders M, Miller E, Lam CH, Perrin DM. Whole cell-SELEX of aptamers with a tyrosine-like side chain against live bacteria. *Organic & Biomolecular Chemistry*. 2017;**15**(9):1980-1989. DOI: 10.1039/C6OB02451C
- [92] Chen F, Zhou J, Luo F, Mohammed AB, Zhang XL. Aptamer from whole-bacterium SELEX as new therapeutic reagent against virulent *Mycobacterium tuberculosis*. *Biochemical and Biophysical Research Communications*. 2007;**357**(3):743-748. DOI: 10.1016/j.bbrc.2007.04.007
- [93] Pan Q, Wang Q, Sun X, Xia X, Wu S, Luo F, et al. Aptamer against mannose-capped lipoarabinomannan inhibits virulent *Mycobacterium tuberculosis* infection in mice and rhesus monkeys. *Molecular Therapy*. 2014;**22**(5):940-951. DOI: 10.1038/mt.2014.31
- [94] Sun X, Pan Q, Yuan C, Wang Q, Tang X-L, Ding K, et al. A single ssDNA aptamer binding to ManLAM of BCG enhances immunoprotective effects against tuberculosis. *Journal of the American Chemical Society*. 2016;**138**(36):11680-11689. DOI: 10.1021/jacs.6b05357
- [95] Baig IA, Moon JY, Lee SC, Ryoo SW, Yoon MY. Development of ssDNA aptamers as potent inhibitors of *Mycobacterium tuberculosis* acetohydroxyacid synthase. *Biochim Biophys Acta—Proteins Proteomics*. 2015;**1854**(10):1338-1350. DOI: 10.1016/j.bbapap.2015.05.003
- [96] Pan Q, Zhang XL, Wu HY, He PW, Wang F, Zhang MS, et al. Aptamers that preferentially bind type IVB pili and inhibit human monocytic-cell invasion by *Salmonella enterica* Serovar typhi. *Antimicrobial Agents and Chemotherapy*. 2005;**49**(10):4052-4060. DOI: 10.1128/AAC.49.10.4052-4060.2005
- [97] Zelada-Guillen GA, Riu J, Düzgün A, Rius FX. Immediate detection of living bacteria at ultralow concentrations using a carbon nanotube based potentiometric aptasensor. *Angewandte Chemie International Edition*. 2009;**48**(40):7334-7337. DOI: 10.1002/anie.200902090

- [98] Wang K, Wu D, Chen Z, Zhang X, Yang X, Yang CJ, et al. Inhibition of the superantigenic activities of staphylococcal enterotoxin A by an aptamer antagonist. *Toxicon*. 2016;**119**:21-27. DOI: 10.1016/j.toxicon.2016.05.006
- [99] Vivekananda J, Salgado C, Millenbaugh NJ. DNA aptamers as a novel approach to neutralize *Staphylococcus aureus*  $\alpha$ -toxin. *Biochemical and Biophysical Research Communications*. 2014;**444**(3):433-438. DOI: 10.1016/j.bbrc.2014.01.076
- [100] Yamamoto R, Katahira M, Nishikawa S, Baba T, Taira K, Kumar PKR. A novel RNA motif that binds efficiently and specifically to the Tat protein of HIV and inhibits the trans-activation by Tat of transcription in vitro and in vivo. *Genes to Cells*. 2000;**5**(5):371-388. DOI: 10.1046/j.1365-2443.2000.00330.x
- [101] Minunni M, Tombelli S, Gullotto A, Luzi E, Mascini M. Development of biosensors with aptamers as bio-recognition element: The case of HIV-1 Tat protein. *Biosensors & Bioelectronics*. 2004;**20**(6):1149-1156. DOI: 10.1016/j.bios.2004.03.037
- [102] Chen F, Hu Y, Li D, Chen H, Zhang XL. CS-SELEX generates high-affinity ssDNA aptamers as molecular probes for hepatitis C virus envelope glycoprotein E2. *PLoS One*. 2009;**4**(12):e8142. DOI: 10.1371/journal.pone.0008142
- [103] Lee S, Kim YS, Jo M, Jin M, ki Lee D, Kim S. Chip-based detection of hepatitis C virus using RNA aptamers that specifically bind to HCV core antigen. *Biochemical and Biophysical Research Communications*. 2007;**358**(1):47-52. DOI: 10.1016/j.bbrc.2007.04.057
- [104] Shi S, Yu X, Gao Y, Xue B, Wu X, Wang X, et al. Inhibition of hepatitis C virus production by aptamers against the core protein. *Journal of Virology*. 2014;**88**(4):1990-1999. DOI: 10.1128/JVI.03312-13
- [105] Ghanbari K, Roushani M, Azadbakht A. Ultra-sensitive aptasensor based on a QGD nanocomposite for detection of hepatitis C virus core antigen. *Analytical Biochemistry*. 2017;**534**:64-69. DOI: 10.1016/j.ab.2017.07.016
- [106] Sung HJ, Kayhan B, Ben-Yedidia T, Arnon R. A DNA aptamer prevents influenza infection by blocking the receptor binding region of the viral hemagglutinin. *The Journal of Biological Chemistry*. 2004;**279**(46):48410-48419. DOI: 10.1074/jbc.M409059200
- [107] Misono TS, Kumar PKR. Selection of RNA aptamers against human influenza virus hemagglutinin using surface plasmon resonance. *Analytical Biochemistry*. 2005;**342**(2):312-317. DOI: 10.1016/j.ab.2005.04.013
- [108] Gopinath SCB, Misono TS, Kawasaki K, Mizuno T, Imai M, Odagiri T, et al. An RNA aptamer that distinguishes between closely related human influenza viruses and inhibits haemagglutinin-mediated membrane fusion. *The Journal of General Virology*. 2006;**87**(3):479-487. DOI: 10.1099/vir.0.81508-0
- [109] Cheng C, Dong J, Yao L, Chen A, Jia R, Huan L, et al. Potent inhibition of human influenza H5N1 virus by oligonucleotides derived by SELEX. *Biochemical and Biophysical Research Communications*. 2008;**366**(3):670-674. DOI: 10.1016/j.bbrc.2007.11.183
- [110] Choi SK, Lee C, Lee KS, Choe SY, Mo IP, Seong RH, et al. DNA aptamers against the receptor binding region of hemagglutinin prevent avian influenza viral infection. *Molecules and Cells*. 2011;**32**(6):527-533. DOI: 10.1007/s10059-011-0156-x

- [111] Park SY, Kim S, Yoon H, Kim K-B, Kalme SS, Oh S, et al. Selection of an antiviral RNA aptamer against hemagglutinin of the subtype H5 avian influenza virus. *Nucleic Acid Therapy (Formerly Oligonucleotides)*. 2011;**21**(6):395-402. DOI: 10.1089/nat.2011.0321
- [112] Gopinath SCB, Kumar PKR. Aptamers that bind to the hemagglutinin of the recent pandemic influenza virus H1N1 and efficiently inhibit agglutination. *Acta Biomaterialia*. 2013;**9**(11):8932-8941. DOI: 10.1016/j.actbio.2013.06.016
- [113] Wongphatcharachai M, Wang P, Enomoto S, Webby RJ, Gramer MR, Amonsin A, et al. Neutralizing DNA aptamers against swine influenza H3N2 viruses. *Journal of Clinical Microbiology*. 2013;**51**(1):46-54. DOI: 10.1128/JCM.02118-12
- [114] Suenaga E, Kumar PKR. An aptamer that binds efficiently to the hemagglutinins of highly pathogenic avian influenza viruses (H5N1 and H7N7) and inhibits hemagglutinin-glycan interactions. *Acta Biomaterialia*. 2014;**10**(3):1314-1323. DOI: 10.1016/j.actbio.2013.12.034
- [115] Woo HM, Lee JM, Yim S, Jeong YJ. Isolation of single-stranded DNA aptamers that distinguish influenza virus hemagglutinin subtype H1 from H5. *PLoS One*. 2015;**10**(4):e0125060. DOI: 10.1371/journal.pone.0125060
- [116] Zhang Y, Yu Z, Jiang F, Fu P, Shen J, Wu W, et al. Two DNA aptamers against avian influenza H9N2 virus prevent viral infection in cells. *PLoS One*. 2015;**10**(3):e0123060. DOI: 10.1371/journal.pone.0123060
- [117] Lai HC, Wang CH, Liou TM, Bin LG. Influenza A virus-specific aptamers screened by using an integrated microfluidic system. *Lab on a Chip*. 2014;**14**(12):2002-2013. DOI: 10.1016/j.vetpar.2015.05.004
- [118] Nguyen VT, Bin SH, Kim BC, Kim SK, Song CS, Gu MB. Highly sensitive sandwich-type SPR based detection of whole H5Nx viruses using a pair of aptamers. *Biosensors & Bioelectronics*. 2016;**86**:293-300. DOI: 10.1016/j.bios.2016.06.064
- [119] Liu J, Yang Y, Hu B, Ma ZY, Huang HP, Yu Y, et al. Development of HBsAg-binding aptamers that bind HepG2.2.15 cells via HBV surface antigen. *Virologica Sinica*. 2010;**25**(1):27-35. DOI: 10.1007/s12250-010-3091-7
- [120] Toscano-Garibay JD, Benítez-Hess ML, Alvarez-Salas LM. Isolation and characterization of an RNA aptamer for the HPV-16 E7 oncoprotein. *Archives of Medical Research*. 2011;**42**(2):88-96. DOI: 10.1016/j.arcmed.2011.02.005
- [121] Rahim Ruslinda A, Tanabe K, Ibori S, Wang X, Kawarada H. Effects of diamond-FET-based RNA aptamer sensing for detection of real sample of HIV-1 Tat protein. *Biosensors & Bioelectronics*. 2013;**40**(1):277-282. DOI: 10.1016/j.bios.2012.07.048
- [122] Zhou J, Swiderski P, Li H, Zhang J, Neff CP, Akkina R, et al. Selection, characterization and application of new RNA HIV gp 120 aptamers for facile delivery of Dicer substrate siRNAs into HIV infected cells. *Nucleic Acids Research*. 2009;**37**(9):3094-3109. DOI: 10.1093/nar/gkp185
- [123] Prokofjeva M, Tsvetkov V, Basmanov D, Varizhuk A, Lagarkova M, Smirnov I, et al. Anti-HIV activities of intramolecular G4 and Non-G4 oligonucleotides. *Nucleic Acid Therapeutics*. 2017;**27**(1):56-66. DOI: 10.1089/nat.2016.0624
- [124] Tuerk C, MacDougall S, Gold L. RNA pseudoknots that inhibit human immunodeficiency virus type 1 reverse transcriptase. *Proceedings of the National Academy of Sciences of the United States of America*. 1992;**89**(15):6988-6992. DOI: 10.1073/pnas.89.15.6988

- [125] Schneider DJ, Feigon J, Hostomsky Z, Gold L. High-affinity ssDNA inhibitors of the reverse transcriptase of type 1 human immunodeficiency virus. *Biochemistry*. 1995;**34**(29):9599-9610. DOI: 10.1021/bi00029a037
- [126] Mosing RK, Mendonsa SD, Bowser MT. Capillary electrophoresis-SELEX selection of aptamers with affinity for HIV-1 reverse transcriptase. *Analytical Chemistry*. 2005;**77**(19):6107-6112. DOI: 10.1021/ac050836q
- [127] Somasunderam A, Ferguson MR, Rojo DR, Thiviyathan V, Li X, O'Brien WA, et al. Combinatorial selection, inhibition, and antiviral activity of DNA thioaptamers targeting the RNase H domain of HIV-1 reverse transcriptase. *Biochemistry*. 2005;**44**(30):10388-10395. DOI: 10.1021/bi0507074
- [128] DeStefano JJ, Nair GR. Novel aptamer inhibitors of human immunodeficiency virus reverse transcriptase. *Oligonucleotides*. 2008;**18**(2):133-144. DOI: 10.1089/oli.2008.0103
- [129] Ferreira-Bravo IA, Cozens C, Holliger P, DeStefano JJ. Selection of 2'-deoxy-2'-fluoroarabinonucleotide (FANA) aptamers that bind HIV-1 reverse transcriptase with picomolar affinity. *Nucleic Acids Research*. 2015;**43**(20):9587-9599. DOI: 10.1093/nar/gkv1057
- [130] Sánchez-Luque FJ, Stich M, Manrubia S, Briones C, Berzal-Herranz A. Efficient HIV-1 inhibition by a 16 nt-long RNA aptamer designed by combining in vitro selection and in silico optimisation strategies. *Scientific Reports*. 2014;**1**(4):6242. DOI: 10.1038/srep06242
- [131] Boiziau C, Dausse E, Yurchenko L, Toulmé JJ. DNA aptamers selected against the HIV-1 trans-activation-responsive RNA element form RNA-DNA kissing complexes. *The Journal of Biological Chemistry*. 1999;**274**(18):12730-12737. DOI: 10.1074/jbc.274.18.12730
- [132] Jing N, Hogan ME. Structure-activity of tetrad-forming oligonucleotides as a potent anti- HIV therapeutic drug. *The Journal of Biological Chemistry*. 1998;**273**(52):34992-34999. DOI: 10.1074/jbc.273.52.34992
- [133] Esposito V, Pirone L, Mayol L, Pedone E, Virgilio A, Galeone A. Exploring the binding of d(GGGT)<sub>4</sub> to the HIV-1 integrase: An approach to investigate G-quadruplex aptamer/target protein interactions. *Biochimie*. 2016;**127**:19-22. DOI: 10.1016/j.biochi.2016.04.013
- [134] De Soultrait VR, Lozach PY, Altmeyer R, Tarrago-Litvak L, Litvak S, Andréola ML. DNA aptamers derived from HIV-1 RNase H inhibitors are strong anti-integrase agents. *Journal of Molecular Biology*. 2002;**324**(2):195-203. DOI: 10.1016/S0022-2836(02)01064-1
- [135] Phan AT, Kuryavyi V, Ma J-B, Faure A, Andreola M-L, Patel DJ. From the cover: An interlocked dimeric parallel-stranded DNA quadruplex: A potent inhibitor of HIV-1 integrase. *Proceedings of the National Academy of Sciences of the United States of America*. 2005;**102**(3):634-639. DOI: 10.1073/pnas.0406278102
- [136] Kim SJ, Kim MY, Jeong S, Kim SJ, Lee JH, You JC. Selection and stabilization of the RNA aptamers against the human immunodeficiency virus type-1 nucleocapsid protein. *Biochemical and Biophysical Research Communications*. 2002;**291**(4):925-931. DOI: 10.1006/bbrc.2002.6521
- [137] Ramalingam D, Duclair S, Datta SAK, Ellington A, Rein A, Prasad VR. RNA aptamers directed to human immunodeficiency virus type 1 gag polyprotein bind to the matrix and nucleocapsid domains and inhibit

- virus production. *Journal of Virology*. 2011;**85**(1):305-314. DOI: 10.1128/JVI.02626-09
- [138] Jensen KB, Green L, MacDougall-Waugh S, Tuerk C. Characterization of an *in vitro*-selected RNA ligand to the HIV-1 rev protein. *Journal of Molecular Biology*. 1994;**235**(1):237-247. DOI: 10.1016/S0022-2836(05)80030-0
- [139] Pang KM, Castanotto D, Li H, Scherer L, Rossi JJ. Incorporation of aptamers in the terminal loop of shRNAs yields an effective and novel combinatorial targeting strategy. *Nucleic Acids Research*. 2017;**46**(1):e6. DOI: 10.1093/nar/gkx980
- [140] Kumar PKR, Machida K, Urvil PT, Kakiuchi N, Vishnuvardhan D, Shimotohno K, et al. Isolation of RNA aptamers specific to the NS3 protein of hepatitis C virus from a pool of completely random RNA. *Virology*. 1997;**237**(2):270-282. DOI: 10.1006/viro.1997.8773
- [141] Fukuda K, Vishnuvardhan D, Sekiya S, Hwang J, Kakiuchi N, Taira K, et al. Isolation and characterization of RNA aptamers specific for the hepatitis C virus nonstructural protein 3 protease. *European Journal of Biochemistry*. 2000;**267**(12):3685-3694. DOI: 10.1046/j.1432-1327.2000.01400.x
- [142] Nishikawa F, Funaji K, Fukuda K, Nishikawa S. *In vitro* selection of RNA aptamers against the HCVNS3 helicase domain. *Oligonucleotides*. 2004;**14**:114. DOI: 10.1089/1545457041526335
- [143] Kikuchi K, Umehara T, Fukuda K, Kuno A, Hasegawa T, Nishikawa S. A hepatitis C virus (HCV) internal ribosome entry site (IRES) domain III-IV-targeted aptamer inhibits translation by binding to an apical loop of domain III. *Nucleic Acids Research*. 2005;**33**(2):683-692. DOI: 10.1093/nar/gki215
- [144] Romero-López C, Barroso-delJesus A, Puerta-Fernández E, Berzal-Herranz A. Interfering with hepatitis C virus IRES activity using RNA molecules identified by a novel *in vitro* selection method. *Biological Chemistry*. 2005;**386**(2):183-190. DOI: 10.1515/BC.2005.023
- [145] Romero-López C, Díaz-González R, Berzal-Herranz A. Inhibition of hepatitis C virus internal ribosome entry site-mediated translation by an RNA targeting the conserved III<sup>h</sup> domain. *Cellular and Molecular Life Sciences*. 2007;**64**(22):2994-3006. DOI: 10.1007/s00018-007-7345-y
- [146] Romero-López C, Lahlali T, Berzal-Herranz B, Berzal-Herranz A. Development of optimized inhibitor RNAs allowing multisite-targeting of the HCV genome. *Molecules*. 2017;**22**(5):E861. DOI: 10.3390/molecules22050861
- [147] Bellecave P, Andreola M-L, Ventura M, Tarrago-Litvak L, Litvak S, Astier-Gin T. Selection of DNA aptamers that bind the RNA-dependent RNA polymerase of hepatitis C virus and inhibit viral RNA synthesis *in vitro*. *Oligonucleotides*. 2003;**13**(6):455-463. DOI: 10.1089/154545703322860771
- [148] Bellecave P, Cazenave C, Rumi J, Staedel C, Cosnefroy O, Andreola ML, et al. Inhibition of hepatitis C virus (HCV) RNA polymerase by DNA aptamers: Mechanism of inhibition of *in vitro* RNA synthesis and effect on HCV-infected cells. *Antimicrobial Agents and Chemotherapy*. 2008;**52**(6):2097-2110. DOI: 10.1128/AAC.01227-07
- [149] Jones LA, Clancy LE, Rawlinson WD, White PA. High-affinity aptamers to subtype 3a hepatitis C virus polymerase display genotypic specificity. *Antimicrobial Agents and Chemotherapy*. 2006;**50**(9):3019-3027. DOI: 10.1128/AAC.01603-05
- [150] Lee CH, Lee YJ, Kim JH, Lim JH, Kim J-H, Han W, et al. Inhibition of



- hepatitis C Virus (HCV) replication by specific RNA aptamers against HCV NS5B RNA replicase. *Journal of Virology*. 2013;**87**(12):7064-7074. DOI: 10.1128/JVI.00405-13
- [151] Kwon HM, Lee KH, Han BW, Han MR, Kim DH, Kim DE. An RNA aptamer that specifically binds to the glycosylated hemagglutinin of avian influenza virus and suppresses viral infection in cells. *PLoS One*. 2014;**9**(5):e97574. DOI: 10.1371/journal.pone.0097574
- [152] Yuan S, Zhang N, Singh K, Shuai H, Chu H, Zhou J, et al. Cross-protection of influenza A virus infection by a DNA aptamer targeting the PA endonuclease domain. *Antimicrobial Agents and Chemotherapy*. 2015;**59**(7):4082-4093. DOI: 10.1128/AAC.00306-15
- [153] Feng H, Beck J, Nassal M, hong Hu K. A SELEX-screened aptamer of human hepatitis B virus RNA encapsidation signal suppresses viral replication. *PLoS One*. 2011;**6**(11):e27862. DOI: 10.1371/journal.pone.0027862
- [154] Zhang Z, Zhang J, Pei X, Zhang Q, Lu B, Zhang X, et al. An aptamer targets HBV core protein and suppresses HBV replication in HepG2.2.15 cells. *International Journal of Molecular Medicine*. 2014;**34**(5):1423-1429. DOI: 10.3892/ijmm.2014.1908
- [155] Orabi A, Bieringer M, Geerlof A, Bruss V. An aptamer against the matrix binding domain on the hepatitis B virus capsid impairs virion formation. *Journal of Virology*. 2015;**89**(18):9281-9287. DOI: 10.1128/JVI.00466-15
- [156] Nicol C, Bunka DHJ, Blair GE, Stonehouse NJ. Effects of single nucleotide changes on the binding and activity of RNA aptamers to human papillomavirus 16 E7 oncoprotein. *Biochemical and Biophysical Research Communications*. 2011;**405**(3):417-421. DOI: 10.1016/j.bbrc.2011.01.044
- [157] Nicol C, Cesur O, Forrest S, Belyaeva TA, Bunka DHJ, Blair GE, et al. An RNA aptamer provides a novel approach for the induction of apoptosis by targeting the HPV16 E7 oncoprotein. *PLoS One*. 2013;**8**:e64781. DOI: 10.1371/journal.pone.0064781
- [158] Belyaeva T, Nicol C, Cesur Ö, Travé G, Blair G, Stonehouse N. An RNA aptamer targets the PDZ-binding motif of the HPV16 E6 oncoprotein. *Cancers (Basel)*. 2014;**6**(3):1553-1569. DOI: 10.3390/cancers6031553
- [159] Shum KT, Tanner JA. Differential inhibitory activities and stabilisation of DNA aptamers against the SARS coronavirus helicase. *Chembiochem*. 2008;**9**(18):3037-3045. DOI: 10.1002/cbic.200800491
- [160] Chen HL, Hsiao WH, Lee HC, Wu SC, Cheng JW. Selection and characterization of DNA aptamers targeting all four serotypes of dengue viruses. *PLoS One*. 2015;**10**(6):e0131240. DOI: 10.1371/journal.pone.0131240
- [161] Liang HR, Hu GQ, Li L, Gao YW, Yang ST, Xia XZ. Aptamers targeting rabies virus-infected cells inhibit street rabies virus in vivo. *International Immunopharmacology*. 2014;**21**(2):432-438. DOI: 10.1016/j.intimp.2014.03.020
- [162] Shubham S, Hoinka J, Banerjee S, Swanson E, Dillard JA, Lennemann NJ, et al. A 2'FY-RNA motif defines an aptamer for Ebolavirus secreted protein. *Science Reports*. 2018;**8**(1):12373. DOI: 10.1038/s41598-018-30590-8
- [163] Lee KH, Zeng H. Aptamer-based ELISA assay for highly specific and sensitive detection of Zika NS1 protein. *Analytical Chemistry*. 2017;**89**(23):12743-12748. DOI: 10.1021/acs.analchem.7b02862

- [164] Que-Gewirth NS, Sullenger BA. Gene therapy progress and prospects: RNA aptamers. *Gene Therapy*. 2007;**14**(4):283-291. DOI: 10.1038/sj.gt.3302900
- [165] Kaur H, Bruno JG, Kumar A, Sharma TK. Aptamers in the therapeutics and diagnostics pipelines. *Theranostics*. 2018;**8**(15):4016-4032. DOI: 10.7150/thno.25958
- [166] O'Sullivan CK. Aptasensors—The future of biosensing? *Analytical and Bioanalytical Chemistry*. 2002;**372**:44-48. DOI: 10.1007/s00216-001-1189-3
- [167] Shamah SM, Healy JM, Cload ST. Complex target SELEX. *Accounts of Chemical Research*. 2008;**41**:130-138. DOI: 10.1021/ar700142z
- [168] Lim YC, Kouzani AZ, Duan W. Aptasensors: A review. *Journal of Biomedical Nanotechnology*. 2010;**6**(2): 93-105. DOI: 10.1166/jbn.2010.1103
- [169] Dhiman A, Kalra P, Bansal V, Bruno JG, Sharma TK. Aptamer-based point-of-care diagnostic platforms. *Sensors Actuators, B Chemical*. 2017;**246**: 535-553. DOI: 10.1016/j.snb.2017.02.060
- [170] Sharma TK. The point behind translation of aptamers for point of care diagnostics. *Aptamers (Synthetic Antibodies)*. 2016;**3**:36-42
- [171] Jayasena SD. Aptamers: An emerging class of molecules that rival antibodies in diagnostics. *Clinical Chemistry*. 1999;**45**:1628-1650
- [172] Zhang P, Zhao N, Zeng Z, Chang CC, Zu Y. Combination of an aptamer probe to CD4 and antibodies for multicolored cell phenotyping. *American Journal of Clinical Pathology*. 2010;**134**(4):586-593. DOI: 10.1309/AJCP55KQYWWSGZRKC
- [173] Abdeevaa IA, Maloshenoka LG, Pogorelkoab GV, Mokrykovaa MV, Bruskin SA. RNA-aptamers—As targeted inhibitors of protein functions in plants. *Journal of Plant Physiology*. 2019;**232**: 127-129. DOI: 10.1016/j.jplph.2018.10.026
- [174] Konopka K, Lee NS, Rossi J, Düzgüneş N. Rev-binding aptamer and CMV promoter act as decoys to inhibit HIV replication. *Gene*. 2000;**255**(2):235-244. DOI: 10.1016/S0378-1119(00)00334-6
- [175] Chaloin L. Endogenous expression of a high-affinity pseudoknot RNA aptamer suppresses replication of HIV-1. *Nucleic Acids Research*. 2002;**30**(18):4001-4008. DOI: 10.1093/nar/gkf522
- [176] Soh JH, Lin Y, Rana S, Ying JY, Stevens MM. Colorimetric detection of small molecules in complex matrixes via target-mediated growth of aptamer-functionalized gold nanoparticles. *Analytical Chemistry*. 2015;**87**(15):7644-7652. DOI: 10.1021/acs.analchem.5b00875
- [177] Ruscito A, DeRosa MC. Small-molecule binding aptamers: Selection strategies, characterization, and applications. *Frontiers in Chemistry*. 2016;**4**(14):1-14. DOI: 10.3389/fchem.2016.00014
- [178] Liu A, Zhang Y, Chen W, Wang X, Chen F. Gold nanoparticle-based colorimetric detection of staphylococcal enterotoxin B using ssDNA aptamers. *European Food Research and Technology*. 2013;**237**(3):323-329. DOI: 10.1007/s00217-013-1995-9
- [179] Shim WB, Kim MJ, Mun H, Kim MG. An aptamer-based dipstick assay for the rapid and simple detection of aflatoxin B1. *Biosensors & Bioelectronics*. 2014;**62**:288-294. DOI: 10.1016/j.bios.2014.06.059
- [180] Candia J, Cheung F, Kotliarov Y, Fantoni G, Sellers B, Griesman T, et al. Assessment of variability in the SOMAscan assay. *Scientific Reports*.

2017;7(1):14248. DOI: 10.1038/s41598-017-14755-5

[181] De Groote MA, Nahid P, Jarlsberg L, Johnson JL, Weiner M, Muzanyi G, et al. Elucidating novel serum biomarkers associated with pulmonary tuberculosis treatment. *PLoS One*. 2013;8(4):e61002. DOI: 10.1371/journal.pone.0061002

[182] Kraemer S, Vaught JD, Bock C, Gold L, Katilius E, Keeney TR, et al. From SOMAmer-based biomarker discovery to diagnostic and clinical applications: A SOMAmer-based, streamlined multiplex proteomic assay. *PLoS One*. 2011;6(10):e26332. DOI: 10.1371/journal.pone.0026332

[183] Lollo B, Steele F, Gold L. Beyond antibodies: New affinity reagents to unlock the proteome. *Proteomics*. 2014;14(6):638-644. DOI: 10.1002/pmic.201300187

[184] Mehan MR, Ayers D, Thirstrup D, Xiong W, Ostroff RM, Brody EN, et al. Protein signature of lung cancer tissues. *PLoS One*. 2012;7(4):e35157. DOI: 10.1371/journal.pone.0035157

[185] Müller J, Friedrich M, Becher T, Braunstein J, Kupper T, Berdel P, et al. Monitoring of plasma levels of activated protein C using a clinically applicable oligonucleotide-based enzyme capture assay. *Journal of Thrombosis and Haemostasis*. 2012;10(3):390-398. DOI: 10.1111/j.1538-7836.2012.04623.x

[186] Yan X, Song Y, Liu J, Zhou N, Zhang CL, He L, et al. Two-dimensional porphyrin-based covalent organic framework: A novel platform for sensitive epidermal growth factor receptor and living cancer cell detection. *Biosensors & Bioelectronics*. 2018;5663(18):30944-30948. DOI: 10.1016/j.bios.2018.11.047

[187] Song Y, Shi Y, Huang M, Wang W, Wang Y, Cheng J, et al. Bioinspired

engineering of multivalent aptamer-functionalized nanointerface to enhance capture and release of circulating tumor cells. *Angewandte Chemie International Edition*. 2018;131:1-6. DOI: 1002/anie.201809337

[188] Hong P, Li W, Li J. Applications of aptasensors in clinical diagnostics. *Sensors*. 2012;12(2):1181-1193. DOI: 10.3390/s120201181

[189] Bhat VG, Chavan P, Ojha S, Nair PK. Challenges in the laboratory diagnosis and management of dengue infections. *The Open Microbiology Journal*. 2015;9:33-37. DOI: 10.2174/1874285801509010033

[190] Tsai WY, Youn HH, Brites C, Tsai JJ, Tyson J, Pedroso C, et al. Distinguishing secondary dengue virus infection from Zika virus infection with previous dengue by a combination of 3 simple serological tests. *Clinical Infectious Diseases*. 2017;65(11):1829-1836. DOI: 10.1093/cid/cix672

[191] Kim YJ, Kim HS, Chon JW, Kim DH, Hyeon JY, Seo KH. New colorimetric aptasensor for rapid on-site detection of *Campylobacter jejuni* and *Campylobacter coli* in chicken carcass samples. *Analytica Chimica Acta*. 2018;1029:78-85. DOI: 10.1016/j.aca.2018.04.059

[192] Labib M, Zamay AS, Kolovskaya OS, Reshetneva IT, Zamay GS, Kibbee RJ, et al. Aptamer-based impedimetric sensor for bacterial typing. *Analytical Chemistry*. 2012;84(19):8114-8117. DOI: 10.1021/ac302217u

[193] Yoon SY, Gee G, Hong KJ, Seo SH. Application of aptamers for assessment of vaccine efficacy. *Clinical and Experimental Vaccine Research*. 2017;6:160-163. DOI: 10.7774/cevr.2017.6.2.160

[194] WHO. Tuberculosis. 2018. Available from: <https://www.who.int/news-room/fact-sheets/detail/tuberculosis>

- [195] WHO. Global Tuberculosis Report 2015. DOI: 978-92-4-156450-2
- [196] Elhassan MM, Elmekki MA, Osman AL, Hamid ME. Challenges in diagnosing tuberculosis in children: A comparative study from Sudan. *International Journal of Infectious Diseases*. 2016;**43**:25-29. DOI: 10.1016/j.ijid.2015.12.006
- [197] Hilman BC. Pediatric tuberculosis: Problems in diagnosis and issues in management. *The Journal of the Louisiana State Medical Society: Official organ of the Louisiana State Medical Society*. 1998;**150**(12):601-610
- [198] Racsa LD, Kraft CS, Olinger GG, Hensley LE. Viral hemorrhagic fever diagnostics. *Clinical Infectious Diseases*. 2016;**62**:214-219. DOI: 10.1093/cid/civ792
- [199] Miyazaki D, Shimizu D, Shimizu Y, Inoue Y, Inoue T, Higaki S, et al. Diagnostic efficacy of real-time PCR for ocular cytomegalovirus infections. *Graefes Archive for Clinical and Experimental Ophthalmology*. 2018;**256**(12):2413-2420. DOI: 10.1007/s00417-018-4111-9
- [200] Nolan N, Halai UA, Regunath H, Smith LP, Rojas-Moreno C, Salzer W. Primary cytomegalovirus infection in immunocompetent adults in the United States—A case series. *IDCases*. 2017;**10**:123-126. DOI: 10.1016/j.idcr.2017.10.008
- [201] O'Hara KM, Pontrelli G, Kunstel KL. An introduction to gastrointestinal tract CMV disease. *Journal of the Academy of Physician Assistants*. 2017;**30**:48-52. DOI: 10.1097/01.JAA.0000524712.40590.76
- [202] Marty AM, Jahrling PB, Geisbert TW. Viral hemorrhagic fevers. *Clinics in Laboratory Medicine*. 2006;**26**(2): 345-386. DOI: 10.1016/j.cll.2006.05.001
- [203] Behring K. Ueber das Zustandekommen der Diphtherie-Immunität und der Tetanus-Immunität bei Thieren. *Dtsch Medizinische Wochenschrift*. 1890;**16**:1113-1114. DOI: 10.1055/s-0029-1207589
- [204] Edelman G. Antibody structure and molecular immunology. *Annals of the New York Academy of Sciences*. 1971;**190**:5-25





*Edited by Muharrem Ince and Olcay Kaplan Ince*

This book focuses on recent and future trends in analytical methods and provides an overview of analytical chemistry. As a comprehensive analytical chemistry book, it takes a broad view of the subject and integrates a wide variety of approaches. The book provides separation approaches and method validation, as well as recent developments and applications in analytical chemistry. It is written primarily for researchers in the fields of analytical chemistry, environmental chemistry, and applied chemistry. The aim of the book is to explain the subject, clarify important studies, and compare and develop new and groundbreaking applications. Written by leading experts in their respective areas, the book is highly recommended for professionals interested in analytical chemistry because it provides specific and comprehensive examples.

Published in London, UK

© 2019 IntechOpen  
© romaset / iStock

**IntechOpen**

